Vision Assisted Tribography
of Rolling-Sliding Contact of Polymer-Steel Pairs

Visiegeassisteerde tribografie van het rol-slip-gedrag van polymeer-staalparen

Jacob Sukumaran

UNIVERSITEIT
GENT

**Promotor**
prof. dr. ir. Patrick De Baets
Ghent University
Faculty of Engineering and Architecture
Department of Mechanical Construction and Production

**Examination Committee**
prof. Rik Van de Walle (Chair)
prof. Wilfried Philips
prof. Wim De Waele
prof. Joris Degrieck
prof. Giorgio Donzella
prof. Gábor Kalácska
   dr. Stijn Hertelé

**Research Institute**
Ghent University
Department of Mechanical Construction and Production
Laboratory Soete
Technologiepark 903
B-9052 Zwijnaarde
Belgium

Tel. +32 9 331 04 75
Fax. +32 9 331 04 90
JacobPremKumar.Sukumaran@UGent
www.tribology-fatigue.ugent.be

இது உங்களால் உண்டானதல்ல, இது தேவனுடைய ஈவு. ஒருவரும் பெருமைபாராட்டாதபடிக்கு இது கிரியைகளினால் உண்டானதல்ல.

எபேசியர் 2:8-9


*It is the gift of God, not by works, so that no one can boast.*

*Ephesians 2:8-9*

# Acknowledgement

First I owe my deepest gratitude to my promoter prof. Patrick De Baets for his untiring support, guidance and providing me with an excellent research atmosphere. His meticulous comments and scientific discussions has led to the development of novel vision system in this thesis. I particularly appreciate the feedback offered by prof. Wilfried Philips. His comments and suggestions on image processing techniques provided new insights in quantitative micrography. The tribological advice given by prof. Gabor Kalascka has also been a great help in this research.

I want to thank Matyas Ando (Matyi), a good friend who gives me constructive comments and warm encouragement. His insightful remarks and suggestions are very valuable in this research. Most of the discussions with Matyi on technical and scientific matters were fruitful. It would have been difficult and a prolonged process in accomplishing modules of the project without the expertise of our project partner from TELIN, UGent. Without fail I should point out Seyfollah Soleimani's (Seyf) substantial contribution in the image processing part. I would also like to thank his fellow team members Koen Dougteroli for the image registration and Dimitri Van Cauwelaert for the camera.

I would like to express my gratitude to Barányi István (Peesta) for the stimulating collaboration on surface characterisation. Discussions with Peesta and Matyi have been illuminating. I would also like to thank Sandeep Kalathimekkad for his timely help on calibrating the illumination system. I am also grateful for the master thesis students Tom Piccin and Michiel Maenhout. Their support on preliminary testing was immense. I would like to thank Cyril Rajesh and Geo J Sangeeth for their suggestions on modification of the test rig. I thank the department of material Science and engineering (UGent), TELIN, and Olympus Benelux for permitting to use the cameras. I would like to thank Mr. Titus Thangam, Golden elevators, India for providing the rollers.

I am grateful for the wonderful colleagues at laboratory Soete the professors, fellow researchers and technicians who has always been supportive and encouraging. The research task would have been all the more difficult were it not for the encouragement and support provided by the researchers: Matyi, Saosomet Chittt, Yeczain Perez, Vanessa Rodriguez, Jan De Pauw, Gusztav Fekete, Patric Neis, Matthias Verstraete, Jeroen Van Wittenberghe, Timothy Galle, Koen Van Minnebruggen, Stijn Hertele, Felicia Jula, Diego Belato Rosado, Nahuel Micone, Reza Hojjati Talemi,

# Summary

Tribological repercussions reflect directly on country's gross national product (GNP). Hence, serious consideration has been given for friction and wear studies. The need for smooth operation, simple design and self-lubrication has led to the replacement of metals with polymers. These polymers having tribological advantage are often investigated under sliding condition. In rolling contact condition these materials are used in wide range of application from domestic products to heavy duty engineering components. However the tribological knowledge in this area is limited. This opens new avenues to perform friction and wear studies of polymers in rolling condition.

Initially, to understand the practical wear problems in rolling and their link with traditional tribological approach, three modes of study were performed. This includes (1) case studies from literature, (2) retrieval analysis of an engineering component and (3) performance based analysis through real-scale laboratory testing. All three modes of study exhibited a common wear scar "groove" which represents abrasion mechanism in rolling contacts. Nevertheless, the fundamental understanding of the grooving mechanism in rolling contacts are limited and scarcely reported. Therefore an extensive tribological study for partial sliding condition was formulated in this study.

Most tribological investigation in rolling contacts addresses the wear performance of polymers using a descriptive study through quantitative mass loss or dimensional change. However, based on the retrieval analysis and real scale testing, it is evident that the observable wear is only at an asperity level. This means the micron scale changes at asperity level can be better observed from worn surface topography and micrographs. Thus, the current research attempts to use quantitative micrography for wear characterisation. Since the quantitative micrography is rarely used in tribological investigations, the methodology and protocol is developed for the same in the current research. Moreover, there is lack of agreement in the used classification for terminologies such as wear scars, phenomena and wear mechanism which hinder the effective use of quantitative micrography. However this is resolved by introducing a new classification for polymer wear through a unique tribo-tree. The tribo-tree inter-relates the wear scars with the corresponding damage mechanism. This also provides possibility to trace back the damage mode from the observed wear scar. The benefit of the tribo-tree may not be instantly discerned however, on a long run this can act as a bridge between the engineers and scientists to deal with common wear problems.

In the current research, two different approaches are followed for wear investigation of polymer composite in partial sliding condition. A traditional tribological study (TTS) for global wear characteristic and damage evolution study (DES) for understanding particle generation. The partial sliding contact is implemented by means of twin disc model where a composite material (polyamide reinforced with 30% glass fibre) is tested against steel counterface material. In TTS, a traditional methodology with reference investigation prior testing is performed which is followed by wear testing and post-mortem analysis. However, in DES the test is paused at specific intervals to monitor the evolution of damage suffered by the polymer composite contact surface. In both methods, priority is given to the quantitative micrography for observing micron level changes on the worn surfaces.

Tests were performed in TTS for pure rolling (0% slip ratio) and partial sliding conditions (9%, 18% and 26% slip ratio). In the polymer composite, the pure rolling specimen was observed with micro-pitting, whereas partial sliding specimen revealed micro-channels or the so called "groove" to affirm the abrasion. Additionally, post-mortem analysis on the steel surface shows two kinds of transfer film: (1) uniformly spread thin primary transfer layer found for all four slip ratios. (2) a lumpy deposit of uneven material on the steel surface is the secondary layer found in the partial sliding condition. The acquired micrographs of composite contact surface from the post-mortem of different slip ratio are compared with mass loss data. In the partial sliding conditions, both mass loss and quantitative micrography (using segmentation by thresholing and grey-scale granulometry) showed similar tendency in the wear behaviour. Among all conditions, 9% partial sliding condition showed increased wear and the same is validated with quantitative micrography by estimating the abrasion marks from the segmented images. On the whole, the high wear rate is reflected from the larger coverage of grooves on the contact surface. In addition to the quantitative micrography and mass loss data of wear, survey of the experts opinion on surface scars was carried out. All three data showed similar trend for wear in partial sliding condition. It is also evident from the wear results that the topographic characteristics of the steel surface play a vital role. The consequence of slip ratio on wear is surpassed by the initial roughness characteristic (Rpk) of steel counter material.

The second is the damage evolution study (DES) which provides sequential data on the morphology of polymer composite contact surface at specific intervals of time. In DES, the newly developed technique called "relocation micrography" is used to locate the same region of interest for studying the development of surface morphology. The evolution of damage in polymer composite surface is clearly mapped and the wear in partial sliding condition is described in a two staged process: fracturing of asperities and plastic flow in the first stage followed by transfer layer formation in the second stage. Image processing technique using energy of the grey scale texture (GST) is effectively used to understand the sequential changes experienced by the composite material. The friction characteristic corresponds to the energy score of the image from composite micrographs. Likewise, the dynamic nature of the transfer layer on counter material is clearly observed from the sequential imaging of the same region.

The partial sliding condition produced unique scar representing the abrasion mechanism. It is evident from both approaches that, in wear analysis the micrograph

of the contact surface have to be dealt both globally and locally to characterize the surface change. The quantitative micrography stands effective in evaluating the wear of polymers in rolling contact. However, the used methodology in both approaches has shortcomings. The TTS does not provide the history of events causing wear, and DES has an unstable thermal condition due to the intermediate pauses. Thus an online vision system to monitor the images of contact surface was proposed.

In the field of tribology, online monitoring refers to the information acquired during a tribotest (real-time). Several attempts are made by researches to understand the wear process by adopting visual means for *in-situ* monitoring. Nevertheless, for the first time in polymer tribology *in-situ* vision system which can acquire online micrographs of contact surface at a frame rate of 35000 fps and 375 ns shutter time is developed. The developed opto-electronic Online Vision System (OVS) was used in rolling-sliding contacts to understand the intermediate mechanisms and reveal dynamic behavior of transfer layer. In the development of OVS the parameters (optical and camera) are optimized to acquire high speed micrographs.

Preliminary tests were performed on the newly developed online vision system. Periodical changes in wear mechanism are evident with resin back transfer, surface cracks and partial exposure of fibres. The self-healing mechanism of composites from the back transfer of resin is identified in the preliminary testing. Thus, the use of OVS indeed supports the hypothesis of dynamic nature of transfer layer. Moreover, the obtained micrographs are post processed and quantified for understanding the online wear trends using blur estimation. The above research has helped to understand the wear mechanisms in the rolling contacts of polymers using advanced microscopic techniques. Besides, the microscopic techniques are effectively used for wear characterisation. Collectively, the research has led to the development of advanced technique of online monitoring through computer vision and has introduced a quantitative micrography for wear analysis of polymers in rolling contacts. It was finally concluded that a combined approach with quantitative and qualitative analysis using OVS is essential for tribography. This approach also opens new avenue for the use of real time micrographs in future condition monitoring of machines and machine components.

# Samenvatting

*(Dutch summary)*

Problemen in verband met wrijving en slijtage weerspiegelen zich onmiddellijk in 's lands bruto nationaal product (BNP). Hun oplossingen moeten worden gevonden in aangepaste ontwerpen en materiaalkeuzen. Zo worden metalen steeds vaker vervangen door polymeren, o.a. omwille van hun droogloopeigenschappen en zelfsmerende werking. Vooraleer in bedrijf te worden genomen, worden deze polymeren doorgaans in laboratoriumomgeving aan wrijvings- en slijtagetesten onderworpen. Niet alleen voor zuivere glijcontacten doch ook voor rollende contacten worden polymeren gebruikt, zowel in de lichte machinebouw als in de zware machinebouw. Over rollende polymeercontacten is vandaag nog bitter weinig geweten, wat natuurlijk wel de mogelijkheid biedt om op dit gebied vernieuwende tribologische studies uit te voeren.

Beter begrip van de prestaties van polymeren in rollende contacten wordt vandaag meestal verworven door middel van praktijkervaring maar soms ook door schaalstudies die opgezet worden om technische problemen en oplossingen voor bepaalde cases te bestuderen. Concreet gesproken worden drie methoden van aanpak gevolgd: (1) gevalstudies uit literatuurgegevens, (2) gedetailleerde analyse van reële componenten en (3) laboratoriumproeven (meestal op schaal). Het microslip gedrag speelt in elk geval een belangrijke rol en het is belangrijk de bijbehorende mechanismen van wrijving en slijtage goed te begrijpen. Traditioneel gaat men hierbij erg beschrijvend te werk. Een kwantitatieve benadering beperkt zich meestal tot het meten van massaverlies veroorzaakt door slijtage en het navenant rangschikken van verschillende polymeermaterialen. In rollende contacten is dit omwille van de erg kleine slijtagemassa's vaak niet erg nauwkeurig noch zinvol. De observatie van de verandering van de oppervlaktetopografie door microslijtage is een betere benadering. Daarom werd in dit werk de nadruk gelegd op kwantitatieve micrografie, welke echter niet tot de standaard tribologische meettechnieken behoort. Een moeilijkheid bij het interpreteren van micrografie is het onvermijdelijk gelijktijdig optreden van diverse slijtagemechanismen met een mix van oppervlaktekarakteristieken in het slijtagespoor. Om hier enige klaarheid in te scheppen, hebben we in dit werk een triboboomstructuur ontwikkeld die het verband

legt tussen de topografische karakteristieken in het slijtagespoor en de verschillende slijtagemechanismen ten grondslag. Met deze structuur kan dus uitgaande van de waargenomen oppervlaktekarakteristieken een verband met de basis schade- en slijtagemechanismen worden gelegd. Is op dit ogenblik de triboboom nog een theoretisch concept, het is wel de bedoeling die op termijn te laten uitgroeien tot een handig instrument dat de brug slaat tussen het fundamentele onderzoek en de praktijkengineering.

In dit werk worden traditionele tribologische studies aangevuld met zogenaamde schadeevolutiestudies, zowel met het oog op de studie van materiaalverlies door slijtage als voor de observatie van het ontstaan van slijtagedeeltjes. Traditionele tribologische analyses bestaan uit slijtagetesten uitgevoerd volgens een voorgeschreven, vaak genormeerd, protocol gevolgd door een post-mortem analyse. In geavanceerde schadeevolutiestudies worden slijtagetesten op geregelde tijdstippen onderbroken om de evolutie van de schade die aan de contactoppervlakken (op microniveau) ontstaat nauwgezet op te volgen. Met de traditionele aanpak wordt vooral de globale slijtage bestudeerd, terwijl de moderne schadeevolutiestudies zich meer richten op het ontstaan van en het dynamisch gedrag van slijtagedebris.

Om een betrouwbare kwantitatieve micrografie te bekomen, moet men voldoende aandacht schenken aan de gebruikte techniek, het meetprotocol en de exacte locatie van de beeldopname op het testmonster. In deze thesis werden testen uitgevoerd bij 0% slip (zuiver rollen) en bij partiële slip (9%, 18% en 26% slip ratio). De beelden die van het slijtagespoor werden gemaakt , werden vergeleken met de beschrijvende gegevens en de kwantificering van het massaverlies door slijtage. Er werd onder andere vastgesteld dat bij 9% slip een maximum in de slijtagecurve wordt bereikt. Deze vaststelling werd ook bevestigd door kwantitatieve micrografie van de abrasiegroeven in het contactoppervlak. Er is met andere woorden een duidelijk verband tussen het aantal abrasiegroeven en de slijtagemassa. Beide metingen werden ook door een onafhankelijk expertpanel visueel gevalideerd.

Een tweede techniek in dit werk is de schadeevolutiestudie die de morfologische verandering van het oppervlak van het polymeer op specifieke tijdsintervallen opvolgt. Een relocatietechniek wordt gebruikt om elke beeldopname op precies dezelfde locatie op het testmonster uit te voeren. De veranderingen aan het oppervlak van het polymeer monster worden aldus in kaart gebracht. Twee slijtagemechanismen worden duidelijk onderscheiden: initiële slijtage wordt hoofdzakelijk gedomineerd door plastische vervorming en lokale breuk van de ruwheidstoppen. Later in het slijtageproces is de opbouw van een transfertlaag op het tegenoppervlak bepalend. Beeldverwerkingstechnieken worden toegepast om uit consecutieve beelden de topografische en morfologische wijzigingen beter te begrijpen. Zodoende kunnen deze beelden gebruikt worden als belangrijke variabele in slijtagedetectie- en analyse. Een nadeel van deze methode is evenwel dat de beeldopnametechniek vereist dat de tribologische test onderbroken wordt, wat op zichzelf het slijtageproces ook beïnvloedt. Daarom werd in deze thesis een online

observatietechniek voorgesteld, waarbij de tribotest ongehinderd kan doorlopen, dus zonder het tribologisch evenwicht te verstoren.

Deze onlinemonitoring techniek laat dus toe slijtage- en schadegegevens te verwerven tijdens de werking van een component of tijdens het uitvoeren van een tribotest. Deze informatie kan vervolgens worden gebruikt voor het karakteriseren van het wrijvings-en slijtagegedrag van de triboparen. Door verschillende onderzoekers werden pogingen ondernomen om door in situ (maar daarom niet online) visuele inspectie het slijtageproces van bepaalde componenten te begrijpen. In deze thesis is het echter de eerste keer dat voor de observatie van een component (in dit geval een polymeer rol) gebruik wordt gemaakt van online microfotografie (frame rate van 35.000 fps en 375 ns sluitertijd). Daartoe werd een optoelektronisch online visiesysteem ontwikkeld dat werd toegepast voor in situ waarnemingen van bewegende (rollende en slippende) oppervlakken in een twin-disk opstelling. De hoofdbedoeling bestond erin transfertlagen te observeren en hun invloed op wrijving en slijtage te begrijpen. O.a. werd het belang van de transfertlaag bevestigd zowel in positieve (beschermende werking) als negatieve (slijtageversterkend) zin.

Een aantal preliminaire testen werden uitgevoerd met het nieuw ontwikkelde online visiesysteem om specifiek de slijtage van een vezelversterkt polymeer te onderzoeken. Periodieke oppervlakteveranderingen door slijtage en de wijzigende slijtagemechanismen zijn duidelijk waarneembaar met o.a. readhesie van het polymeer, het ontstaan van oppervlaktescheuren, het gedeeltelijke bloot komen te liggen van vezels, etc. Onscherpteschattingen werden gebruikt om het slijtageproces kwalitatief te begrijpen. Tijdens deze testen kon ook de slijtagebeschermende werking van het gereadheerde polymeer worden bevestigd.

# Contents

**Appendices**

# Symbols
# and acronyms

## Symbols

| | | |
|---|---|---|
| $\alpha$ | Thermal expansion coefficient | x10$^{-6}$ °K$^{-1}$ |
| $c$ | Specific heat of the disc | J/kg.°K |
| D | Sliding distance | m |
| $E_i$ $(i = 1,2)$ | Young's modulus | GPa |
| e | Exposure time | Seconds |
| $\xi$ | Relative slip | m |
| $Ff$ | Friction force | N |
| $F$ | Applied normal load | N |
| $F^*$ | Excitation function | - |
| fps | Frames per second | - |
| HV | Vickers hardness | kg/mm$^2$ |
| $K$ | Thermal conductivity of the disc | W/m.°K |
| $l_m$ | Evaluation length | mm |
| $\mu$ | Coefficient of friction | - |
| M | Number of points in the profile | - |
| NP | Number of pixels spanning in the field of view | µm |
| $p$ | Contact pressure | MPa |
| $p_m$ | Mean Hertzian contact pressure | GPa |
| $p_{max}$ | Maximum Hertzian contact pressure | GPa |

| $R_a$ | Arithmetical mean roughness | μm |
|---|---|---|
| $R_{Ku}$ | Kurtosis | μm |
| $R_{sk}$ | Skewness | μm |
| $R_{pk}$ | Mean height of peaks | μm |
| $R_{vk}$ | Mean depth of valleys | μm |
| $R_{max}$ | Maximum height of the profile | μm |
| $T$ | Test temperature | °C |
| $T$ | Wear volume | mm³ |
| $s$ | Slip velocity | m/s |
| $υ$ | Part velocity | m/s |
| Δw | Weight changes | mg |
| $WR$ | Specific wear rate | mm³/N-m |
| $Δx$ | sampling distance in x direction | μm |
| $λ_c$ | Cut-off | mm |
| $ω$ | Rotational speed | rpm |
| $v_i \ (i = 1,2)$ | Poisson's ratio | - |
| $z(x_i)$ | Height co-ordinate | μm |

# Definitions and acronyms

| ASTM | American society for testing and materials |
|---|---|
| AISI | American iron and steel institute |
| Al2O3 | Aluminium oxide |
| Ag | Argentum |
| Au | Aurum |
| AFM | Atomic force microscopy |
| CCFM | Constant compliance force modulation |
| CCD | Charge coupled device |
| CMOS | Complementary metal–oxide–semiconductor |

| | |
|---|---|
| CF30 | Carbon fibre 30 % |
| CNT | Carbon nano tubes |
| Cu | Copper |
| DES | Damage evolution study |
| DSC | Differential scanning calorimetry |
| DIN | Deutsches institut für normung |
| EDX | Energy disperse X-ray spectrometer |
| FFM | Friction force microscope |
| FIB | Focus ion beam |
| FOV | Field of view |
| FZG | Forschungsstelle fur zahnrader und getriebebau |
| GST | Grey scale texture |
| GF30 | Glass fibre 30% |
| HDPE | High density polyethylene |
| IA | Image acquisition module |
| ISO | International organization for standardization |
| LDPE | Low density polyethylene |
| LIMS | Liquid-metal ion sources |
| LVDT | Linear variable differential transformer |
| LED | Light emitting diode |
| MS | Microscopic system module |
| MOS | Mean observer score |
| OM | Optical micrscopy |
| OVS | Online vision system |
| PA | Polyamide |
| PU | Polyurethane |
| PPS | Poly phenyl sulphide |
| PEEK | Polyetheretherketone |

| | |
|---|---|
| PET | Polyethylene terephthalate |
| PES | Polyethersulfone |
| PBT | Polybutylene terephthalate |
| PFM | Photonic force microscopy |
| PC | PolyCarbonate |
| PMMA | Poly (methyl methacrylate) |
| PSD | Power spectral density |
| POM-C | Polyoxymethylene homopolymer |
| POM-H | Polyoxymethylene co-polymer |
| PTFE | Polytetrafluoroethylene |
| PCM | Point contact microscope |
| RMS | Royal microscopical society |
| RWAT | Rotating wheel abrasion tester |
| ROI | Region of interest |
| SEM | Scanning electron microscopy |
| SCF | Short carbon fibres |
| SPM | Scanning probe microscope |
| STM | Scanning tunnelling microscope |
| SiC | Silicon carbide |
| SIMS | Secondary ion mass spectrometry |
| TFT | Thin film transistor |
| TiO$_2$ | Titanium oxide |
| TTS | Traditional tribological study |
| TMM | Tool makers microscope |
| TPU | Thermoplastic polyurethane |
| UHMW-PE | Ultra high molecular weight polyethylene |
| VZM | Video zoom microscope |

**Chapter 1**

# Polymers in rolling-sliding applications
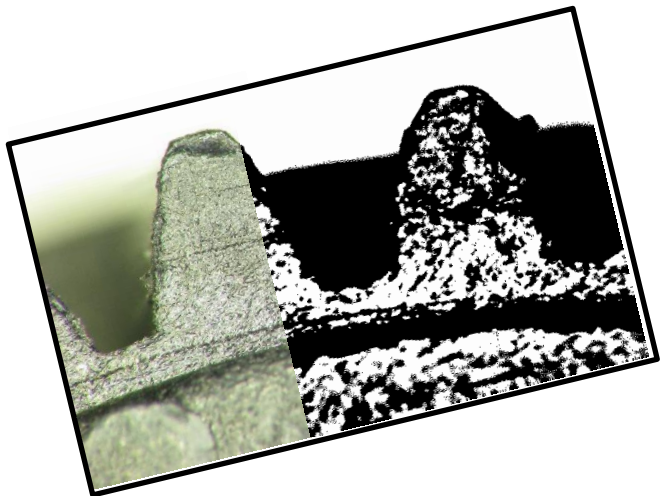
## Goal

This chapter is designed to establish a link between science and engineering by familiarizing practical examples, case studies and their relation with earlier scientific work on polymers in rolling contact. The underlying mechanisms for wear of polymers in rolling contact condition, and its applications are less explored. Though numerous applications from copy machine to heavy duty engineering subjects depend on rolling contact of polymers, more research were focussed on polymer sliding. Hence, the aim of this chapter is to elaborate the importance of polymers in rolling contact on practical issues. To understand the practical wear problems and their connection with traditional tribological approach, three modes of study were performed which includes (1) case studies from literature, (2) a retrieval analysis of an engineering component (3) and performance based analysis from real-scale laboratory test on an engineering component.

## 1.1 Polymers and their tribological implications

The influence of tribology on the economy of a country are reported since mid '60s [1.1]. Tribology repercussions on the scale of a country's gross national product (GNP) were reported for UK, USA, China and Germany [1.2, 3]. Especially in Belgium a country with automated and well developed industrial society will have positive influence of about 1.1 – 1.3 % of the GNP from a correct tribological practise. This has led to keen focus on tribological research for efficient design and engineering practice. Based on tribological considerations, the need for simple design, dry running, extended service life and smooth operation has led to an extensive replacement of metals with polymers in different applications. Freedom in altering material properties by using fillers and additives provides a new prospect for polymers in tribological studies [1.4-6].

The polymers had their start from the Mayan periods where the natural rubbers have been used as a play tool. However, the credit goes to Leo Hendrik Bakeland for introducing the modern synthetic polymer (Bakelite). The tribological market for polymers has gained its importance during WWII, where the phenolic resins are used as bearing material [1.7]. However, the advancements in polymer science has eventually replaced the phenolic resins with engineering polymers. Thermoplastic polymers are divided into various subgroups according to their application range: for example, utility polymers, engineering polymers and high performance polymers. Even though a huge variety of thermoplastics are available in the market only high performance polymers and a few engineering polymers are considered for the tribological applications [1.8, 9]. Engineering polymers are mostly used when low friction is a primary requirement. The commonly used engineering polymers are Polyamide (PA), Polyoxymethylene (POM), Polytetrafluoroethylene (PTFE) and Polyethylene terephthalate (PET). These polymers are often tested for their tribological properties using traditional standards (ASTM G132, G65, G99-95a) with pin-on-disc or block on ring configuration. These standards represents pure sliding conditions nevertheless, polymers are also used in pure rolling and partial sliding components such as cam, gears, rollers and bearings [1.8, 10-16]. The existing

standards for tribological investigation do not accommodate the testing of polymers in rolling contact and partial sliding condition. Moreover, in rolling contacts of polymer, wear characterisation is uncertain due to the poor compliance of the rolling components with the wear monitoring techniques in terms of dimensional tolerances and scaling effects. Besides, in-lab investigations are mostly at accelerated conditions may introduce synergetic effects from temperature increase and its corresponding material response. For these reasons the rolling and partial sliding contacts has been scarcely investigated which opens prospects for wear studies in this area.

## 1.2 Polymers in pure rolling and partial sliding contacts

Polymers are frequently used in the domestic and engineering applications particularly in rolling contacts [1.17, 18]. An advantage of rolling contacts over pure sliding is the reduced rigorous mechanical interaction at asperity level between the contacting bodies. Hence, rolling is a preferential contact condition in components with relative movements. Moreover, the polymers in rolling contact have a relatively less resistance to motion on comparing with partial sliding or full sliding contacts. In contrast, partial sliding (rolling-sliding) is sometimes involuntarily introduced by means of misalignment, poor dimensional fits and foreign particles entrapment. The partial sliding in a rolling contact is estimated in terms of slip ratio from relative sliding. Even though relative sliding of rolling contacts is experienced in diverse applications, very limited research has been performed to understand its influence [1.14, 1.19-1.30]. Table 1-1 lists the application regime of polymers and the related fundamental studies. Polymers with rolling-sliding contacts are used based on three main tribological advantages: (1) dry running capability, (2) adaptability in aggressive environmental condition, (3) bio-compatibility. Even though polymers could be used in wet or water lubricated conditions, majority of applications are performed in dry running.

Table 1-1 Three major areas for polymers in pure rolling and partial sliding condition

| Condition | Requirements | Application |
|---|---|---|
| Dry operations | Simple design, service life and low friction and wear | Bearings, gears, etc. [1.20, 21, 26] |
| Transportation and aggressive environment | Precise frictional characteristics and vibration suppressor | Automatic shelf, positioning roller, elevator rollers, conveyors [1.17, 31] |
| Low debris formation | Clean environment, slow speed and bio-compatibility are critical. | Prosthesis [1.32], rollers in food industry and transportation rolls [1.18] |

Table 1-2 clearly shows the slow progress in tribological research made in pure rolling and partial sliding contacts of polymers. It is evident that in most cases of polymer rolling, the material loss due to wear is estimated in terms of mass loss. Attempts to use advanced wear monitoring techniques at asperity level are scarcely reported for

polymer in rolling contacts. However, the existing studies provides knowledge on the usage of specific model and operational range such as speed and slip ratio (relative sliding). In regards to the operational speed and slip ratio a range between 0.1 – 3.14 m/s and 0 - 30% is used respectively. Table 1-2 also highlights the real engineering problem [1.18] (transportation rolls in cold rolling mill) and application (bearing) investigated [1.20] in real scale. This partly shows the limited connection between real scale problems and the fundamental testing in rolling-sliding contacts of polymers.

Table 1-2 Existing studies on pure rolling and partial sliding contacts of polymers

| Author | Contact kinematic | Tribo-pairs | Velocity |
|---|---|---|---|
| Avanzini *et al* [1.19] | #Twin-disc | PEEK - Steel | 500 rpm (0.7m/s) |
| Avanzini *et al* [1.19] | #Twin-disc | PEEK/GF30/CF30/ PTFE - Steel | 800 rpm (1.25 m/s) |
| Koike *et al* [1.14] | *Real scale test | PEEK-Alumina | 172 N , 1200 rpm (2.13 m/s) |
| Ren *et al* [1.18] | *Cold rolling | PA6 roller - Steel | |
| Chen *et al* [1.22] | #Twin-disc (28% Slip) | PA 66-PA66 | 200 N, 1000 rpm (1.5 m/s) |
| Apichartpattanasiri *et al* [1.33] | Twin-disc | Nylon 66 - Nylon 66 | 200 N, 1000 rpm |
| Charles *et al* [1.21] | #Twin-disc | Nylon 6 nano composite - Nylon 6 | 225 N, 2000 rpm (3.14 m/s) |
| Gordon *et al* [1.30] | #Twin-disc (2% slip) | PA46-PA46 | 400 N, 1000 rpm (1.5 m/s) |
| Gordon *et al* [1.30] | #Twin-disc (2% slip) | PA46+12% aramid fibers-PA46 composite | 600 N, 1000 rpm (1.5 m/s) |
| Harrass *et al* [1.23] | Ball on plate | PA6, POM, PEEK - steel | 100N, 1 m/s |
| Hooke *et al* [1.25] | #Twin-disc (6% slip) | POM-POM | 200 N, 1000 rpm |
| Francisco *et al* [1.34] | Twin-disc | Epoxy – stainless steel | 600 N, 500 rpm (1.04 m/s) |
| Hooke *et al* [1.24] | #Twin-disc (Slip 20%) | GF/PA66-GF/PA66 | 300 N, 1000 rpm (1.5 m/s) |
| Kukureka *et al* [1.26] | #Twin-disc (Slip 4%) | POM-POM | 600 N, 1500 rpm (2.3 m/s) |
| Lawrence *et al* [1.28] | #Four ball machine | PA66, POM-Steel | 154 N, 400 rpm (0.1 m/s) |

*Real application testing at laboratory scale, #Mass loss

# 1.3 Importance of polymers in rolling-sliding applications

In polymer rolling, the occurrence of partial slip is unavoidable a.o. due to local (elastic) deformation, surface damage and misalignment of components. As a consequence, erroneous operation is experienced which is common in applications such as rolling doors, conveyors, transportation rolls, bearings and many others [1.18, 20, 31]. Apart from partial sliding, polymers as a material have other limitations such as poor load carrying capabilities, ageing characteristics and thermal softening behaviour [1.35]. Furthermore, the poor thermal conductivity could cause melting of polymers from the accumulation of heat in tribological contact. All these limitations may significantly affect the material removal rate considering the progressive damage caused by wear.

It has earlier been suggested that an effective use of material in real application can be achieved by understanding wear behaviour at real contact configuration [1.36], which should be true for polymers as well. Thus, in this chapter we have also considered the wear of real engineering component. Considering real engineering applications, the degree of wear or the intensity of wear is a subjective factor which depends upon the selected application. For example, the scale of wear for polymer in a contaminated environment (for example conveyor rollers) will be several fold higher than the precision components (polymer ball bearing). Nevertheless, this subjective factor is generalized in the laboratory scale based on the so called traditional "wear rate". The wear rate has its own definition by different authors, but the commonly used definition relates to service life (sliding distance, number of cycles) and the material properties. Having a relatively minor share of sliding from the view point of contact kinematics, the expressed dominant mechanisms are deformation of asperities dominated by rolling and partly by abrasion. Thus, with mechanisms such as local plastic deformation through low stress abrasion (partial sliding) and plastic flow without material removal does not yield significant material loss to use the stereometric analysis. However these mechanisms might be well reflected in the topographic values. Thus, the wear is merely a damage at surface level which can be effectively indicated by topographic features and surface scars for characterisation.

In wear characterisation three basic modes of testing are generally adopted (1) model testing, (2) laboratory scale testing and (3) real scale testing. It is noteworthy that all three modes use visual inspection of surface scars for validating the wear, which is partly subjective. In our case, for rolling-sliding conditions the primary techniques used to measure the wear are mass loss, stereometric analysis and partly by topographic characterisation. To elaborate the disadvantage of measuring wear through linear displacement, it is important to mention the dimensional scale of the specimen and its wear values. Most of the existing research from literature on rolling-sliding of polymers has sample sizes in millimetres (30 mm) and their measured wear is in few microns (50 - 500 µm). Besides, scars such as crater, groove or pit with a depth profile more than 50 µm can produce a significant material loss which is not accounted in the wear measurement through linear displacement. However, the mass loss would consider the material loss from the individual craters and pits but it has other influences from the mechanism itself. A typical tribological characteristic of

polymer is the transfer layer on the counter material and back transfer of these layers to the parent material. This creates a dynamic state for which the stereometric value or the mass loss from post-mortem analysis may provide partly incorrect information on wear. Based on the transfer layer characteristics, the formed transfer film is still a part of the tribo system to consider its quantity as wear. Besides, it is evident from literature that the mass loss is in few milligrams, which might be contributed by the transfer layer. Also, topographic measurements are very local in nature and provides more information on the surface condition than wear. Since the contour profiling or depth profiling technique also considers only a relatively small area for investigation a high scatter can be expected in the quantitative wear.

The objective of this chapter is also to understand how close lab experiments simulate the real situation in terms of worn surface of the polymer in rolling-sliding contacts. Thus, an approach consisting of three different modes of wear investigation were used to elucidate the representativeness between each other.

(1) Desktop research: Case studies and fundamental work reported in literature
(2) Retrieval analysis of a practical case: Rollers in a sliding door
(3) Laboratory scale test on polymer rollers.

The first approach consists of extensive survey of literature and case studies. However, to understand the closeness of literature with real applications, experimental work by means of retrieval analysis and laboratory test was made (second and third approach). To understand the wear mechanism from the view point of morphological changes 3D profilometry and micrographic inspections were carried out.

## 1.4 Literature case studies

Among different wear studies present in the literature we considered two extreme applications (domestic and heavy duty engineering) to cover a wide range. Starting with the heavy duty engineering application, Ren *et al* made an elaborate study on the wear mechanisms observed in PA roller which is used as a transportation roller in cold rolling process [1.18]. In this, misalignment of roller is explained from the surface scars which also act as an indicator of wear mechanism. The worn surface morphology of roller has revealed information on flow direction of the debris which provides evidence for misalignment. The observed thin film on the rollers was reported as a consequence of melting and plastic flow. It was revealed that side slipping (partial sliding) causes formation of foam like substance on the contact surface. However, generally these foam or thin layer of substance can be a protective layer for enhancing the wear resistance of material. Having a large difference in hardness between polymer and the metal provides high chance of particle generation for transfer layer formation. This may rise question on the choice of suitable tribo-pair (polymer (PA) /metal). In this regard, Olsson concluded that among different combination of tribo-pairs in rolling-sliding condition polymer-metal pairs produces beneficial frictional characteristics provided smooth surface of the counter material [1.17]. In regards to the material for specific applications Polyetheretherketone (PEEK) and polyurethane (PU) are investigated for use in industrial cams [1.35].

In domestic applications, rolling-sliding contact is manifested in many components. A good example of combined rolling-sliding contact is gears where pure rolling contact occurs at the pitch point and partial sliding at flank. Extensive research exists for plastic gears focusing on the global wear as a parameter for performance based design. However, in case of gears, complex mechanisms can be expected due to the combination of partial sliding and dynamic loading condition. In most research, real gears are tested at laboratory scale [1.11, 37, 38], where different kinds of surface defects such as crack formation, tearing of gear flank, pitting and spalling are reported. Wear testing of acetal gear by Mao *et al* clearly displays the two regions of wear which corresponds to pure rolling and partial sliding condition. The SEM image of the gear (Figure 1-1) clearly shows protrusion (indicated by arrow) due to relatively less wear at the pitch point which in-turn is due to pure rolling. However, the region close to the root and tip of the flank shows a severe material removal from partial sliding condition.

In rolling contacts of polymer it is evident that the parametric investigations uses cracks and surface defects as validation tools. The ultimate failure of the specimen is evaluated from the surface damage (sometimes irrespective to the number of cycles). Such methodologies of using surface morphologies are frequently followed by engineers in deciding the reliability of component. This clearly indicates that the surface scars could act as a potential wear indicator in rolling-sliding conditions. Finally, the literature survey for polymer in rolling-sliding applications it is clear that phenomena such as pitting, surface cracks, plastic flow and abrasion for indicating the severity of wear.
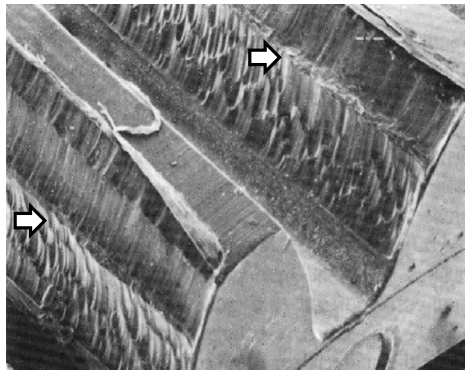


Figure 1-1 Scanning electron micrograph of acetal gear tooth [1.11].

## 1.5 Retrieval analysis of worn out roller

The retrieval analysis is aimed at understanding the link between the literature and its representativeness to applications. From literature, it was understood that plastic flow, micro-pits and cracks are the common mechanisms for polymers in rolling contact [1.30]. To observe the global presence of these mechanisms in real components, a retrieval analysis was performed on real engineering component. A common tribological problem related to both domestic and engineering application

is chosen for retrieval analysis. From automatic parking to elevator doors, steel rollers have been replaced with polymer rollers for their capability to be used in dry running and noise free operations. However, these rollers have to be replaced frequently due to the poor friction characteristics, wear and failure owing to plastic deformation. During replacement of these rollers, the elevator doors need to be completely dismounted for replacing the rollers, which is rather time consuming and cumbersome. Even though the direct cost of the rollers is relatively low, it is expensive considering the installation cost and the indirect costs such as down time and discomfort for the users. For investigation purpose a worn rollers from a sliding door of an elevator (Golden elevators, Chennai, India) was chosen. The rollers were removed due to poor functionality from noisy operation and poor friction at opening and closing cycles. Onsite visual inspection of rollers and the vibration exerted on the doors are the main source for validation. Figure 1-2 shows the roller contact surface and the schematics of the arrangement. The rollers are accommodated in the elevator shaft and it is evident that these rollers operate in a dusty environment and are poorly accessible for frequent maintenance. Polymer rollers are in contact over structural steel surface.
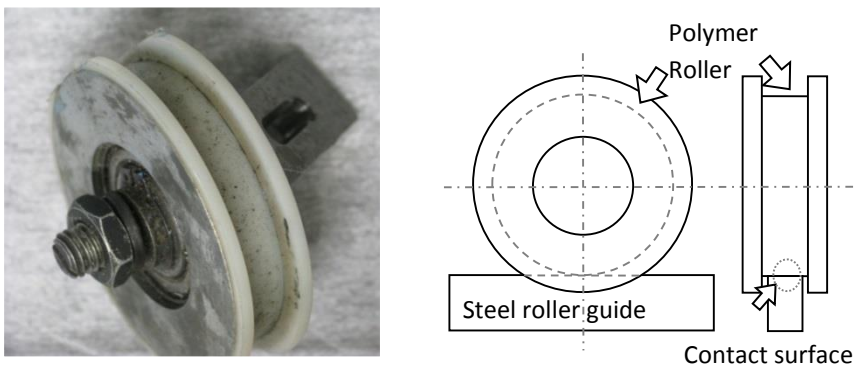


Figure 1-2 Retrieved polymer roller and its mounting schematic.

In wear evaluation, the human eye is still one of the most reliable observation tools because of its high performance metadata-acquisition and processing system. The rollers have experienced severe damage from pitting as seen in Figure 1-2. Inspection on the 3D profile (see Figure 1-3) clearly indicates micro pits of diameter between 50 – 100 µm and large craters on the surfaces with diameter ranging between 500 µm – 2000 µm. Similar surface morphology with micro-pits on the polymer surface was earlier reported from a twin-disc testing by Gordon *et al* [1.30]. Considering the distribution of these surface scars, micro-pits are dominant feature in the retrieved roller. Also abrasion as a consequence of partial sliding is observed in the topography (indicated with arrow) Figure 1-3 (a) and (b). Although these wear scars such as craters, micro-pits and abrasion grooves occupy a significant area in the contact surface, their quantitative characteristics are seldom considered for tribological characterisation at the laboratory scale.

During the post-mortem, particles were collected from the contact surface. Moreover, the micrographs also shows evidences of entrapped particles in the pits

are clearly seen in Figure 1-3 (indicated by arrow). This is common for rolling components operating in contaminated environment, where the third bodies interferes the surface interaction. It can be assumed that these third bodies can act as an asperity in generating audible noise during its contact with steel counter face material. A detailed inspection report of the retrieved roller is provided in appendix A. Stereometric wear analysis in this case is impractical considering the required reference before mounting the rollers. However based on the tolerances there is almost no global wear. The retrieval analysis concludes that the mechanisms (micro-pits, craters and abrasion) experienced in literature are partly observed in the polymer rollers.
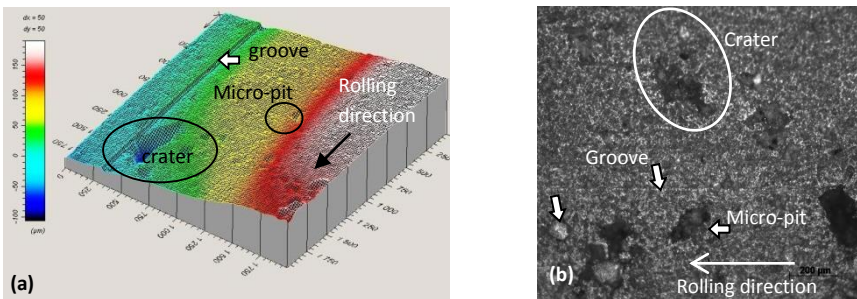


Figure 1-3 shows the contact surface of roller (a) 3D profile (b) micrograph.

## 1.6 Laboratory scale testing of an engineering component

In the laboratory scale testing "roller conveyor chain" was chosen for its industrial relevance and their use in contaminated environment. Roller conveyors are generally used in mass production as a transportation tool. A typical example of the roller conveyor chain and its arrangement is shown in Figure 1-4. The rollers are selected based on the requirements such as load, operating environment and the product to be transported. For high loads, steel is used as a load carrying component however, in food and pharmaceutical industry high load is not a pre-requisite. Formation of debris and it wear behaviour is critical in these applications, therefore, polymer rollers are used in these application areas. To understand the material behaviour under controlled condition a polymer roller conveyor test rig is used to perform wear test of conveyor rollers. Details and specification of the test rig is given elsewhere [1.31]. In the laboratory testing acetal (POM-H) roller is tested against steel counterface material.
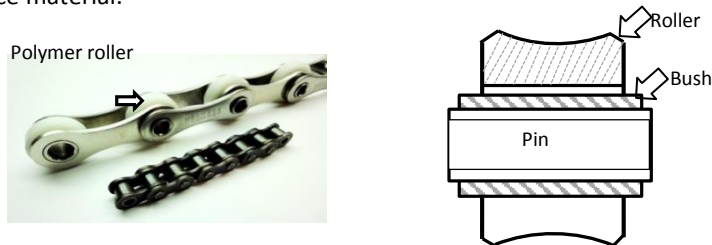


Figure 1-4 Roller conveyor chain and its arrangement.

The contact condition is described in the schematic (Figure 1-5) where a polymer roller comes in contact with the steel counterface material. A detailed test report on the wear analysis of conveyor rollers is provided in appendix B. As a part of wear analysis, the surface morphology of worn rollers are investigated by means of reflected light bright field microscopy and stylus profilometry. The conveyor rollers used in our case have a specific "parabolic" profile in the contact surface as shown in Figure 1-5. Wear measurements are done by tracing the profile to understand the change in depth before and after testing. A schematic of the contact condition and the observed change as a consequence of wear is shown in Figure 1-5. The conveyor chain has 50 rollers out of which 8 were considered for investigation. The average of five measurements for each roller at 5 locations (0°, 72°, 144°, 216°, and 288°) was made to understand the change in surface roughness.
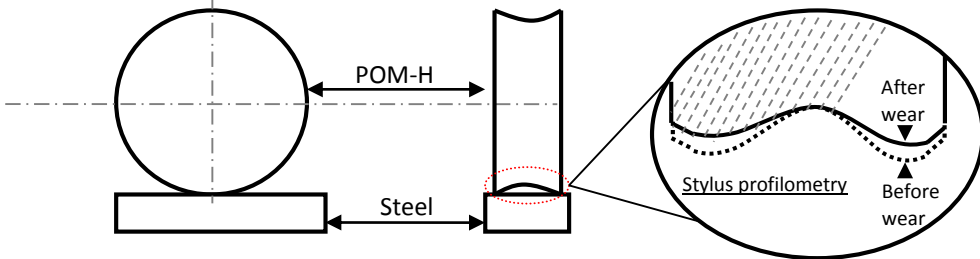


Figure 1-5 Shows the contact schematics and wear changes.

The scars due to wear of polymers are also observed by visual inspection. The contact surface of the steel counterface was partially covered with a transfer layer. From Figure 1-6 (a), the dimensional change of polymer roller due to wear can be clearly seen from the profile. However, this could also be partly attributed to plastic deformation of polymer rollers. The average measured roughness Ra of the untested polymer roller ranged between 1.8 – 3.5 µm. Nonetheless, on wear testing, smoothening of roller surface is evident from the reduction in roughness to 0.7 – 1.4 µm. The removal of roughness peaks from the wear of polymer roller is clearly seen from the traced profile (Figure 1-6 (a) indicated with arrow). Analysis of the topography of the counter surface shows that there is an increase in roughness from 0.17 µm to 0.24 µm. The increase in roughness should be attributed to the deposition of third body (transfer layer, see Figure 1-6 b). The width of surface scar (7 mm) from the steel counter material clearly indicates a full contact is established between the counter face and the polymer which has a roller width of 7mm.

In regards to the surface morphology of polymer rollers, micro scratches were present even before the wear testing which may be due to material handling (Figure 1-7 a). Additionally, dimple like features on the unworn surface can be attributed to the manufacturing defects of rollers. In the microscopic inspection of the worn polymer, lateral cracks perpendicular to the rolling direction are visible in Figure 1-7 (b). Similar feature was observed in a model testing of polymers in a twin disc test rig [1.30]. The groove or the scratch pattern in the polymer surface can be attributed to the partial sliding of rollers. The partial sliding was identified by acquiring a video of the contacts during the test using an endoscope camera. It is also to be noted that with debris formation the polymers cannot be used for conveyors in food or

pharmaceutical industry. On comparing the observed micrographs from the test results and existing literature, similar morphologies were observed by Gordon *et al* [1.1] and Avanzini *et al* [1.19] where it was described as severe wear condition.
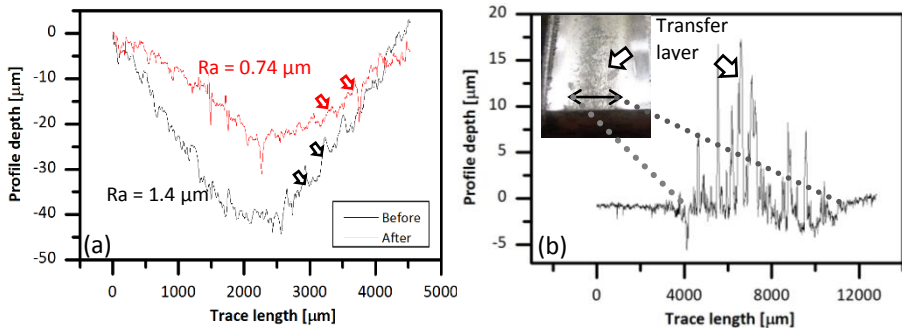


Figure 1-6 Topography of (a) roller (b) counter material after wear testing.
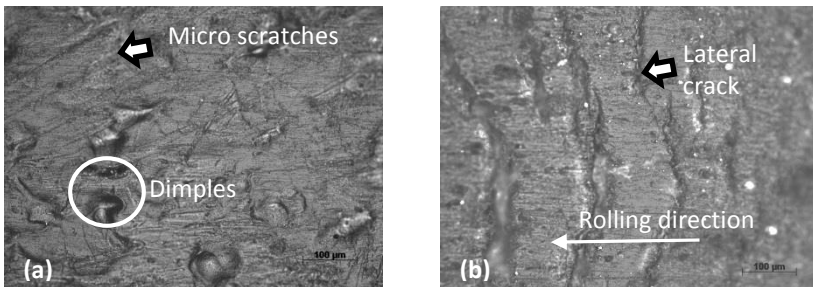


Figure 1-7 Micrograph of polymer roller (a) before testing (b) after testing.
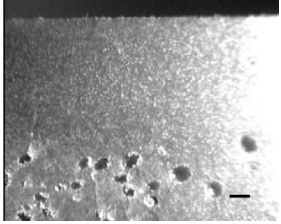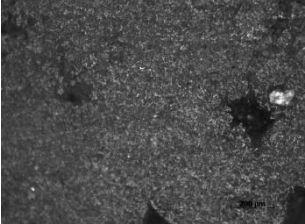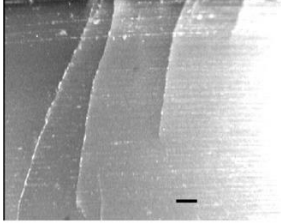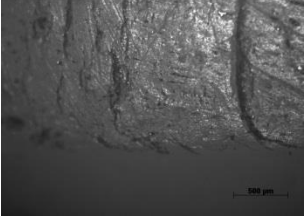
## 1.7 Comparative study on literature, component retrieval and lab testing

It is evident from the literature, retrieval study and lab testing that polymer wear in rolling contacts is rather at an asperity level and also limited within few microns. It is further clear from Table 1-3 that the mechanisms observed in lab-scale (cracks and pits) are partly observed in real engineering components. However, a connection has to be established between the application and laboratory scale testing.

Moreover, the ignored facts in rolling contacts of polymers are the nature of transfer layer and its consequences on the wear process. Transfer layer which is often discussed as an influencing member in polymer sliding has not been given equal importance in rolling contacts. Assuming that the transfer layer is fully formed during the running-in process, the nature of contact changes from polymer-metal to a polymer-polymer contact. This might influence the transition of wear from severe to a mild wear due to the reduction in asperity interaction between hard steel material and polymers. Both the transfer layer characteristic and surface scars due to progressive surface damage acts as indicators of the wear process. If these surface scars are repetitive in nature from the lab scale testing, they can be effectively used for wear characterisation. However a methodology is to be followed in studying the surface scars for rolling contacts of polymers. On comparing with literature, the

retrieval analysis and lab-testing explicitly express similar wear surface characteristics (see Table 1-3).

Table 1-3 Comparison of wear mechanisms between literature and real-scale testing

| Literature | Experimental | Wear mechanism |
|---|---|---|
|  Twin-disc testing PA 46: Gordon *et al* [1.30] 400 N Load 1000 rpm |  Retrieval analysis Elevator roller ≈60 rpm | Micro pits Third particles |
|  Twin-disc testing PA 46/6% aramid, Gordon *et al* [1.30] 400 N Load 1000 rpm |  Real scale lab test With roller conveyor, 60 -70 rpm | Lateral cracks |

Failure mechanisms commonly described in literature are crack formation and pitting. These mechanisms are also observed in engineering components at this stage of work. It is our assumption that the involvement of partial sliding results in abrasive wear scars representing abrasion. Such characteristics are not confirmed in the discussed literature. A reason could be the local plastic deformation incurred by deformation of rolling supersedes the abrasion grooves. It is evident from both the retrieval analysis and conveyor testing that the grooves pattern is formed as a consequence of partial sliding (Figure 1-8). The abrasion marks support the hypothesis of increased material removal and formation of transfer layer. In order to completely relate the nature of contact used in laboratory testing close to reality, the morphological and topographic characteristics of both polymer and its counter material are to be included for wear characterisation.

With prior knowledge that polymer wear in rolling condition occurs at asperity level, conventional stereometric analysis is not fully sufficient for tribological characterization. From literature, it is concluded that visual inspection and microscopic observations are used as a validation tool. Most authors have reported wear mechanisms from the observed wear scars qualitatively. However, the severity of wear is quantitatively understood from stereometric analysis and is non-uniform on considering different scar types (grooves, pits and transfer layer). In traditional practise, the wear scar characteristics are studied locally and on relatively narrow region of interest. However, to understand the global presence, wear characterization based on quantitative microscopy with sufficient coverage of contact surface would be more appropriate. Altogether the investigation recommends for a quantitative connection between the wear scars and traditional wear parameters (mass loss and dimensional loss). Additionally the topographic characteristics can be used as a validation tool.

In engineering practice straight forward information on contact surface damage is obtained from worn surface morphology (micrographs). Observed details on wear mechanisms and the wear mode provide valuable information on the component's condition and necessary corrective measures. As a start, quantitative micrography for wear studies could be an initial validation tool to bridge the science and engineering by complementing each other for tribological solutions.
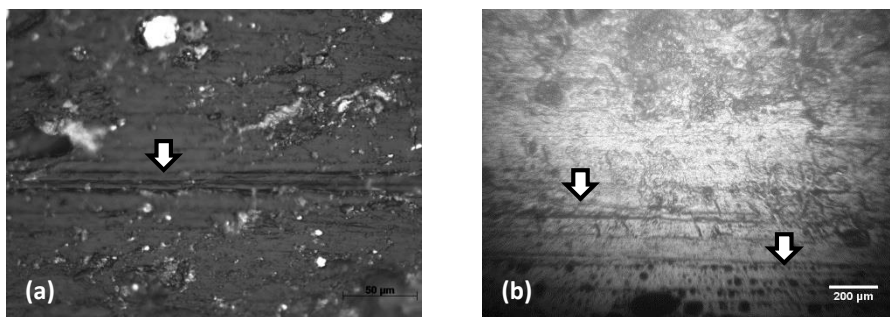


Figure 1-8 Abrasion grooves as a consequence of partial sliding (a) conveyor roller (laboratory test specimen) (b) elevator roller (retrieval specimen).

## 1.8 Summary and scope of the thesis

From the above discussion it is evident that the rolling-sliding of polymers has received less attention regarding the partial sliding characteristics. The basic mechanism governing the wear behaviour and friction response from partial sliding is less understood: especially, the particle generation process and the transfer layer characteristics. This is due to the complex contact condition from the combination of rolling and sliding motion. Besides, the currently used techniques for wear quantification are not fully reliable. Advancements in this area of research to improve measuring techniques and methodologies for polymers in rolling-sliding contacts would be highly beneficial to the scientific community.

The observation from the retrieval analysis elucidate grooves from partial sliding condition. Such mechanism is not earlier reported in the literature for which a better understanding about the wear process is necessary. Moreover, the lab-testing also confirms partial sliding of real component from the view point of wear scar observations. From the comparative study it is evident that quantitative microscopy techniques can serve as a better source for wear characterisation for polymer in rolling-sliding contacts.

The goal of the current research can be listed out as:

- Identifying the contributing mechanism governing the wear process and its tribological performance for polymers in rolling-sliding contacts.
- The wear scar observations are made at a random location in the traditional practise. Since both sliding and rolling creates different wear scar, a local effect with different kinds of mechanism is bound to occur. Thus, a methodology is to be developed to have reference of the investigated area for comparison purpose.
- Understand the evolution of wear process in the progressive damage condition.
- Better understanding of the mechanism and the particle generation process requires observation of wear scar during the wear process. This could be accomplished by introducing a high speed imaging of wear scars which is been developed in the current research.

The research goals will be individually address by separate chapters. In chapter 2, a clear understanding of available wear mechanisms and the corresponding surface scars in polymer tribology will be described. In addition the various state of art techniques used in tribography will also be discussed in detail. Chapter 3 is a guideline for the testing procedures. The methods, material and test protocols are clearly described for the two different approaches traditional tribological study (TTS) and Damage evolution study (DES).

Chapter 4 is the experimental study to understand the influence of roll-slip phenomena. The effect of partial sliding and the transfer layer characteristics are studied in detail. A traditional approach with post-mortem analysis is used for topographic and morphological inspection. However, this chapter takes advantage of the quantitative micrography using image processing techniques for wear characterisation. Chapter 5 is designed to understand the limitations of TTS and reveal the damage mechanism involved in the wear process. This will be accomplished by means of experimental investigations using DES. The intermediate mechanism and the evolution of surface morphology in both polymer and steel surface are better studied using DES.

Chapter 6 is dedicated to the design and development of a novel online vision system. In this chapter the design of a high speed-online vision system is described in detail. Optical, camera and illumination parameters are optimised for an effective use of OVS. Tests were performed for identifying the capability of the newly developed OVS. Besides, a sample material was investigated to reveal the benefits of the newly developed OVS. Chapter 7 summarises and provides the overall conclusion from the thesis. It also describes the potential of the newly developed OVS for future work.

# References

[1.1] B. Flitney, "Bob's bit," Sealing Technology, vol. 2009, pp. 3, 2009.

[1.2] S. Zhang, "Current Industrial Activities of Tribology in China," in Advanced Tribology, J. Luo, Y. Meng, T. Shao, and Q. Zhao, ed: Springer, pp. 3-3, 2010.

[1.3] I. Tzanakis, M. Hadfield, B. Thomas, S. M. Noya, I. Henshaw, and S. Austen, "Future perspectives on sustainable tribology," Renewable and Sustainable Energy Reviews, vol. 16, pp. 4126-4140, 2012.

[1.4] V. K. Srivastava and J. P. Pathak, "Friction and wear properties of bushing bearing of graphite filled short glass fibre composites in dry sliding," Wear, vol. 197, pp. 145-150, 1996.

[1.5] K. Friedrich and A. K. Schlarb, Tribology of polymeric nanocomposites: friction and wear of bulk materials and coatings, Tribology and interface engineering series, vol. 55 , 2011.

[1.6] W. G. Sawyer, K. D. Freudenberg, P. Bhimaraj, and L. S. Schadler, "A study on the friction and wear behavior of PTFE filled with alumina nanoparticles," Wear, vol. 254, pp. 573-580, 2003.

[1.7] A. B. Strong, "History of Composite Materials," ed: July, 2002.

[1.8] G. Kalácska, "Abrasive wear of polymer/steel gear drives," Progress in Agricultural Engineering Sciences, vol. 4, pp. 1-26, 2008.

[1.9] G. Kalácska, "An engineering approach to dry friction behaviour of numerous engineering plastics with respect to the mechanical properties," Express Polymer Letters, vol. 7, pp. 199-210, 2013.

[1.10] H. Düzcükoğlu, "Study on development of polyamide gears for improvement of load-carrying capacity," Tribology International, vol. 42, pp. 1146-1153, 2009.

[1.11] K. Mao, W. Li, C. J. Hooke, and D. Walton, "Friction and wear behaviour of acetal and nylon gears," Wear, vol. 267, pp. 639-645, 2009.

[1.12] S. Senthilvelan and R. Gnanamoorthy, "Effect of gear tooth fillet radius on the performance of injection molded Nylon 6/6 gears," Materials & Design, vol. 27, pp. 632-639, 2006.

[1.13] C. H. Chue and H. H. Chung, "Pitting formation under rolling contact," Theoretical and Applied Fracture Mechanics, vol. 34, pp. 1-9, 2000.

[1.14] H. Koike, K. Kida, E. C. Santos, J. Rozwadowska, Y. Kashima, and K. Kanemasu, "Self-lubrication of PEEK polymer bearings in rolling contact fatigue under radial loads," Tribology International, vol. 49, pp. 30-38, 2012.

[1.15] T. McGloughlin and A. Kavanagh, "The influence of slip ratios in contemporary TKR on the wear of ultra-high molecular weight polyethylene (UHMWPE): An experimental view," Journal of Biomechanics, vol. 31, Supplement 1, p. 8, 1998.

[1.16] D. Scott and G. H. Mills, "A scanning electron microscope study of fracture phenomena associated with rolling contact surface fatigue failure," Wear, vol. 16, pp. 234-237, 1970.

[1.17] M. Olsson, "Tribological evaluation of some potential tribo materials used in column lift rolling contacts—A case study," Wear, vol. 270, pp. 720-724, 2011.

[1.18] C. Ren, J. Chen, H. Pan, X. Huang, and H. Zhu, "Wear mechanism of PA6 roller used in cold rolling process," Engineering Failure Analysis, vol. 28, pp. 311-317, 2013.

[1.19] A. Avanzini, G. Donzella, A. Mazzù, and C. Petrogalli, "Wear and rolling contact fatigue of PEEK and PEEK composites," Tribology International, vol. 57, pp. 22-30, 2013.

[1.20] A. F. Beke, R. S. Dwyer-Joyce, F. R. Jones, and J. Gregory, "Wear testing of acetal for the prediction of polymer rolling bearing durability," Tribology Series. vol. Vol. 41, , pp. 175-182, 2003.

[1.21] D. F. Charles, R. Gnanamoorthy, and P. Ravindran, "Rolling contact fatigue behavior of polyamide clay reinforced nanocomposite—Effect of load and speed," Wear, vol. 269, pp. 565-571, 2010.

[1.22] Y. K. Chen, S. N. Kukureka, C. J. Hooke, and M. Rao, "Surface topography and wear mechanisms in polyamide 66 and its composites," Journal of Materials Science, vol. 35, pp. 1269-1281, 2000.

[1.23] M. Harrass, K. Friedrich, and A. A. Almajid, "Tribological behavior of selected engineering polymers under rolling contact," Tribology International, vol. 43, pp. 635-646, 2010.

[1.24] C. J. Hooke, S. N. Kukureka, P. Liao, M. Rao, and Y. K. Chen, "Wear and friction of nylon-glass fibre composites in non-conformal contact under combined rolling and sliding," Wear, vol. 197, pp. 115-122, 1996.

[1.25] C. J. Hooke, S. N. Kukureka, P. Liao, M. Rao, and Y. K. Chen, "The friction and wear of polymers in non-conformal contacts," Wear, vol. 200, pp. 83-94, 1996.

[1.26] S. N. Kukureka, Y. K. Chen, C. J. Hooke, and P. Liao, "The wear mechanisms of acetal in unlubricated rolling-sliding contact," Wear, vol. 185, pp. 1-8, 1995.

[1.27] S. N. Kukureka, C. J. Hooke, M. Rao, P. Liao, and Y. K. Chen, "The effect of fibre reinforcement on the friction and wear of polyamide 66 under dry rolling/sliding contact," Tribology International, vol. 32, pp. 107-116, 1999.

[1.28] C. C. Lawrence and T. A. Stolarski, "Rolling contact wear of polymers: A preliminary study," Wear, vol. 132, pp. 183-191, 1989.

[1.29] M. Rao, C. J. Hooke, S. N. Kukureka, P. Liao, and Y. K. Chen, "The effect of PTFE on the friction and wear behavior of polymers in rolling-sliding contact," Polymer Engineering & Science, vol. 38, pp. 1946-1958, 1998.

[1.30] D. H. Gordon and S. N. Kukureka, "The wear and friction of polyamide 46 and polyamide 46/aramid-fibre composites in sliding/rolling contact," Wear, vol. 267, pp. 669-678, 2009.

[1.31] V. Kerremans, T. Rolly, P. De Baets, J. De Pauw, J. Sukumaran, and Y. P. Delgado, "Wear of conveyor chains with polymer rolls," Sustainable construction and design. Vol.2(3). pp.378-387, 2011.

[1.32] A. Reinholz, M. A. Wimmer, M. M. Morlock, and E. Schnelder, "Analysis of the coefficient of friction as a function of the slide/roll ratio in total knee replacement," Journal of Biomechanics, vol. 31, Supplement 1, p. 8, 1998.

[1.33] S. Apichartpattanasiri, J. N. Hay, and S. N. Kukureka, "A study of the tribological behaviour of polyamide 66 with varying injection-moulding parameters," Wear, vol. 251, pp. 1557-1566, 2001.

[1.34] A. Francisco, H. Abbouchi, and B. Villechaise, "A New Approach for Rolling Contact Fatigue Numerical Study. Application to a Brittle Epoxy Resin," Journal of Tribology, vol. 133, pp. 031101-031101, 2011.

[1.35] A. Avanzini, G. Donzella, and D. Gallina, "Failure analysis and life prediction of polymeric rollers for industrial applications," International Journal of Materials and Product Technology, vol. 38, pp. 362-385, 2010.

[1.36] S. M. Hosseini and T. A. Stolarski, "Morphology of polymer wear debris resulting from different contact conditions," Journal of Applied Polymer Science, vol. 45, pp. 2021-2030, 1992.

[1.37] S. Senthilvelan and R. Gnanamoorthy, "Damage mechanisms in injection molded unreinforced, glass and carbon reinforced nylon 66 spur gears," Applied Composite Materials, vol. 11, pp. 377-397, 2004.

[1.38] H. Imrek, "Performance improvement method for Nylon 6 spur gears," Tribology International, vol. 42, pp. 503-510, 2009.

# Chapter 2

# Morphological features of polymer wear
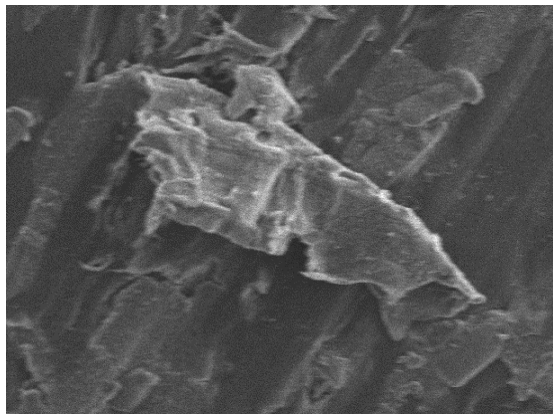
## Goal

In this chapter an overview of the various wear mechanisms in polymer tribology is summarised. This overview focuses on the diverse surface scars or morphologies of polymer wear. Different imaging techniques used for characterizing the worn surface morphologies are discussed. The correspondence between images of contact surface and descriptive information from the previously reported experimental results is also elaborated. The generic wear mechanisms proposed by different authors are compared and classified according to their morphological characteristics. A tribo-tree for polymer wear is established for easy understanding of the interrelationship between morphology of worn surface, phenomena leading to surface modification, wear mechanism and the deformation mode. Specific type of wear mechanisms (abrasion, adhesion, fatigue-wear and therformation) and their corresponding surface morphology, influenced by the contact kinematics, operational parameters and materials are also discussed in detail. The review concludes that standardization of imaging techniques is essential for effective tribological inspection. Additionally, for each tribo-pair it is advantageous to have evolution of wear surface for better understanding of the wear process.

## 2.1 Wear Classification

Polymer, being a low cost material and having advantage over metals in terms of light weight, vibration resistance and dry running capabilities, are studied extensively for tribological applications. The enormous amount of research work on polymer tribology focuses on wear response from the view point of material composition and parametric influences [2. 1, 2, 3, 4, 5]. In polymers, the wear responses are substantiated in terms of wear mechanisms both qualitatively and quantitatively, from surface morphology and topography respectively. For easy understanding of the wear process a generic classification of wear mechanism is in practice for metals, non-metals and ceramics etc. Also, polymer wear classification was proposed by different authors [2. 1, 2, 6, 7, 8]. Reviews on polymer wear mechanism based on the surface characteristics dates back to more than a decade [2. 7]. With the development of new technologies it is thus essential to recapitulate the developments of polymer tribology and contemplate the latest interventions. The generic classification for wear mechanisms considers lubrication, hard materials and environmental condition which might not be entirely appropriate for polymer tribology. In this section, all factors obtained from three major mechanisms (abrasion, adhesion and fatigue) and wear classification by various authors are explored.

Different approaches such as energy, phenomenological [2. 8], material response [2. 6], and surface condition [2. 9] were used to categorise the wear mechanisms. Bartnev *et al* and Lancaster's wear classifications were primarily based on the process endured by the material [2. 1, 6]. Clerico *et al* also addressed on the major divisions of polymer wear mechanism into distinct types such as abrasion, adhesion and fatigue[2. 10]. However, in their description it had been reported that the wear mechanism itself is rather progressive with abrasion during the initial stage of wear followed by adhesion. The change in wear mode from abrasion to adhesion was earlier experienced by Kim *et al.* This transition from adhesion is supported by the

formation of transfer film which is a critical factor in the wear classification [2. 11]. Yamaguchi classified the wear mechanism based on the observed phenomenon such as ploughing, pitting cracking, etc. which were resultants of a progressive damage process [2. 8]. The most widely used classification is of Briscoe *et al*, in which wear of polymer is basically divided into three broad groups. In their wear classification, polymer has been rationalized by summing up the different approaches to a specific group (1) generic approach, (2) phenomenological approach and (3) material response [2. 7]. This classification is categorised as open type where all mechanisms including fatigue and abrasive wear from Bartnev *et al*, are brought under one single umbrella. However, in an open classification when experts or engineers categorize their material response, it can result in deviations due to subjective nature of involved experts. Another interesting classification is by Bayer, who classified wear mechanisms into seven major generic categories [2. 9]. In fact, his classification can be considered as a global model for all materials. However, this classification does not hold good for polymers. This is because among the seven generic mechanisms, repeated-cycle deformation is not entirely true for polymer. In the polymer-metal tribo-pairs, from the first instant of interaction the soft material deforms either in plastic or elastic mode which rules out the repeated cycle deformation. Also, according to the delamination theory, several cycles are required to form crater by polymer adhesion [2. 12]. Thus, adhesion mechanism can be grouped under repeated cycle deformation, but the classification gets complicated due to the creation of an overlap between adhesion and repeated cycle deformation. Also most of these classification does not consider the polymer composites which bring in sub-mechanisms (three body abrasion, rolling of debris etc.) from the debris. The easiest method to classify wear is based on the surface response to the tribo-system, for which the scars are the representatives.

"Seeing is believing" is often followed by tribologists to explain the frictional behaviour, wear and the processes involved in tribological interaction. Visualizing the worn surface of polymer is more interesting due to the immediate surface morphological response as a consequence of wear. Phenomenological approach would be more appropriate where the defined mechanisms can be validated based on observed scars or morphological changes. Bayer had already reported that scars were used as a classifier of wear mechanism [2. 9]. These scars are the consequence of a chain of events occurring during the course of interaction. Several authors have explained the phenomenology of wear. However, without including wear scars as a variable, the classification remains incomplete. A definitive classification specifically for polymers accommodating the scars produced by various wear mechanisms is an absolute must. This classification would be easily approachable by both engineers and scientists for decision making on materials design, manufacturing and maintenance.

Based on existing classifications the wear scars can be correlated with the corresponding mechanisms using the interrelationship established by Lancaster and the damage map of Bayer [2. 1, 9, 13]. Bayer had already indicated the existence of three different classifications which were based on (1) scars (2) physical mechanisms and (3) conditions. However, these three classifications are not related to each other. With simple adaptations, we have established a tribo-tree for polymers and its

composites as shown in Figure 2-1. The tree has the following four levels (1) wear mode, (2) wear mechanisms, (3) wear phenomenon and (4) wear scars. The tribo-tree basically represents the interrelationship between wear mechanism and the corresponding surface scars. To understand the difference between wear mechanism, phenomenon and scars, they are to be individually defined. In the wear process, the phenomenon is the resulting event caused by wear mechanism to produce a certain type of wear scar. Figure 2-1 shows the interrelation between the levels and their subdivisions.
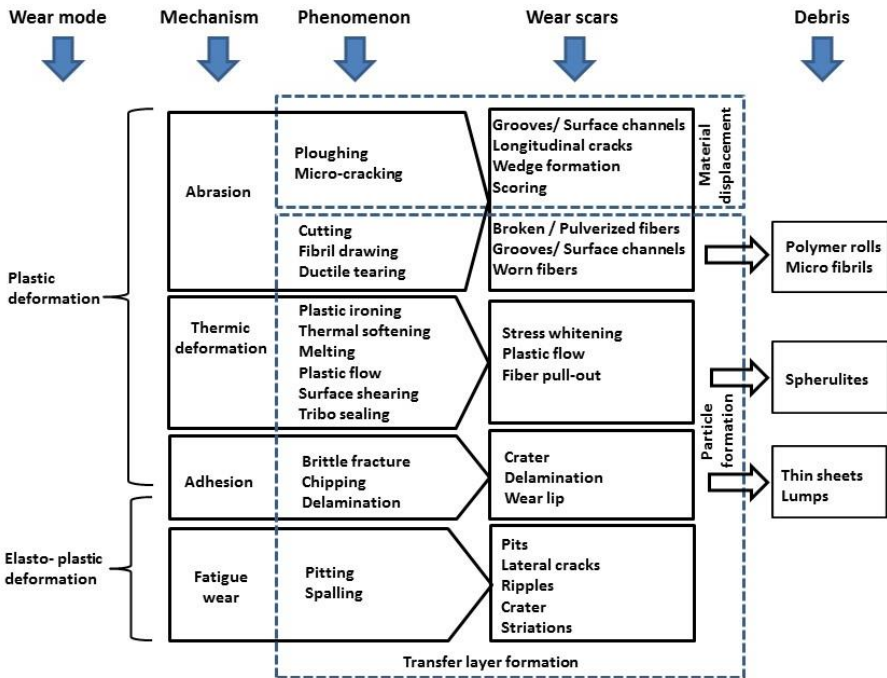


Figure 2-1 Tribo-tree with surface scars, debris and the phenomenon for wear classification of polymer and its composites.

The wear mode, which is the fundamental way of describing the damage, is divided into two groups, plastic and elasto-plastic. The wear mechanisms follow one of the two wear modes to produce surface scars. They are related to the column of wear mechanisms with four subdivisions. Three of these mechanisms (abrasion, adhesion and fatigue) already exist in the generic classification. The mechanism of therformation is based on temperature effect for which the polymers are susceptible, on altering the surface morphology severely. Thus, we have termed the fourth subdivision as "Therformation" (surface scars caused by temperature change) that is dominated by the heat developed in the course of interaction producing scars by thermal softening and melting. In the tribo-tree the phenomena and scars corresponding to these four mechanisms are also included. The tribo-tree can assist in damage investigations whereby the scars can be traced back to primary failure modes. This flow diagram helps to resolve practical questions on material design and maintenance. When an effective database is created for the tribo-tree, the debris also

can be used as a diagnostic tool. The tribo-tree concept proposes the requirement of an effective database of surface scars/morphology from the worn polymer surface.

## 2.2 Wear mechanisms: a survey of tribo scars

Although, the friction and wear of polymers are broadly reviewed [2. 2, 6, 7, 8] the connection between the wear mechanism fundamentals and the scars are scarcely surveyed. Most tribological report has micrograph representing the surface before and after wear to validate the descriptive wear/friction data and to relate them with specific wear mechanism. Besides, wear scars are also used as a direct measure to visually validate damage levels and to put forth theories and hypotheses for interpreting the wear processes. To study the wear mechanisms, we consider surface damage as a form of qualitative/quantitative changes during interaction between any two materials, in our case, the polymer and its counterface. Therefore, wear mechanism is defined as an ongoing process in the tribo-system contributing to the change in surface morphology of the contacting bodies. For metals, definitions based on material model also exist, where mechanisms is described from the perspective of plastic slip line pattern [2. 14]. However, such models do not consider the temperature effect as an important factor in polymer tribology. Generally, the wear mechanisms are based on the type of material, tribo-system and surface characteristics. On comparing with steel, polymers have different mechanical, physical and chemical characteristics that result in different wear scars. A clear list of scars representing the mechanisms for polymers does not exist and has to be compiled from the existing literature. To accommodate a broad group of materials used in polymer tribology, the polymers and their composites are considered in the current discussion.

Based on the classification introduced in the tribo-tree, polymer tribology has four subdivisions which are (1) abrasion, (2) adhesion, (3) fatigue-wear and (4) therformation. An additional important phenomenon in polymer tribology is the transfer layer formation, which persists (with different levels) in all four mechanisms. The four mechanisms in the tribo-tree together with the transfer layer formation are elaborately discussed below.

## 2.2.1 Polymer abrasion

Polymer abrasion is a widely found wear mechanism where phenomena such as ploughing and cutting persist. These phenomena cause geometrical change on the surface with or without progressive material loss to incur wear scars such as grooves and cracks. In the abrasion of polymers, the most dominant scars are grooves along the sliding direction caused by ploughing or cutting phenomenon. Several authors concluded their studies with the dominancy of abrasion mechanism from these wear scars called "grooves" [2. 11, 15, 16, 17, 18, 19]. Lancaster, in categorising the abrasive wear mechanism of polymers, briefs them as an elastic-plastic deformation of polymer for which the particle detachment occurs through plastic grooving, cutting and fatigue [2. 1]. Zhum and Ghar classify abrasive wear with four different phenomena (1) micro-ploughing, (2) micro-cutting, (3) micro-fatigue and (4) micro-cracking [2. 20]. For having a groove as a wear scar, two possible phenomena are

relevant (1) ploughing and (2) cutting. A two dimensional sketch followed by pictorial representation and real scars from literature for abrasive wear is shown in Figure 2-2. Ploughing in abrasion is the local plastic deformation by material displacement within the solid body without particle generation. Cutting can be defined as micro-machining process where particle removal is evident [2. 14]. In both cases, a groove distinguishes the scar produced from ploughing and cutting. It was earlier reported that the grooves produced by cutting are narrow and steep whereas ploughing yields wide and shallow scars [2. 14]. However, particle generation, debris formation and transfer layer presence show clear signs of micro-cutting.

Ploughing of polymers was earlier reported by Lancaster *et al* where fibre reinforced polymer of Nylon 66 and PTFE was investigated from photo-micrographs [2. 21]. Scoring marks resembling a groove pattern has been used to compare UHMWPE and PET [2. 22]. Also a similar feature with micro channels in UHMWPE as a ductile tearing were reported by Bohm *et al* [2. 23]. Besides micro-channels, grooves at nanometer size were observed by Chang *et al* on short carbon fibres in composites [2. 24]. The phenomenon of ploughing and cutting are common in case of pure plastics, however, with the inclusion of reinforcements it changes. For example, on introducing glass fibre as reinforcements in PET, mechanism changed from micro-ploughing to micro-cracking [2. 25]. A similar feature with fracture of individual fibres was also observed by Chen *et al* for PA66 and PPS composites [2. 26, 27]. The abrasion in fibre reinforced composites can be attributed to brittle failure. In composites, the hard fibres are ruptured by indentation steel asperity and subsequent sliding fractures the fibres. This is schematically represented in Figure 2-2 c. In certain cases, when the bond strength between fibre and matrix is significantly strong, the matrix supports the fibres and thus thinning of fibres occurs through abrasion by a hard asperity [2. 24].
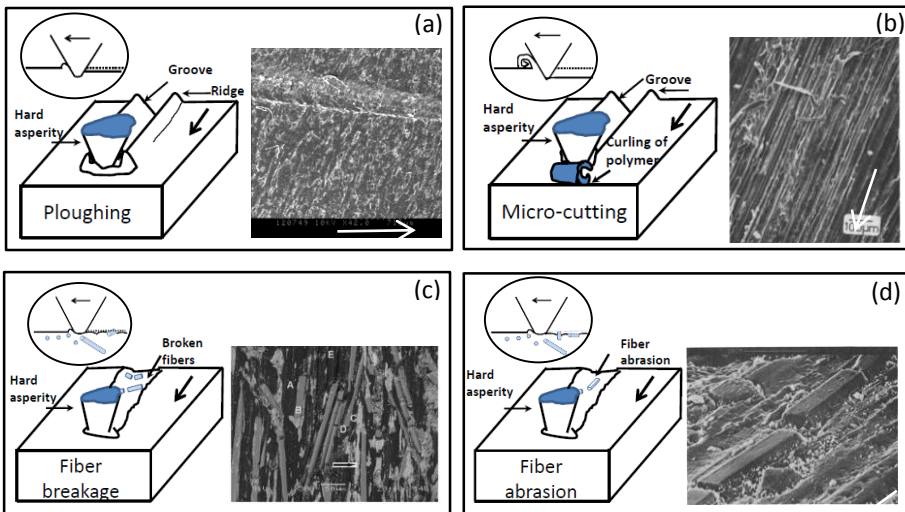


Figure 2-2 Different types of abrasion scars (a) ploughing (b) micro-cutting (c) fibre breakage (d) fibre abrasion (Arrow mark indicate the sliding direction in the pictorial representation) [2. 26, 28, 29].

Even though, grooves are generalised from its surface morphology and its appearance, the observed grooves from different studies have size variations. Starting from Lancaster [2.21] to Chang *et al* [2.24] the grooves have been reported at different levels of magnification. With the recent developments in material composition and instrumentation, groove size are described in nano scale. Taking a closer look the variations in size can be attributed to material properties or parameters such as load, speed, roughness etc. This denotes that the qualitative aspects related with grooves such as size and its coverage can be related to the wear behaviour. While it is still unclear on understanding the scale of investigation in grooving, discrepancies do exist in linking them to polymer abrasion. After all Harsha *et al* outlined the influencing mechanisms for abrasion as fracture, fatigue and melting [2. 30]. Thus, encountering an overlap between phenomena and mechanisms.

Abrasion can also occur in two different ways (1) two body abrasion and (2) three body abrasion. The fragmented fibre debris or generated particle having higher hardness than the matrix creates a situation of third body wear. Hence, pure plastic has higher chances for experiencing two body abrasions. However, when there are reinforcements in the polymer such as glass or carbon fibres, three body abrasion prevails. This was reported by Byett *et al* for Polycarbonate with glass fibre tested against hardened stainless steel AISI 431 [2. 28]. A similar mechanism with three body abrasion was also reported by Chen *et al* for PA66 and PPS composites with 5% glass and carbon fibres [2. 26, 27]. A schematic representation of the fiber breakage, fiber abrasion and a SEM image for the same are shown in Figure 2-2 (c & d).Two more phenomena of abrasion had been reported in the literature excluding micro-cracking [2. 20] and micro-fatigue. For the combination of polypropylene against steel, Ghandi *et al* reported that cracking was induced by grooves [2. 31].

Summing up all the phenomena of abrasion in a common umbrella, the wear scars with rectangular pattern or smooth long lines parallel to the sliding direction is the typical morphological representation. Reports exist with comparable sizes of wear scars in validating their descriptive score on wear rate [2. 32]. Thus, one can assume that from the statistical evaluation of the area covered by the groove pattern on a worn surface, the severity of abrasion and its dominancy could be concluded. It is noteworthy to understand that particle detachment is not necessarily the only form of abrasion. Local plastic displacement of polymer within their confined place is also likely to occur in polymers producing the same morphology.

## 2.2.2 Polymer adhesion

Initially adhesive wear scar was described as a fragmentation of softer material in the tribo-pair [2. 33]. Seabra *et al* postulated that the main cause for polymer adhesion is due to Van der Waals force during interaction [2. 22]. On the other hand, Czichos *et al* described adhesion and abrasion from the perspective of adhesion energy and material property (rupture strength) respectively [2. 34]. On the whole, adhesion mechanism is a process in which the shearing of bonded junctions during the course of interaction between two bodies. Such mechanisms leave scars of the fragmented region and adhered debris in the counterface material. In the wear classification,

scars representing the adhesion mechanism are craters, surface flake, lumps of polymer and wear lips which can be seen by post microscopy. Adhesion as reported by Koike *et al* for PEEK against alumina balls results in lumpy transfer of polymer as observed from micrographs [2. 35]. Similar results were observed for polyethylene (UHMWPE) where lumpy transfer layer on steel surface was considered as a sign of adhesion. Kar in his work identified the adhesive nature of POM from the fiber like structures formed under excessive heating [2. 36]. The adhesive wear mode is also confirmed from the type of debris observed in the vicinity of contact, where plate like debris is a consequence of adhesive delamination. A similar feature on delaminated surface was reported by Rodriguez *et al* for PEEK composites [2. 37]. Figure 2-3 (a) shows a schematic representation and SEM micrograph of delamination.

Surface morphology with torn out patches in the polymer-polymer contact (PA6-POM) is also considered as a sign of adhesive wear [2. 32]. It is well known that the adhesion mode is more dominant in polymer–polymer contact than polymer-metal contact. This is due to the joining of hot junctions: the heat dissipation in polymer-polymer tribo-pairs is relatively less which promotes adhesion through thermal softening. Generally, in adhesion mechanism the formation of transfer layer is the result of particle generation from the fracture of adhesive junctions. Myskhin *et al* extensively reviewed the polymer adhesion in terms of friction and wear [2. 38]. Excessive heating and third body occurrence is a typical sign of adhesive wear in which spherical particles are produced from local melting. In a research by Lhynm *et al* the prevalence of adhesion by means of decohesive flaking was reported for carbon fiber reinforced PTFE [2. 39]. They also reported that the smooth surface as seen from post microscopy indicated adhesive wear. In a recent review, Dasari *et al* described delamination as the nucleation of crack in the subsurface, and the resulting damage was due to repeated cycle deformation [2. 12]. However, scratch testing with a single cycle in PEEK nanocomposites and diamond indenter also showed signs of delamination as seen in SEM micrograph Figure 2-3 (a). [2. 37]. The inconsistencies in describing the adhesion mechanism by specific means such as failure mode or wear scar create a misconception of the material removal. This reveals the importance of a holistic approach in explaining the mechanism. A parametric description in combination with surface scars at different instance of wear process aids better understanding of the mechanism.

The schematics of the two common features in the adhesive wear are shown Figure 2-3 with examples of real scars of polymer surfaces. Summing up, as a consequence of adhesion wear scars such as craters, decohesive flaking, smoothening of surface, transfer layer and torn-out patches are produced. In other words all these features can be morphologically categorised using an irregular platelet with sharp edges indicating the decohesive flaking or craters. It is evident that the edges are clearly indicates the border between the parent material and the transferred part.
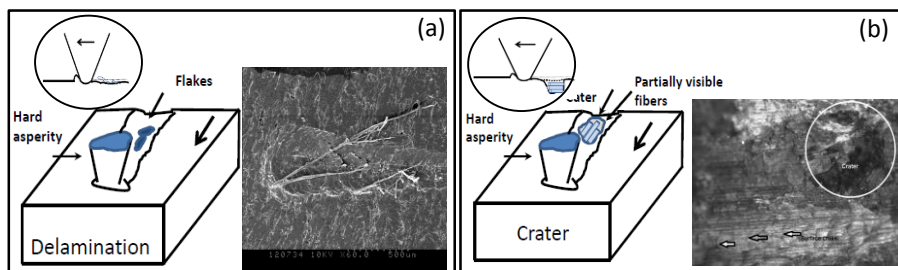
Figure 2-3 Different types of adhesion scars (a) delamination (b) craters (Arrow mark indicates the sliding direction in the pictorial representation).

## 2.2.3 Fatigue-wear of polymers

Fatigue is one of the passive modes of particle removal which requires substantial amount of time to produce macroscopically visible wear scars on the surface level. Considering the type of scars for fatigue wear, striations are common in fractured specimens. However, this morphological feature is also seen in tribo-contacts. Clerico *et al* described fatigue as a severe wear condition which is prevalent in the final stage of wear [2. 10]. Thus, effective information on fatigue-wear can be obtained mostly by post-microscopy. The comparison of a worn surface morphology to a fatigue fractured HDPE specimen was earlier done by Jain *et al* [2. 40]. In their investigation, features of arced ripples were observed in both fatigued and wear tested specimen revealing fatigue-wear of polymer. In-fact, these ripples are considered as a consequence of surface plasticisation. However, without a cross-sectional study it is hard to interpret the involved mechanism. A cross-sectional investigation of a similar ripple like surface for PES sliding against steel in n-propanol showed deep cracks in micron scale [2. 41]. In sliding of UHMWPE similar crack like features oriented perpendicular to the sliding direction which were reported earlier [2. 42]. Some of these ripples can be seen only at high magnification. Therefore, this can only conclude the final mode of failure. Ripples are not only associated with fatigue but also with other mechanisms such as fretting wear and thermal softening. For example, a ripple like surface morphology was observed in fretting of PMMA sliding against steel [2. 43].

The common fatigue phenomenon in steel is pitting and spalling which is seen as craters in the contact surface and is also observed in polymer rolling [2. 44]. Spalling was also observed in polymer rolling due to networking of cracks nucleated from the fiber-matrix interface [2. 45]. However, in the rolling contact fatigue of PEEK composite, the variations in the surface scars are attributed to the adhesion process. Apart from pitting, the rolling contacts subjected to fatigue also showed transverse cracks [2. 45, 46, 47]. It has been reported by Storlarski that the most common feature in polymer rolling is plastic flow [2. 48]. Polymer rolling has been studied by few authors where the common feature observed was plastic flow and transverse cracks (cracks perpendicular to the rolling direction [2. 35, 46, 49, 50, 51, 52, 53]). Figure 2-4 (a & b) shows similar transverse cracks from the micrograph of the worn surface. Plastic flow observed in the rolling contacts of polymer can also be attributed

to the thermal effect, especially when high speeds are involved. Under high surface velocity thermal effects play a significant role in creating surface morphologies like streaky flow of material. The schematics of the ripples, pitting and lateral cracks are shown in Figure 2-4 with examples from real scars of polymer surface.

An interestingly common feature in fatigue-wear of polymer is the arced ripples, craters, pits and the surface cracks. Ample research work exists on studying crack length growth in steel surface. Nevertheless, such information on crack length and its characteristics are limited for polymers. Summing up the wear scar features from fatigue, the close morphological feature which can represent these wear scars are thin irregular line profiles and a circular geometry. Additionally the size of the pits decides its category as micro-pits or craters.
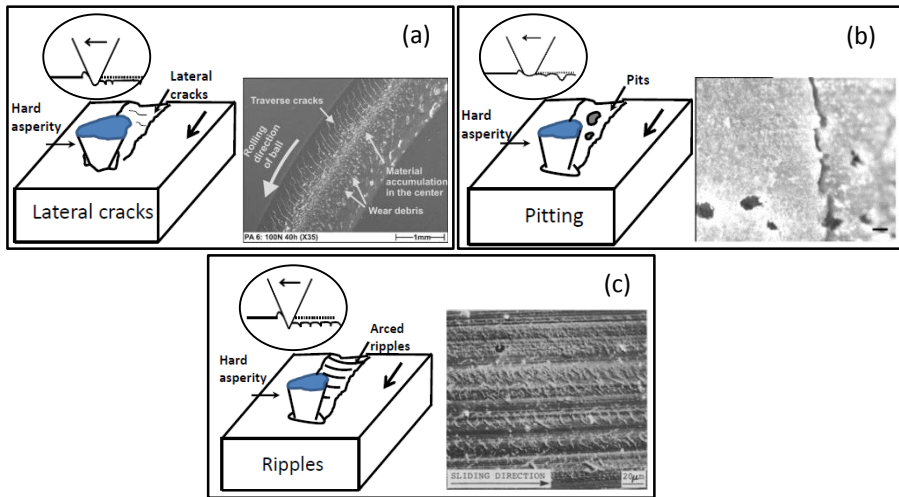


Figure 2-4 Different types of fatigue-wear scars (a) lateral cracks (b) pits (c) arced ripples) (Arrow mark indicate the sliding direction in the pictorial representation) [2. 40, 46, 54].

## 2.2.4 Therformation

The fundamentals behind the generic mechanisms developed for metals partially fits for polymers. One of the vital classifications in polymer wear is therformation. Even though the scars produced by thermal softening or melting are distinct, they are related to the generic mechanisms. Phenomena related to therformation are localised flow, melting and thermal softening. In general, the thermal behaviour varies with respect to the type of polymer: thermosetting polymers fail in a brittle mode and thermoplastics undergo thermal softening or melting.

One of the surface features commonly found in polymer tribology is plastic flow in both abrasion and adhesion [2. 19, 32, 36]. These patterns are generally present as a wavy discontinuous pattern in the direction of sliding [2. 19]. Kar *et al* has observed localized flow of POM caused by thermal softening at a sliding speed of 2.5 m/s. In rolling contact, the formation of such patterns is explained as a consequence of increased temperature [2. 44, 52]. In most reported cases, the localized flow has been identified from scars such as ridges, wavy substance and discontinuous steaks. A

schematic representing the plastic flow with an example of real scar from literature is shown in Figure 2-5. In a SEM micrograph plastic flow seen as white patches, is generally referred as stress whitening. This is because of the change in refractive index due to the micro void clusters with size of light's wavelength present in the surface [2. 55]. It is clear that in most cases flow like features are prevalent at higher temperature. Only limited literature reports about plastic flow of polymer surface nevertheless, the reasoning from individual authors on the plastic flow is significantly different [2. 19, 35, 44, 56].
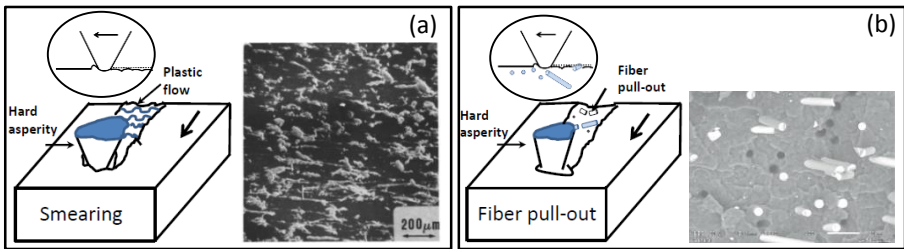


Figure 2-5 Different types of thermic deformation scars (a) smearing (b) fiber pull-out (Arrow mark indicate the sliding direction in the pictorial representation) [2. 31, 34].

Apart from the viscous flow an additional mechanism experienced as a consequence of therformation is fibre pull-out. For example, Chang *et al* reported groove like features in polyamide composite as a consequence of fibre pull-out. In this case, at high magnification the surface scar showed similar appearance as a groove formed by micro-cutting. The cause for these grooves is thermal softening of matrix at high contact pressure which reduces the interface strength between the fibre and matrix and thus debonding of fibres occurs [2. 19]. Unlike the other three generic mechanisms, no distinct features are categorised for characterising the therformation. However, the wear scars show promising distinguishable features such as pulled out fibres represented by a dark phase in the micrograph. Also the clarification can be made based on the size of fibres. Broken fibres have significantly different size compared to pulled out fibres. The wavy streak of material is an easy indicators in the perspective of image processing that can be used to quantify the severity of wear mechanism. This streaky substance can also be estimated from a geometrical view point. The streaky substance has a specific wave like morphology. The size and the elongation of these waves, can be taken as a direct measure for understanding the severity of plastic flow during the wear process. Summarising the scar type for therformation the commonly occurring plastic flow can be morphologically represented as wavy discontinuous pattern.

## 2.2.5 Third body and transfer layer formation

The variability in friction and wear behaviour of polymers can be primarily related to the formation of the transfer layer. This protective layer significantly affects the tribological characteristics: covering hard asperities with an interfacial layer modifying the state of stress [2. 57]. Among abrasion, adhesion and fatigue, the persuasive mechanism contributing to the formation of transfer layer is still a matter

of question. The formation of thin layer has been previously studied by several authors for understanding the process and also for its characteristics [2. 58, 59, 60, 61, 62]. Based on the morphological features as observed on the counterface, Franklin *et al* classified the transfer layer into four distinct types [2. 63]. Type A has smaller clumps of diameter 20 µm. Type B is continuous and smoothly deposited and Type C shows a relative discontinuous and large clumps up till 100 µm [2. 63]. And the fourth category is a combination of type B and C. Nevertheless, Briscoe *et al* segregated the transfer layer into two distinct divisions (1) adiabatic and (2) isothermal based on which this can also be correlated to specific surface morphologies [2. 7]. Within the same classification the isothermal type is further divided into (1) no transfer, (2) smooth molecular profile and (3) lumpy or unordered transfer layer. The transfer layer formation was also explained from the phenomenological view point by Brisco and Chandrashekar *et al* [2. 7, 64]. Various theories were put forward on the formation of transfer film such as conjoining of adjacent semi-crystalline slices, filling of roughness valleys and surface shearing [2. 15, 24, 65] and conglomeration of wear particles.

The reported transfer film formation are mostly for high stress abrasion where particle generation is evident. These particles are trapped in the interface and milled between the two surfaces to form a uniform thin layer. A schematics of similar mechanism was proposed by Chang *et al* where the nano-particles trapped between the polymer composite and the steel asperities (counter material) was found to be acting as a protective agent against wear [2. 24]. Discontinuous transfer layers were very often observed by different authors [2. 61, 63, 65]. Marcus *et al* proposed that the transfer film was formed by surface shearing of UHMWPE [2. 65]. Once the transfer layer is fully formed there is possibility for peeling off due to poor adherence at the interface [2. 66]. The peeled transfer layer has high chances of adhering back to the parent material, termed as "back transfer" [2. 34, 35, 67]. The formation of the back transfer is influenced by the ridges present in the parent material from micro-cutting and by the protruding fibres which conglomerates the polymer collected from the transfer layer [2. 34]. Thus rough surfaces are susceptible to back transfer and transfer occurs in places where the surface irregularities are large. Similar characteristics of polymer accumulation was also observed on the protruding fibres of polyamide composite under high contact pressure in sliding condition [2. 24]. Morphologically, the transfer layer has no regular pattern. The pattern depends upon the contact kinematics and the material used. However, when two materials are in contact, the transfer layer can be identified from the difference in colour between the transfer layer and the parent material. This can be a source of information to recognise transfer layer.

Apart from the formation of transfer layers, the third body generation is prevalent in polymer wear. The most common form of particle generation is roll formation by polymer abrasion. Using a phenomenological approach Aharoni elucidated the roll-formation process [2. 68] from micro-machining of soft polymer by hard asperity followed by curling of debris in pure sliding condition. Chen *et al* also reported debris in fibrils form with diameter ranging from 0.1 – 10µm for PA66 in rolling-sliding condition where abrasion is less expected [2. 44]. Thus, we can assume that formation

of rolls is independent to the sequence of motion. It is also understood that these rolls are shaped by plastic flow leading to the formation of flakes which are rolled into special type of debris in the course of interaction. In another research by Byett *et al*, the roll like debris with particle diameter ranging between 2 – 4 µm were accumulated as the wear progresses [2. 28]. Benabdallah in his work on UHMWPE, PA66 and POM found that the roll formation occurs post to the formation of transfer layer [2. 42]. In this case, the asperities which are already covered by the transfer layer might restrict the curling phenomenon promoted by asperity interaction as described by Aharoni [2. 68] and also by Sampathkumaran *et al* [2. 69]. It is evident that roll formation persists in engineering plastics [2. 19, 28, 42, 44, 68, 70], however, its occurrence was recently found also in high performance polymers PPS composite (PPS +15% Ethylene butyl acrylate) [2. 11]. Besides micro-machining, delamination and pitting phenomena, the temperature influences the particle formation significantly. In a research by Varziri *et al* spherical particles were produced as a consequence of local melting [2. 18]. Still discrepancies exist on relating the formed debris to specific mechanism. One typical example is the phenomenon of roll-formation itself. In roll formation three different mechanisms such as abrasion, adhesion and fatigue were proposed [2. 42, 68, 71].

Benabdallah reported that fine debris are a consequence of mild abrasion [2. 42]. Harsha *et al* has observed morphologies for cutting in terms of surface channels, which involves debris in forms of fine fibrils [2. 30]. Apart from the fine fibrils, Cortellucci *et al* also observed simple shear type chips in the abrasion testing of PMMA [2. 29]. In an investigation by Ren *et al* on cold rolling, black coloration on PA 6 roller in form of flakes indicates the misalignment of rollers [2. 72]. It is now evident that the generated particle can provide information about the wear mode and its condition. Consequently, a thorough study on the generated debris can serve as a diagnostic tool similar to the ferrography.

## 2.3 Morphological changes from contact kinematics, load and speed

Having understood the classification of mechanisms, it is vital to study the parameters influencing the change in surface morphology. Unlike steel, the polymer wear process is more dynamic in nature by the synergetic effect of contact condition, operational parameters and material properties. These factors either together or individually contribute to different wear mechanisms which can be observed as a morphological change. Factors such as environment, production process and alignment errors produces parasitic effects while studying the influence of individual variable on wear mechanism. Additionally, there is also a possibility of a combined effect of two or more different parameters contributing to specific type of wear mechanism.

Among different variables, the contact kinematics (reciprocating/continuous sliding/partial sliding/rolling) have an influence in altering the tribological process. It is a common fact that sliding produces more severe wear scars than rolling. In rolling, elastic- plastic deformation is the dominant mechanism but in case of sliding plastic deformation is prevalent. It has been mentioned earlier in this thesis that the cause of failure in rolling contacts of polymers are mainly due to plastic flow rather than

fatigue [2. 73]. In case of partial sliding, there is a high possibility of encountering representative scars from rolling as well as partial sliding condition. This means grooves and micro-pits as a consequence of abrasion and pitting should prevail. However, reports on such features are meagre apart from Koike *et al* who identified the overlap in mechanism with abrasion and adhesion [2. 35]. This creates new avenues for investigating the overlap in mechanisms. Also the dominating mechanism and its corresponding tribological characteristics can be studied. The influence for nature of contact studied by Mergler *et al* articulates that severe damage of polymer was observed in pin-on-disc apparatus compared to reciprocating sliding test [2. 61]. The severity of wear was attributed to the inadequacy in formation of transfer layer.

Apart from the nature of contact, other parameters were also discussed. For example, Pogacnik *et al*, experienced different mechanisms by changing the parameters such as materials and speed [2. 32]. Besides the nature of contact and materials, the testing speed also has significant influence on the wear mechanism. Parallel micro-channel of the worn surface of PA6 specimen tested against POM was identified with mild abrasive scratches. For the same combination of tribo-pairs with increased speed at 1 m/s plastic deformation was observed, forming a streaky flow of material. It is evident that transition in mechanism from abrasion (groove) to adhesion (streaky flow) is observed by increasing the speed from low to high for both polymer-metal and polymer-polymer contacts. Similar observations were also reported for HDPE, POM and PTFE where morphological change was visualised [2. 36].

The influence of the contact pressure is described by Chang *et al*. In their report, the increase in load creates a transition in mechanisms from removal of partial phase (short carbon fibres) to cratering of the bulk material (epoxy and fibres) by the formation of micro-cracks in the brittle mode [2. 24]. The differences in mechanisms related to contact pressure are also highly pronounced through debris characteristics. In a research on PEEK materials, the back transfer of transfer layer is governed by the contact load [2. 35]. The formation of the film also depends upon the load where increased loads plastically deforms the generated wear particle [2. 68]. However, in another research at low loads the particles were removed as debris. The fragments of PEEK generated in the initial stage of wear adhere to the counter material (alumina balls) where the retaining capacity of these deposited PEEK on alumina balls depend upon the loading condition. At low load the transfer layer is retained however at higher loading condition the transfer layer is peeled off and adheres back to the polymer raceways [2. 35].

## 2.4 Influence of material

It has been reported repeatedly that material is a major influencing factor in changing wear mechanisms. The general rule of hard and soft materials failing in a brittle and ductile mode respectively also holds for polymer wear. In polymers, a relatively hard material (polyamide) undergoes brittle micro facture whereas a soft and tough material such as UHMWPE is abraded by ductile tearing. In a recent study, Liu *et al* compared the wear behaviour of two materials from the perspective of scratch marks (grooves) [2. 74],that changed with altering the filler material. By adding PTFE, the ploughing effect reduced, but on the other hand carbon nanotube (CNT) fillers

increased the ploughing effect. Chang *et al* stated the significant role of material composition as observed from the worn surface. Epoxy based polyamide composites have severe wear behaviour in form of micro-cracking and removal of material in the bulk mode. However on adding $TiO_2$ nanoparticles, the severity of wear has been reduced due to changes in bulk properties [2. 24]. The thermo-mechanical response of material also contributes in changing the micro-mechanism. The ductile and brittle response of polyamide and epoxy composites due to their thermo-mechanical behaviour is seen as a fracture of matrix in the epoxy and plastic flow by thermal softening for polyamide in high loading condition [2. 24].

Zhang *et al* compared the surface morphology of composite materials with different fibre length and found that the worn surface showed similar characteristics at 1 MPa contact pressure [2. 2]. Fibre size from the worn surface can be used to reason the process underwent by two different materials. From SEM micrographs, it can be concluded that, short fibres are easily susceptible to fibre pull-out. Long fibres due to the large surface area interaction with the matrix resist better to the pull-out [2. 75]. From the perspective of observations made through SEM on the worn surface, Chairman *et al* compared the damage intensity between basalt-E composite and glass-E composite sliding against SiC abrasive paper (400). The observations showed the partial removal of matrix in glass-E composites whereas a significant amount of matrix still remain in the worn surface of basalt E composites remain on the worn surface [2. 76]. The frequently used polymers POM and PTFE while sliding against steel exhibited variation in the observed mechanisms. POM has a localised plastic flow due to thermal softening at a speed of 2.5 m/s but for the same conditions such features are not observed in PTFE [2. 36].

It is evident that mechanisms are unique for different materials and parameters. This can aid in using the knowledge of basic wear mechanism for deciding on the operational parameter. On the whole, it is clearly understood that the wear mechanism is affected by a combination of factors within the material properties itself.

## 2.5  Techniques used in tribography

Hogmark *et al* on the grounds of topography and microstructure defined tribography as a methodology validating the tribological characteristics pertaining to micro level changes in the contacting surfaces [2. 77]. Usually, researchers use a tribographical approach in explaining wear mechanisms. The tribological consequences are represented both quantitatively and qualitatively from surface topography and morphology. The topographic characteristics have quantitative dimensions to relate it to the wear behaviour. However, to a certain extent the morphological features such as grooves, pits, transfer layer can be strongly associated to the specific mechanisms based on the operational and material characteristics. Quantitative texture evaluation through contact and contactless techniques (optical profilometry, stylus profilometry) are time consuming. A faster indicator of the surface condition is the morphology of the worn surface observed by microscopy techniques. In general, authors follow three different approaches which are, (1) microscopy to morphologically monitor and identify the type of mechanism from the micrographs,

(2) cross-section analysis for understanding the sub-surface damage and (3) topographic measurements as a quantitative tool

Even with all the available investigating methodologies the failure initiated from the subsurface due to shearing of top layer/transfer layer thickness which cannot be explored without destructive cross-sectional studies. Research supports the subsurface deformation and surface shearing observed as thin sheets, in the cross-sectional studies. It should be noted that under severe conditions or close to seizure, the formed wear scar is significant which can also damage the sub surface evidences thus providing no better information. It is also evident from the literature that the cross-sectional studies are scarcely reported in a tribological investigation.

## 2.6   Microscopy for morphological monitoring

Different kinds of monitoring techniques are used to visualize the worn surface. Visual inspection is one of the oldest and most common techniques of inspecting surface morphology. Stolarski in his work on polymer rolling uses visual inspection for preliminary investigation, followed by post microscopy using SEM and AFM [2. 53]. Maintenance engineers use similar methodology where the equipment is inspected with naked eyes for first-hand information on damage scars. Naked eye inspection has constraints in terms of resolution which is limited to 130 µm [2. 78]. At such resolution only few details are known from the scars where in the previous section (Figure 2-2, Figure 2-3, Figure 2-4) it is clear from the SEM images that patterns illustrating wear mechanisms were in the order of few microns. Also surface scars with easily detectable features by naked eye correspond to severe wear or a condition close to seizure. From the features seen in the visual inspection engineers/technicians intuitively forecast the severity of wear. Such a conclusion from naked eye observations is mostly pointing towards global wear characteristics. To identify the mode of failure and to segregate into corresponding wear mechanisms a microscopic view of the worn surface is required. Also for understanding wear progress the naked eye visualisation might not be appropriate, because morphology of materials at the early stage of wear is not detectable at a macro scale.

According to the literature, there are two broad categories of microscopic techniques, classified based on the imaging principle [2. 79]. However with the overlap in categories, we have included a third category. The three basic groups of imaging systems are (1) lens-imaging (2) scanning-imaging classes and (3) intermediate classes [2. 78]. The classification is defined based on formation of images for which instantaneous image formation, sequential image formation (scanning) and a combination of these two persist. These three categories comprises almost all techniques used in tribological studies. Optical microscopy (OM) and transmission electron microscopy (TEM) falls in the lens imaging category, whereas scanning probe microscopy (SPM) and Focus Ion Beam (FIB) falls in the scanning imaging technology. The scanning probe microscopy in-turn has different techniques such as Atomic Force Microscopy (AFM) and Scanning Tunnelling Microscopy (STM). Scanning electron microscopy falls in the third class. Figure 2-6 shows the techniques and their capability on revealing interesting features of the contact surface in terms of spatial resolution.

Among the different techniques in practice, SEM and OM are widely used due to its high resolution imaging, good contrast and segregation of different phases in polymer composites with reinforced materials. Though SEM is an expensive technique, images using SEM are more commonly found in all research articles than using OM. In fact most of the papers hold a separate section on "Scanning electron microscopy" or SEM microscopic observations validating the wear characteristics of worn surfaces [2. 24, 30, 42, 59, 80, 81]. Even stand-alone investigation using scanning electron micrography on polymer wear mechanisms are published earlier [2. 40, 82]. This is due to the fact that high resolution distortions free images can be acquired using SEM. OM has some limitations such as depth of field which, due to variations in topography of the contact surface, distort the image significantly, and illumination that can bring in disturbing artefacts. Depending on the severity of wear the worn surface has asperities with significant difference between peaks and valleys for which OM produces a highly distorted image. Tanaka *et al*, using OM, has observed significant differences in the morphology of worn surface however, it was also reported that the information obtained with OM is not useful for PTFE tested against glass possibly due to the required high magnification to witness the difference in mechanism [2. 15].
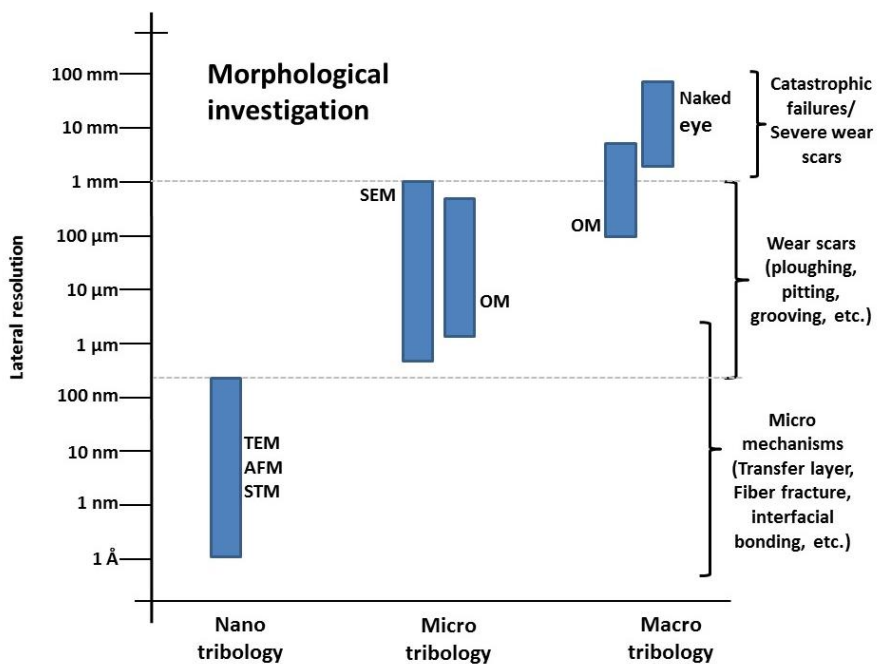


Figure 2-6. Microscopic techniques used in tribological investigation.

The resourcefulness of OM cannot be however underestimated. The optical microscopy is advantageous over electron beam microscopy because the OM does not cause potential damage to the investigated surface by radiation or beam damage. Marcus *et al* investigated the transfer layer of polymer on the steel surface with optical microscopy [2. 65]. Also in a sliding test on Polybutylene Terephthalate (PBT) surface, the scratch marks representing abrasion as observed by OM were reported [2. 83]. Ovaert *et al* also used OM to identify transfer film characteristics formed on steel by PEEK. Transfer film observed in optical microscopy seems darker than the steel surface due to the poor scattering effect of polymer [2. 84]. Pooley and Tabor on studying the tribological characteristic used OM and electron microscopy as the primary techniques to investigate the transfer film. In their study the transfer layer with the appearance of streaky substance of PTFE, LDPE and HDPE were found with a thickness ranging from 10 nm to 100 nm [2. 33].

Apart from SEM and OM, the other most commonly used microscopy technique is scanning probe microscopy which has several modules starting from scanning tunnelling microscope (STM). The focusing error, which is a measure of displacement, can be obtained by using different methods such as optical beam deflection, optical interferometry, laser beam reflection, tunnelling current and electrostatic forces [2. 85, 86]. Scanning with spatial resolution up to sub-angstrom level is already in practice since the late 80's [2. 86]. Such a measurement also provides quantitative data in terms of surface topography. The choice of technique for higher magnification relies on the information revealed in lower magnification. Stolarski adopted AFM since no sign of damage was observed in the SEM micrographs for the particular case of polymers in rolling contact [2. 53]. AFM is used more in making quantitative measurements and micro-tribological testing rather than imaging. A stage prior to AFM is scanning tunneling microscopy which uses the tunnelling current between the surface to be investigated and the contacting surface. This technique is effective in case where the material is a conductive material, however, in some case conductive coating should be applied for a high resolution image. Several modes of AFM are used: (1) tapping mode,(2) non-contact mode, (3) contact mode and (4) imaging mode. The disadvantage with the STM on investing surface has been overcome by the AFM. Optimization of the technique for soft materials was done to have better repeatability. Within AFM, limitation persists on using the type of technique to monitor the morphology without damaging the contact surface. One of the major constraints of the contact mode is that the soft material is susceptible to change morphology during the interaction between the tip and the surface. Both modes have limitation of their own in terms of scanning speed and also the damage caused to the surface [2. 87].

Apart from topographic features additional advantage can be sought from these advanced techniques to characterise material at a micron level, and to perform tribo tests. For example, in AFM, when heavily loaded against the test material, the sharp pin can produce wear scars which can be studied in detail. Stroup *et al* had used constant compliance force modulation (CCFM) in scanning force microscopy for characterising the mechanical properties locally [2. 91]. AFM is also used for understanding the friction force distribution and to study the micro wear

characteristics rather than micro morphology. The use of AFM has been adopted by different authors with respect to their requirement, Kaneko *et al* studied the change in properties from the molecular level in altering the intermolecular bond in PC [2. 88]. Hamada used two types of AFM (Point contact microscope (PCM) & Friction force microscope (FFM) to study the micro-tribological characteristics of polymer [2. 89]. Phase differentiation using the tapping mode in the AFM was earlier introduced by Hoper *et al* where they used material-contrast imaging in aluminium substrate with copolymer [2. 90].

Table 2-1 summarises some of the imaging techniques and the wear scars identified with these technique and their corresponding field of view. The table accommodates images of wear scars belonging to the four different mechanisms. It is clear that SEM is the dominant technique used in the tribological investigation. The range of field of view (FOV) as understood from the table is between 25 and 40000 μm. In Table 2-1, smearing has the smallest FOV and can also be detectable in low resolution and 1300 μm FOV [2. 10]. It is evident that most of the scars produced can be accommodated in an image with FOV of not less than 500 μm for which the OM can be an inexpensive and suitable technique if distortion free images can be produced.

Even though many microscopic techniques exists, only few are used in polymer tribology investigations. FIB is one among the high end microscopes which aids in cross-sectional studies. FIB also uses similar principle of the SEM but instead of electron, FIB uses ions to scan the surface. The market of FIB was started in the 80s. One of the advantages of the FIB is that *in-situ* cross-section can be made for studying the subsurface features. In FIB microscopy, advancements have been made by introducing secondary ion mass spectrometry (SIMS) or liquid-metal ion sources (LMIS) [2. 92]. FIB-SEM is one of the recent advancements is using a combination of techniques to study the cross section without disturbing the contact surface. Tribology grade polymer hybrids are being investigated for their distribution of filler by making a pocket in the bulk material and thereby studying the cut section from the milled region.

In general, the FIB-SEM can be used to understand the subsurface cracks from tribo mechanisms without significantly disturbing the contact surface. Brosotow *et al* used a similar combination of FIB and SEM, to study the dispersion of polymer in the subsurface of hybrid composites of LDPE. Aluminium particle (1 micron size) dispersed in the subsurface can be clearly seen in the scanned image. Similar methodology can be used to study the transfer layer thickness on the counter face material through back scattered electron [2. 93]. The difference in the atomic mass of the transfer layer and the counterface material aids in measuring the thickness from a pocket made on the contacting surface of the counter material.

Table 2-1. Details of wear scars revealed using different imaging techniques.

| | Nature of contact | Tribo-pairs | Imaging technique | FOV (μm) | Wear scar |
|---|---|---|---|---|---|
| **Polymer abrasion** | | | | | |
| Byett et al [2. 28] | Pin on disc | Polycarbonate/glass fiber- AISI 431 | SEM | 50 | Fiber abrasion |
| Harsha et al [2. 30] | Pin on disc | PEEK - Abrasive paper (120 grit SiC) | SEM | 100 | Cutting |
| Harsha et al [2. 30] | RWAT | PEK - Abrasive paper (120 grit SiC) | SEM | 100 | Microcracks |
| Pogacnik et al [2. 32] | Pin on disc | PA6-POM | SEM | 60 | Scratches |
| Cortellucci et al [2. 29] | Pin on cylinder | PTFE-Abrasive paper (120, 220, 320 SiC) | SEM | 700 | Surface channels |
| Chang et al [2. 24] | Pin on disc | NanoTiO2+Graphite +SCF+PTFE/Epoxy - 100Cr6 | AFM | 40 | Nano grooves |
| Kim et al [2. 11] | Block on ring | PPS10%EBA- ASTM 1046 | SEM | 1200 | Grooves |
| Chang et al [2. 19] | Pin on disc | PA66 -Steel | SEM | 4500 | Grooves |
| Bohm et al [2. 23] | Pin on Plate | UHMPE- 431 SS | SEM | 1000 | Ductile tearing |
| Vaziri et al [2. 18] | Pin on disc | PA6- Abrasive paper (800 grit) | SEM | 25 | Grooves |
| Mergler et al [2. 61] | Pin on disc | POMC-AISI 304 | SEM | 100 | Grooves |
| **Therformation** | | | | | |
| Chen et al [2. 44] | Twin-disc | PA 66-PA66 | SEM | 25 | Smearing /melting |
| Liu et al [2. 56] | Pin on disc | UHMWPE-316 SS | SEM | 600 | Wave like pattern |
| Koike et al [2. 35] | RCF testrig | PEEK-Alumina | OM | 800 | Plastic flow |
| Chang et al [2. 19] | Pin on disc | Nano TiO2/PA66 - Steel | SEM | 60 | Fiber removal |
| **Adhesive wear** | | | | | |
| Benabdallah et al [2. 42] | Reciproca-ting sliding | UHMWPE- AISI 4340 | SEM | | Cracks |
| Pogacnik et al [2. 32] | Pin on disc | PA6-POM | SEM | 60 | local melting |

| | | | | | |
|---|---|---|---|---|---|
| Mergler *et al [2. 61]* | Pin on disc | POM-POM | SEM | 50 | Melting |
| Kaltzakort a *et al* [2. 94] | Reciproca -ting sliding | TPU - cast iron GG25 | SEM | | Delamination |
| Chang *et al* [2. 19] | Pin on disc | PA66 -Steel | SEM | 4500 | Smooth surface |
| Avanzini *et al* [2. 45] | Twin-disc | PEEK - Steel | OM | 12000 | Delamination |
| **Fatigue wear** | | | | | |
| Charles *et al* [2. 71] | Twin-disc | Nylon 6 nano composites - Nylon 67 | | | Surface cracking |
| Gordon *et al* [2. 46] | Twin-disc | PA46+12% aramid fibers against itself | OM | 15000 | Pitting/ cracks |
| Chang *et al* [2. 19] | Pin on disc | Nano TiO2/PA66 - Steel | SEM | 30 | Micro cracks |
| Avanzini et al [2. 45] | Twin-disc | PEEK/GF30/CF30/ PTFE - Steel | OM | 1500 | Transversal cracks |
| Avanzini *et al [2. 45]* | Twin-disc | PEEK/CF30 - Steel | Optical Camera | 40000 | Macro- spalling |
| Jain *et al* [2. 40] | Pin on disc | POM-Hardened AISI 4340 Steel | SEM | 100 | Arced ripples |

Starting with the qualitative techniques, tribologists are keen to observe the changes in surface morphology from micron to nano scale. For polymers, different types of microscopic techniques are used based on the specific type of information required. The common limitation is the cost involved in the use of high end techniques such as TEM, AFM and SEM etc. An approximation of the cost involved in using these techniques is given in Table 2-2. These service costs were taken from different source of information including quotes from service providers. The investigations from macro scales were partially justified based on the microlevel information obtained from the worn surface. Hence images of worn surfaces are acquired by different microscopic techniques for most publications and engineering reports.

Table 2-2 Service cost for using the morphology imaging techniques

| Technique | Cost |
| --- | --- |
| TEM | 90 -108 EUR/hour |
| Confocal | 54 EUR/hour |
| FIB | 137 EUR /hour |
| AFM | 143 EUR/half day session |
| Scanning electron microscopy | 150 EUR/hour |
| Energy dispersive spectrometer (EDSS) | 150 EUR/hour |
| Image analysis | 160 EUR/sample |
| Auger | 162 EUR/hour |
| SEM factrography /EDS micro analysis | 400 EUR/sample |
| Sputtering conductive coating (Au, Ag, Cu,C) | 10 EUR/sample |

## 2.7   Advances in monitoring techniques

In all investigations a specific protocol is advisable for having repeatable and reliable results. Since the last decade, usage of protocols and standards are outdated due to the introduction of new materials, equipments and softwares. For instance, most of images reviewed in the last section did not have any imaging protocol in their report to compare with each other. Image resolution is very important in case of tribological studies, misinterpretation is prone to occur if care is not taken for understanding the overall appearance of the worn surface. Chang *et al* reported groove like features in polyamide composite as a consequence of fibre pull-out, where the surface scar showed similar appearance as a groove formed by micro-cutting or third body rolling while investigating under high magnification [2. 24]. The cause for these grooves is thermal softening of the matrix at high contact pressure. Thus, the importance of magnification is very clear and high magnification micrograph could also mislead or create false interpretation [2. 19]. Having understood the importance of morphology imaging which is faster than the quantitative measurements the existing imaging techniques in practice are studied.

The short-comings addressed by the advancements in the monitoring techniques have given a new dimension for tribography. In the recent years the understanding on the development of worn surface "evolution studies" has gained importance. An evolution study by Koki *et al* on real scale PEEK ball bearing with alumina balls showed an adhesion film on the alumina balls [2. 35]. The sequence of events in the wear process showed the formation of a transfer film followed by fragmentation of PEEK deposits on the alumina ball and subsequent back transfer of these fragments to the raceways.

Evolution of wear is required to tell the history of wear process. As reported in the beginning of this chapter, the wear mechanisms change during the wear process. Post

microscopy of the wear scars is rather insufficient to express the damage process experienced by the contact pairs. The change in mechanism as a function of time can be supported by the hypothesis of Shu *et al* who demonstrated the asperity-asperity contact being converted to asperity plane contact [2. 95]. This is similar to polymer-metal tribo-pairs, where the filling of valleys in the steel counterface with polymer debris can be attributed to the change in morphology and geometry from point to plane contact at a local level. Also in polymers, the ductile mode of wear changes the nature of contact through smoothening of the polymer surface by plastic flow [2. 10]. Successive occurrence of micro-ploughing followed by micro-cutting for PET matrix slid against $Al_2O_3$ abrasives was earlier studied [2. 25].

In the evolution studies both *ex-situ* and *in-situ* measurements on the worn surface with different microscopy techniques are already in practice [2. 96, 97, 98, 99, 100, 101, 102, 103, 104, 105, 106, 107, 108, 109, 110, 111]. To understand the evolution, *ex-situ* studies were also performed by Chang *et al* in identifying the change in friction characteristics from the SEM micrographs [2. 19]. The reported friction characteristics seem to correspond with the observed change in surface morphology. An important characteristic feature to be concluded from the discussion is that similarities in terms of friction characteristics are evident due to comparable microstructure between two materials. While comparing PA66 composite and its alternative (nano additives), both materials show similar surface morphology until the running-in phase. In the evolution of wear for both materials, removal of fibres and fracture of surfaces was observed in the running-in stage. As the wear progresses the nano material smoothens the surface, reflected in lower friction characteristics. However, in conventional material friction behaviour remains the same where in the steady state regime the surface morphology also remains the same as in the running stage [2. 19]. Evolution studies were also done by Belin *et al* to understand the changes undergone by the interface during the course of wear [2. 112].

Schofer *et al* performed evolution studies using atomic force microscopy, but it is rather an *in-situ* technique with intermediate pauses. In their case, the specimen was not disturbed by dismounting. However, the test is paused for acquiring the morphological and topographical information [2. 113]. Advanced techniques are used in parallel with conventional techniques for elucidating minute wear, where atomic force microscopy is used together with image processing technique to quantitatively elucidate the wear precisely. Similar investigations were also performed by Kaneko *et al* using a AFM to describe the different stages of micro-wear process of polymer, where three stages with formation of plateau followed by distortion and particle formation in PC, PMMA and EP polymers were observed [2. 88].

In most cases, the counterface material is a relatively harder material. Having a hard counterface, the change undergone by the polymer surface will be significant and produce quantitatively measurable scars at a micro or even on macro scale. Recent advancements in the image processing or 3D scanning techniques can aid in measuring such variables. Apart from hardware oriented advancements, interventions in the software of image processing and analysing contributes significantly in easy understanding and error free interpretation. Advanced techniques such as mathematical morphology, segmentation, blur correction are

effectively used for wear analysis in tribological investigation [2. 96, 114, 115, 116, 117, 118]. Recent advancements in the image processing helps to overcome these constrains in the OM based on depth of field. Z stacking is a technique where several images acquired at different focus plane are fused together to form a single 3D image. Also the 3D microscopy though being an optical system can still acquire image with large depth field. Thus, the latest advancements in the image processing have enabled us to use the optical microscope in a more efficient manner.

## 2.8 Quantitative estimate for tribography

In polymer tribology, most of the research analyse different parameters at several levels. The resulting wear trends are explained from the view point of consequential wear mechanism from selected surface scars. These tests are with several levels of individual parameter due to limited understanding of wear process. The repeatability of specific wear scars characteristics (quantitatively) for one specific condition is scarcely reported. This indicated that among different parameters studied, the surface scars are barely used as a representative in relating the wear characteristics. In spite of it, this can be partly attributed to the limited use of image processing techniques in tribological investigation. Specific operating parameters result in producing a unique output in form of scars and debris. The quantitative value such as roughness profile by itself is merely statistical information on the surface profile. However, qualitative details such as change in surface morphology, colour etc. complement the quantitative data for evaluating the wear mechanism. What is required for the polymer tribological investigation is a balance between the fundamental understandings and engineering implication. However, subjective interpretations are mostly based on the images obtained from the contact surfaces which are more qualitative in nature.

In tribological investigation, microscopy is used for both qualitative and quantitative investigations. The qualitative and quantitative results complement each other and effort has been put on converting the qualitative data to quantitative numbers [2. 119, 120, 121, 122, 123, 124]. The information on the surface appearance correlating to the wear mechanism is subjective and true only to a qualitative extent. Qualitative (micrographs) and quantitative (profile, wear) measurements are effectively used by computer vision only at an engineering level and mostly for metrological inspection of metals. Moore *et al* briefed the measuring techniques and the advantages and disadvantages of quantitative characterization of texture [2. 125]. Such information of qualitative data if looked upon on a micro level leads us further to the fundamental understanding of material behaviour. A qualitative approximation on the severity of the mechanisms was done by many researchers comparing the micrographs. For example, comparing contact conditions, Pogacnik *et al* explained  the intensity of wear in-terms of the depth of scratches [2. 32]. From existing reports the severity in mechanism has been explained from the view point of surface features observed such as depth and width of the scratches. Justification or rationalization of the wear intensity or severity was also done from the SEM images as reported by Quintelier *et al* [2. 126].

In all the existing reports, it is clear that the mechanisms are investigated from the qualitative perspective. However the use of quantitative values is appropriate to define thresholds based on the severity of wear. A statistical approach would be more appropriate in quantitatively estimating the surface features. Chen *et al* also described the severity of the mechanism vaguely estimating the groove width [2. 127]. The width of grooves formed due to abrasion have been approximately estimated as 2 – 7 μm from visual inspection of micrographs images by Vaziri [2. 18]. Harsha *et al* compared the size of the grooves to the particles formed as a consequence of wear, and provide an estimate about the type of mechanism (cutting/ploughing). Byett *et al* determined a quantitative coverage of transfer layer which is in-between 0 – 20 % [2. 28]. Ovaert *et al* also made similar assumptions on the quantitative occupation of transfer film [2. 84]. For the back transfer of polymers from the counter material, Bijwe *et al* described the quantitative measurements from the micrographs [2. 67]. All such quantitative measurements are made from the visualization of micrographs. These document the quantitative measurements on the severity of wear mechanisms.

## 2.9    Summary and conclusions

In polymers, tribological characteristics are affected by its surface morphology and it is evident that they are altered by factors such as sequence of motion, materials and operational parameters. One should bear in mind that these factors result in producing a specific type of wear scars. It is also clear that a disparity exists on segregating the information from the worn surface into (i) wear mechanism, (ii) phenomenon and (iii) wear scars. In our discussion on wear scars we conclude that the observation (wear scar) is a consequence of phenomenon led by specific wear mechanism. The wear mechanism itself is dominated by the operational parameters and the materials.

It is a question of who is investigating what? An engineer in the maintenance or manufacturing or design sector primarily controls the wear process by altering the working parameters. Scientists look from more of a fundamental perspective to understand underlying mechanisms thus, leaving less priority to the practicality by creating ideal conditions (laboratory testing at microscale) for the investigations. Apart from the classical fundamental understanding of wear mechanisms, the practice of justifying wear hypothesis is performed from monitoring the worn surface in the post-mortem analysis. Both the engineers and the scientist look at the worn surface to understand the wear process. But the aim of two groups vary where the engineers look at the macro level correlating with the global behaviour and the scientists look at the submicron level to estimate the consequence of micro modification on the overall behaviour of the material.

Connecting both groups is the tribo-tree where an atlas of the wear scars is required for which images from different stages of wear can serve as a template for both engineering studies and fundamental studies. Polymers being a crucial material in tribological application a sequential understanding of their wear process are essential. The template by means of evolution studies can be obtained by online

monitoring system so that the images from different stages are recorded *in-situ* without disturbing the equilibrium of the testing. From an engineering perspective these images can serve to monitor the condition of the surface from time to time. Also information about the severity using inline testing can aid material designers to modify their composition based on the dominating mechanism observed on the testing which can be compared with the earlier obtained template.

In the selection of an appropriate microscopy for an efficient usage, optical microscopy is effective in terms of cost, resolution and portability. Online measurements for morphological changes are still a challenge for tribologists but with the recent advancements in the image processing the online images through OM can be effectively made. On achieving a certain degree of repeatability, standardization of imaging techniques has to be made for which a protocol has to be strictly followed in terms of size, and other influencing factors producing artefacts.

It is evident in the discussion that an approach common to both the groups has to be made which is economic, less time consuming and revealing the important details in a wear process. Such an approach will be applicable only in the case of standardisation of wear micrographs at a laboratory scale and using them as a template for field investigations.

# References

[2.1]    J. K. Lancaster, "Material-specific wear mechanisms: relevance to wear modelling," Wear, vol. 141, pp. 159-183, 1990.

[2.2]    S. W. Zhang, "State-of-the-art of polymer tribology," Tribology International, vol. 31, pp. 49-60, 1998.

[2.3]    J. K. Lancaster, "Dry bearings," Tribology International, vol. 11, pp. 19-20, 1978.

[2.4]    J. K. Lancaster, "Dry bearings: a survey of materials and factors affecting their performance," Tribology, vol. 6, pp. 219-251, 1973.

[2.5]    J. W. M. Mens and A. W. J. de Gee, "Friction and wear behaviour of 18 polymers in contact with steel in environments of air and water," Wear, vol. 149, pp. 255-268, 1991.

[2.6]    G. M. Bartenev and V. V. Lavrentev, Friction and Wear of Polymers: Elsevier Science, 1981.

[2.7]    B. J. Briscoe and S. K. Sinha, "Wear of polymers," Proceedings of the Institution of Mechanical Engineers, Part J: Journal of Engineering Tribology, vol. 216, pp. 401-413, 2002.

[2.8]    Y. Yamaguchi, Tribology of Plastic Materials: Their Characteristics and Applications to Sliding Components: Elsevier Science, 1990.

[2.9]    R. G. Bayer, Mechanical Wear Fundamentals and Testing, Taylor & Francis, 2004.

[2.10]   M. Clerico and V. Patierno, "Sliding wear of polymeric composites," Wear, vol. 53, pp. 279-301, 1979.

[2.11]   S. S. Kim, M. W. Shin, and H. Jang, "The Wear Mechanism of a Polyphenylene Sulfide (PPS) Composite Mixed with Ethylene Butyl Acrylate (EBA)," Tribology Letters, vol. 47, pp. 165-173, 2012.

[2.12]   A. Dasari, Z.-Z. Yu, and Y.-W. Mai, "Fundamental aspects and recent progress on wear/scratch damage in polymer nanocomposites," Materials Science and Engineering: R: Reports, vol. 63, pp. 31-80, 2009.

[2.13]   R. G. Bayer, Wear Analysis for Engineers: HNB Publishing, 2002.

[2.14]   J. D. Huffington, "Abrasion groove sizes and shapes in relation to the mechanism of abrasion," Wear, vol. 49, pp. 327-337, 1978.

[2.15]   K. Tanaka, Y. Uchiyama, and S. Toyooka, "The mechanism of wear of polytetrafluoroethylene," Wear, vol. 23, pp. 153-172, 1973.

[2.16]   J. D. Huffington, "The frictional method of measuring contact area between surfaces and its relation to the surface microtopography of some abraded metals and polymers," Wear, vol. 12, pp. 343-356, 1968.

[2.17]   A. P. Harsha, "An investigation on low stress abrasive wear characteristics of high performance engineering thermoplastic polymers," Wear, vol. 271, pp. 942-951, 2011.

[2.18]   M. Vaziri, R. T. Spurr, and F. H. Stott, "An investigation of the wear of polymeric materials," Wear, vol. 122, pp. 329-342, 1988.

[2.19]   L. Chang, Z. Zhang, H. Zhang, and A. K. Schlarb, "On the sliding wear of nanoparticle filled polyamide 66 composites," Composites Science and Technology, vol. 66, pp. 3188-3198, 2006.

[2.20]   K. H. Z. Gahr, "Microstructure and wear of materials," in Tribology Series. vol. Volume 10, G. Karl-Heinz Zum, Elsevier, pp. v-vi, 1987.

[2.21]   J. K. Lancaster, "The effect of carbon fibre reinforcement on the friction and wear of polymers," Journal of Physics D: Applied Physics, vol. 1, p. 549, 1968.

[2.22]   L. C. Seabra and A. M. Baptista, "Tribological behaviour of food grade polymers against stainless steel in dry sliding and with sugar," Wear, vol. 253, pp. 394-402, 2002.

[2.23]   H. Böhm, S. Betz, and A. Ball, "The wear resistance of polymers," Tribology International, vol. 23, pp. 399-406, 1990.

[2.24]   L. Chang and K. Friedrich, "Enhancement effect of nanoparticles on the sliding wear of short fiber-reinforced polymer composites: A critical discussion of wear mechanisms," Tribology International, vol. 43, pp. 2355-2364, 2010.

[2.25]   K. Friedrich and M. Cyffka, "On the wear of reinforced thermoplastics by different abrasive papers," Wear, vol. 103, pp. 333-344, 1985.

[2.26]   Z. Chen, X. Liu, R. Lü, and T. Li, "Mechanical and tribological properties of PA66/PPS blend. III. Reinforced with GF," Journal of Applied Polymer Science, vol. 102, pp. 523-529, 2006.

[2.27]   Z. Chen, X. Liu, R. Lü, and T. Li, "Friction and wear mechanisms of PA66/PPS blend reinforced with carbon fiber," Journal of Applied Polymer Science, vol. 105, pp. 602-608, 2007.

[2.28]   J. H. Byett and C. Allen, "Dry sliding wear behaviour of polyamide 66 and polycarbonate composites," Tribology International, vol. 25, pp. 237-246, 1992.

[2.29]   R. Cortellucci, C. J. Heim, T. D. Koshy, and P. J. Phillips, "Abrasion of plastics," Wear, vol. 47, pp. 397-405, 1978.

[2.30]   A. P. Harsha and U. S. Tewari, "Two-body and three-body abrasive wear behaviour of polyaryletherketone composites," Polymer Testing, vol. 22, pp. 403-418, 2003.

[2.31]   R. Ashok Gandhi, K. Palanikumar, B. K. Ragunath, and J. Paulo Davim, "Role of carbon nanotubes (CNTs) in improving wear properties of polypropylene (PP) in dry sliding condition," Materials & Design, vol. 48, pp. 52-57, 2013.

[2.32]   A. Pogačnik and M. Kalin, "Parameters influencing the running-in and long-term tribological behaviour of polyamide (PA) against polyacetal (POM) and steel," Wear, vol. 290–291, pp. 140-148, 2012.

[2.33]   C. M. Pooley and D. Tabor, "Friction and Molecular Structure: The Behaviour of Some Thermoplastics," Proceedings of the Royal Society of London. A. Mathematical and Physical Sciences, vol. 329, pp. 251-274, 1972.

[2.34]   H. Czichos, "Influence of adhesive and abrasive mechanisms on the tribological behaviour of thermoplastic polymers," Wear, vol. 88, pp. 27-43, 1983.

[2.35]   H. Koike, K. Kida, E. C. Santos, J. Rozwadowska, Y. Kashima, and K. Kanemasu, "Self-lubrication of PEEK polymer bearings in rolling contact fatigue under radial loads," Tribology International, vol. 49, pp. 30-38, 2012.

[2.36]   M. K. Kar and S. Bahadur, "Micromechanism of wear at polymer-metal sliding interface," Wear, vol. 46, pp. 189-202, 1978.

[2.37]  V. Rodriguez, J. Sukumaran, Y. P. Delgado, M. Staia, A. Iost, and P. De Baets, "Scratch evaluation on a high performance polymer," Mechanical Engineering Letters, Szent István University, pp. 76, 2013.

[2.38]  N. Myshkin, M. Petrokovets, and A. Kovalev, "Tribology of polymers: adhesion, friction, wear, and mass-transfer," Tribology International, vol. 38, pp. 910-921, 2006.

[2.39]  C. Lhymn, "Microscopy study of the frictional wear of polytetrafluoroethylene," Wear, vol. 107, pp. 95-105, 1986.

[2.40]  V. K. Jain and S. Bahadur, "An investigation of the markings on wear and fatigue fracture surfaces," Wear, vol. 75, pp. 357-368, 1982.

[2.41]  M. K Omar, A. G. Atkins, J. K. Lancaster, "The role of crack resistance parameters in polymer wear," Jounal of physics D: Applied physics, vol. 19, pp. 18, 1986.

[2.42]  H. S. Benabdallah, "Reciprocating sliding friction and contact stress of some thermoplastics against steel," Journal of Materials Science, vol. 32, pp. 5069-5083, 11997.

[2.43]  B. J. Briscoe, A. Chateauminois, T. C. Lindley, and D. Parsonage, "Contact damage of poly (methylmethacrylate) during complex microdisplacements," Wear, vol. 240, pp. 27-39, 2000.

[2.44]  Y. K. Chen, S. N. Kukureka, C. J. Hooke, and M. Rao, "Surface topography and wear mechanisms in polyamide 66 and its composites," Journal of Materials Science, vol. 35, pp. 1269-1281, 2000.

[2.45]  A. Avanzini, G. Donzella, A. Mazzù, and C. Petrogalli, "Wear and rolling contact fatigue of PEEK and PEEK composites," Tribology International, vol. 57, pp. 22-30, 2013.

[2.46]  D. H. Gordon and S. N. Kukureka, "The wear and friction of polyamide 46 and polyamide 46/aramid-fibre composites in sliding-rolling contact," Wear, vol. 267, pp. 669-678, 2009.

[2.47]  M. Rao, C. J. Hooke, S. N. Kukureka, P. Liao, and Y. K. Chen, "The effect of PTFE on the friction and wear behavior of polymers in rolling-sliding contact," Polymer Engineering & Science, vol. 38, pp. 1946-1958, 1998.

[2.48]  T. A. Stolarski, "Tribology of polyetheretherketone," Wear, vol. 158, pp. 71-78, 1992.

[2.49]  C. J. Hooke, S. N. Kukureka, P. Liao, M. Rao, and Y. K. Chen, "Wear and friction of nylon-glass fibre composites in non-conformal contact under combined rolling and sliding," Wear, vol. 197, pp. 115-122, 1996.

[2.50]  C. J. Hooke, S. N. Kukureka, P. Liao, M. Rao, and Y. K. Chen, "The friction and wear of polymers in non-conformal contacts," Wear, vol. 200, pp. 83-94, 1996.

[2.51]  S. N. Kukureka, Y. K. Chen, C. J. Hooke, and P. Liao, "The wear mechanisms of acetal in unlubricated rolling-sliding contact," Wear, vol. 185, pp. 1-8, 1995.

[2.52]  S. N. Kukureka, C. J. Hooke, M. Rao, P. Liao, and Y. K. Chen, "The effect of fibre reinforcement on the friction and wear of polyamide 66 under dry rolling-sliding contact," Tribology International, vol. 32, pp. 107-116, 1999.

[2.53]   T. A. Stolarski, S. M. Hosseini, and S. Tobe, "Surface fatigue of polymers in rolling contact," Wear, vol. 214, pp. 271-278, 1998.

[2.54]   M. Harrass, K. Friedrich, and A. A. Almajid, "Tribological behavior of selected engineering polymers under rolling contact," Tribology International, vol. 43, pp. 635-646.

[2.55]   M. Wong, G. T. Lim, A. Moyse, J. N. Reddy, and H. J. Sue, "A new test methodology for evaluating scratch resistance of polymers," Wear, vol. 256, pp. 1214-1227, 2004.

[2.56]   C. Z. Liu, J. Q. Wu, J. Q. Li, L. Q. Ren, J. Tong, and A. D. Arnell, "Tribological behaviours of PA/UHMWPE blend under dry and lubricating condition," Wear, vol. 260, pp. 109-115, 2006.

[2.57]   J. K. Lancaster, "Polymer-based bearing materials: The role of fillers and fibre reinforcement," Tribology, vol. 5, pp. 249-255, 1972.

[2.58]   S. Bahadur, "The development of transfer layers and their role in polymer tribology," Wear, vol. 245, pp. 92-99, 2000.

[2.59]   M. H. Cho, "The role of transfer film and back transfer behavior on the tribological performance of polyoxymethylene in sliding," Journal of Mechanical Science and Technology, vol. 23, pp. 2291-2298, 2009.

[2.60]   A. Kapoor and S. Bahadur, "Transfer film bonding and wear studies on CuS-nylon composite sliding against steel," Tribology International, vol. 27, pp. 323-329, 1994.

[2.61]   Y. J. Mergler, R. P. Schaake, and A. J. Huis in't Veld, "Material transfer of POM in sliding contact," Wear, vol. 256, pp. 294-301, 2004.

[2.62]   S. H. Rhee and K. C. Ludema, "Mechanisms of formation of polymeric transfer films," Wear, vol. 46, pp. 231-240, 1978.

[2.63]   S. E. Franklin and A. de Kraker, "Investigation of counterface surface topography effects on the wear and transfer behaviour of a POM–20% PTFE composite," Wear, vol. 255, pp. 766-773, 2003.

[2.64]   M. Chandrasekaran, L. Y. Wei, K. K. Venkateshwaran, A. W. Batchelor, and N. L. Loh, "Tribology of UHMWPE tested against a stainless steel counterface in unidirectional sliding in presence of model synovial fluids: part 1," Wear, vol. 223, pp. 13-21, 1998.

[2.65]   K. Marcus, A. Ball, and C. Allen, "The effect of grinding direction on the nature of the transfer film formed during the sliding wear of ultrahigh molecular weight polyethylene against stainless steel," Wear, vol. 151, pp. 323-336, 1991.

[2.66]   A. I. Sviridyonok, V. A. Bely, V. A. Smurugov, and V. G. Savkin, "A study of transfer in frictional interaction of polymers," Wear, vol. 25, pp. 301-308, 1973.

[2.67]   J. Bijwe and R. Rattan, "Influence of weave of carbon fabric in polyetherimide composites in various wear situations," Wear, vol. 263, pp. 984-991, 2007.

[2.68]   S. M. Aharoni, "Wear of polymers by roll-formation," Wear, vol. 25, pp. 309-327, 1973.

[2.69]   P. Sampathkumaran, S. Seetharamu, A. Murali, R. K. Kumar, and Kishore, "Sliding wear studies in glass-epoxy system through scanning microscopic observations," Bulletin of Materials Science, vol. 21, pp. 335-339, 1998.

[2.70]   S. M. Hosseini and T. A. Stolarski, "Morphology of polymer wear debris resulting from different contact conditions," Journal of Applied Polymer Science, vol. 45, pp. 2021-2030, 1992.

[2.71]   D. F. Charles, R. Gnanamoorthy, and P. Ravindran, "Rolling contact fatigue behavior of polyamide clay reinforced nanocomposite—Effect of load and speed," Wear, vol. 269, pp. 565-571, 2010.

[2.72]   C. Ren, J. Chen, H. Pan, X. Huang, and H. Zhu, "Wear mechanism of PA6 roller used in cold rolling process," Engineering Failure Analysis, vol. 28, pp. 311-317, 2013.

[2.73]   C. C. Lawrence and T. A. Stolarski, "Rolling contact wear of polymers: A preliminary study," Wear, vol. 132, pp. 183-191, 1989.

[2.74]   Y. Liu and S. K. Sinha, "Wear performances and wear mechanism study of bulk UHMWPE composites with nacre and CNT fillers and PFPE overcoat," Wear, vol. 300, pp. 44-54, 2013.

[2.75]   H. Zhang, Z. Zhang, and K. Friedrich, "Effect of fiber length on the wear resistance of short carbon fiber reinforced epoxy composites," Composites Science and Technology, vol. 67, pp. 222-230, 2007.

[2.76]   C. A. Chairman and S. P. Kumaresh Babu, "Mechanical and abrasive wear behavior of glass and basalt fabric-reinforced epoxy composites," Journal of Applied Polymer Science, vol. 130, pp. 120-130, 2013.

[2.77]   S. Hogmark, S. Jacobson, O. Vingsbo, "Surface damage", ASM Handbook: ASM International,A. I. H. Committee ed. 1992.

[2.78]   "Introduction to Polymer Morphology," in Polymer Microscopy, ed: Springer New York, pp. 1-25, 2008.

[2.79]   L. C. Sawyer, D. T. Grubb, and G. F. Meyers, Polymer Microscopy: Springer, 2008.

[2.80]   D. H. Buckley, "The use of analytical surface tools in the fundamental study of wear," Wear, vol. 46, pp. 19-53, 1978.

[2.81]   A. P. Harsha and U. S. Tewari, "Tribo performance of polyaryletherketone composites," Polymer Testing, vol. 21, pp. 697-709, 2002.

[2.82]   D. Scott and G. H. Mills, "Scanning electron microscopical study of fibre reinforced polymeric cage materials for rolling bearings," Polymer, vol. 14, pp. 130-132, 1973.

[2.83]   J. R. T. Branco and S. V. Campos, "Wear behavior of thermally sprayed PET," Surface and Coatings Technology, vol. 120–121, pp. 476-481, 1999.

[2.84]   T. C. Ovaert and H. S. Cheng, "Counterface topographical effects on the wear of polyetheretherketone and a polyetheretherketone-carbon fiber composite," Wear, vol. 150, pp. 275-287, 1991.

[2.85]   R. Kaneko, S. Oguchi, S. Hara, R. Matsuda, T. Okada, H. Ogawa, "Atomic force microscope coupled with an optical microscope," Ultramicroscopy, vol. 42–44, Part 2, pp. 1542-1548, 1992.

[2.86]   E. Meyer, H. Heinzelmann, P. Grütter, T. Jung, H. R. Hidber, H. Rudin, "Atomic force microscopy for the study of tribology and adhesion," Thin Solid Films, vol. 181, pp. 527-544, 1989.

[2.87]   M. Špírková, M. Šlouf, O. Bláhová, T. Farkačová, and J. Benešová, "Submicrometer characterization of surfaces of epoxy-based organic–

inorganic nanocomposite coatings. A comparison of AFM study with currently used testing techniques," Journal of Applied Polymer Science, vol. 102, pp. 5763-5774, 2006.

[2.88]    R. Kaneko and E. Hamada, "Microwear processes of polymer surfaces," Wear, vol. 162–164, Part A, pp. 370-377, 1993.

[2.89]    E. Hamada and R. Kaneko, "Micro-tribological evaluations of a polymer surface by atomic force microscopes," Ultramicroscopy, vol. 42–44, Part 1, pp. 184-190, 1992.

[2.90]    R. Höper, T. Gesang, W. Possart, O. D. Hennemann, and S. Boseck, "Imaging elastic sample properties with an atomic force microscope operating in the tapping mode," Ultramicroscopy, vol. 60, pp. 17-24, 1995.

[2.91]    E. W. Stroup, A. Pungor, and V. Hlady, "A constant compliance force modulation technique for scanning force microscopy (SFM) imaging of polymer surface elasticity," Ultramicroscopy, vol. 66, pp. 237-249, 1996.

[2.92]    M. W. Phaneuf, "Applications of focused ion beam microscopy to materials science specimens," Micron, vol. 30, pp. 277-288, 1999.

[2.93]    W. Brostow, B. P. Gorman, and O. Olea-Mejia, "Focused ion beam milling and scanning electron microscopy characterization of polymer + metal hybrids," Materials Letters, vol. 61, pp. 1333-1336, 2007.

[2.94]    O. Kaltzakorta, R. Wäsche, M. Hartelt, A. Aginagalde, and W. Tato, "Influence of Polymer Filler on Tribological Properties of Thermoplastic Polyurethane Under Oscillating Sliding Conditions Against Cast Iron," Tribology Letters, vol. 48, pp. 209-216, 2012.

[2.95]    N. P. Suh, "An overview of the delamination theory of wear," Wear, vol. 44, pp. 1-16, 1977.

[2.96]    S. Kano, H. Homma, S. Sasaki, and H. Shimura, "In situ monitoring of friction surfaces and their sequence pattern analysis," Philos Trans A Math Phys Eng Sci, vol. 366, pp. 665-71, 2008.

[2.97]    J. Ye, H. S. Khare, and D. L. Burris, "Transfer film evolution and its role in promoting ultra-low wear of a PTFE nanocomposite," Wear, vol. 297, pp. 1095-1102.

[2.98]    T. R. Bates Jr, K. C. Ludema, and W. A. Brainard, "A rheological mechanism of penetrative wear," Wear, vol. 30, pp. 365-375, 1974.

[2.99]    R. R. Chromik, C. C. Baker, A. A. Voevodin, and K. J. Wahl, "In situ tribometry of solid lubricant nanocomposite coatings," Wear, vol. 262, pp. 1239-1252, 2007.

[2.100]  I. Etsion, "Discussion of the Paper: Optical In Situ Micro Tribometer for Analysis of Real Contact Area for Contact Mechanics, Adhesion, and Sliding Experiments," Tribology Letters, vol. 46, pp. 205-205, 2012.

[2.101]  W. A. Glaeser, "Wear experiments in the scanning electron microscope," Wear, vol. 73, pp. 371-386, 1981.

[2.102]  K. Hokkirigawa and K. Kato, "An experimental and theoretical investigation of ploughing, cutting and wedge formation during abrasive wear," Tribology International, vol. 21, pp. 51-57, 1988.

[2.103]  T. Kayaba, K. Hokkirigawa, and K. Kato, "Analysis of the abrasive wear mechanism by successive observations of wear processes in a scanning electron microscope," Wear, vol. 110, pp. 419-430, 1986.

[2.104]  B. Krick, J. Vail, B. J. Persson, and W. G. Sawyer, "Optical In Situ Micro Tribometer for Analysis of Real Contact Area for Contact Mechanics, Adhesion, and Sliding Experiments," Tribology Letters, vol. 45, pp. 185-194, 2012.

[2.105]  S. C. Lim and J. H. Brunton, "A dynamic wear rig for the scanning electron microscope," Wear, vol. 101, pp. 81-91, 1985.

[2.106]  J. Michler, R. Rabe, J. L. Bucaille, B. Moser, P. Schwaller, and J. M. Breguet, "Investigation of wear mechanisms through in situ observation during microscratching inside the scanning electron microscope," Wear, vol. 259, pp. 18-26, 2005.

[2.107]  B. Murarash and M. Varenberg, "Tribometer for In Situ Scanning Electron Microscopy of Microstructured Contacts," Tribology Letters, vol. 41, pp. 319-323, 2011.

[2.108]  A. Ovcharenko, G. Halperin, I. Etsion, and M. Varenberg, "A novel test rig for in situ and real time optical measurement of the contact area evolution during pre-sliding of a spherical contact," Tribology Letters, vol. 23, pp. 55-63, 2006.

[2.109]  D. A. Rigney, L. H. Chen, M. G. S. Naylor, and A. R. Rosenfield, "Wear processes in sliding systems," Wear, vol. 100, pp. 195-219, 1984.

[2.110]  T. W. Scharf and I. L. Singer, "Role of Third Bodies in Friction Behavior of Diamond-like Nanocomposite Coatings Studied by In Situ Tribometry," Tribology Transactions, vol. 45, pp. 363-371, 2002.

[2.111]  H. E. Sliney, "Dynamics of Solid Lubrication as Observed by Optical Microscopy," A S L E Transactions, vol. 21, pp. 109-117, 1978.

[2.112]  M. Belin and J. M. Martin, "Triboscopy, a new approach to surface degradations of thin films," Wear, vol. 156, pp. 151-160, 1992.

[2.113]  J. Schöfer and E. Santner, "Quantitative wear analysis using atomic force microscopy," Wear, vol. 222, pp. 74-83, 1998.

[2.114]  J. Sukumaran, S. Soleimani, P. De Baets, V. Rodriguez, K. Douterloigne, W. Philips, "High-speed imaging for online micrographs of polymer composites in tribological investigation," Wear, vol. 296, pp. 702-712, 2012.

[2.115]  Y. C. Tasan, M. B. de Rooij, and D. J. Schipper, "Measurement of wear on asperity level using image-processing techniques," Wear, vol. 258, pp. 83-91, 2005.

[2.116]  C. Gunkel, A. Stepper, A. Müller, and C. Müller, "Micro crack detection with Dijkstra's shortest path algorithm," Machine Vision and Applications, vol. 23, pp. 589-601, 2012.

[2.117]  J. Sukumaran, P. De Baets, V. Rodriguez Fereira, Y. Perez Delgado, J. De Pauw, and M. Ando, "The need for online microstructural image acquisition for tribological charecterisation in rolling/sliding contacts," in 29th Meeting of the International research group on wear of engineering materials IRG-OECD, pp. 21-22, 2013.

[2.118]  S. Soleimani, J. P. Sukumaran, K. Douterloigne, F. Rooms, W. Philips, and P. De Baets, "Correction, stitching and blur estimation of micro-graphs obtained at high speed," in Advanced Concepts for Intelligent Vision Systems, pp. 84-95, 2012.

[2.119]  BY Lee, and H. Juan,, "The model of surface roughness inspection by vision system in turning," Mechatronics, vol. 14, p. 12, 2001.

[2.120]  S. Damodarasamy and S. Raman, "Texture analysis using computer vision," Computers in Industry, vol. 16, pp. 25-34, 1991.

[2.121]  H. A. ElMaraghy and D. J. Bullis, "Expert inspector of surface defects," Computers in Industry, vol. 11, pp. 321-331, 1989.

[2.122]  G. Galante, M. Piacentini, and V. F. Ruisi, "Surface roughness detection by tool image processing," Wear, vol. 148, pp. 211-220, 1991.

[2.123]  D. E. P. Hoy and F. Yu, "Surface quality assessment using computer vision methods," Journal of Materials Processing Technology, vol. 28, pp. 265-274, 1991.

[2.124]  N. K. Myshkin, A. Y. Grigoriev, and O. V. Kholodilov, "Quantitative analysis of surface topography using scanning electron microscopy," Wear, vol. 153, pp. 119-133, 1992.

[2.125]  D. F. Moore, "A history of research on surface texture effects," Wear, vol. 13, pp. 381-412, 1969.

[2.126]  J. Quintelier, P. De Baets, P. Samyn, and D. Van Hemelrijck, "On the SEM features of glass–polyester composite system subjected to dry sliding wear," Wear, vol. 261, pp. 703-714, 2006.

[2.127]  Z. Chen, T. Li, X. Liu, and R. Lü, "Friction and wear mechanisms of polyamide 66/high density polyethylene blends," Journal of Polymer Science Part B: Polymer Physics, vol. 43, pp. 2514-2523, 2005.

# Chapter 3

# Materials and test methods
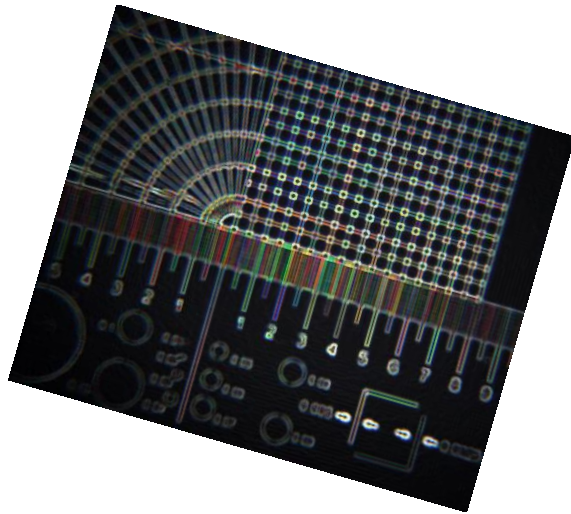
# Goal

Chapter 1 suggests that the present understanding on wear of polymers in rolling contact is insufficient and far from the real application. From chapter 2 it is clear that the morphological feature of surface scars can provide evidence of the wear process and its severity. This chapter discusses the different test methodologies which can be used for an efficient wear monitoring system using morphological characteristics. Possibilities for using the traditional tribological study (TTS) and damage evolution study (DES) are discussed in detail. In TTS a traditional protocol describes the conventional practises where the study includes reference investigation before testing, followed by wear testing and post-mortem analysis. However, in the test protocol of DES, intermediate pauses at specific intervals are made for wear investigation. Both the protocols are designed prioritizing the observation of micron level changes on the worn surfaces. The objectives for developing the protocol are clearly defined where the global and local wear is to be monitored in TTS and DES respectively. Particle generation and dynamicity involved in the wear process are to be understood through *ex-situ* methodology in the "damage evolution study". Moreover, this chapter also includes a detailed explanation on the materials choice and operating parameters. This chapter clearly describes the measuring procedure and the imaging technique used in chapters 4 and 5 are also discussed.

# 3.1 Test methodologies for wear phenomenon studies

Lab experiments are the most complicated and interesting part of tribological research. Care should be taken on choosing the contact conditions, instrumentation, material preparation and test methodology. A stringent protocol is necessary to have ideal conditions for achieving comparable results (repeatability). An exploratory approach is used in investigating the wear mechanism of polymer-metal pairs in rolling-sliding contacts. The tribological behaviour of applications is generally studied using standardized contact configurations. Investigations using real components are less effective due to its extensive time consumption and rather expensive. Besides result related challenges such as dynamicity in transfer layer formation, unknown wear process, and complexity in the contact geometry are unavoidable. However, to a large extent such complexities are eliminated in the model testing.

In the current research, a twin-disc model with Hertzian line contact for contacting bodies at different velocity replicates the partial sliding of a tribological system. In polymer sliding it is well known that the tribological characteristics is primarily dominated by features related to asperities of the counterface material (steel) [3.1]. The morphological characteristics at micron scale are studied through SEM, stylus profilometry and optical microscopy. Post-mortem imaging of the contact surface for both polymer and the counterface material is made to explore the interaction between the mating surface and transfer layer deposition.

Dimensional changes or mass loss in the wear processes are assessed using offline techniques. The asperity morphology in both polymer and steel changes significantly as a function of particle generation in polymers. For this reason the evolution study

is a major point of interest in the present research. Also, from the previous chapters it was evident that traditionally techniques alone cannot completely articulate the history of the wear process. Moreover, it was understood that the traditional post-mortem analysis cannot display intermediate wear mechanisms. Thus, two separate sets of test sequences were followed to understand the wear process of polymers in rolling-sliding contacts:

1. "A traditional tribological study" (TTS) to understand the transition in mechanism from pure rolling to partial sliding.
2. "A damage evolution study" (DES) of wear process through *ex-situ* techniques.

The TTS follows a set of standard procedures with conventional wear measurements (mass loss and dimensional change) for studying the influencing parameter of interest (in our case, slip ratio). The DES is a time-series study to understand the evolution of surface morphology.

Any tribological investigation comprises three steps: (1) specimen preparation (2) wear testing and (3) surface analysis. For specimen preparation a protocol was developed which is same for both test sequences (TTS and DES). In the present research, the novelty in terms of the used techniques is introduced in both the approaches. "Relocation micrography" is a newly developed technique to locate the same region of interest (ROI). Moreover, quantitative micrography is introduced for wear scar investigation. In the below section the importance of TTS and DES are discussed in detail. A schematic of both approaches is given in Figure 3-1. More details about the protocol for TTS and DES can be found in Appendix C.
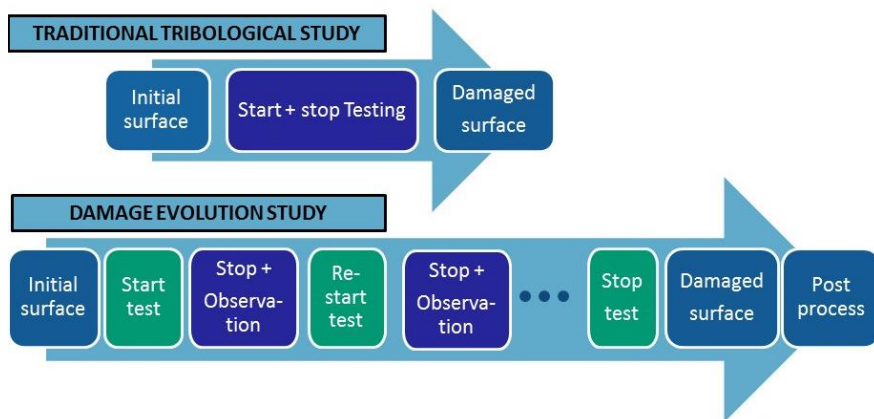


Figure 3-1 Schematic of the testing protocol for TTS and DES.

## 3.2 Traditional tribological study (TTS)

In rolling, commonly manifested phenomena are micro-pitting, spalling and surface cracks [3.2, 3]. When partial sliding is introduced, there is a high possibility for grooving phenomena. These grooves can be formed by both ploughing and micro-cutting. However, in a combined rolling-sliding condition, a combination of these two surface scars is expected, but their dominancy and the transition of wear mechanism

are still unknown. Even existing reports does not clearly discusses the transition in wear mechanism [3.3, 4, 5, 6]. Our ultimate aim here in this test sequence is to understand the transition of wear mechanism as a function of partial sliding and its effects on global wear behaviour. In TTS wear testing of different slip ratio is realized by different tests. The sequence aids to understand the change in surface morphology as a consequence of wear mechanism transition from pure rolling to partial sliding condition in polymer-metal pairs.

Only few studies were carried out on rolling contact of polymers, most of them evaluate wear from the nominal contact dimensions [3. 4, 6, 7]. However, the link between severity of wear and its mechanisms are less explained. In literature post-mortem analysis of worn polymer surface show evidence of the initial surface texture (machine marks) [3. 3, 8]. This clearly describes the damage of such contacts are merely at the asperity level. Thus, in TTS two scales of wear are studied (1) wear (from mass loss and change in nominal contact dimension) and (2) surface texture modification in the wear scars.

It was understood from chapter 2 that the wear scar provides information about specific mechanism (in our case abrasion or fatigue). However, severity of the mechanisms are still unclear, which will be studied using quantitative micrography. Thus, in the current chapter, a novel approach of quantitative micrography, is introduced in the tribological science. The evaluation of surface scars has always been subjective, where an expert qualitatively characterizes the severity of wear mechanisms. Thus in the current investigation using TTS a combined approach of qualitative and quantitative analysis of wear mechanism transition was studied using contact measurements (stylus profilometry), micrographs and image analysis. Image segmentation was performed for characterizing the surface features quantitatively. Comparison of quantitative values and the observer scores were carried out for validation. Further to which SEM studies were also performed for selected specimens (0% and 26% partial sliding). One of the dominating phenomena in polymer tribology is transfer layer formation which is also evaluated by cross-sectional study and roughness measurements.

Apart from these objectives, the output from the TTS provides the limits for "damage evolution studies" in terms of test duration and maximum operation temperature. Adaptations of range in test parameters for contact pressure and test duration are done based on the observation in the preliminary testing to improve the experimental results and to attain precision and repeatability.

## 3.3 Damage evolution study (DES)

In damage evolution study, the experiments are focused on understanding the sequential surface modification at micron scale and the corresponding tribological response. The set of data (images of surface scars) obtained from partial sliding conditions will clearly point out the variation in friction behaviour of the tribo-system. An interrupted wear testing methodology is adopted to monitor the momentary change of the polymer and steel surface. Consequently, during the intermediate pause an *ex-situ* approach for microscopic inspection was used. *Ex-situ* approach is already in practice for transfer layer studies [3. 10]. At each intermediate pause,

surface characteristics are recorded using photomacrograph, optical micrograph and a 2D line trace of the surface. The roughness parameters are used to validate and understand the representativeness of the image analysis in wear characterization. The steel surface which has roughness valleys from the machine marks is monitored by measuring Ra, Rmax, Rsk, Rku, Rpk and Rvk in the same region at different intervals of time. It is evident from the literature that the transfer layer formation is a dynamic process. However, by conventional post-mortem wear scar observations does not provide any details on these dynamic tribological behaviours. Thus in the DES the dynamicity of the transfer layer formation is studied from the surface characteristics of counterface material.

The total number of rotations is partly dependent on contact pressure, velocity and the operational temperature and observable wear. Thus, parameters such as rpm, load and duration of testing has been decided based on the results from TTS and preliminary testing. In TTS, tests are performed for $3.0 \cdot 10^5$ rotations. The preliminary testing in TTS elucidates the running-in, transition and steady stage. Thus the number of intermediate pauses was decided based on the time/rotations required for completing the running-in and transition stage. To segregate the effect of temperature or melting, the temperature profile is monitored.

In regards to image analysis, the damage evolution study follows techniques such as granulometry, segmentation and energy of the grey scale texture. The images were registered in the first place to follow the sequence of events for logical reasoning of the tribological process.

## 3.4 Materials

A basic engineering polymer composite which is commonly used in rolling contact condition has been chosen. In the current investigation, a commercially available polyamide composite (GF/PA 66) reinforced with 30% short glass fibers (DOCAMID 66-GF30, Quattroplast, Hungary) was used. GF/PA 66 has been frequently used in rolling-sliding applications such as gears, cams and rollers. The detailed material properties as provided by the supplier are specified in Table 3-1. GF/PA66 is not a novel material, the composite is known for its high strength and abrasion resistance. Very often, researches choose a basic material (polyamide composite) for an exploratory research (which is in our case the representativeness of surface cars for wear characterisation). Besides, the focus is to study the particle generation process in polymers and understand the transfer layer characteristic. The main objective of our investigation is to study the wear scars from partial sliding condition thereby understanding the mechanism observed on the worn surface. Existing researches on polymers in rolling-sliding contact have already used polyamide composites as the test material [3. 4, 8]. The use of similar material acts as a reference for validation purpose. An additional advantage of selecting short fibre reinforced polymer composite is that the role of third body abrasion can be easily understood from the glass fibre debris. Having short glass fibre as reinforcement, the condition of the debris will also reveal the aggressive nature of contact. The damage caused by the glass fibre to the counterface was already reported [3. 12]. On this basis the abrasive nature of partial sliding condition will also be reflected in the counterface material.

In polymer tribology, frequently used counter materials are metals due to their heat dissipative nature and wear compensation character. As a counter material, alloy steel 40CrMnNiMo8 (M238 Bohler, Hungary) was used. The thermal advantage and the wear compensation characteristics are the two main reasons to use steel as a counterface material. Polymer composite has relatively poor thermal conductivity which introduces localized thermal spikes. This is mitigated by introducing steel counter material which dissipates the accumulated frictional heat [3. 11]. Table 3-2 shows the mechanical properties of the counter material.

Table 3-1 Mechanical and thermal properties of test materials material

|  | Units | Standard | GF/PA66 |
|---|---|---|---|
| **Physical properties** | | | |
| Color | | | Black |
| Density | g/cm $^3$ | ISO 1183 | 1.35 |
| Water absorption | % | | 1.5-1.9 |
| **Mechanical properties** | | | |
| Yield strength (tensile strength) | N/mm $^2$ | ISO 527 | 185 |
| Elongation at break ( tensile test) | % | ISO 527 | >3 |
| Young's modulus (tensile test) | N/mm $^2$ | ISO 527 | 10000 |
| Ball indentation hardness | N/mm $^2$ | ISO 2039-1 | 270 |
| Shore D Hardness | | ISO 868 | 85 |
| **Thermal properties** | | | |
| Melting temperature | ˚C | 3146-DSC | 260 |
| Thermal conductivity (20C) | W/(K·m) | | 0.24 |
| Specific heat capacities | KJ/(kg·m) | | 1.5 |
| Coefficient of linear thermal expansion (Between 20 - 60 °C) | m/(m·K)X10 $^6$ | | 20 |
| Max. service temperature (long period) | ˚C | | 130 |

Table 3-2 Mechanical and thermal properties of counter material

| Properties | 40CrMnNiMo8 |
|---|---|
| Young's modulus [GPa] | 210 |
| Hardness [HB] | 300 |
| Thermal conductivity (20˚C) [W/(m·K)] | 34 |

## 3.4.1 Specimen preparation

The initial steps in the specimen preparation process are common for both polymer and steel discs. The polymers and the steel samples which are obtained in rod form are subsequently machined in a turning centre (Schaublien 135) to the required diameter for the corresponding slip ratio. Automatic feed was chosen to maintain

similar topographic profile in all the samples. However, the steel specimens are polished further using SiC abrasive papers. Markings were engraved on the steel and polymer specimen for locating the region of interest for topographic studies. Additionally, the mounting holes indicated by the arrows in Figure 3-2 acts as a fool proof for locating the same sector. A more detailed description on the locating principle is explained in the relocation micrography. A technical drawing of the polymer and steel disc is given in Figure 3-2.
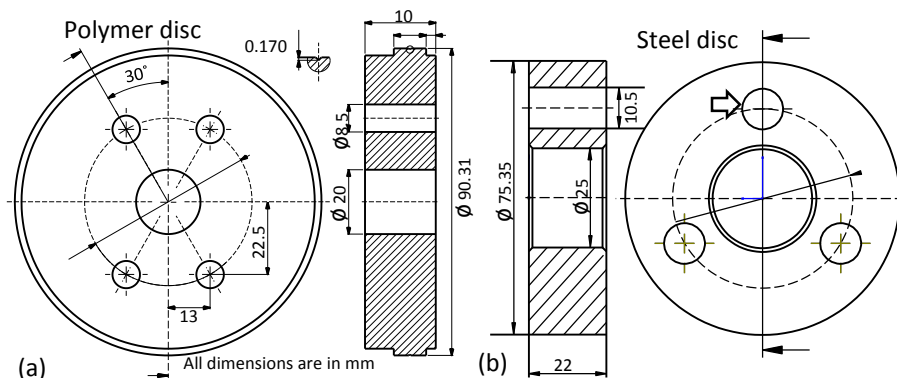


Figure 3-2 Shows drawing of (a) polymer and (b) steel counter material.

## 3.4.2 Polymers disc

A dedicated cutting insert CCGT with 80° included angle was used for machining polymer surface to ensure uniformity in surface topography in terms of roughness. A radial (hoop) groove (see Figure 3-2) was set up in the middle of the polymer contact width to be used later for understanding the deformation behaviour of the polymer disc. The edges of the contact surface are chamfered at 45° to avoid edge effects and acceptable stress concentration. Moreover, the contact width (6.5 ± 0.3 mm) for polymer disc is chosen to be lesser than the steel disc width in order to eliminate cutting effect of the steel edges into the polymer and to release the debris.

## 3.4.3 Steel disc

A special procedure was developed for iterative polishing of the steel discs. In the polishing process, SiC grinding paper of grit size P80D, P240, P320 and P400 from Buehler (Ø 305 mm) was used. Each paper was polished at 500 rpm for 60 seconds to achieve a roughness Ra of approximately 0.2-1.0 μm. The polished steel discs were ultrasonically cleaned in acetone bath for 20 minutes using Sono Swiss (Type SW12H) ultrasonic cleaner. An additional advantage of the steel specimen is the total width (22 mm) compared with the contact width. On the whole, with a wide surface, the steel specimen has a reference (untested) surface for comparing the roughness profile after the contact.

## 3.5 Surface characterisation

## 3.5.1 Surface topography

The topographic profile characteristics of polymer composite and steel disc was measured parallel to the disc axis at predefined locations. A systematic tracing of profile was made using the profilometer (Somicronic® EMS Surfascan 3D, type SM3, needle type ST305) equipped with modules for contour analysis, surface texture analysis and 3D form. In the surface characterization a cut-off wavelength $\lambda_c$ = 0.8 mm at 0.3 mm/s traverse speed was used. The selection criterion for the $\lambda_c$ and $l_m$ was based on DIN 4768 and ISO 4288 standards. Based on a calibrated groove, the three-dimensional instruments conformity certificate (Hommel Somicronic) has an absolute error depth of 0.186 μm on 110.0 μm full scale and independently to this 1 μm in the positioning direction [3.12]. Apart from the 2D profiles, the 3D topography was scanned to find specific features such as grooves and micro-pits as shown Figure 3-3. For the post-mortem analysis of TTS, the worn surfaces were cleaned with pressurized air. Apart from the 3D profile, the V-groove on the contact surface is measured for its depth profile for understanding the global deformation characteristics of the polymer composite.

In DES, the roughness of the polymer and the steel was monitored at every interval. As discussed in the introduction, the transfer layer formed by the entrapment of polymer particles in the roughness valleys of the counterface material tends to modify the Ra as a function of time. Thus during the intermediate pauses the corresponding roughness (average of five measurements) was also measured.
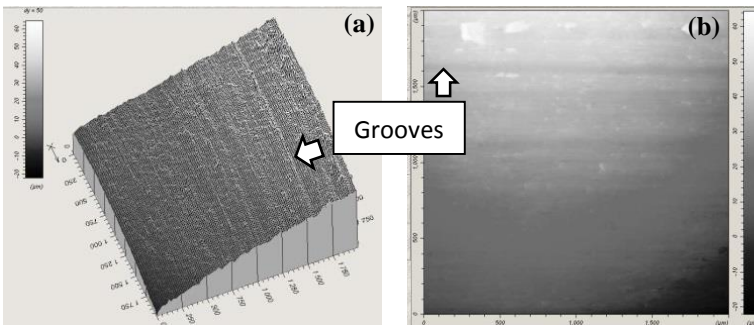


Figure 3-3 (a) 3D (b) 2D scanned topography of a worn surface of polymer.

## 3.5.2 Spectral analysis

In case of DES the roughness measurements were made at each interrupted pause to understand the evolution of surface roughness and to approximately estimate the changes made by transfer layer. For precise evaluation the form error and waviness are corrected using polynomial regression (see Figure 3-4). In cooperation with Department of Machine and Industrial Product Design, Budapest University of Technology and Economics an algorithm was developed to filter these errors. The changes as a consequence of transfer layer deposition were interpreted from the power spectrum density (PSD) using Fourier analysis on the original 2D profile of the steel counterface. A sample profile is shown in Figure 3-5. Characterization of the transfer layer was done by means of PSD analysis on the corrected topographic profile of the steel surface.
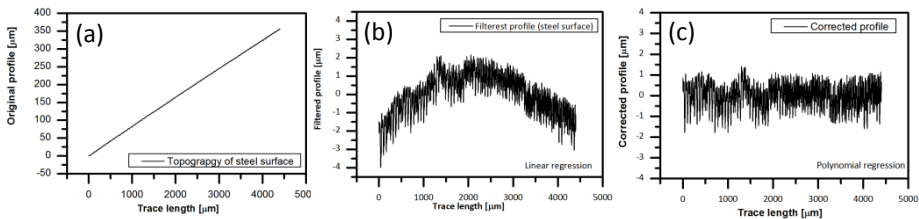


Figure 3-4 (a) original profile with form error (b) waviness (c) corrected profile used for PSD.

The mathematical backgrounds of the PSD analysis adopted from Baryani *et al* are summarized as follows.

$$F(q_p) = \Delta x \sum_{i=1}^{M} z(x_i) e^{-j2\pi q_p x_i}$$

eq. 3-1

And the PSD amplitude made as follows:

$$A(q_p) = \frac{F(q_p) F^*(q_p)}{M \Delta x}$$

eq. 3-2

Where:

|  |  |
|---|---|
| $q_p$ | frequencies in x direction, |
| $x_i$ | spatial coordinate in x direction |
| $z(x_i)$ | height coordinate, |
| M | number of points in profile, |
| $\Delta x$ | sampling distance in x direction |
| $F^*$ | Excitation function |

In a 2D surface profile, the PSD amplitude as a function of wavelength is estimated at each intermediate pause of the DES. As the roughness peaks are filled with transfer layer the amplitude changes correspondingly. Thus the amplitude for the dominant

wavelength indicates the change in height of the roughness valleys. This can be used as a factor to characterize transfer layer formation.
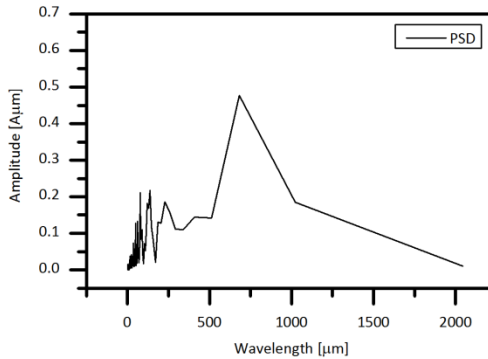


Figure 3-5 Power spectrum density evaluated for 2000 μm trace length.

# 3.6 Tribography

Advanced techniques on image processing were implemented to quantitatively evaluate the severity of wear scar. The micrographs of the specimen were acquired using a 10 bit AVT colour CCD camera in conjunction with an Olympus BXFM reflected light bright field microscope. A xenon NOVA® KARL STROZ high power 300 watt (6000 K) light source with fiber optic guide was used as an illumination. Images were taken at different magnifications from 10X to 60X.

In conventional investigation (TTS) a random segment of the worn surface is analysed for representing the surface modification as a consequence of wear. However, the random surface cannot identify the damage evolution neither can conclude the global surface characteristics. Such challenges has been overcome in DES by a locating fixture where a field of view (FOV) of approximately 1300 μm (using 10X lens) can be located within ±100 μm. Thus via monitoring the same segment by relocation principle, the evolution of transfer layer can be studied. For extracting changes from images and to further process images for comparison, the illumination intensity and exposure time are retained. The used lenses in both TTS and DES are listed in Table 3-3.

Table 3-3 Objective lenses and characteristics

| Objective lens | Characteristic |
| --- | --- |
| 5X | NA 0.12, Achromat |
| 10X | NA 0.25, (SWIFT), Achromat |
| 20X | NA 0.35, SLM PLN (Olympus), Ultra long working distance |
| 40X | NA 0.65, Achromat |
| 60X | NA 0.85 (SWIFT), Achromat |

## 3.6.1 Relocation micrography

From the principle of apparent area of contact, we assume that not all the asperities come in contact during the test. Thus a 2D roughness profile used in regular engineering practice may not completely represent the surface condition. A significant area which can accommodate several asperities for investigation is required. Hence, micrograph serves better to investigate the changes in contact surface incurred during interaction. It was earlier described that *ex-situ* will be followed in the DES sequence for understanding the sequential wear evolution process. In such a case, microscopic features from both the polymer and the steel surface are monitored. Using *ex-situ* methodology for microscopy with several intermediate pauses, locating the same region at micron scale is tedious, time consuming and practically not viable. Thus, we developed a new technique called "relocation micrography" for locating the same region of interest.

Relocation systems have already been used in stylus profilometry. In earlier research, relocation of the same region was done by tracking the stylus mark on the soft material [3. 13]. A simple method for relocating the region of interest can be performed by a fool proof locating fixture. This technique is commonly used in the production shop floor to locate the same region of interest at micron scale. The fool proof system was adapted from the geometric features of the samples and the steel discs itself. The fixture as shown in Figure 3-6 is rigidly mounted to a standard microscope base (Olympus SZX-ST). After each intermediate pause in the DES sequence, the specimen is mounted onto the fixture for image acquisition. With the combined dimensional tolerances of the specimen and the fixture, an average of 100 μm - 200 μm mismatch could be observed in the acquired micrograph which is affordable for investigating an image with large (more than 1000 μm) field of view. The region is matched using image processing technique "registration", where the mismatched regions in the micrograph are removed by cropping.
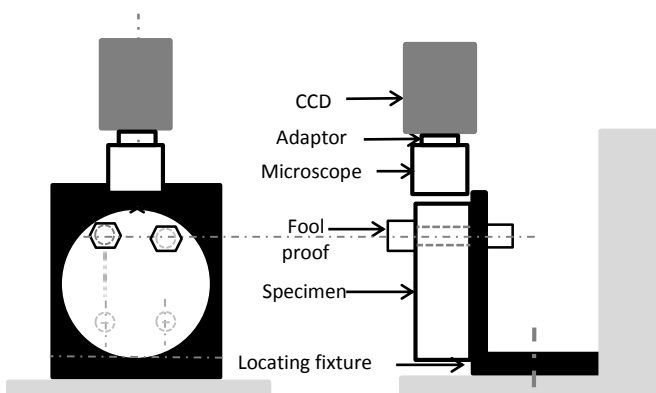


Figure 3-6 Arrangement of the relocation micrography.

Table 3-4 Methodology for image processing

| Sequence | TTS | DES |
|---|---|---|
| **Objective lens used** | 10X | 10X |
| **Exposure time steel** | 300 µs | 300 µs, 25 sec |
| **Exposure time polymer** | 1500 µs | 1500 µs |
| **Post processing** | Grey scale granulometry, segmentation by thresholding | Registration, cropping, Energy of an image |

## 3.6.2 Image analysis

In microscopic analysis, identifying the same region was done by locating fixture to follow the evolution of wear and transfer layer deposition in polymer and metal surfaces respectively. Precise location of the features was done by registering the images. Image processing techniques (segmentation by thresholding, grey-scale granulometry and energy of the image) are used for characterizing the surface change. Image processing includes manual registration of images, local thresholding for segmentation which then used for segregation of characteristic feature such as grooves and pits. Generally, segmentation is defined as partitioning of the image into different regions of similar grey values. Though there are many methods for image segmentation, due to its simplicity, the present work uses segmentation method by means of thresholding. It can be performed globally or locally. Thus, the area occupied by the scar can be characterized. The raw image shows significant difference between contact surface of pure rolling and partial sliding condition (see Figure 3-7). The results of binarised images from segmentation by local thresholding reflects the changes. A mathematical morphology technique with the operation of granulometry by binary opening is used to analyse the size distribution of surface scars. The change in size of the pits and grooves is estimated by filtering the surface scars by using structuring elements (SE). A square shaped SE is used for filtering the pitting and a rectangular shape SE was used for abrasion. Though surface modification are revealed by the segmentation using local thresholding, it does not precisely represent the change in quantitative area of the texture. This is because the binary image does not clearly define the edges and the boundaries of the cavities Figure 3-7.

For converting a grey scale image to binary image via global thresholding, a single threshold value is used for the whole image. The local thresholding segmentation uses a variable threshold throughout the image. In local thresholding, threshold is calculated for each pixel in the image. This method includes the local statistics of the image in small patches. Several window sizes were chosen for the the neighbouring pixels in the local thresholding. The minimum window size was chosen from the rough estimate of the wear scar. Also the estimation from different window sizes are correlated with a mean observer score. Thus it can be assumed that the local changes of illumination are negligible within such small patches. In this study, the mean of neighbouring pixels around each pixel is used as the threshold (including the given

pixel). The desired neighbourhood is specified by a window of size w × w pixels while the given pixel is located at the centre of the window. The window size is specified with prior knowledge on the size of features as observed in the image.

Comparing the segmented images and the raw image it is evident that bright objects having resemblance rectangular pattern can be attributed to the ridges of abrasion (abrasion). Similarly, the black regions which mostly resembles a crater (due to pitting) should be segregated. These patterns are compared also agrees good with the literature as described in chapter 2. For abrasion, the black region between the white horizontal regions are assumed to be grooves hence an appropriate SE is a rectangle. Therefore, to estimate the severity of the abrasion mechanism, granulometry by opening is applied to the segmented images using a rectangular SE. The image processing part is carried out by S. Soleimani and K. Douterloigne from IPI group of the TELIN department (telecommunication and information processing) of Ghent University.
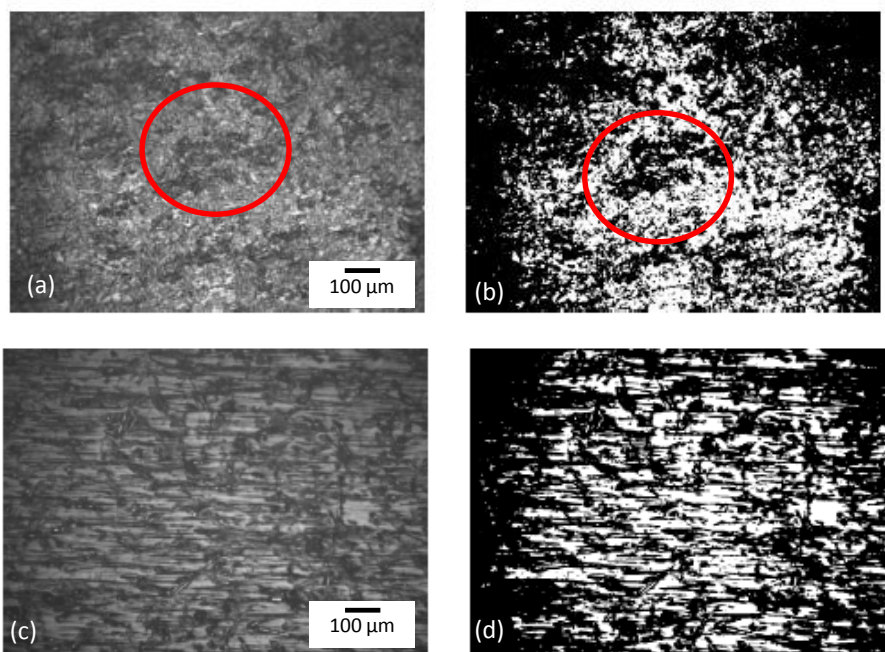


Figure 3-7 (a) raw image pure rolling (b) segmentation using global thresholding (c) partial sliding (9%) (d) segmented image partial sliding.

Subjective analysis was made to validate the results of image processing. In the subjective investigation a methodology for quality assessment of pictures from ITU standard BT.500-11 was followed. In this analysis randomly chosen images (15 numbers) were presented to the subject experts (comprising mainly tribologist and mechanical engineers). The observers indicate the intensity of mechanism (abrasion and pitting) on a scale between 0% - 100%. These subjective scores from the observers are compared with the mean objective score calculated by mathematical morphology and granulometry.

## 3.7 Methodology

## 3.7.1 Definition of roll-slip phenomenon

As understood from chapter 1, roll-slip is a common phenomenon which originates from the relative sliding of rolling components used in day to day life. To explain in detail, we will outline the rolling and sliding components individually as understood from the literature. In pure rolling, there is no difference in the contact velocity between two non-conformal contacts (for example two discs). However, when there is a difference it can be referred to the sliding part. Thus, in a non-conformal contact, the roll-slip phenomenon can be defined as the combination of sliding and rolling in a single cycle of operation. The sliding occurs partially due to the difference in velocity between two bodies. In pure rolling condition the partial sliding is achieved due to the difference in velocity between two moving bodies. Hence the superposition of the velocity fields are considered for calculating the slip ratio. The velocity fields for pure rolling, rolling-sliding and pure sliding condition is given in Figure 3-8. The ratio between rolling and sliding part is defined as the slip ratio [3.14].
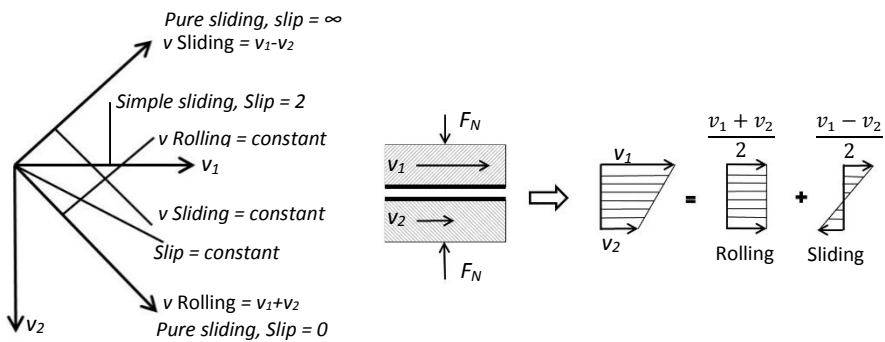


Figure 3-8 Velocity field for pure rolling, rolling-sliding and pure sliding condition [3. 14].

The partial sliding in our study is due to the difference in diameter between the discs. The expression for the slip ratio is adapted from the literature where the ratio between sliding velocity and rolling velocity is assumed as a slip ratio [3. 4, 6, 7]. In defining the slip ratio, the material of interest (polymer) has velocity vector $v_1$ and the counter material is assigned with $v_2$. Thus, the corresponding diameter of the polymer disc is $d_1$ and the steel disc is $d_2$. Henceforth, the surface velocity of both discs differs in constant rotational speed. The slip ratio can be calculated from the ratio between sliding and rolling velocity:

$$Slip\ ratio\ s\ [\%] = \frac{(v_1 - v_2)}{(v_1 + v_2)} \times 200\% \qquad\qquad \text{eq. 3-3}$$

In one cycle of operation the sliding part can be varied between 0 % and 200%. When it is 0% it is pure rolling condition and at 200% it is pure sliding. This can be experienced in a gear mesh, with pure rolling at pitch point and at other locations on the tooth flank a combination of rolling and sliding.

## 3.7.2 Experimental simulation of roll-slip phenomenon

Roll-slip phenomenon described in literature is produced is mainly on non-conformal contact with a relative sliding between two bodies on the course of rolling. Generally, model testing is primarily done for understanding the wear mechanism. One of the main reason to adopt model testing is ti eliminate the variability experienced by field test in terms of load, velocity and environment. Additionally model testing is used to make comparative study on elucidating the influencing parameter. In literature, we have come across different test configuration for simulating the non-conformal contact. This involves twin-disc configuration which is widely used [3. 4 – 7, 9, 15, 16] followed by modified four ball machine [3. 17, 18]. Twin disc has the advantage of controlling the rolling-sliding ratio hence, it is appropriate for the current experimental simulations.

The pure rolling and partial sliding condition is experimentally simulated using a twin disc model. Therefore an existing Forschungsstelle fur Zahnrader und Getriebebau (FZG) gear oil tester is refurbished to a twin-disc tester fulfilling the requirements for measuring the friction force, wear and temperature. The schematic of the twin disc is shown in Figure 3-9. The system basically consists of two shafts synchronized by a drive gear system. The discs in contact have slightly different tangential velocities, resulting into a mixed rolling-sliding condition. The test rig is equipped with sensoric devices to measure friction torque, contact temperature and normal displacement (wear). All measurements are done online and recorded using NI DAQ (National instruments BNC 2100).

Table 3-5 Slip ratio and the corresponding diameter of the specimen

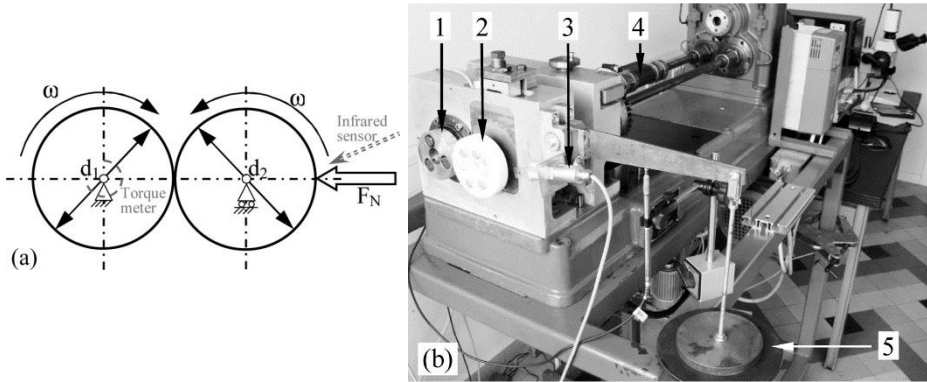| Slip ratio (%) | Polymer diameter (mm) | Steel diameter (mm) |
|---|---|---|
| 30 | 95.22 | 70.38 |
| 26 | 94.04 | 71.93 |
| 18 | 90.31 | 75.35 |
| 9 | 86.78 | 78.86 |
| 0 | 82.81 | 82.84 |

Figure 3-9 (a) Schematic of the test rig and (b) digital photograph (1) steel disc (2) polymer disc (3) temperature sensor (4) torque sensor (5) dead weight.

### 3.7.3 Wear experiments

Preliminary tests were made to optimize the test parameters. The initial tests were performed for 33, 55 and 72 MPa average Hertzian contact pressure at 26 % partial slip ratio and 500 rpm. From literature it is evident that a contact pressure ranging between 33.9 – 59.1 MPa and a slip ratio of 0 – 30% is used for polyamide composites (PA46 + aramid fibers) [3. 4]. For 55 and 72 MPa at 26 % partial sliding resulted in severe wear by producing high frictional heating (60 °C). Also the SEM analysis at 55 and 72 MPa showed severe damage of fibers. However, for 33 MPa contact pressure the frictional heat was lesser than 50 °C, henceforth the same contact pressure is used further in traditional testing. Test duration of ten hour corresponding to $3.0\ 10^5$ rotations was adopted for TTS. The test conditions followed for TTS and DES is shown in Table 3-6. The protocol for both TTS and DES is given in appendix C.

Table 3-6 Test condition for TTS and DES sequence

| Wear testing | TTS | DES |
|---|---|---|
| Material used | GF/PA66 | GF/PA66 |
| Slip ratio | 0-26% | 0 and 30% |
| Test sequence | Continuous rolling/sliding test | Interrupted testing |
| Test duration | 10 hours | 8 hours |
| Number of cycles | $3\ 10^5$ | $2.4\ 10^5$ |
| Mode | Continuous testing | Interrupted (every 15000 cycles) |

## 3.8 Wear evaluation

Research reports reveal that, with model testing of polymer-metal rolling contacts after millions of cycles, the observed wear is in few micrometres (between 50 -500 µm) [3. 4, 5, 9]. Also while using the gravimetric analysis the measured mass loss is between 20 and 50 mg [3. 19]. The critical factor in measuring polymer wear is the difference of scale. A narrow range of wear at submicron to micrometre level is measured on a tribo pair of several millimetres size. The measurable wear after such long duration of testing is not fully reliable due to the scale difference and also due to the involved dynamicity. Repeatability test on wear measurements were performed for 26% slip ratio.

### 3.8.1  Mass loss

It is known from chapter 1 (see table 1.2) that mass loss in very often used for wear characterization.  A procedure involving preheating the specimen for moisture removal was already in practice [3. 5, 6], the same is adopted in our experiments for the TTS. Prior to testing the polymer disc were heated in an oven at 70 °C for a period of 20 hours to remove moisture. Subsequently, the mass loss is measured in an OHAUS explorer weighing balance with a maximum limit of 210 g and an accuracy of 0.0001g.

### 3.8.2  Diameter loss

We adopted an offline and online approach, for offline measurements of diameter reduction. A contact point measuring method employing electronic micrometre (outside micrometre at an accuracy of 0.001 mm) for diameter measurements was used. Alternatively, an online monitoring system was used based on a linear variable differential transformer (LVDT) Solartron AX/10/S. Online signals acquired at 1 kHz are averaged for every second to monitor the diameter change. In offline method (micrometre), polymer being an elastic material, the induced pressure might not be uniform and measured human error (is prevalent in such a technique.

### 3.8.3  V groove depth profile

A technique similar to reference mark wear evaluation by Khruschov was adapted in our offline measurement [3. 20]. A geometrical alteration is done to the polymer specimen in the contact surface. A radial (hoop) V groove (deep 150 ± 30 µm) is intentionally made on the contact surface as shown in the Figure 3-10. The variation in dimension due to wear was reflected from the change in size of the V groove. Mechanisms such as global plastic deformation can be identified from the slope of the V groove. These grooves are measured for its depth profile using a profilometer, Somicronic® EMS Surfascan 3D.
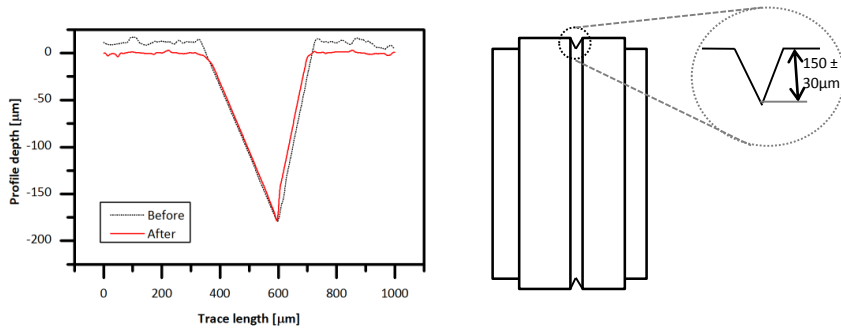
Figure 3-10 profile depth of the v-groove on contact surface.

## 3.9 Scanning electron micrography

For sub-micron scale investigations the specimen and the steel surfaces were parted to analyse the worn surface by SEM. Morphological characterization and investigation on the presence of transfer layer were carried out using an Environmental SEM (XL30, FEI) with a LaB6 filament operated at 20 kV and equipped with an energy disperse X-ray spectrometer (EDX). The surface of polymer specimen to be used in SEM inspection was coated with gold to increase the electrical conductivity. An unworn sample was also investigated and considered as a reference. Additionally the collected debris was further investigated for specific morphological features in order to understand the mechanism experienced by the polymer composite during roll-slip testing.

## 3.10 Cross-section studies

Even though profilometry explains the deposited transfer layer characteristics, it has to be validated for the thickness of transfer layer. Hence, a cross-sectional study was made on the steel specimen. For this study the steel surface of pure rolling condition and 26% partial sliding condition was chosen. Initially the steel surface is sawed in dry condition to prepare the cold mould. A cold mould was chosen because high temperature involved in hot pressing can deteriorate the transfer layer. Moulding was done by mixing 25 g of epoxy resin, (EPOFIX) to 3 g of epoxy hardener (EPOFIX hardener). The mix was then thoroughly stirred and kept in the fume hood for 20 hours to cure.  The first step was polishing in wet condition using 120 grit SiC abrasive paper on KNUTH-ROTO 2 polishing machine. Additionally a Struers MD-Allegro 250 mm grinding disc with a 9 µm grade diamond paste and a Struers MD-Dur 250 mm polishing cloth with 3 µm grade diamond paste in STRUERS-ROTOPOL 22 polishing machine was used. Both steps were performed with a load of 75 N and a rotational speed of 150 rpm for 10 minutes. In cross sectional studies, an AXIOSCOP 2 MATmot, Carl Ziess metallurgical microscope equipped with Axiocam MRc5 was used. Illumination at full intensity (3200K) was used in acquiring the images.

## 3.11 Summary

The test methodology clearly considers the objective for understanding the polymer wear in rolling-sliding contact and monitoring the wear process (as understood from chapter 1). Test sequence was formulated based on literature and results from the preliminary testing. The traditional tribological study will elucidate the global wear characteristics for which a model is developed in chapter 4. In regards to the damage evolution study the change in surface morphology and its corresponding surface response helps in understanding the dynamic behaviour of polymer wear. *Ex-situ* methodology with intermediate pauses reveals the progressive wear mechanism. Adaptation of technique such as relocation micrography and image processing in tribological investigation brings in novelty to the methodology itself. Such techniques aids precise tribological mapping of worn surface for logical reasoning.

# References

[3.1]   W. Wieleba, "The statistical correlation of the coefficient of friction and wear rate of PTFE composites with steel counterface roughness and hardness," Wear, vol. 252, pp. 719-729, 2002.

[3.2]   A. Avanzini, G. Donzella, and D. Gallina, "Failure analysis and life prediction of polymeric rollers for industrial applications," International Journal of Materials and Product Technology, vol. 38, pp. 362-385, 2010.

[3.3]   A. Avanzini, G. Donzella, A. Mazzù, and C. Petrogalli, "Wear and rolling contact fatigue of PEEK and PEEK composites," Tribology International, vol. 57, pp. 22-30, 2013.

[3.4]   D. H. Gordon and S. N. Kukureka, "The wear and friction of polyamide 46 and polyamide 46/aramid-fibre composites in sliding/rolling contact," Wear, vol. 267, pp. 669-678, 2009.

[3.5]   C. J. Hooke, S. N. Kukureka, P. Liao, M. Rao, and Y. K. Chen, "The friction and wear of polymers in non-conformal contacts," Wear, vol. 200, pp. 83-94, 1996.

[3.6]   S. N. Kukureka, Y. K. Chen, C. J. Hooke, and P. Liao, "The wear mechanisms of acetal in unlubricated rolling-sliding contact," Wear, vol. 185, pp. 1-8, 1995.

[3.7]   S. N. Kukureka, C. J. Hooke, M. Rao, P. Liao, and Y. K. Chen, "The effect of fibre reinforcement on the friction and wear of polyamide 66 under dry rolling/sliding contact," Tribology International, vol. 32, pp. 107-116, 1999.

[3.8]   J. Ye, H. S. Khare, and D. L. Burris, "Transfer film evolution and its role in promoting ultra-low wear of a PTFE nanocomposite," Wear, vol. 297, pp. 1095-1102.

[3.9]   Y. K. Chen, S. N. Kukureka, C. J. Hooke, and M. Rao, "Surface topography and wear mechanisms in polyamide 66 and its composites," Journal of Materials Science, vol. 35, pp. 1269-1281, 2000.

[3.10]  J. H. Byett and C. Allen, "Dry sliding wear behaviour of polyamide 66 and polycarbonate composites," Tribology International, vol. 25, pp. 237-246, 1992.

[3.11]  W. Glaeser, Materials for tribology vol. 20: Elsevier, 1992.

[3.12]  Hommel Somicronic, "Three-dimensional instruments conformity certificate," No. 380027 ed, 2003.

[3.13]  M. J. Edmonds, A. M. Jones, P. W. O'Callaghan, and S. D. Probert, "A three-dimensional relocation profilometer stage," Wear, vol. 43, pp. 329-340, 1977.

[3.14]   D. J. Schipper, Transition in the lubrication of concentrated contacts, PhD Dissertation, Twente University, 1988.

[3.15]  D. F. Charles, R. Gnanamoorthy, and P. Ravindran, "Rolling contact fatigue behavior of polyamide clay reinforced nanocomposite—Effect of load and speed," Wear, vol. 269, pp. 565-571, 2010.

[3.16]  M. Rao, C. J. Hooke, S. N. Kukureka, P. Liao, and Y. K. Chen, "The effect of PTFE on the friction and wear behavior of polymers in rolling-sliding contact," Polymer Engineering & Science, vol. 38, pp. 1946-1958, 1998.

[3.17] C. C. Lawrence and T. A. Stolarski, "Rolling contact wear of polymers: A preliminary study," Wear, vol. 132, pp. 183-191, 1989.

[3.18] T. A. Stolarski, S. M. Hosseini, and S. Tobe, "Surface fatigue of polymers in rolling contact," Wear, vol. 214, pp. 271-278, 1998.

[3.19] H. Koike, K. Kida, E. C. Santos, J. Rozwadowska, Y. Kashima, and K. Kanemasu, "Self-lubrication of PEEK polymer bearings in rolling contact fatigue under radial loads," Tribology International, vol. 49, pp. 30-38, 2012.

[3.20] M. M. Khruschov, "A new method for the determination of wear of machine parts," Wear, vol. 3, pp. 60-71, 1960.

Chapter 4

# From pure rolling to partial sliding: a traditional tribological study
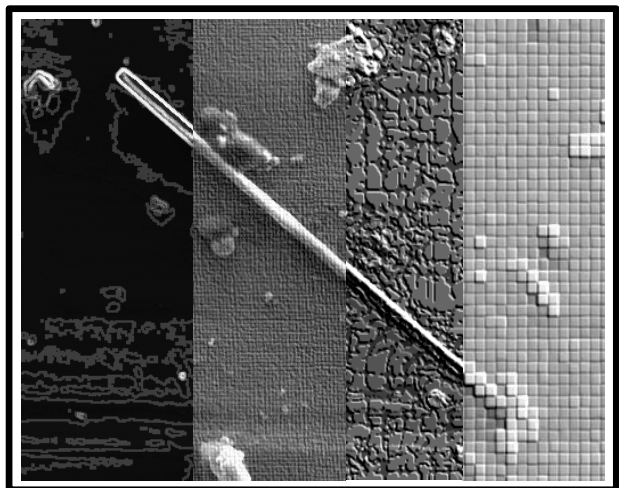
# Goal

This chapter primarily focuses on the change in wear mechanism from pure rolling to partial sliding condition. In the rolling contact of polymers, chapter 1 clearly reveals signs of abrasion due to partial sliding. Existing scientific reports of polymers in rolling contact show increased wear for partial sliding when compared with pure rolling. However, the mechanism behind increased wear for partial sliding is not fully understood. Having identified from chapter 2 that wear scar is an effective means for understanding the wear mechanism and also for wear characterization; questions related to partial sliding are addressed from the view point of wear scars. A more rational approach to study the wear scar is by means of quantitative micrography. Experimental work on pure rolling and partial sliding condition is realised based on the twin-disc model testing using traditional tribological study (TTS) defined in chapter 3. Attempts were made to use the image processing techniques (granulometry and segmentation) for quantitative micrography in evaluating the wear intensity from wear scar. The competence of image processing techniques in describing the quantitative characteristics of wear scars is compared with expert opinion. Thus the followed methodology allows or a clear understanding wear process suffered by the polymers in rolling-sliding contact. Moreover, existing mathematical model for wear of rolling contacts do not consider the partial sliding or the topographic characteristics. Thus, a mathematical model based on dimensional analysis is developed by accommodating parameters related to partial sliding condition. Additionally, the unknown of the polymer tribology which is the transfer layer characteristics are also analysed in detail.

## 4.1 Wear mechanisms of polymers in rolling-sliding contacts

In tribological application, for an appropriate material selection, wear testing is done prior to the design stage for "choosing" a wear resistant material. It would be logical to use the term explore rather than "choose", because of the limited work on polymers in rolling contacts, specifically in partial sliding condition. It is also understood that wear testing of polymers in rolling contact is vaguely connected to the wear patterns observed in real industrial components (see chapter 1). For example, the grooving phenomena due to partial sliding are scarcely reported. Generally, the difference in wear between pure rolling and partial sliding are addressed descriptively by material loss [4. 1, 2, 3] or surface morphology [4. 4, 5]. It has been reported earlier that in pure rolling the material removal is through mechanical fatigue [4. 6] whereas the particle generation in sliding wear is due to softening of polymer surface [4. 7]. Most scientific work associates the wear of rolling contact primarily to contact fatigue. However, the current research attempts to relate the basic wear mechanisms in rolling-sliding contacts to particle generation through abrasion.

Rolling contact produces smooth surfaces due to the flattening of polymer asperities by phenomenon such as plastic flow and the deformation. With two different contact conditions (pure rolling and partial sliding), variability in wear scars can be expected

between each other. Since pure rolling experience contact fatigue, the particle generation is rather at the final stage of wear process (depending upon load condition) [4. 8]. Nevertheless, in partial sliding, particle generation could be expected even in the initial stage of wear. This is due to the micro-machining of polymers from relative sliding. In other words high stress abrasion will be experienced on polymer surface in the form of micro-cutting. The roughness peaks of the steel counter material stands responsible for the micro-cutting phenomena. This progressive material loss due to micro-cutting has a higher chance of indicating increased material loss in partial sliding. However, low stress abrasion can also persist due to micro-ploughing from local plastic deformation for which material loss will be relatively less. Irrespective to the above mechanisms, literature elaborates the variation in wear rate for pure rolling and partial sliding merely from the view point of frictional heating.

In order to relate the wear rate to a specific mechanism, the experimental protocol with traditional tribological study (TTS) mentioned in Chapter 3 is realized in the present chapter. Investigating the wear mechanism in both pure rolling and partial sliding condition will describe the cause for increased wear rate in partial sliding condition. An unanswered question in partial sliding condition is the role of transfer layer in altering the tribological characteristics. These questions and hypothesis narrow down to one specific aspect which is the analysis of surface scars from both polymer and counter face material. Thus quantitative micrography is adopted to characterize the wear scars to understand the tribological behaviour at rolling-sliding condition.

In the current approach, preliminary tests were performed for narrowing down the test parameters. Further to which the techniques to be used for wear measurement are narrowed down from the repeatability test. In regards to the wear analysis the contact surface of both materials are analysed using tribography that includes imaging of the surface and profilometry. Finally the optical micrographs are processed for evaluation of surface scars using quantitative micrography.

## 4.2 Preliminary testing

### 4.2.1 Influence of contact pressure

In the current investigation, polymer composite (GFPA66) is tested against steel counter material using twin-disc model. The influencing factor is the partial sliding condition for which comparative study between pure rolling and partial sliding is made. The operational parameters such as load and speed are chosen based on the preliminary testing.

It is evident that operational parameters close to real working condition are rather impractical due to the wide range of rolling-sliding applications. Also in certain applications the operating condition will have working parameters (speed) that may require extensive test duration. Thus a test condition with increased speed is followed in the current research (500 rpm) which is also followed in most model testing. The range (30 – 70 MPa) of operational load is decided based on literature and also from the comparative study prepared in chapter 1. Initially three tests were

made at different contact pressures (33 MPa, 55, MPa and 72 MPa) at 26% partial sliding condition. The temperature profile and friction curve measured during the course of testing are shown in Figure 4-1. It is evident that the measured polymer surface temperature is higher than the glass transition temperature Tg (50°C) of the composite at 55 MPa and 72 MPa contact pressure. Polymer material at glass transition temperature turns to a rubbery state. Also the significant difference in temperature between the three contact pressures may encounter variations in mechanical properties of the material. These factors may alter the contact area based on the Hertzian contact pressure. This significantly influences the tribological characteristic which can bring in parasitic effects in altering the wear mechanism by introducing plastic flow or softening of the polymer surface. Additionally, the softening of polymer can have aggravated wear characteristics by clearly allowing the steel asperities to easily micro-machine the soft polymer surface. Nevertheless, the primary focus of our research is to individually study the influence of partial sliding and understand the wear mechanism and its advantages. Thus 55 MPa and 72 MPa contact pressures are eliminated. On this basis an operating pressure of 33 MPa is chosen for our further investigation.
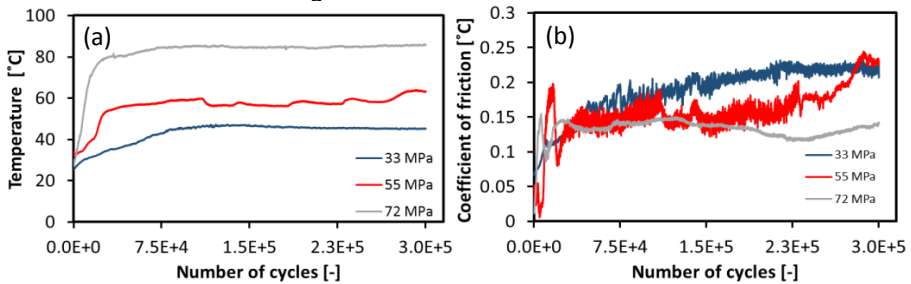


Figure 4-1 Preliminary test (a) temperature curves (b) friction curve.

## 4.2.2 Wear measurement techniques

In literature two commonly used techniques for wear measurement of polymers in rolling-sliding contacts are mass loss and diameter loss. In our investigation the effectiveness and the repeatability of these measuring techniques were studied. In addition to mass loss and diametric change, V-groove measurement which is also a linear measure of diameter change using contour profilometry is included. The change in depth of the V-groove present in the contact surface is measured for wear characterisation. Three tests were conducted for the same condition with 33 MPa contact pressure at 500 rpm and 26% slip ratio. The precise measuring technique in wear estimation from the view point of repeatability was investigated from the three tests. Table 4-1 shows wear measurements in terms of mass loss, diameter loss and contour profilometry from the depth measured in the V-groove of polymer contact surface. It is evident that V-groove has minimum error with less deviation. However, both V-groove and diameter change does not consider the stereometric material loss in terms of volume from pits and grooves. In chapter 1 it was evident that a significant area was covered by micro-pits of diameter between 50 to 100 μm. Assuming each micro-pit as a hemi-sphere carrying a specific volume, a significant amount of material loss will be unaccounted with the linear displacement techniques. Hence the

mass loss is used as a reliable tool for wear evaluation. A protocol mentioned in Chapter 3 (also see Appendix C) in terms of drying and weight measurements of composite discs was used for mass loss measurement. In most polymer-metal contacts, the generated wear particles are milled between the contact surfaces to form a tribo film on the counter material. Though these wear particles are consequences of progressive damage of polymer surface, a portion of the wear particle are still a part of the tribo-system for which it may not be fully considered as a material loss. These wear particle from the steel counter material can also transfer back to polymer surface in creating a self-healing effect for existing damages. It is evident from the repeatability test that there arises 33.8% of RSD for an average 6.26 mg mass loss measurement. From these three tests it is rather clear that repeatability in wear measurements for polymers in rolling-sliding contact is not consistent. From chapter 1 it is evident that the initial contact surface has changed as a function of wear. The machine marks from initial contact surface are still visible on the worn surface indicating the mild wear condition. A similar consideration is made in the current research where the material removal from polymer roller is correlated to the change in surface morphology.

Table 4-1 Repeatability test for 26% partial sliding condition

|  | Mass loss (mg) | Diameter loss (µm) | V-Groove (µm) |
|---|---|---|---|
| Test 1 | 6.6 | 11 | 8 |
| Test 2 | 8.2 | 82 | 11 |
| Test 3 | 4 | 48 | 7 |
| Average | 6.26 | 47 | 8.66 |
| RSD (%) | 33.70 | 75.55 | 24.01 |

From the measured mass loss the wear rate is calculated using the relationship given in eq. 4-1. The calculation for specific wear rate was adopted from literature used in characterising wear for polymer rollers [4. 9]. The following equation provides the specific wear rate

$$WR = \frac{\Delta m}{\rho \pi dwN}$$  eq. 4-1

Where $\Delta m$ is the mass loss can be taken from Table 4-1, $\rho$ is the density of the material, d is the diameter of the polymer disc, w is the specimen width and N is the number of cycles.

## 4.3 Pure rolling to partial sliding condition

Four levels of contact kinematics, starting with pure rolling and three levels (9 %, 18% and 26%) of partial sliding conditions were tested to study the influence of partial sliding. The wear rate for the four conditions is given in Figure 4-2. It is evident that among the four conditions, 9% rolling-sliding has the highest wear rate. Previous researches also had similar findings where wear rate increases at 9% and 10% slip ratio [4. 4, 10]. However, in our case this non-linearity in wear rate can be attributed

to the surface characteristics. Having near ideal conditions, slip ratio is the only changing variable; the worn surface is further studied thoroughly to understand the non-linear wear characteristics. Irrespective of the wear characteristics, the friction behaviour is partly linear with increasing slip ratio. This means friction heating has no significant role for having increased wear rate at 9% slip ratio. From Figure 4-2 it is evident that the steady stage is achieved after $1.5 \cdot 10^5$ rotations. Also, there exist a remarkable similarity of friction trend in the beginning of all four test conditions with a rapid increase and a change in rate at $2.0 \cdot 10^4$ rotations. The pure rolling condition follows another trend with a smooth transition from unsteady to a steady stage attained at $1.0 \cdot 10^4$ rotations. With dynamic tribological characteristics for polymer-metal tribopairs it is not commendable to use statistical interpretations. Thus a detailed study on the wear process is executed through tribography.
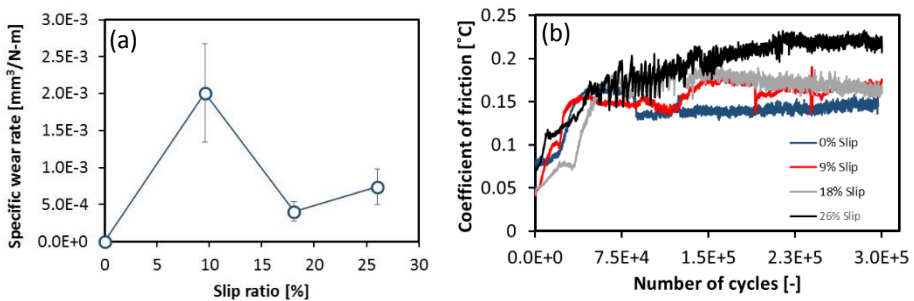


Figure 4-2 (a) Wear rate (b) COF for polymer metal tribo-pairs under rolling-sliding condition.

## 4.3.1 Tribography of polymer contact surface

From the view point of wear mechanisms, a considerable difference in polymer surface morphology was observed between pure rolling and partial sliding condition.. The three methods in tribography (1) morphological study, (2) cross-sectional studies and (3) topographic study are adopted for a complete understanding of the wear process. The difference in surface scars between pure rolling and partial sliding condition is explained from the topographic analysis, micrographs, SEM images. The transfer layer characteristics are described from the cross-section studies.

## 4.3.1.1 Morphological investigation: Optical micrography

Since the surface under investigation is an opaque object, a reflected light bright field microscopy is used for morphological investigation. Surface scars representing micro-pits and grooves are studied in detail. In pure rolling, micro-pits, cracks and craters were observed on the polymer surface (see Figure 4-3). Existing researches demonstrates the pitting phenomena as a consequence of heterogeneity in the contact surface [13, 14]. In our study, heterogeneity in form of surface defects does exist from the machining process. A closer look is made to understand the reason for the formation of the micropits (Figure 4-3). Stolarski *et al* reported that the surface failure of polymers in rolling condition occurs through crack formation, propagation and networking of cracks which finally result in pitting [13]. Rao *et al* briefs that surface cracks are influenced by frictional heating and vary with respect to the

materials [15]. In the present case surface cracks are seen in the pure rolling specimen. It is also evident that these cracks are networking between each other which may result in formation of craters. Crack indicated by C1 in Figure 4-3 (b) is connected to another crack formed individually at location C2. Research report suggest that crack formation is a consequence of fatigue behaviour [4. 11].
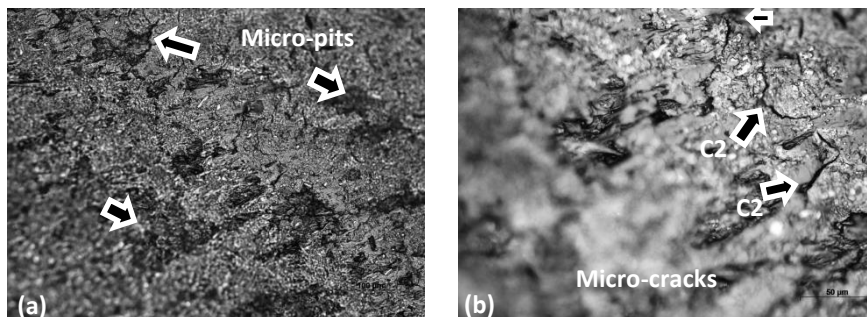


Figure 4-3 Micrographs of polymer composites (GF/PA 66) (a) contact surface showing micropits (b) cracks in pure rolling condition.

In a surface morphological investigation at high magnification, it can be assumed that the observed wear scars such as cracks and micro-pits are present locally. Besides, the visual inspection of the expert on the region of interest, quantitative data on the distribution of crack, its size and characteristic features are not generally investigated. Thus it will be trivial to mention their global presence without any statistical and quantitative information of wear scars. It is insufficient to conclude the incurred wear mechanism based on few qualitative observations on a specific region of interest. However, those few observations can be used to extract the quantitative data about wear scar.

From the surface analysis no signs of therformation or abrasion was found. Literature suggests that the morphological features for thermally induced wear can be identified from wear patterns such as plastic flow [4. 12, 13, 14] and spherical particles. It is evident from the temperature curve and the surface morphology that no evidence of thermal damage in all four contact condition. The cause of material removal in pure rolling can also be attributed to the micro-slip due to the Hertzian contact. The contact width is rather small and thus the micro-slip does not produce significant amount of wear debris. The experiment is conducted within the plastic limit of the polymer thus the axial deformation of bulk material can be neglected. However, the micro topography has rather small asperities which may yield under the action of rolling and also break due to mechanical interlocking with steel asperities. In pure rolling surface cracking is the main cause of material deterioration [4. 15], which is also observed in our case from the micrographs of pure rolling specimen. However, without sequential observations, these hypotheses are only assumptions.
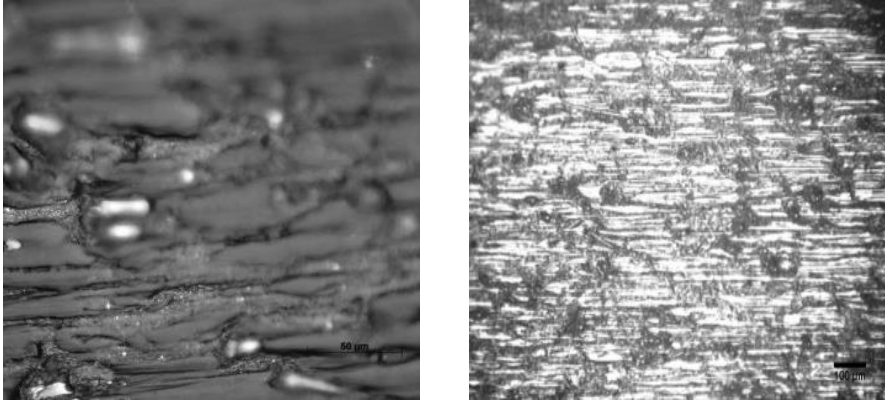
Figure 4-4. Micrographs of polymer composite (GF/PA 66) contact surface showing abrasion patches in partial sliding condition at (26 % slip ratio).

In case of sliding, an entirely different surface morphology was observed. All three specimens (9%, 18% and 26% slip ratio) were observed with grooves as a dominant wear scar as seen in Figure 4-4. Micro-channels observed in the composite contact surface (Figure 4-4) can be attributed to the abrasion of polymer surface. The micro-pits produced by pure rolling are dominated by the partial sliding characteristics. Due to the relative sliding between polymer and steel discs, combination of single and repeated cycle deformation occurs. Besides, the counterface material is investigated for the presence of transfer layer and to understand the process undergone by the material in the course of interaction. It is possible that these micro-channels are a consequence of either micro-cutting or ploughing through local plastic deformation. Nevertheless, only with micro-cutting excessive amount of particle generation occurs. The significant amount of transfer layer shows that substantial amount of particle is generated in the course of wear. From the groove marks in the contact surface and the substantial amount of transfer layer the dominating process for material removal in partial sliding can be concluded as micro-cutting.

## 4.3.1.2 Morphological investigation: SEM

The contact surfaces were further investigated at a higher magnification for understanding the mechanism at a sub-micron level. Figure 4-5 shows the SEM micrographs of GF/PA66 at pure rolling and partial sliding respectively. Peculiarities in wear mechanism in terms of morphological features are clearly seen between the two contact conditions.

At 0% slip ratio, the polymer surface shows stress whitening which is a stage prior to micro-pitting and this is referred as localised flow by earlier researches [4. 16]. These white regions referred as localised flow (see Figure 4-5) appear brighter in the micrographs as a consequence of local plastic deformation. In 26% sliding a clear notification of abrasion groove was observed between the fibre and the matrix. The micro-channels (micro-grooves) as a consequence of partial sliding are indicated with white arrows in Figure 4-5. Moreover, wear lip formation on the polymer surface as

a consequence of poor adhesion (indicated with black arrow) is also observed. The adhesive nature of the polymer does not support sufficiently, thus only limited amount of material is delaminated leaving a relatively small portion with a lip like feature. These shear tongue are formed due to the combined action of ploughing and adhesion where the ploughing action is seen through the nano grooves on the shear tongue (encircled).

The transition from micro-pitting mechanism to micro-grooving and micro-cutting plays a vital role in producing the transfer layer. Even though grooves were present in earlier research, [4. 17] such patterns (micro-channels) in partial sliding are less investigated. These patterns do not only reveal the severity of wear but, also the generated particles being moved to the counter material indicate the formation of transfer layer on the counterface. From the above discussion it is clear that the transition in wear mechanism is due to the difference in material removal. For polymer rolling, a repeated cycle deformation contributes to a relatively lesser material loss. However, in partial sliding condition, single cycle deformation dominated through micro-cutting has significant wear.
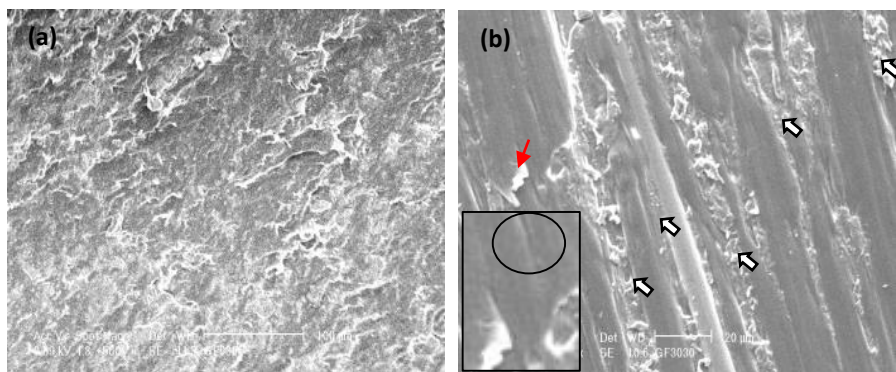


Figure 4-5 SEM micrographs of GF/PA 66 composite at (a) pure rolling condition (b) 26% sliding condition.

## 4.3.1.3 Topographic measurements

In the 3D profiling, the micro-pits and grooves (indicated by arrow) are detected on the polymer surface for pure rolling and partial sliding condition respectively. The grooves in partial sliding can be attributed to the abrasion of soft polymer by steel asperities. However, these scratch marks are not present in the polymer surface tested for pure rolling condition.
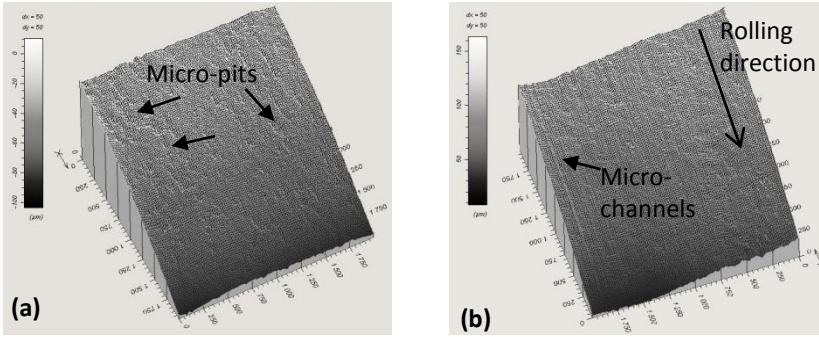
Figure 4-6 stylus profilometry of GF/PA66 surface (a) 00% sliding (b) 26% sliding.

Amplitude density function of the roughness profile were used for validation of the mechanisms observed in the morphological inspection. In this regards, skewness (Rsk) and kurtosis (Rku) which are the third and fourth central moment of the surface profiles were used. These factors are sensitive to the details of surface profiles such as crest and troughs. A negative Rsk indicates a profile with deep valleys or removed peaks. And the positive skweness are the profiles with dominant roughness peaks. A schematic on the skewness is shown in Figure 4-7.
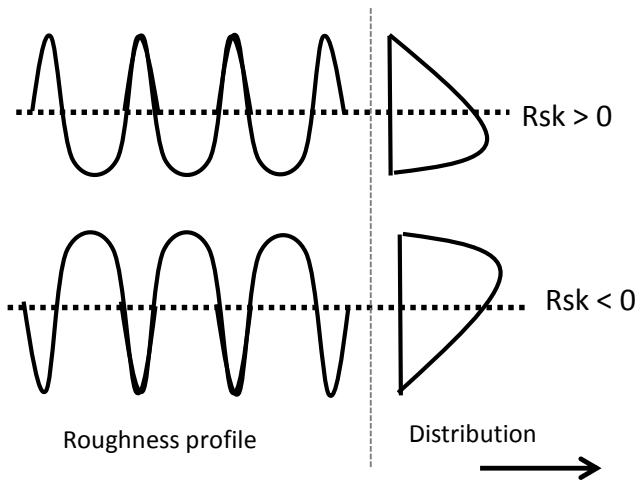


Figure 4-7 Schematic representing the roughness profile height characteristics (skewness).

The observed distribution characteristics (Rsk and Rku) of 2D roughness profile from the stylus profilometric measurement is listed in Table 4-1. It is noteworthy to mention that the positive Rsk before test has altered to negative Rsk for polymer disc at pure rolling condition. The positive Rsk on the initial contact surface can be related to the asperities present in polymer surface. However, from the interaction between composite disc and counter material, these relatively soft polymer asperities are plastically deformed. The negative Rsk indicate predominant valleys in the roughness micro-topography. The surface texture with micro-pits can also be better represented with the negative Rsk. It is possible that the asperity has deformed plastically from the repeated cycle deformation.

In partial sliding condition other than 26%, no significant smoothening was observed from the Ra values. Except 18% slip ratio the Ra has changed by a factor of two, thus, smoothening of surface is evident which can be attributed to the plastic deformation. When compared with partially sliding condition, the pure rolling discs shows with large values of Rku. This can be attributed to the flattening of asperities due to plastic deformation which is common in pure rolling. In all three profiles of the initial contact surface of partial sliding specimen a negative Rsk was observed. This clearly indicates the characteristics of a turned profile. However, this has after wear testing changed to positive Rsk, indicating the prevailing peak characteristics of the ridges formed due to grooving (from partial sliding). It is also possible that the debris present in contact surface could result in positive Rsk. The kurtosis Rku for all three partial sliding specimens is greater than 3, thus having leptokurtic profile. This might also be possibly caused by ploughing of steel asperity.

Table 4-2 Surface roughness profile for the polymer material [μm]

| Slip | Ra | | Rsk | | Rku | | Rmax | |
|---|---|---|---|---|---|---|---|---|
| | Before | after | Before | After | Before | After | Before | After |
| 0 | 1.07 | 0.56 | 0.22 | -1.587 | 2.95 | 7.1 | 6.35 | 4.91 |
| 9 | 1.19 | 0.71 | -0.18 | 1.18 | 2.83 | 6.49 | 7.05 | 5.91 |
| 18 | 0.87 | 0.70 | -0.61 | 0.27 | 2.66 | 3.24 | 4.70 | 4.39 |
| 26 | 1.92 | 0.81 | -0.16 | 0.17 | 2.94 | 4.36 | 11.47 | 6.00 |

## 4.3.2 Transfer layer characteristics

In the previous section from the surface analysis it was evident that no signs of thermal softening from the wear scars was found, thus the wear process can be assumed isothermal according to the classification of Briscoe *et al* [4. 18]. An approach similar to the polymer tribography was used, to investigate the transfer layer characteristics

## 4.3.2.1 Morphological investigation: Optical microscopy

Based on surface morphology the transfer layer for both pure rolling and partial sliding condition can be categorized into two types: (1) uniform layer within steel the roughness peaks are called primary transfer layer, mostly found in pure rolling specimen and (2) secondary layer is the thick dark deposit of polymers on the steel surface and is common in partial sliding condition. The secondary transfer layer can be easily removed (using acetone), but the primary layer has stronger adhesive characteristics. Even after cleaning the counter material disc for 25 minutes in ultrasonic bath we can still see the primary layer. Various theories based on Van der Waals force, Columb's electrostatic force and chemical bonding were proposed for transfer layer formation. However, from our observations, both transfer layers (primary and secondary) of GF/PA66 composite were formed from fractured particles trapped between the contacting surfaces that are mechanically milled to form the transfer films. The limitation in formation of the primary transfer layer and its uniformity is due to the inadequacy in debris formation.

However, in secondary transfer layer, sufficient amount of debris are generated by the abrasion process in partial sliding condition. Thus a thick layer (approximately 8 μm) is formed from the generated particles. It is also evident from Figure 4-9 that three distinct regions are clearly seen on the steel counter face. Region 1 in Figure 4-9 indicates the steel surface where for the given constant exposure time and illumination, the surface appears brighter. Region 2 is the primary layer understood from the defocused image, thus indicating the plane of region 2 lower than region 3 which is fully in focus. Also from the texture the primary and the secondary layer can be easily distinguished. Such characteristics are seen in different places of the steel counter face. In regards to the texture, the primary transfer layer has a smooth surface (similar to any coated material) as seen from Figure 4-8(a). The secondary transfer layer is always found with irregular pattern and also embedded with fibers (see Figure 4-8 ). Thus, it can be concluded that the transfer layer formation is a mostly a mechanical process and depends on the availability of debris to form uniform layer or chunk material.

The tribological nature of the transfer layer acting as a protective agent is frequently discussed in literature [4. 18, 19]. From the view point of surface interaction the aggressiveness of the hard steel asperity is reduced with the presence of a transfer layer. Nevertheless this has other consequences like heat dissipation and adhesion characteristics. It can be postulated that the transfer layer carrying the thermal property of the parent material may possess a relatively low thermal conductivity and thus retaining the frictional heat within the contact. Nevertheless, among four tests, the high surface temperature was recorded for 26% slip ratio has less transfer layer thickness than the 9% specimen. Thus we can conclude that the thickness of transfer layer up to 8 μm has negligible influence on heat accumulation/dissipation. This means that the source of temperature increase is mainly the frictional heating due to relative slip.
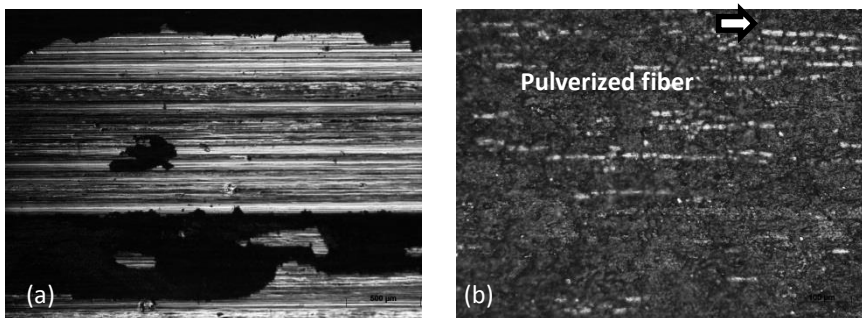


Figure 4-8 Transfer layer (a) with primary and secondary layer for 18% slip (b) embedded with pulverized fibers.
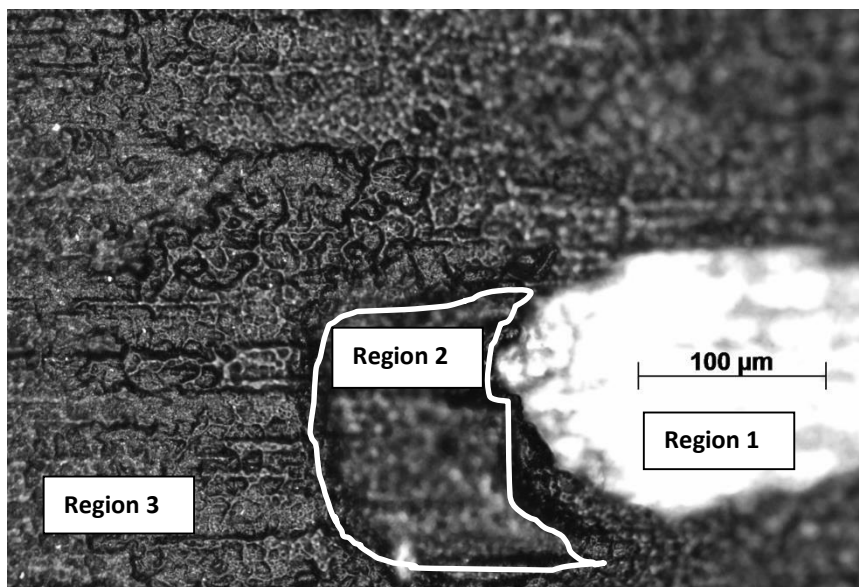
Figure 4-9 transfer layer on the steel counterface material of 9% partial sliding condition (optical microscopy).

## 4.3.2.2 Morphological investigation: SEM

Transfer film roles are well described by Briscoe *et al* for advantageous friction and wear behaviour. Comparing the SEM images of pure rolling and partial slid specimens, it is evident that the transfer layer is promoted by partial sliding which indeed should positively alter the tribological behaviour [4. 19, 20]. From the counterface material at the same level of magnification a dark spongy region (transfer layer) (see Figure 4-10 b) for 26% sliding specimen elucidates the consequence of contact kinematics for transition in wear mechanism. In pure rolling conditions fibres and matrix material are clearly seen in Figure 4-10. On comparing with partial sliding the inadequate quantity of debris present in steel contact surface for pure rolling condition is clearly understood from the SEM micrograph. It is evident that partial sliding increases the transfer layer formation but its contribution to act as a protective layer is not completely true in our case. If in case the transfer layer acts as a protective film, the partial sliding should be intentionally introduced in mechanical components to take advantage of the transfer layer formation. Nevertheless, it is evident that with transfer layer no noticeable friction and wear characteristics were observed. Especially in 9% sliding the friction and wear rate increases. Thus, the self-lubricating characteristics are not prevalent in the used GF/PA66 composite. It is evident that the SEM also provides a similar information as that of optical micrography. Also the higher magnification for transfer layer characteristics reveals limited information about the wear process.
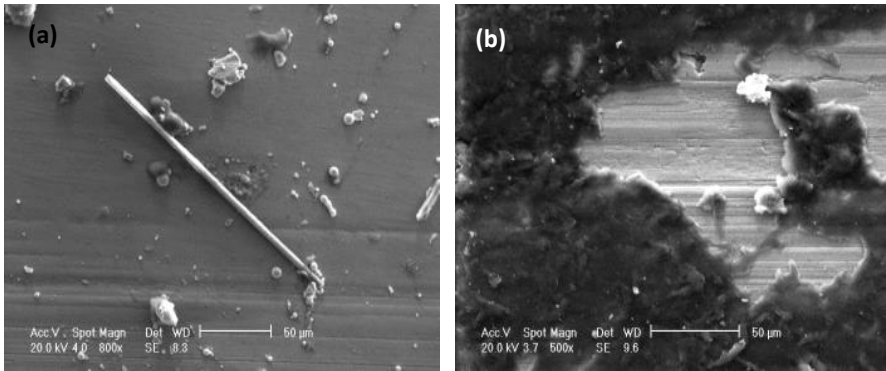
Figure 4-10 shows SEM micrographs of (a) steel counterface at 0% sliding (b) steel counterface at 26% sliding.

To study the thickness of the transfer layer, cross sectional studies were made. In the cross-section of contact surface across the rolling direction a substantial amount of deposit is found for partially sliding condition. The steel asperities are completely covered with the transfer layer by chunks of polymer debris. However, in pure rolling condition the primary layer was not clearly visible. The partial formation of a layer up to 2.9 µm thickness was observed. It is noteworthy to mention that the primary layer takes the geometry of steel asperity.
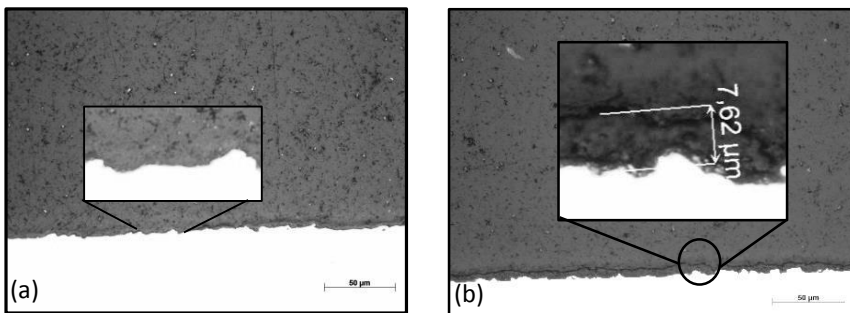


Figure 4-11 Cross-section of steel surface (a) 00% sliding (b) 26% sliding.

## 4.3.2.3 Topographic measurements

The thickness of the deposit correlates well with the surface profile "Rmax" which is the average peak to valley distance. For example Rmax of the 26 % partial sliding condition has a measured thickness of 8.23 µm which is less than ± 1 µm difference in thickness measured through cross section studies (Figure 4-11). The same holds for the pure rolling condition where the Rmax is 2.91 µm and the measured thickness is less than 3 µm.

The kurtosis from the roughness profile supports this theory by having a value greater than 3 for the entire specimen, thus indicating a distribution with sharp peaks. The measured roughness characteristics of the worn profile for four conditions are shown in Table 4-3. It is noteworthy to see the positive skeweness for the partially sliding

condition. A distribution of peaks above the average line can be attributed to the formation of the secondary transfer layer in all three specimens. The negative skewness in the pure rolling condition refers to the predominance of valleys, thus the absence of secondary transfer layer is evident from both topographic measurement and micrograph. Rku having values higher than 3 shows sharp surface characteristics with a leptokurtic profile. Having sharp peaks in the counter material markedly promote grooving by means of abrasion. However, this abrasive action of the asperities is severe only in partial sliding condition as observed from the surface channels.

Table 4-3 Roughness characteristics of steel counter material [µm]

| Slip ratio [%] | Ra | | Rsk | | Rku | | Rmax | | Rpk | |
|:---:|---|---|---|---|---|---|---|---|---|---|
| 0 | 0.80 | 0.45 | -0.34 | -0.76 | 2.41 | 3.28 | 4.76 | 2.91 | 0.43 | 0.24 |
| 9 | 0.79 | 1.13 | -1.4 | 0.27 | 4.44 | 3.32 | 7.68 | 12.89 | 2.07 | 3.42 |
| 18 | 1.03 | 0.99 | -0.91 | -0.44 | 3.34 | 3.66 | 7.25 | 7.85 | 0.25 | 0.96 |
| 26 | 0.20 | 1.16 | -0.94 | 0.21 | 5.46 | 3.68 | 2.46 | 8.23 | 0.13 | 2.36 |

The excessive deposit on the steel surface as a consequence of secondary transfer layer originates from the partial sliding. The micrographs with surface channels (micro-grooves) in Figure 4-4 explicitly indicate the indentation caused by asperity from the counter material. Even after significant deposit of transfer layer abrasion is prevalent. At this stage it is still a qualitative evaluation of the micro-channels from the micrographs. However, among the four conditions, the measured Rpk after testing for 9% and 26% are higher which is a consequence of transfer layer deposition from increased wear. Increased wear rate as seen in Figure 4-2 can be attributed to the ploughing effect of the roughness peaks of counterface (9 %). As it can be seen from the morphological inspection that secondary layer is not entirely present, similar conditions are also experienced in earlier works [4. 19, 20, 21]. Tracing the stylus across such a profile can partially indicate the height difference between primary layer and secondary layer. Figure 4-12 shows such profiles for all four conditions and it is evident that 9% has the highest peaks. Also a difference in level between primary and secondary layer is clearly seen in all the three partial sliding condition.

When there is a thick transfer layer formed on the steel surface it is less likely that the grooves are formed as a consequence of steel polymer interaction. In our case, the formed transfer layer consist of glass fibers which can also act as an asperity in abrading the polymer surface thus increasing the wear rate of the material. It is certain that the partial sliding produces significant amount of debris from the aggressive action of abrasion. In order to have significant quantity of polymer material to form secondary transfer layer, it is required to generate sufficient particle through the wear process. In pure rolling the free particle formation is originated from micro-pitting.
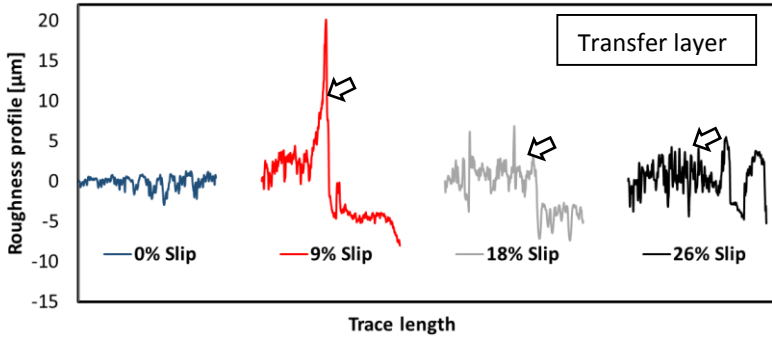
Figure 4-12 Roughness profile of steel counter material for pure rolling and partial sliding condition (trace length 3000 µm).

## 4.3.3 Image analysis: Quantitative microscopy

Even though most tribological tests are validated through wear scar observation from the micrographs, they are still a qualitative estimate. In the current research attempts were made to understand if the quantitative nature of wear scars can represent the wear rate shown in Figure 4-2(a). Also, in order to understand the interaction or estimate the severity of interaction the occurrence of micro-channels is measured using image analysis. Here we propose that the severity of the wear is based on the coverage of micro-channels on the contact surface. Even though there is partial sliding, rolling is still the dominating process. The micro-pits are clearly visible in image analysis from the binary images (Figure 4-13).

It is known that in real industrial practice, depending upon the specific application (rollers, cams and gears), visual inspection of the worn surface is used as a factor for wear evaluation. Nevertheless, in laboratory practice material loss from stereometric analysis is predominantly used. This is partially unrealistic when compared to real industrial practice. In industrial practice, visual inspection is used to a certain degree to estimate wear or service life. Even research reports support theories where visual inspection is made to understand the severity of wear [4. 15]. In such a case these features and their coverage in the contact surface play a vital role in indicating the wear severity.

In our experimental results, pits and grooves observed are rather in-between micro and macro level, which is approximately between the sizes of 30 to 150 µm. Figure 4-13 shows a binary image where micro-channels can be clearly seen. Also, on comparing with the pure rolling surfaces, the micro-pits which are not clearly observed in the grey scale images of partial sliding condition can be well distinguished.

These regions were estimated mathematically through image processing techniques (granulometry) to understand the size distribution of micropits in the micrographs. In partial sliding, the micropits (black regions) persist even in the case of partial sliding condition, which means abrasion is an additional mechanism to micro-pitting. This also answers the elevated wear rate for partial sliding condition. A research by Rao *et*

*al* on POM and PA66 at partial sliding condition shows similar micro-grooves, but rather unclear about the involved mechanisms [4. 17].
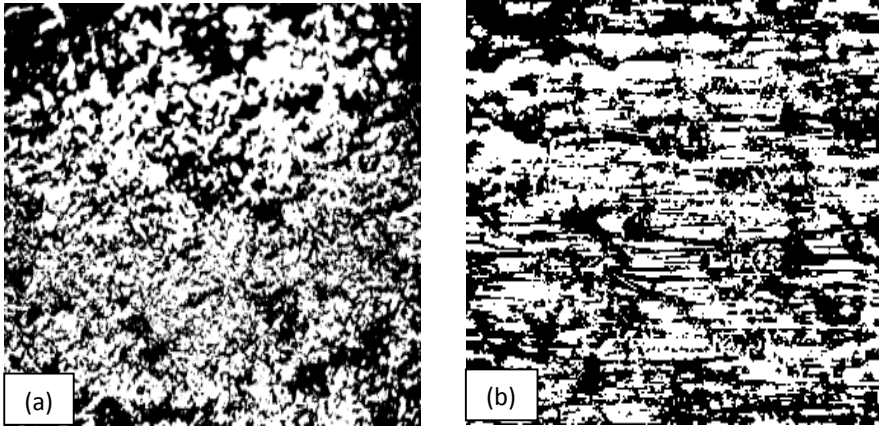


Figure 4-13 *S*egmented micrographs GF/PA 66 at (a) 0% and (b) 26% sliding (include scale).

Aiming at a practical implementation of these image analysis techniques, the quantitative image results are compared with subject experts. A set of 15 images were randomly chosen from these four conditions, including the unworn surface. The level of intensity, with a score between 0 – 100%, on abrasion and pitting as observed by the experts from the details seen on the images were surveyed. This survey is conducted according to the ITU standard BT.500-11. Figure 4-14 shows the estimated score on severity according to the granulometry and its corresponding subjective scores have good correlation for abrasion. The results shown in Figure 4-14 are processed for uneven illumination using local thresholding. Furthermore, for calculating the area occupied by the wear scars, granulometry is done for a sieve size with a rectangular supporting element SE 1 pixel as explained in Chapter 3. A correlation coefficient of 0.99 was found between the objective and subjective curves for abrasion. However, errors persisted for pitting, where the dark corners as seen in Figure 4-13 (a) were considered as pitting. Also the initial unworn surface is taken as a reference image and the surface defects present before wear are to be neutralized to avoid marginal errors in the evaluation of pitting.
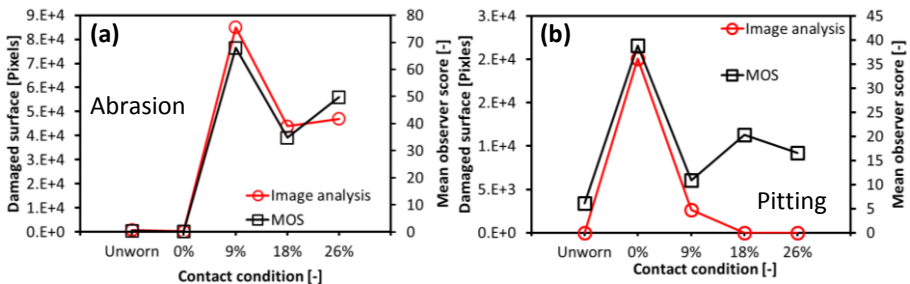


Figure 4-14 comparison of results between image processing and subject experts (a) severity plot (a) abrasion (b) pitting.

Quantitative micrography shows micro-pitting as a dominant mechanism for pure rolling condition. Comparing the four contact conditions, elevated scores for micro-pits were given by experts and the same was estimated by the image analysis (see Figure 4-14). For 18 and 26 % partial sliding condition the area occupied by the grooves due to abrasion is precisely estimated by the image analysis. The severity in wear from the indentation marks made by the hard asperity on soft polymer were segmented and found to be substantially high for 9% partial sliding condition. Both tribography techniques (topographic characteristic and morphology of worn surface) and the quantitative micrography results show increased wear behaviour for 9% slip ratio. The quantitative micrography shows a clear distinction between pure rolling and partial sliding condition. From the wear rate, the transition is not in accordance with the increasing slip. Thus, other topographical factors may dominate the wear characteristics from partial sliding. The abrasion from image analysis, the mean observer score and the wear rate (Figure 4-2 (a) show a similar tendency with increased wear for 9% partially slid specimen. Abrasion of partially slid specimen with 9% sliding ratio has the highest coverage of grooves. Thus, the topographic feature for 9% slip was analysed for characteristics such as RpK, Rmax, Rku and Rsk. The positive skewness in 9% and 26 % sliding indicate the reason for increased presence of transfer layer from severe wear scars.

## 4.4 Development of wear equation for rolling-sliding contacts

While earlier researches alleged the complexity of wear mechanism in polymer sliding, the combination of contact condition having both rolling and partial sliding creates poor understanding of wear mechanism. The fundamental understanding of wear mechanisms has to compliment the experimental data. Here the fundamental interpretations are scattered due to the involvement of different parameters, variations experienced from manufacturing process and also materials used in wear testing. In case of sliding there exists a huge amount of data for creating new wear models. However, a relatively less or insufficient data persist for rolling contacts of polymer-metal tribo-pairs. Moreover, to incorporate all these parameters such as topographic information, material characteristics and operational characteristics, it would take substantial amount of time to perform idealized tribological testing. One way to harmonize this parameter is by using these physical quantities (parameters) in dimensional analysis.

Dimensional analysis is a mathematical tool already being used by tribologist in wear modelling [4. 22, 23]. Though it is not the first time to follow such an approach, novelty is brought in terms of using this tool for wear estimation of rolling-sliding condition and incorporating the surface characteristics of counterface material. A new equation is developed based on the topographic detail (Rmax).

For dimensional analysis it is critical to point out the importance of different parameter considered for the analysis. In our case, the surface topography and contact kinematics are the two most influencing factor. From the topography of steel counter face it is evident that the non-linear characteristics on wear rate represented in Figure 4-2 is a consequence of steel surface. Thus, the topographic characteristics

should also be incorporated in the wear equation. From literature it is also known that compared to pure rolling, the partial sliding had increased wear. Andersson model for rolling-sliding of cams is adopted for describing the relative sliding. In this model, when two contact points $p_1$ and $s_1$ of the dissimilar disc comes in contact at time $T = 0$, the difference in the distance between these two contact point $p_2$ and $s_2$ at time $T = n$ on leaving the Hertzian contact can be considered as a relative slip (see Figure 4-15).
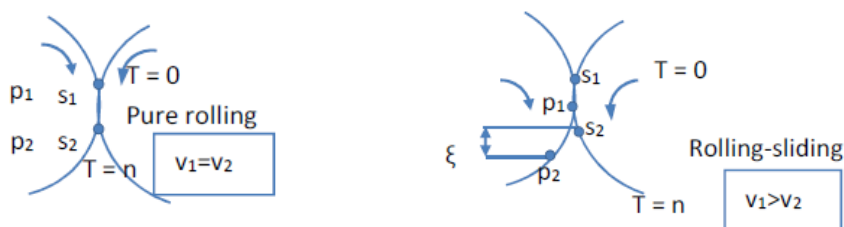


Figure 4-15 Schematic representation of the relative sliding in rolling-sliding contact.

Together with the relative slip, the present equation considers the velocity of polymer disc ($v_1$) and steel disc ($v_2$) for the relative slip velocity. The physical law governing the rolling-sliding condition is the velocity vector which is dissimilar in magnitude. This is required to be included in the wear equation to forecast the trend and the behaviour of polymer-metal tribo pairs. Difference in velocity between the polymer and steel discs are accounted for the relative sliding velocity.

The difference in sliding velocity is given as v

$v = v_1-v_2$

Though in the present case we may use a reference material, the experiments and the model should be allowed to accommodate the usage of other materials in future. Thus the material property (elastic modulus E) is included in the wear equation. In responding to the wear characteristics of polymer-metal pairs in rolling-sliding contact, 7 parameters were chosen for the dimensional analysis. These parameters are rearranged to form 4 dimensional groups using the Buckingham Pi theorem. These 7 parameters are based on three different groups such as (1) operating condition (2) material properties and (3) surface properties.

As understood from the literature each parameter caries a significant importance to be included in the analysis. For example the normal force F is included which can partly represent the scaling factor. The relative slip $\xi$ and the slip velocity s are the primary parameters representing the partial sliding condition. The average peak height Rmax is chosen for representing the initial surface condition. And the sliding distance which normalises the rate dependency is also included. In constructing the dimensionless variables, 7 parameters were selected including the dependent variable V which is the volume loss.

$V = f (F, s, Rmax, E, D, V \xi)$                                    (4.2)

The physical quantities for the selected parameters are given in appendix D.

The difference between the total number of variables (7) and the fundamental dimensions (3) gives the number of dimensionless pi parameters (4)

First, a core group is selected with n=3. The core group is required to have three physical quantities (Rmax, s, F) with at least one fundamental unit in each. In our case the same condition was followed, besides care was taken that the core group contains one variable representing individual characteristics of surface parameter (Rmax) and operational characteristics (s and F). The representative variables in the core group variable are given below.

Core group = [F, s, Rmax, E]                                                                    (4.3)

Next, using core group a set of product groups is formed. Each product group consists of the core group and one variable outside the core group.

$\qquad$ [F, s, Rmax, E]                                                              (4.4)
$\qquad$ [F, s, Rmax, D]                                                              (4.5)
$\qquad$ [F, s, Rmax, V]                                                              (4.6)
$\qquad$ [F, s, Rmax, ξ]                                                              (4.7)

After the selection of product groups, arbitrary exponents are assigned to the variables in the product group (4.4 to 4.7). The product groups are given as

$\qquad$ $\Pi 1 = [(F)^{a1}, (s)^{b1}, (Rmax)^{c1}, (E)]$                                  (4.8)
$\qquad$ $\Pi 2 = [(F)^{a2}, (s)^{b2}, (Rmax)^{c2}, (D)]$                                  (4.9)
$\qquad$ $\Pi 3 = [(F)^{a3}, (s)^{b3}, (Rmax)^{c3}, (V)]$                                 (4.10)
$\qquad$ $\Pi 4 = [(F)^{a4}, (s)^{b4}, (Rmax)^{c4}, (ξ)]$                                 (4.11)

By requiring each product group to be dimensionless, it is possible to solve for those arbitrary exponents. Solving the exponents results in the following four dimensionless Pi parameters (see Table 4-4). Each representing a factor connected to the wear characteristics (The details of the derivation are given in Appendix D).

It is evident from the four Pi groups that each signifies a specific physical nature of the tribo system. For example the group $\pi_1$ which contains the elastic modulus and normal force is a good representative for material characteristics and scaling factor. In general the wear equation uses hardness of the material a critical parameter. However, having a huge difference in hardness ratio between the tribo pair and a relatively less difference in the Shore D hardness between polymer the harness does not play a vital role here. Besides the elastic property of the material decides the progressive damage from plastic flow and fracturing of asperities. Thus this group is strongly associated with the material characteristics. Likewise the significance of other groups are mentioned in Table 4-4.

Table 4-4 Dimensional group and its physical significance

| Dimensionless group | Physical significance |
|---|---|
| $\pi1 = \dfrac{(Rmax)^2 E}{F}$ | Mechanical characteristics are included if in case other materials are to be used for future investigations this equation can also be used. |
| $\pi2 = \dfrac{D}{Rmax}$ | The sliding distance which has significant contribution in creating a damage from abrasion as understood from the micrographs |
| $\pi3 = \dfrac{V}{Rmax^3}$ | The wear volume in this case is the calculated quantity from the mass loss and the density of the material. |
| $\pi4 = \dfrac{\xi}{Rmax}$ | Relative slip is related to the partial sliding condition. It is also found in the results and in literature the wear increases as a function of slip ratio, thus, this group represents the rolling sliding factor. |

The four groups can be put as

$$\left( \frac{(Rmax)^2 E}{F} \right) \left( \frac{D}{Rmax} \right) \left( \frac{V}{Rmax^3} \right) \left( \frac{\xi}{Rmax} \right) \qquad (4.12)$$

This can be redefined in favour of wear by adding a constant k in the depended group. The objective is to understand the undetermined factor k relating to the included variables that represent all three groups such as operating parameters, material characteristics and surface characteristics. The initial surface topographic information Rmax is know from the stylus profilometry, the wear volume V is calculated from the mass loss. The other known factors on normal force and E modulus of the materials will be used to find the unknown factor k.

$$\frac{V}{Rmax^3} = k \left( \frac{(Rmax)^2 E}{F} \right) \left( \frac{D}{Rmax} \right) \left( \frac{\xi}{Rmax} \right) \qquad (4.13)$$

This further result in

$$V = k. \frac{Rmax^3 E \xi D}{F} \qquad (4.14)$$

Where k is the wear dependence constant.

$$k = \frac{V F}{Rmax^3 E \xi D} \qquad (4.15)$$

Using equation (4.15) for dimensionless wear trend, a choice on favorable physical parameter can be investigated for its influence using experiments. The direct proportionality of the surface feature, operational parameter and material characteristics is well represented in equation (4.14). It is evident that with increased Rmax of the counter material the polymer deposition is significantly high. Thus proportional exist between Rmax and wear volume. The same also fits good for the increased slip ratio, where the relative sliding increases leads to increased wear. The model clearly includes the effect of transfer layer deposition from the average peak measurements Rmax. However, the basic understanding of the involved mechanism which is micro-cutting on polymer surface by roughness peaks, coverage of transfer layer in the XY plane and surface change from polymers are yet to be realised in the wear equation.

Considering the linear increase in the slip ratio an intermediate raise in wear rate at 9% slip can be attributed to Rpk found on the initial contact surface of steel discs which is higher than the rest. This wear equation for the given experimental data provides a trend similar to the non-dimensional theoretical wear as shown in Figure 4-16 (the axis are not mentioned in the plot due to different dimensional quantities). It is evident from Figure 4-16 that the wear trend for the Avanzini et al, theoretical non dimensional wear, mean observer score, image analysis and the experimental results shows similar trend for the considered rolling-sliding condition.
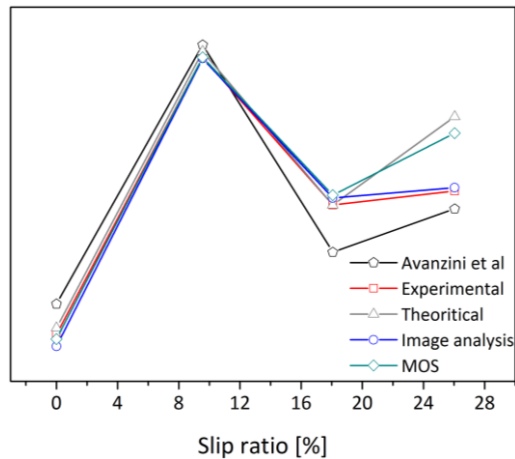


Figure 4-16 Wear trend calculated based on the dimensional analysis and wear trend from image analysis and Avanzini *et al.*

The severity of wear in terms of the included parameters on rolling-sliding condition can be evaluated by the non-dimensional wear rate. From the experimental implication of the current study for the developed equation shows that the surface topography has dominating characteristics than the partial sliding condition. The developed equation serves better to understand the dominating wear characteristics for a set of condition.

## 4.5 Summary and conclusion

In classical wear testing of rolling-sliding of polymer-metal components, it is assumed that the tribosystem remains unchanged. However, in the course of wear the contact condition changes from polymer-metal to polymer-polymer contact, thus effectively changing the nature of the tribological system. The transfer layer characteristics are clearly studied. Two types of transfer layer were observed in pure rolling and partial sliding condition. Thin uniform layer was observed in the pure rolling specimen and thick chunk of material referred as secondary transfer layer was found in partially slid specimen. These transfer layers do not affect the heat dissipation process. Beside micrographs and wear characterisation by mass loss it is necessary to identify the root cause of transfer layers formation.

From the current experiments it is evident that a significant change in wear mechanism occurs when moving from pure rolling to partial sliding. Pure rolling specimen is dominated by micro-pitting. This is confirmed by the microscopic inspections as well as by the image analysis. However, the pitting behaviour is also observed in the partial sliding condition where abrasion is the dominant mechanism.

The methodology (image analysis) stands effective in analysing the dominant mechanism and its severity. For example, the 9% partial sliding specimen has undergone the most severe wear. To understand more about the transfer layer a time scale- study is necessary to acquire the complete knowledge on the formation of these layers. An appropriate way to do that is the *ex-situ* technique which will be discussed in Chapter 5.

Based on the mass loss and the mechanism observed from tribography the following conclusions are made in answering the questions raised in Chapter 1 and 2:

- Laboratory scale model testing can fully represent the real application for experimentally simulating rolling-sliding wear of polymers.
- Polymers at pure rolling contact has micro-pits and cracks as dominant wear scars to represent the repeated cycle deformation.
- The high wear rate for partial sliding condition is due to the abrasive action of the steel asperities. The abrasive action is clearly observed in the SEM, 3D topography, and also in optical microscopy.
- Besides the partial sliding, the initial topographic height parameter of steel which is the Rpk plays a vital role. The peaks found in the steel surface acts as an indenter in the contact surface to perform the micro-cutting.
- The wear scars as a quantitative representative for wear characterization are clearly revealed from the subjective and objective scores.

# References

[4.1]     D. H. Gordon and S. N. Kukureka, "The wear and friction of polyamide 46 and polyamide 46/aramid-fibre composites in sliding/rolling contact," Wear, vol. 267, pp. 669-678, 2009.

[4.2]     C. J. Hooke, S. N. Kukureka, P. Liao, M. Rao, and Y. K. Chen, "Wear and friction of nylon-glass fibre composites in non-conformal contact under combined rolling and sliding," Wear, vol. 197, pp. 115-122, 1996.

[4.3]     S. N. Kukureka, C. J. Hooke, M. Rao, P. Liao, and Y. K. Chen, "The effect of fibre reinforcement on the friction and wear of polyamide 66 under dry rolling/sliding contact," Tribology International, vol. 32, pp. 107-116, 1999.

[4.4]     Y. K. Chen, S. N. Kukureka, C. J. Hooke, and M. Rao, "Surface topography and wear mechanisms in polyamide 66 and its composites," Journal of Materials Science, vol. 35, pp. 1269-1281, 2000/03/01 2000.

[4.5]     H. Koike, K. Kida, E. C. Santos, J. Rozwadowska, Y. Kashima, and K. Kanemasu, "Self-lubrication of PEEK polymer bearings in rolling contact fatigue under radial loads," Tribology International, vol. 49, pp. 30-38, 2012.

[4.6]     S. N. Kukureka, Y. K. Chen, C. J. Hooke, and P. Liao, "The wear mechanisms of acetal in unlubricated rolling-sliding contact," Wear, vol. 185, pp. 1-8, 1995.

[4.7]     T. A. Stolarski, "Tribology of polyetheretherketone," Wear, vol. 158, pp. 71-78, 1992.

[4.8]     H. Czichos, "Influence of adhesive and abrasive mechanisms on the tribological behaviour of thermoplastic polymers," Wear, vol. 88, pp. 27-43, 1983.

[4.9]     A. Avanzini, G. Donzella, A. Mazzù, and C. Petrogalli, "Wear and rolling contact fatigue of PEEK and PEEK composites," Tribology International, vol. 57, pp. 22-30, 2013.

[4.10]    C. J. Hooke, S. N. Kukureka, P. Liao, M. Rao, and Y. K. Chen, "The friction and wear of polymers in non-conformal contacts," Wear, vol. 200, pp. 83-94, 1996.

[4.11]    C. Ren, J. Chen, H. Pan, X. Huang, and H. Zhu, "Wear mechanism of PA6 roller used in cold rolling process," Engineering Failure Analysis, vol. 28, pp. 311-317, 2013.

[4.12]    L. Chang, Z. Zhang, H. Zhang, and A. K. Schlarb, "On the sliding wear of nanoparticle filled polyamide 66 composites," Composites Science and Technology, vol. 66, pp. 3188-3198, 2006.

[4.13]    A. Pogačnik and M. Kalin, "Parameters influencing the running-in and long-term tribological behaviour of polyamide (PA) against polyacetal (POM) and steel," Wear, vol. 290–291, pp. 140-148, 2012.

[4.14]    M. K. Kar and S. Bahadur, "Micromechanism of wear at polymer-metal sliding interface," Wear, vol. 46, pp. 189-202, 1978.

[4.15]    T. A. Stolarski, S. M. Hosseini, and S. Tobe, "Surface fatigue of polymers in rolling contact," Wear, vol. 214, pp. 271-278, 1998.

[4.16]    M. Wong, G. T. Lim, A. Moyse, J. N. Reddy, and H. J. Sue, "A new test methodology for evaluating scratch resistance of polymers," Wear, vol. 256, pp. 1214-1227, 2004.

[4.17]   M. Rao, C. J. Hooke, S. N. Kukureka, P. Liao, and Y. K. Chen, "The effect of PTFE on the friction and wear behavior of polymers in rolling-sliding contact," Polymer Engineering & Science, vol. 38, pp. 1946-1958, 1998.

[4.18]   B. J. Briscoe and S. K. Sinha, "Wear of polymers," Proceedings of the Institution of Mechanical Engineers, Part J: Journal of Engineering Tribology, vol. 216, pp. 401-413, 2002.

[4.19]   S. Bahadur, "The development of transfer layers and their role in polymer tribology," Wear, vol. 245, pp. 92-99, 2000.

[4.20]   Y. J. Mergler, R. P. Schaake, and A. J. Huis in't Veld, "Material transfer of POM in sliding contact," Wear, vol. 256, pp. 294-301, 2004.

[4.21]   A. I. Sviridyonok, V. A. Bely, V. A. Smurugov, and V. G. Savkin, "A study of transfer in frictional interaction of polymers," Wear, vol. 25, pp. 301-308, 1973.

[4.22]   N. Viswanath and D. G. Bellow, "Development of an equation for the wear of polymers," Wear, vol. 181–183, Part 1, pp. 42-49, 1995.

[4.23]   J. K. Lancaster, "Material-specific wear mechanisms: relevance to wear modelling," Wear, vol. 141, pp. 159-183, 1990.

# Evolution of wear in rolling-sliding of polymers

# Goal

This chapter emphasises on the dynamicity involved in wear process of polymers in rolling-sliding contact. The previous chapter elucidates the wear mechanisms and transfer layer characteristics from post-mortem analysis, which signifies the information taken only after substantial change. Debris characteristics observed in chapter 4 raises questions about the dynamic tribological nature of polymer-metal pairs. Attempts were made to answer questions regarding the dynamicity in the formation of a transfer layer by means of *ex-situ* investigation. Surface characteristics are acquired at specific intervals to understand the evolution of damage in the wear process. Imaging techniques are effectively used and validated by means of roughness measurements. The hypothesis on repeated cycle deformation behaviour in polymer rolling is studied. Also, evidences about abrasion process are clearly understood from the sequential imaging of a well-defined region in the contact surface. The dynamic nature of transfer layer occurrences is understood from the calculated energy score of the grey scale texture. The dynamic wear behaviour in these contacts is explained from the view point of both the transfer layer formation and asperity modification.

## 5.1 Limitations in the traditional tribography

In general, polymer-metal tribo pairs under rolling-sliding condition are descriptively studied [5. 1, 2, 3, 4, 5]. Stolarski reported that though polymers have numerous applications in rolling contacts, the basic mechanisms for material removal are still unclear. Some of the wear phenomena reported for rolling-sliding of polymers as observed in the post-mortem analysis are micro-pitting, lateral cracks, transfer layer, roll formation, fibre debonding, surface flaking, fibre damage, delamination and melting [5. 1, 3, 6, 7, 8, 9, 10]. Assumptions on wear process from post-mortem analysis might be only partially correct; thus, a damage evolution study is essential. In an evolution study, the driving factors for wear particle generation and transfer layer formation can be easily understood by following the damage process. Investigations on transfer layer formation are imperative in tribological characterisation of polymer metal tribo-pairs. From chapter 4, the quantitative descriptions (in Rmax) were given for the so-called "transfer layer" based on the post-mortem analysis. However, the variations in the coverage of transfer layer based on its global presence on the complete contact surface are not considered. Hence, its characteristics from the post-mortem analysis through topographic data may contain high level of uncertainty. Without knowing the variations in the occurrence of transfer layers as a function of time, it will be ambiguous to consider it as a parameter influencing tribological characteristics. The poor adhesive nature of transfer layer on the counter material and its tendency of adhering back to the initial material leads to inconsistency in friction behaviour [5. 11]. Thus, it is necessary to describe a step-by-step process in wear particle generation and transfer layer formation for the given tribosystem.

## 5.2 Advantages of damage evolution studies (DES) on wear particle generation

Monitoring the evolution of wear has always been an interest to scientists to understand the underlying mechanisms [5. 12, 13, 14, 15, 16]. Surface topography and morphology are representative quantities and qualities that elucidate the tribological nature of a contact pair. Moore, in his review, explains that the surface texture plays a vital role in modifying the friction characteristics [5. 17]. However, the topographical measurement and its analysis are partly sufficient to outline the surface change. Thus, both morphological measurement using optical technique and stylus profilometry are used by means of *ex-situ* approach. The difficulty arises in locating the same region for repeated measurements. Relocation profilometry was one of the techniques, which were used for locating the same region. Tasan *et al* used an alternative semi-online monitoring technique on topographic analysis where the specimen is brought to rest and measurement is made without dismounting [5. 15]. However, in these cases, only two dimensional topographic changes are measured. Willamson *et al* suggested that only limited number of asperities undergo modification during a tribological contact. Hence, reference mapping for wear studies using topographic characterization is tedious and requires statistical data, which is also laborious. However, mapping of large surface area in XY plane based on micrographs may provide sufficient information to track the changes qualitatively and quantitatively.

It is evident that, in the conventional tribological studies, the cumulative damage from progressive material loss hinders the understanding of the wear process. It is noteworthy to mention that the existing damage evolution studies performed for steel or lubricated surfaces clearly elucidate the wear process [5. 18, 19]. The change in surface texture during a wear process could be further used to understand the material characteristics based on the observations from wear evolution or surface damage. In this thesis, the polymer surfaces are investigated to understand the wear process via damage evolution studies by *ex-situ* techniques.

## 5.3 A different approach (Reflected dark field illumination)

It has been reported earlier that the minute details of the wear scars are difficult to observe by bright field illumination. However, this can be overcome by using an old technique called as dark field illumination [5. 20]. Thus, in the current chapter, in addition to bright field imaging, a dark field imaging technique is used. The latter type of imaging is not new in microscopy; however, very limited literature on its use in the tribological investigation could be found [5. 20]. The main criterion in dark field microscopy is that the light cannot enter through the objective. However, the reflected light from the surface can use the optical path to capture the image of the worn surface in the CCD. In our equipment, we adopted simple modifications to produce the dark field image. An external illumination by means of fibre optic guided lights is directed to the worn surface at a certain angle (90° ± 5°) (See Figure 5-1). This ensures only the reflected light to travel via the optical path to the CCD for image

acquisition. Both the bright field and dark field imaging were used in the *ex-situ* methodology.
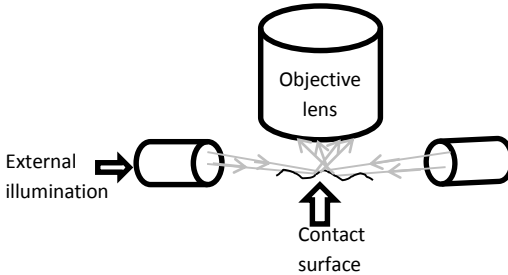


Figure 5-1 Adaptation for external illumination.

## 5.4 The approach of damage evolution studies (DES)

A limited number of studies exist focusing on the understanding of the rolling-sliding behaviour of polymers. However, these studies always followed the traditional tribography approach. There are few reported works on damage evolution but limited to pure sliding contacts representing severe wear. This research will examine the evolution of wear surface of rolling contacts in polymer composites. Both the composite and steel surfaces are monitored, and correlation between the changes in surface morphology and its corresponding tribological behaviour are deduced.

Like traditional tribological study (TTS), the damage evolution study (DES) also uses the same material combination with glass fibre-reinforced polyamide composite against steel counterface. The partial sliding condition is investigated with the focus on understanding the surface modification using photomacrographs, micrographs and topographic information. Qualitative and quantitative information from the micrographs are used for discerning the changes suffered by the polymer surface. A step-by-step process of wear was schematically described based on the observations. Furthermore, the steel counterface surface was investigated for the transfer layer characteristics.

In the DES, wear tests of $2.4 \cdot 10^5$ cycles, corresponding to approximately 8 hours of testing clearly indicate the dynamic behaviour of the transfer layer. From interrupted testing the peak temperature at all intervals was considered for the time series plot. Figure 5-2 shows friction and temperature curve from $0 - 2.4 \cdot 10^5$ cycles that were interrupted for every $1.5 \cdot 10^4$ cycles until $1.2 \cdot 10^5$ rotations (see Appendix C). Later, the intermediate pause was made for every $3.0 \cdot 10^4$ rotations. This threshold was made based on the test results from TTS study (chapter 4) and visual interpretation of the images. It is evident from Figure 5-2 that, after each intermediate pause both the friction and temperature profile experiences a sharp increase followed by transition and steady stage. It is apparent that both the temperature and the friction curves show a running-in phase at every intermediate pause. Though the intermediate pause in *ex-situ* may reveal the development of wear process, it will disturb the equilibrium of testing, both mechanically and thermally.
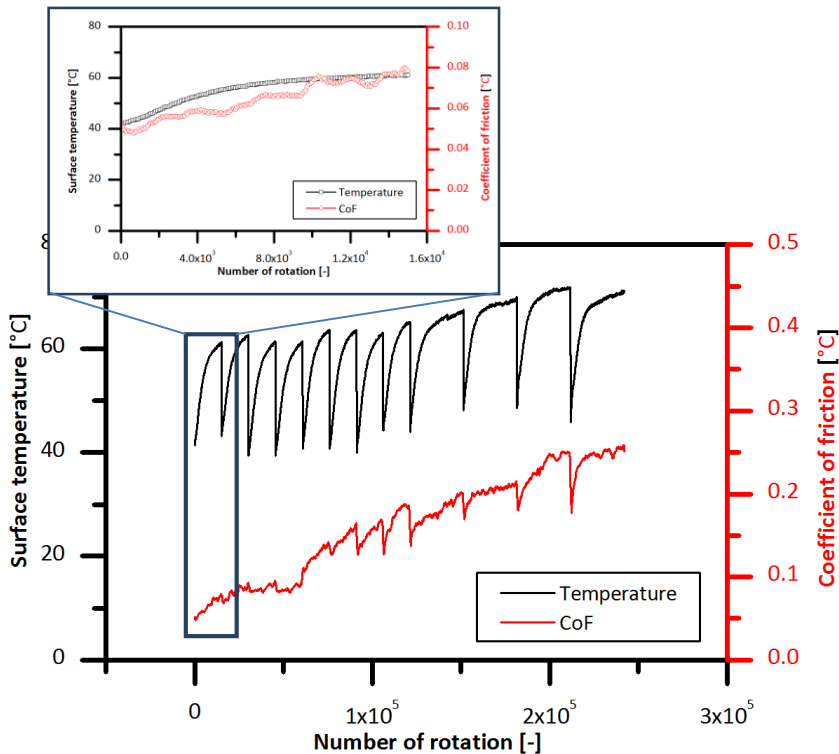
Figure 5-2 Shows the friction and temperature curve for one intermediate pause and complete cycles.

Two tests (Test 1 and Test 2) for repeatability were performed with 30% slip ratio. These tests were made to verify if the material shows similar behaviour in terms of friction, surface morphology and temperature characteristics. The recorded temperature plot shows less than 1°C of temperature change between the two tests (except for $9 \cdot 10^4$ rotations) at all intervals. For the same temperature profile of test 1 and test 2, variations in friction characteristics were observed for both the tests after $9.0 \cdot 10^4$ rotations. This implies that differences in friction coefficient cannot be explained by temperature effects. Thus, any variations in friction should rather be attributed to the change in physical surface characteristics such as morphology, asperity heights or wear patterns.
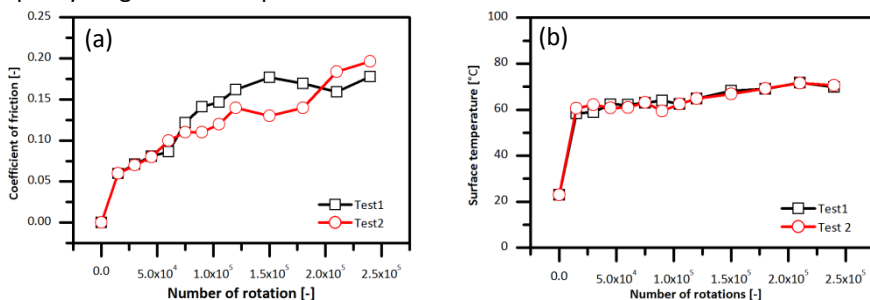


Figure 5-3 Test 1 and Test 2 (a) CoF curve (b) temperature profile.

It is noteworthy to mention that the wear measurements using gravimetric analysis cannot be performed in DES due to less material removal at each intermediate pause. In addition, the drying procedure followed in chapter 4 requires 20 hours of drying, which is not feasible with the intermediate pause. Also, the reference profilometry through V-groove does not show significant change and thus not considered for wear analysis. The friction curves for both tests follow a similar trend until $9.0 \cdot 10^4$ rotations. Thereafter, variations in friction characteristics can be observed (see Figure 5-3a). The dissimilarity in friction between the two tests after $9.0 \cdot 10^4$ rotations can be attributed to the surface change. Figure 5-4 shows the roughness Rmax of the polymer surfaces at all intervals, where the changes between the test 1 and test 2 are clearly observed after $9.0 \cdot 10^4$ rotations. Such changes were not observed for steel counter face material. Thus, the changes in friction characteristics can be related mainly with the Rmax of the polymer specimen. However, this roughness evolution and the friction and temperature profile do not provide enough information to describe the sequential surface modification suffered by the material. Consequently, the polymer and steel surface were investigated at a microscopic scale for better understanding of the morphological changes. The details of the microscopic technique were already described in Chapter 3.
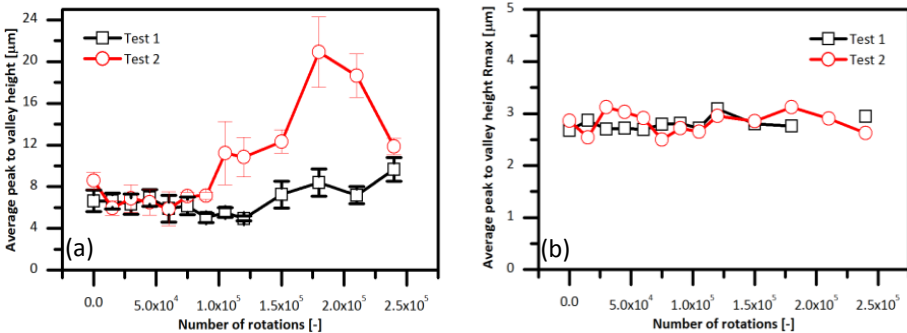


Figure 5-4 Rmax of the (a) polymer surface (b) steel surface.

## 5.4.1  Evolution of the polymer contact surface

## 5.4.1.1 Photomacrographs

During intermediate pauses, the photomacrographs of the worn contact surface were acquired using CANON PC1234 optical camera with ring light near vertical illumination. Comparing the images taken at initial surface and $2.4 \cdot 10^5$ rotations a significant surface change was observed (Figure 5-5). After $2.4 \cdot 10^5$ rotations in Test 1 specimen, the polymer contact surface was observed to be covered with thin sheet of polymers. This can be ascribed as a transfer layer on the polymer surface. In literatures, transfer layer was generally examined on the steel counter material. In our case, from the *ex-situ* technique, it was concluded that both the parent material and the counter material are important for the formation of transfer layers. These transfer layers on polymer surface have specific morphology, with a curl on the trailing (receding) edge.
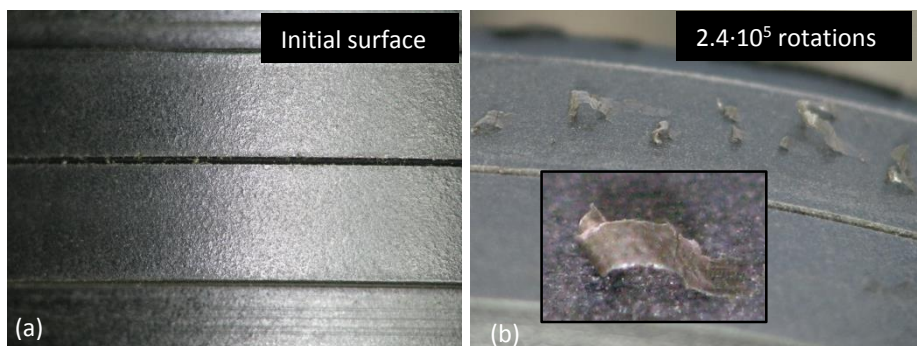
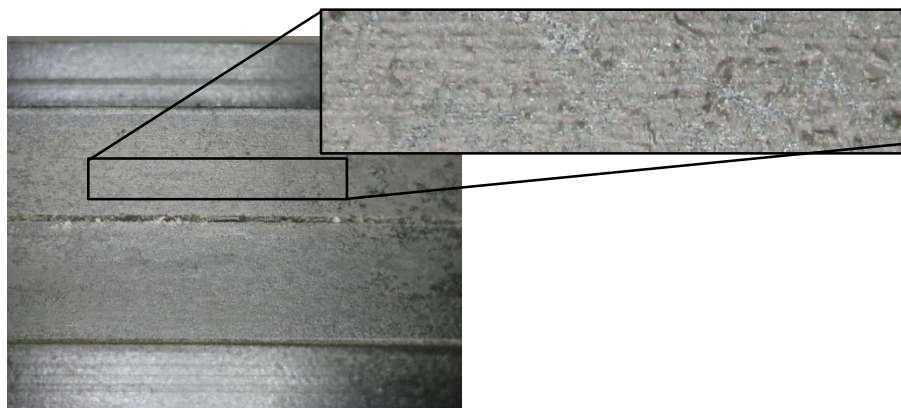Figure 5-5 Photomacrographs of polymer contact surface for Test 1 (a) initial surface (b) $2.4\cdot10^5$.



Figure 5-6 Photomacrographs of polymer contact surface for Test 2 at $2.4\cdot10^5$ rotations.

For the same operating condition, the major difference between Test 1 and Test 2 is the formation of the thin layer (see Figure 5-5 b) on polymer contact surface in Test 1. The reason for the formation is strictly from the generated particle, which relies on the topographic details of counter face material that will be discussed later in this chapter. In Test 2, the worn polymer contact surface is observed with grooves as a consequence of partial sliding (see zoomed out portion). Patches of spongy material (debris) are unevenly spread throughout the contact. Nevertheless, the thin sheet like substance present in Test 1 was not found in Test 2.

## 5.4.1.2 Micrography with bright field illumination

The images of worn contact surface are acquired with reflected brightfield microscope, which is commonly used for opaque specimens. Selected micrographs of GF/PA66 at specific intermediate pauses are shown in Figure 5-7. The relationship between consecutive images is explained later. All brightfield images were taken with same exposure time of 1500 µs. Registration of images was done to identify the same location for every intermediate pause. The global view of images might look different; however, there are bridging features between consecutive images, which act as a reference to track the evolution of wear. The reference scars are marked on the consecutive images to point out the common features between two images (Figure 5-7). From the micrographs in Figure 5-7, it can be seen that no substantial change was found until $4.5 \cdot 10^4$ rotations. The dark regions pointed out with white arrows are the only changes recognised until $4.5 \cdot 10^5$ rotations. Evidence of partial abrasion is clearly seen only after $2.1 \cdot 10^5$ rotations. After $2.1 \cdot 10^5$ rotations, micro-channels are clearly visible as pointed out with white arrows. Similar kinds of surface scars with micro-channels are seen in the post-mortem analysis in chapter 4 for partial sliding conditions. From the obtained micrographs and the corresponding Rmax values, the explanation of the evolution can be made.
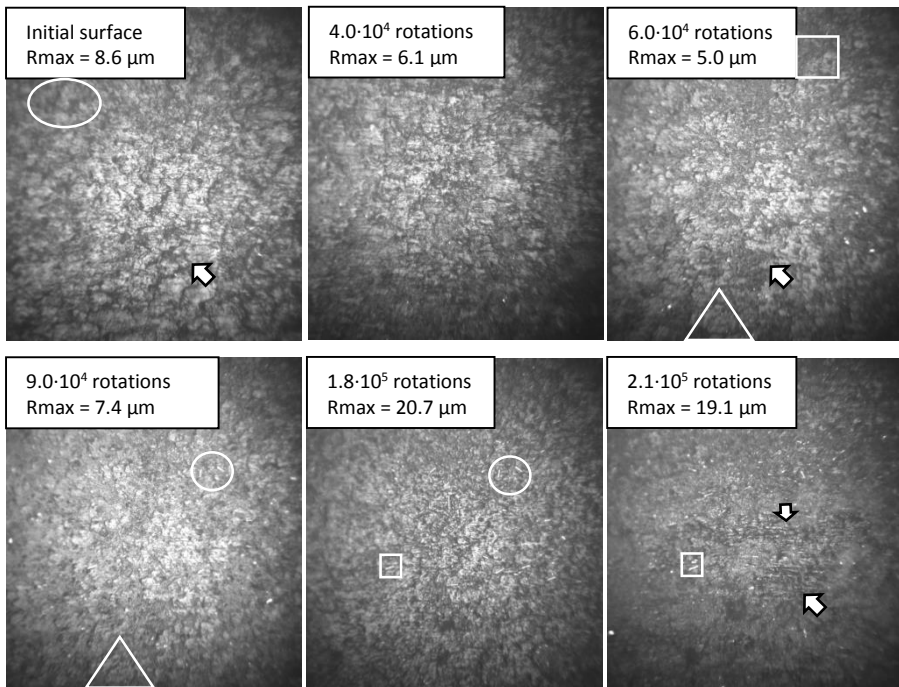


Figure 5-7 selected sequence of micrographs from Test 2 representing the evolution of polymer surface morphology (Raw image, 1500 µs exposure time).

Table 5-1 Topographic characteristic (polymer) at each intermediate pause [μm]

| Rotations | Test 1 | | | | Test 2 | | | |
|---|---|---|---|---|---|---|---|---|
| | Ra | Rsk | Rku | Rmax | Ra | Rsk | Rku | Rmax |
| $0.00 \cdot 10^0$ | 0.91 | 0.05 | 2.89 | 6.64 | 1.03 | 0.31 | 3.29 | 8.67 |
| $1.50 \cdot 10^4$ | 0.88 | -0.04 | 2.90 | 6.62 | 0.89 | -0.19 | 2.85 | 6.02 |
| $3.00 \cdot 10^4$ | 0.92 | -0.18 | 2.85 | 6.33 | 0.90 | 0.01 | 3.13 | 7.31 |
| $4.50 \cdot 10^4$ | 0.94 | 0.15 | 2.85 | 6.91 | 0.88 | -0.08 | 2.70 | 6.16 |
| $6.00 \cdot 10^4$ | 0.85 | 0.10 | 3.03 | 5.89 | 0.76 | 0.15 | 2.52 | 5.06 |
| $7.50 \cdot 10^4$ | 0.88 | 0.23 | 2.86 | 6.15 | 0.78 | -0.49 | 3.10 | 6.95 |
| $9.00 \cdot 10^4$ | 0.78 | 0.30 | 2.96 | 5.02 | 1.00 | 0.27 | 2.99 | 7.45 |
| $1.05 \cdot 10^5$ | 0.88 | -0.03 | 2.66 | 5.52 | 1.20 | 0.21 | 3.39 | 12.02 |
| $1.20 \cdot 10^5$ | 0.78 | 0.00 | 2.61 | 4.96 | 1.43 | -0.14 | 3.62 | 10.84 |
| $1.50 \cdot 10^5$ | 0.98 | -0.07 | 2.94 | 7.25 | 1.49 | -0.15 | 2.97 | 12.23 |
| $1.80 \cdot 10^5$ | 1.06 | 0.16 | 2.66 | 8.40 | 2.41 | -0.41 | 2.85 | 20.76 |
| $2.10 \cdot 10^5$ | 1.04 | 0.02 | 3.26 | 7.19 | 2.39 | -0.38 | 3.06 | 19.13 |
| $2.40 \cdot 10^5$ | 1.24 | -0.13 | 3.01 | 9.66 | 1.73 | -0.69 | 3.40 | 11.87 |

Comparing polymer worn surface from Test 1 and 2, both show similar surface morphologies and patterns. Hence, images of polymer surface only from Test 2 are shown. Topographic values listed in Table 5-1 display difference in Rmax from $9.0 \cdot 10^4$ rotations. Starting from zero rotation, dark patches are seen even before contact, and are encircled in the gray scale image (see Figure 5-8). The edges for the texture in the encircled region are clearly visible in the binary images. However, investigating further the area of the dark regions reduces at the first intermediate pause after $1.5 \cdot 10^4$ rotations.



0 rotations
Rmax = 8.6 μm
Rsk = 0.31

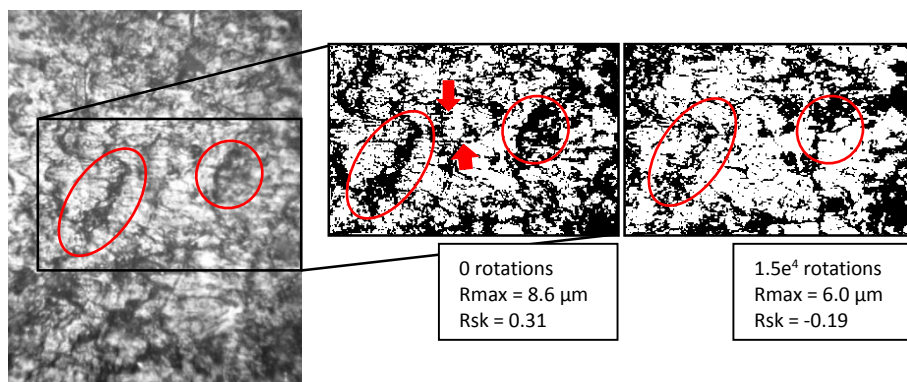1.5e⁴ rotations
Rmax = 6.0 μm
Rsk = -0.19

Figure 5-8 shows the transition in surface morphology in the initial stage of wear (Images processed for contrast).

This observation can be linked to the filling of micro-voids (dark region) as observed in Figure 5-8 and also reflected in the decrease of Rmax from 8.5 to 5.9 µm. The mechanism behind filling these holes can be attributed to plastic flow of the matrix (PA66). However, in the used bright field imaging, due to the saturation of light, limitation in terms of resolution exists in pointing out the plastic flow from the obtained texture. Thus, later in this chapter, another technique (dark field imaging) will be used to validate the plastic flow. Proceeding further to $6.0 \cdot 10^4$ rotations, the micrographs show characteristics with dark regions and its corresponding Rmax is 5.06 µm. Nevertheless, this specific intermediate pause has a positive skewness for Rsk = 0.15 on comparing with the previous intermediate stops. Thus, it can be assumed that a predominant peak zone appears from the deposit of polymer debris. Starting from $1.8 \cdot 10^5$ rotations, mild signs of abrasion are partially revealed; however, it becomes more dominant in the later stage.

It is evident that more and more glass fibres are seen after $2.1 \cdot 10^5$ rotations and also the texture has changed significantly. In these textures, abrasion lines are clearly visible and the Kurtosis value (Rku=3.09) above 3 indicates sharp peak profiles. The peak profiles from kurtosis with negative skewness (Rsk = -0.38) in the polymer contact surface shows deep and narrow valleys. This can be attributed as micro-cutting of polymer surface by steel asperities. Supporting the earlier statement grooves with narrow and steep valleys are already reported as micro-cutting in the literature [5. 21]. However, reference values for comparing micro-cutting and micro-ploughing from the kurtosis and skewness are yet to be investigated. It was previously understood from the literature that shallow grooves represent micro-ploughing while sharp and narrow grooves represent the micro-cutting [5. 22]. This texture of polymer contact surface show abrasion grooves represented by parallel lines. Such a mechanism is seldom reported for model testing. To effectively demonstrate the usefulness of image processing technique, the images from $2.1 \cdot 10^5$ and $2.4 \cdot 10^5$ are compared between each other (Figure 5-9). The patches (encircled in red) found after $2.1 \cdot 10^5$ rotations are partially removed in the subsequent cycles. However, for an expert, the visualisation of these two images may represent dissimilar region and appear completely different, or it might take considerable time to find similarity between these two images to follow the evolution process. Registration is the appropriate technique to identify the similarity between two different profiles at pixel level. In the micrographs, the encircled region at $2.1 \cdot 10^5$ and $2.4 \cdot 10^5$ rotations are the common features, which are hardly possible to detect without effective image processing. The image processing part is carried out by S. Soleimani and K. Douterloigne from IPI group of the TELIN department (telecommunication and information processing) of Ghent University.
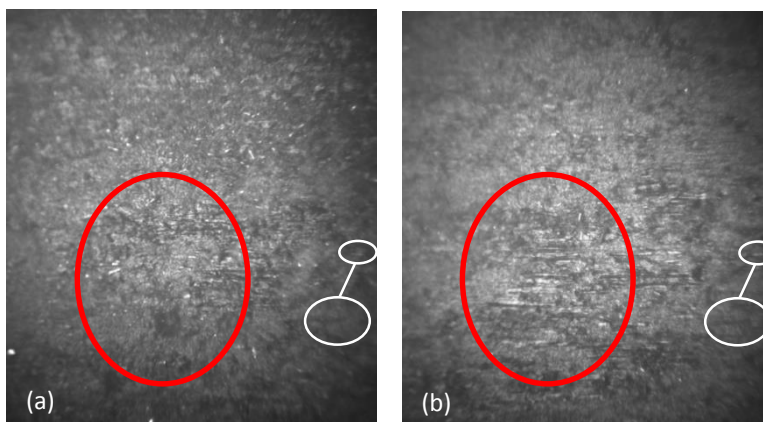
Figure 5-9 Polymer morphology (a) $2.1 \cdot 10^5$ rotations (b) $2.4 \cdot 10^5$ rotations. (Raw images, 1500 μs exposure time).
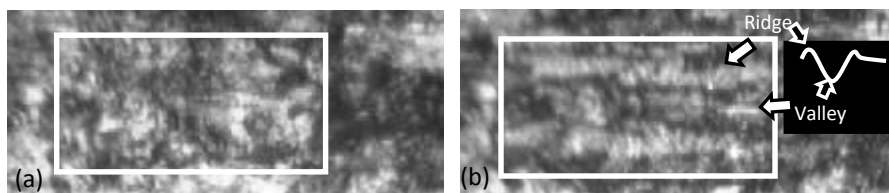


Figure 5-10 Polymer contact surface Test 2 (a) $1.5 \cdot 10^4$ cycles (b) $3.0 \cdot 10^4$ cycles.

As understood from Chapter 2, the morphological features for grooving, which are parallel lines in the sliding direction or a rectangular element, are clearly observed in Figure 5-9. Also, these abrasion grooves are partly visible even at the beginning of testing at $3.0 \cdot 10^4$ cycles. However, this can be seen only at high magnification by digital zooming. A schematic representation of the ridges and the valley made from grooving is shown in Figure 5-10. Nevertheless, due to the increased coverage of these patterns, they are clearly visible from the micrographs only after $2.1 \cdot 10^5$ cycles.

## 5.4.1.3 Microscopy by dark field illumination

It was earlier reported by Zhang *et al* that small details are not clearly revealed in bright field imaging [5. 20]. However, such intricate details can be monitored in dark field imaging. Thus, for dark field imaging, an external illumination at oblique angle is provided via halogen cold light (GOSSEN GKL 300) for a higher exposure time (25 sec). The optical path receives light only from the reflected surface; thus, the sharp corners and protruding wear particles appears with better contrast, thus revealing details such as deformation of asperities and plastic flow. The same surface acquired with two different technique shows completely different appearance (Figure 5-11). However, the dark field image has higher resolution for revealing intricate features. For example, the white particles seen in Figure 5-11 (b) are the asperities in the beginning of contact and are smeared off in the course of wear, as seen in Figure 5-12 (b).
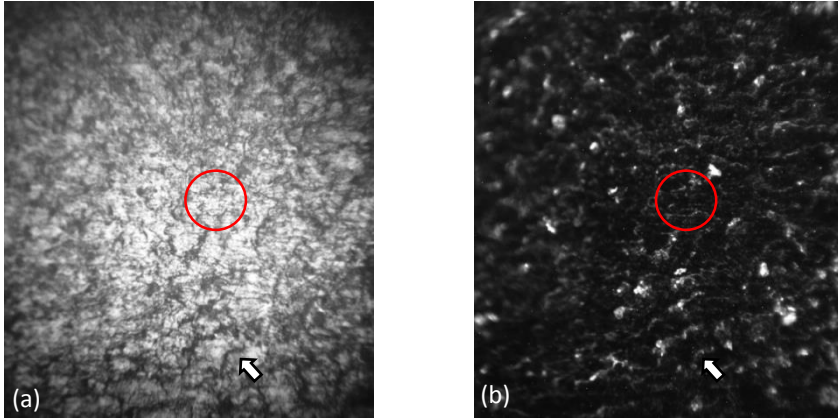
Figure 5-11 Images of initial surface (a) reflected light bright field image (b) dark field image (Images processed for contrast).
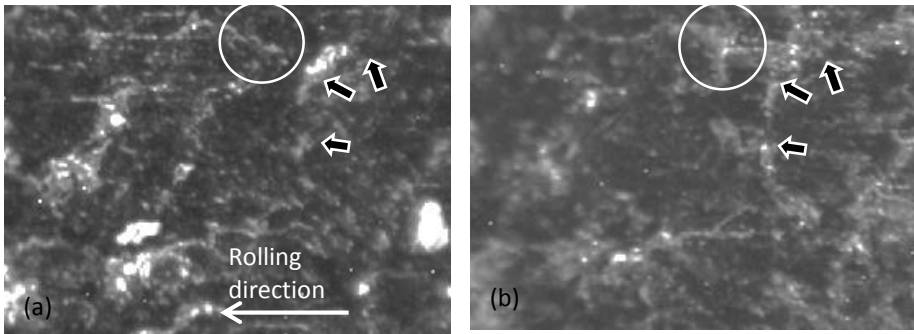


Figure 5-12 Transition in surface morphology from dark field illumination (a) Initial surface (b) $1.5 \cdot 10^5$ rotations (Images processed for contrast).

Figure 5-12 is the dark field image taken from the same region as shown in Figure 5-8. Supporting the earlier statement that initial stage of wear plastic flow is the dominant mechanism, a clear evidence of it can be seen in Figure 5-12. On comparing the initial image with the image taken at $1.5 \cdot 10^5$ rotation, the region indicated with arrows has a clear border and smooth appearance of the texture to validate plastic flow, thus, closing the voids present in the initial stage of wear as seen in Figure 5-8. These features are not clearly seen in bright field imaging due to the saturation of image details. There are also other mechanisms carried out in the initial stage. The encircled region in both the images articulates that the sharp nose like morphology in Figure 5-12(a) has been removed in the course of wear and small fractured elements combine together to form wear debris. This debris are either displaced to another location on polymer contact surface due to the partial sliding or discarded from the contact zone.

Figure 5-13 shows the dark field image at intermediate pauses. It is obvious that for the same region of interest, the contrast of the image increases at every intermediate pause. This is a consequence of damage and plastic flow of polymers. From these

images (Figure 5-13), it is very clear that at $1.05 \cdot 10^5$ rotation, the debris deposited on the surface begin to form a layer. Such a phenomenon for the given condition at the intermediate stage has never been reported. After the accumulation of debris reaches a substantial amount, a layer of polymer is formed all over the contact surface. In Figure 5-13, the bright patches found at $1.5 \cdot 10^5$ rotations disappear at the next intermediate pause ($1.8 \cdot 10^5$) rotations. Nevertheless, these layers reappear at $2.1 \cdot 10^5$ rotations. These findings are not well reflected in the topographic information (Rmax). It is evident that the topographic information is local; even with 4 repeats of measurements on the surface profile, the surface information are merely from four line profiles. The images on the other hand cover a significant area. From these images, we can hypothesize that the transfer layer investigation should not only be focused exclusively on the counter material but also on the polymer that has characteristics with respect to transfer layer formation. The layers formed over the abrasion groove are clearly seen at $2.1 \cdot 10^5$ and $2.4 \cdot 10^5$ rotations. It can be alleged that the significant amount of debris in these stages is a consequence of partial abrasion. In case of polymer, the conformity in contact surface based on the asperity interaction is mediated by this layer; hence, the formation of these layers is an important aspect.
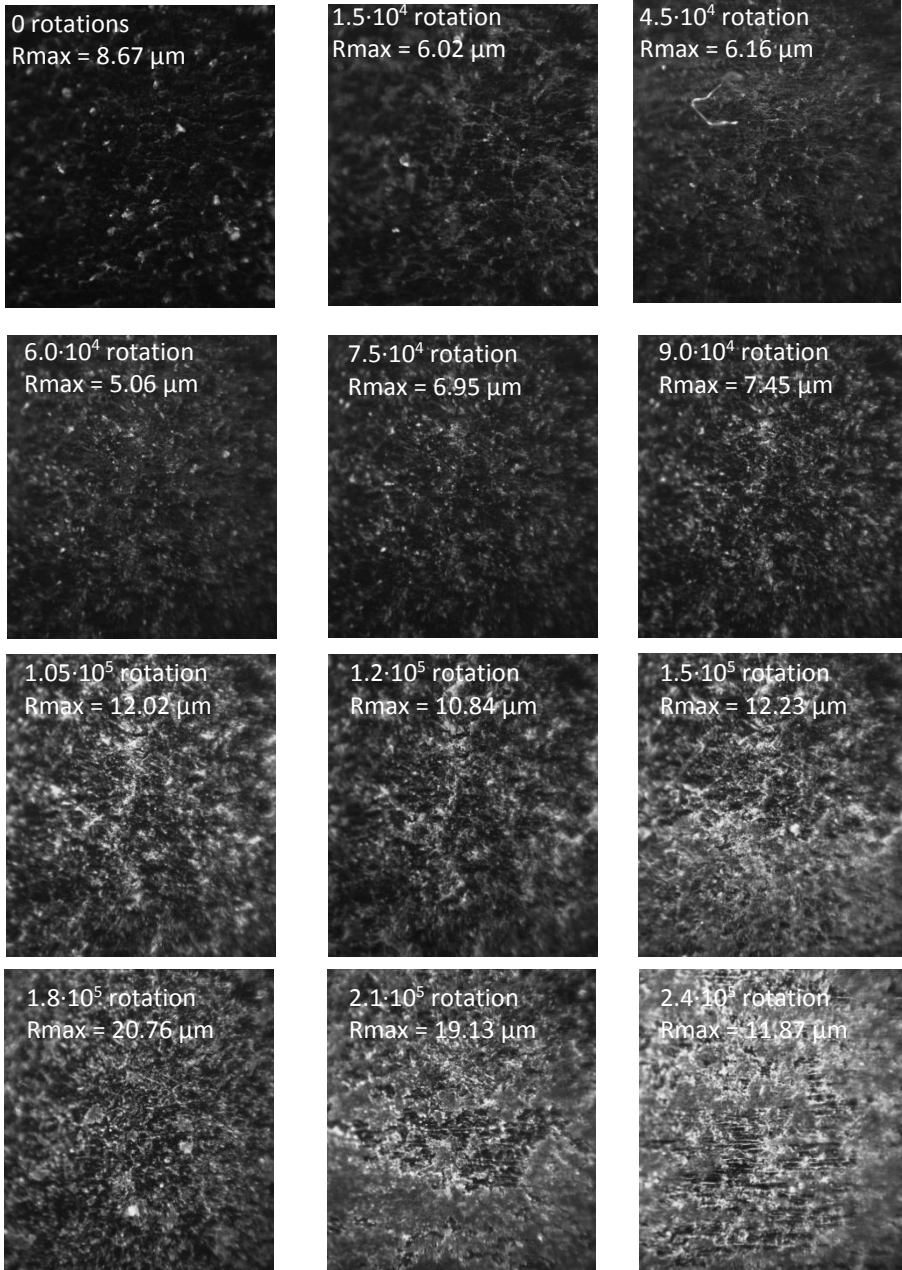
0 rotations
Rmax = 8.67 µm

$1.5 \cdot 10^4$ rotation
Rmax = 6.02 µm

$4.5 \cdot 10^4$ rotation
Rmax = 6.16 µm

$6.0 \cdot 10^4$ rotation
Rmax = 5.06 µm

$7.5 \cdot 10^4$ rotation
Rmax = 6.95 µm

$9.0 \cdot 10^4$ rotation
Rmax = 7.45 µm

$1.05 \cdot 10^5$ rotation
Rmax = 12.02 µm

$1.2 \cdot 10^5$ rotation
Rmax = 10.84 µm

$1.5 \cdot 10^5$ rotation
Rmax = 12.23 µm

$1.8 \cdot 10^5$ rotation
Rmax = 20.76 µm

$2.1 \cdot 10^5$ rotation
Rmax = 19.13 µm

$2.4 \cdot 10^5$ rotation
Rmax = 11.87 µm

Figure 5-13 Dark field image of the polymer contact surface at all the intermediate pauses (Raw images, 25 s exposure time).

## 5.4.1.4 Quantitative evaluation of micrographs

As described earlier, comparing zero rotation and following at each intermediate pause, change in contrast of the image could be noticed. These differences can be estimated by various methods such as grey scale histogram, segmentation of the bright and dark phase and energy score from grey scale texture (GST). After careful consideration based on the analysis of different methods (segmentation using local and global thresholding and granulometry), we have adopted the energy score from the grey scale micrograph, which allows us to investigate the morphology statistically at a global level between the images. Also for evaluating the energy score, we use the equation, which considers the sum of squared elements given by the below expression (5.1).

The energy of an image p(x,y) with size of $M \times N$ pixels is defined as follows:

$$E = \sum_{x=1}^{M} \sum_{y=1}^{N} p(x, y)^2 \hspace{4cm} \text{eq. 5-1}$$

It was earlier described in the literature that not all the asperities in the contacting surface are necessarily in contact. Thus, to understand if there is uniformity among the surfaces, images were acquired from two locations (at 0° and 180° on the circumference of the disc). The calculated energy of images from two locations of Test 2 were taken and their corresponding energy scores were estimated. Out of all these, the energy score has shown similar tendency between the two locations (see Figure 5-14). The peaks at $1.05 \cdot 10^5$ rotations and $1.5 \cdot 10^5$ rotations are due to the bright phase. From the three images next to the plot in Figure 5-14, it can be clearly seen that the micrograph at $1.2 \cdot 10^5$ has less bright phases among the three images. Though it might be difficult to interpret these details with our naked eye, the energy score plays a vital role in providing information on surface modification from an image (sum of the square of pixel value). The reason for the bright phase is the existence of a transfer layer and debris on the polymer surface.
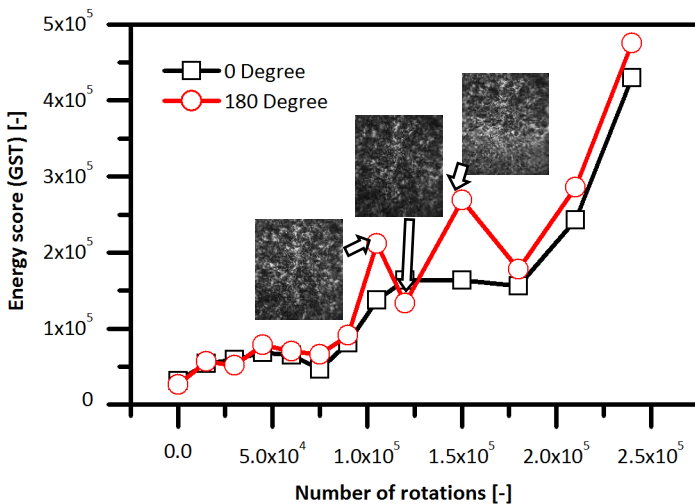


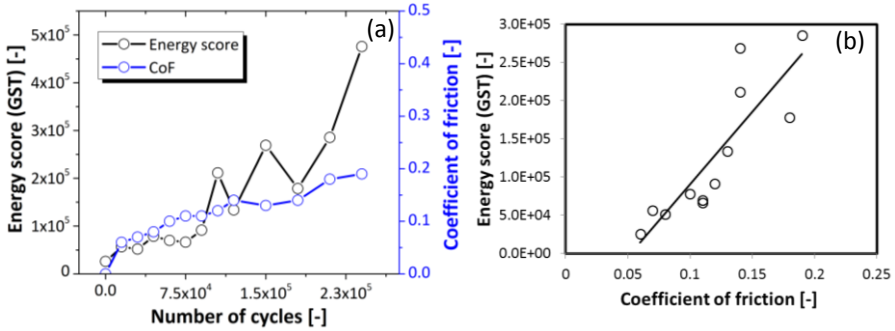Figure 5-14 Energy score of images taken from Test 2 at locations 0° and 180°.

Figure 5-15 Shows (a) Energy score (GST) and CoF as a function of rotations (b) scatter plot for correlation coefficient.

In Test 2, the correlation coefficient between Rmax and the energy score does not show a significant match. Also, one should understand that it is not obligatory for the Rmax to correspond the energy score. Because, the energy score considers image information, which is from XY plane, the stylus profilometry takes in account of the depth profile in the Z direction. However, as wear progresses more debris are formed. This deposition into a transfer layer with certain thickness will be reflected in the Rmax. However, this quantity in Z plane cannot be observed in the 2D image. What is clearly understood from the Rmax and the energy score is the dynamicity in the transfer layer on the polymer specimen. Nevertheless, in both Test 1 and Test 2, the energy score has Pearson's correlation coefficient 0.76 and 0.81 with Rmax.

Both the scores (energy) show similar tendency for Test 1 and 2 in Figure 5-16. On comparing this with the tendency of frictional characteristics, the variation in friction characteristics between both tests begin after $9 \cdot 10^4$ rotations (see Figure 5-3), which is also the same in case of energy scores. However, further variations after $9 \cdot 10^4$ rotations in energy scores correspond to the formation of transfer layer (Figure 5-16). Comparing these two, the variations in friction behaviour can be attributed to transfer layer characteristics. This can be referred to as the dynamic tribological characteristics of transfer layer on polymer surface.
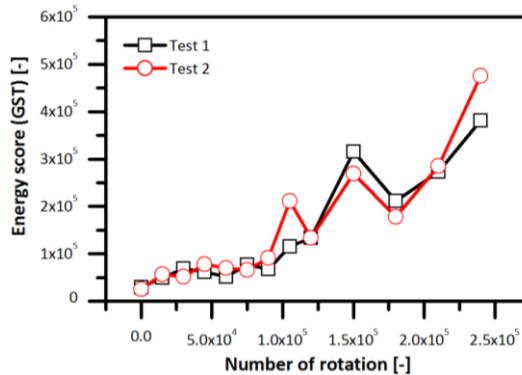


Figure 5-16 Energy scores for the dark field images at intermediate pauses for Test 1 and Test 2.

# 5.4.1.5 Schematic representation of polymer wear process

From the above results, we will schematically represent the evolution of the wear process based on bright and dark field images. The evolution of polymer wear can be divided into two stages with Stage 1 articulating the initial surface modification from plastic flow and fracture of asperities, followed by Stage 2, where formation of transfer layer is the dominant mechanism. Figure 5-17 shows the step-by-step process of polymer wear. In the initial stage, the sharp asperities and weak junctions are fractured. Simultaneously, these fractured debris adheres to the polymer to form a thin layer. The debris, which has different morphology than the bulk material, shines in the dark field imaging; this is highly pronounced after $9 \cdot 10^4$ rotations. The thin layer is a consequence of smearing of debris on the polymer contact surface. Thus, the debris significantly modifies the surface morphology as seen in Figure 5-11 at $2.1 \cdot 10^5$ rotation as in the way represented in stage 2 (Figure 5-17). Depending upon the state of this transfer layer, the friction characteristics are modified. At the later stage after $2.1 \cdot 10^5$ cycles, the transfer layer is clearly seen on the polymer contact surface. The corresponding skewness for both tests has negative value, which means the topography has been significantly changed by the transfer layer formation. Furthermore, a Kurtosis RKu (Rku= 3.01 and 3.4) greater than three at these specific intermediate pauses ($2.4 \cdot 10^5$) for Tests 1 and 2 evidences sharp surface profile. This means the transfer layer is not homogenously formed at this stage of wear.
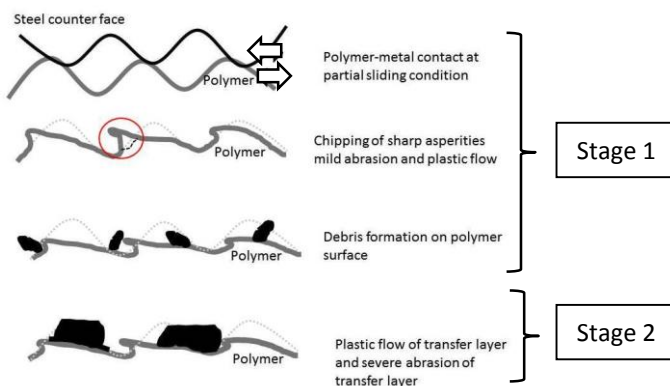


Figure 5-17 Schematic representation of transfer layer formation.

## 5.4.2 Transfer layer formation on steel surface

Transfer layer plays a significant role in polymer-metal contact. Due to the dynamic nature of film formation, the relation between friction and transfer layer can be partly established from the steel surface micrographs acquired using DES approach. The modification of frictional properties due to transfer layers also depends upon the temperature involved in the process, where solidification or free flow of transfer layer alters the tribological properties. Megler *et al* have observed modification in frictional characteristics due to the transfer layer formation [6]. The wear mechanism is also affected by the thickness of the transfer film. Despite having wide variety of

researches on transfer layer formation in polymer metal contact, its true nature is only partially known. The statistical data (roughness, thickness) based on post-mortem are often invalid due to the dynamic nature of the transfer layer formation. In our research, we attempted to bring out the true characteristics of transfer layer and its occurrence.

Starting with the photomacrographs of the steel surface, both Test 1 and Test 2 showed significant difference in the surface morphology of transfer layer (Figure 5-18 and Figure 5-19). In Test 2, as shown in Figure 5-18, the deposition of transfer layer is evident even after $1.5 \cdot 10^4$ rotations. Proceeding further, the partially dark phase at $1.5 \cdot 10^4$ rotations increases its intensity until it reaches a thick dark coloration of the counter material. This can be referred to the primary layer of the transfer film, which is uniformly distributed. However, secondary layers with lumpy mass were also present at different intermediate pauses. In Test 1, clear evidence of secondary transfer layer is shown in Figure 5-19. These results agrees well with the photomacrographs of polymer surface where thin sheets are also seen in Test 1.
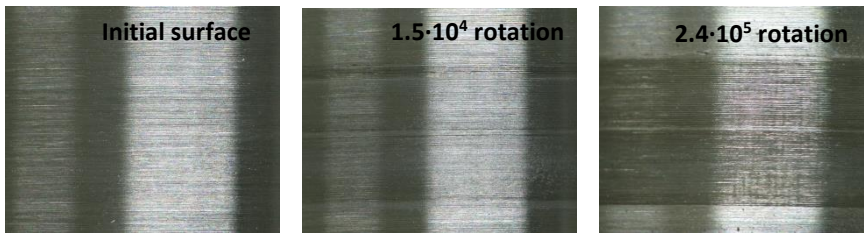


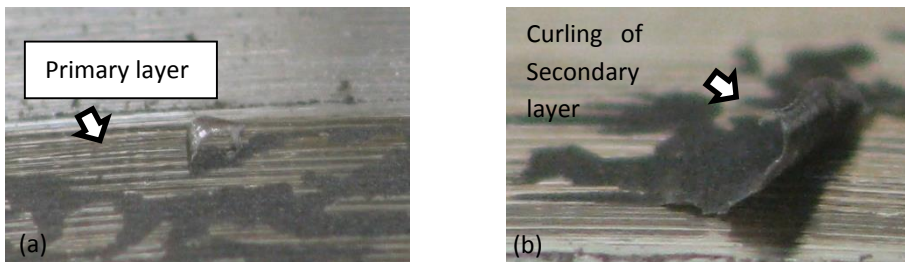Figure 5-18 Steel counterface material at different intermediate pause for Test 2.



Figure 5-19  Secondary transfer layer as observed from photomacrographs for Test 1 at (a) $2.1 \cdot 10^5$ rotations and (b) $2.4 \cdot 10^5$ rotations.

## 5.4.2.1 Micrographs as a qualitative evaluator

Traces of transfer layer are seen after $1.5 \cdot 10^4$ rotations. In Figure 5-20, regions marked with arrows at $1.5 \cdot 10^4$ rotations showed increase in dark coloration and its intensity continued increasing until the end of testing. Comparing the final stage of wear, the surface change to the dark phase on the steel surface due to GF/PA66 debris is less in the initial periods until $3.0 \cdot 10^4$ (Figure 5-22). This is merely due to the progressive damage causing the additional deposition of polymer composite debris on the steel surface. A similar mechanism is seen in the post-mortem analysis in Chapter 4 with different levels of transfer layer deposition. Moreover, steel being a

material with high light reflecting property than polymer, transfer layer visibility at the initial stage is less owing to limited deposition. After roughness valley is packed, conformity in contact at an asperity level is achieved. The difference between the initial contact surface and first intermediate pause at $1.5 \cdot 10^4$ rotations is shown in Figure 5-20.
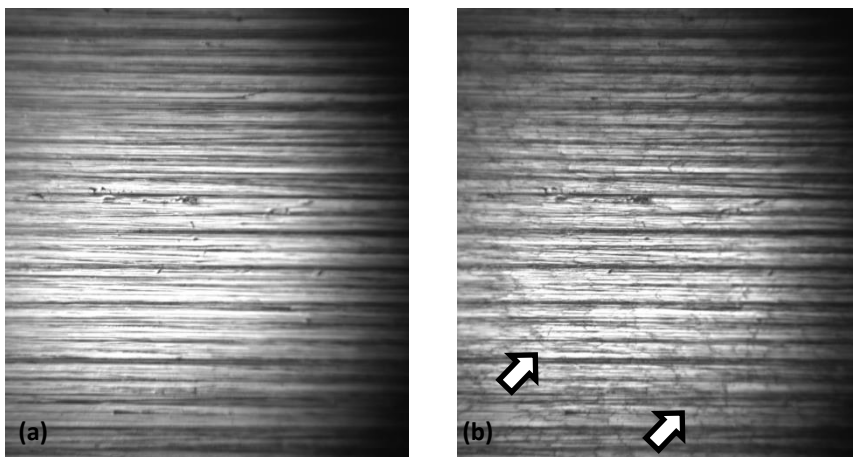


Figure 5-20 Shows steel counterface material (a) initial surface (b) $1.5 \cdot 10^4$ cycles.

A similar approach as in chapter 4 was followed to understand the transfer layer deposition. The Rmax at each intermediate pause is plotted as a function of rotation. In addition, the spectral density is calculated from the roughness profile. Using the power spectrum density (PSD), three dominant wavelengths pertaining to the feed rate of machining at 70 µm and microtopography from polishing process at 50 and 30 µm were identified. Power spectrum density (PSD) amplitude of a specific wavelength (say 70 µm) is used to reveal the polymer deposition in valleys at each intermediate pause. A representative model is shown in Figure 5-21 (a), where the PSD amplitude calculated from the dominant frequency of Test 2 at the beginning of the test is compared with a profile with low PSD amplitude. It is evident from the Figure 5-21 (b) that PSD amplitude can be a representative on comparing with the Rmax, where both show similar tendency. A PSD amplitude from a roughness profile can be a better indicator for transfer layer characteristics than other sources of information such as Rmax and thickness from cross-sectional analysis. Factors such as Rmax and Ra average the amplitude from different wavelength arising from micro and macro topography of a surface. However, in case of PSD amplitude, it takes in account of the dominant wavelength and its corresponding amplitude to understand the transfer layer behaviour. Thus, the reference from one specific wavelength is accounted for studying the transfer layer growth.

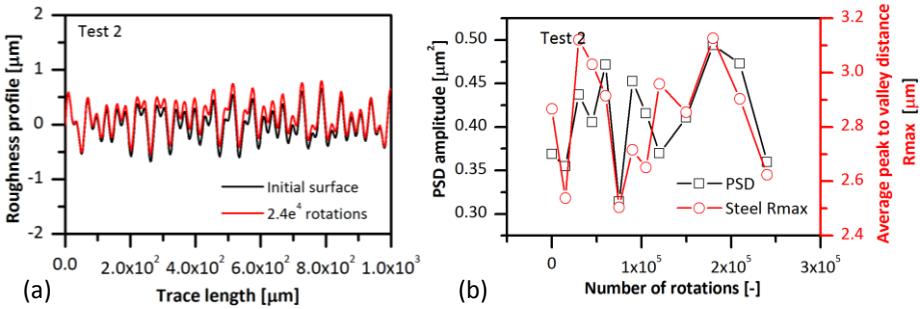(a)                                            (b)

Figure 5-21 Steel surface topography (a) model of roughness profile from Test 2 (b) comparison of PSD amplitude with Rmax of Test 2.

However, with the information obtained from the micrographs, these data on topography with Rmax do not precisely represent the transfer layer formation. From Figure 5-22, it is clear that for the same illumination and region of interest (ROI), the images are darkened at each intermediate pause due to the formation of transfer layer. Also, the blackening cannot be attributed to heating effect because the non-contact region has the same bright phase during the course of testing (see Figure 5-18). From the acquired micrographs of steel surface, it is evident that the transfer layer growth is clearly related to the increase in intensity of the dark phase on the contact surface. Both primary and secondary transfer layer are observed in the steel counterface (similar to the observations in Chapter 4). Although the secondary layers play a dynamic role, the primary layer formation can be assumed to be a continuous process. However, these dynamic characteristics cannot be acknowledged in the topographic details (see Figure 5-4 b). The images of the steel counter face of Test 2 at each intermediate pause are shown below (Figure 5-22). It is evident from Figure 5-22 that the secondary transfer layer seen as a darker region at $1.2 \cdot 10^5$ rotations is absent in the later stage, thus confirming its dynamicity. However, the primary transfer layer is still intact.

The steel surface shows different behaviour between Test 1 and Test 2. For comparison purpose, images of steel surface at specific intermediate pauses are shown in Figure 5-23. It is evident that Test 2 undergoes significant change in the intensity of dark phase. One such example is the surface scar (encircled region) of the steel counter material at Test 2 after $6.0 \cdot 10^4$ rotation, where deposition of black primary layer was absent. However, after $7.5 \cdot 10^4$ rotations, it is partly darkened, which is encircled in the Figure 5-23. On the other hand, in Test 1, the counter surface shows similar contrast for all three images. Thus, we can conclude that a limited or no formation of primary layer at these three specific pauses resulted for Test 1. This means, the primary layer in these specific pauses are different between Test 1 and 2, which is not reflected in the stylus profilometry. These differences can be identified from the energy scores of the images from the steel surfaces. A comparison of these values (energy) between Test 1 and Test 2 from steel counterface micrographs reveals that these differences observed in Figure 5-23 can globally be calculated from the contact surface.
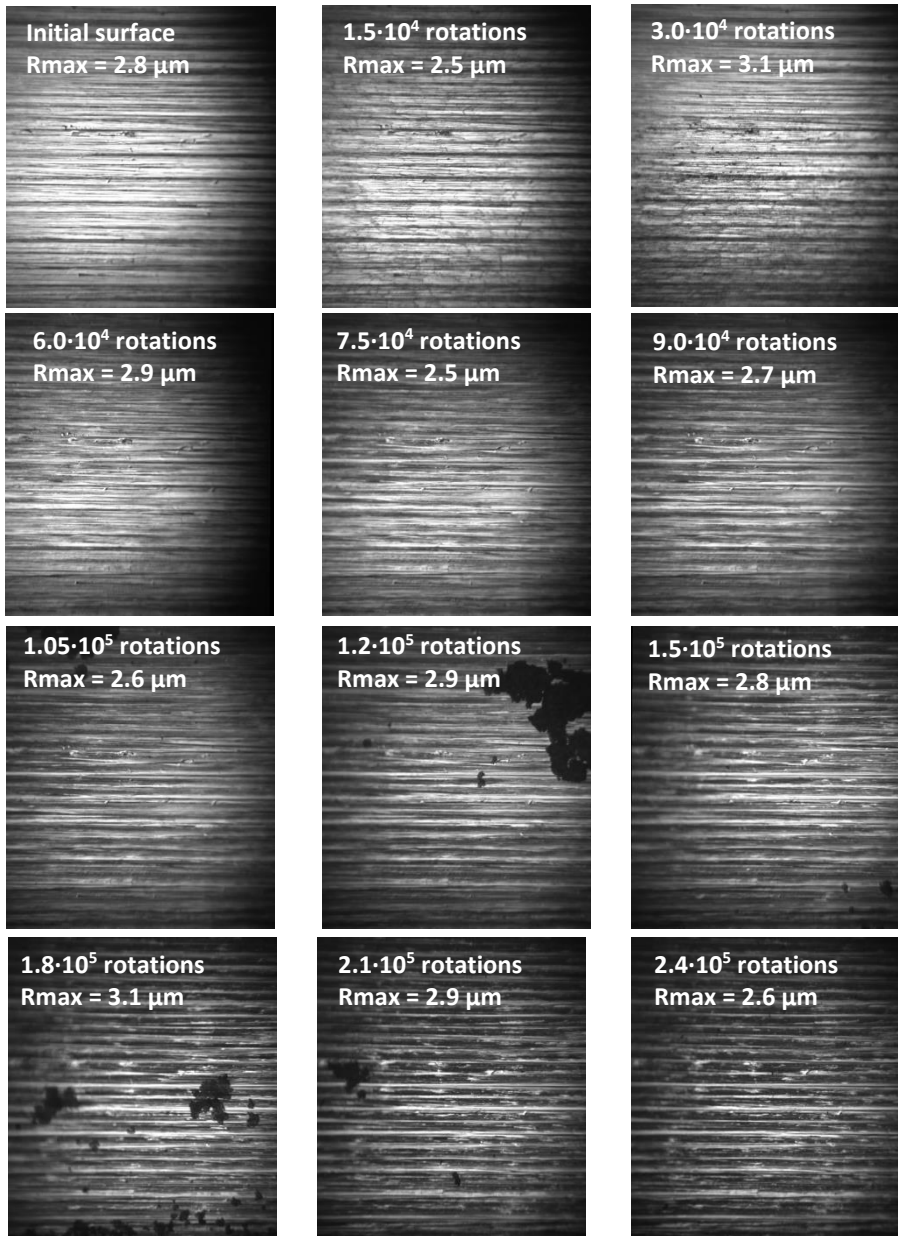
Figure 5-22 Bright field images of steel contact surface acquired at intermediate pause for test 2 (raw images at 300 μs exposure time).

In Figure 5-24, the differences seen between the micrographs of steel surface from $6.0 \cdot 10^4$ to $9.0 \cdot 10^4$ rotations are revealed in the energy scores. Thus, this methodology is an effective indicator for the transfer layer deposition. Also these energy scores partially respond to the variations of friction characteristics.
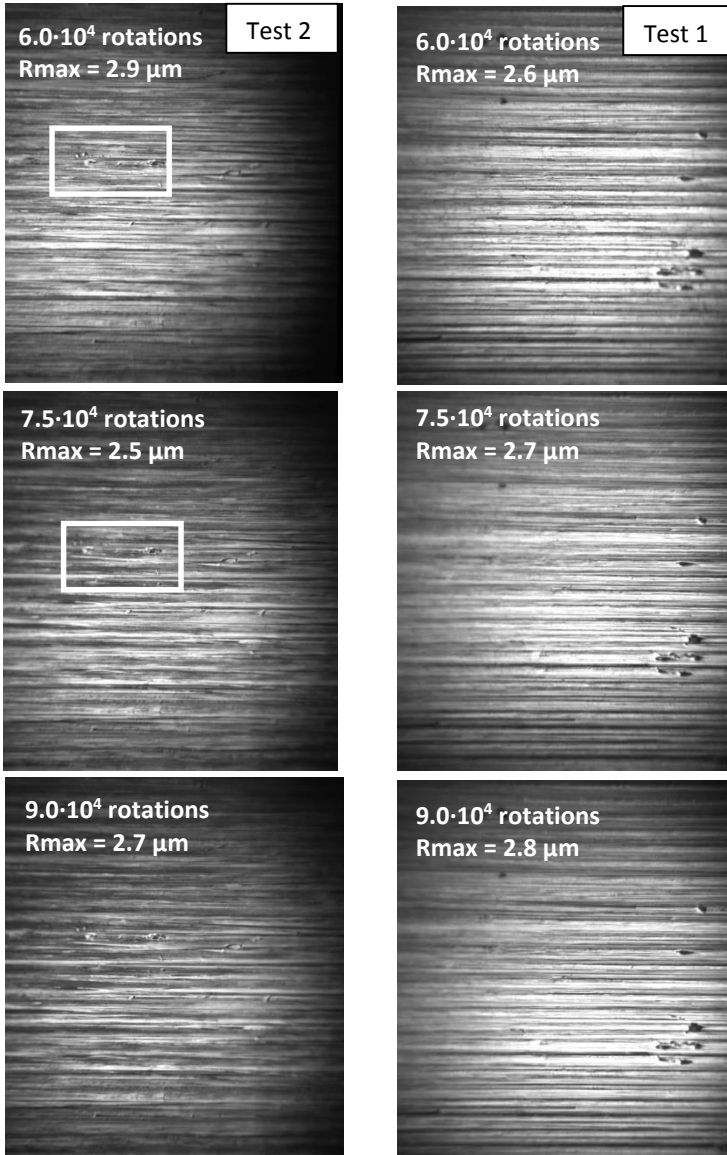
Figure 5-23 Shows comparison of steel counter surface between Test 1 and Test 2 from $6 \cdot 10^4$ rotations to $9 \cdot 10^4$ rotations (raw images at 300 µs exposure time).
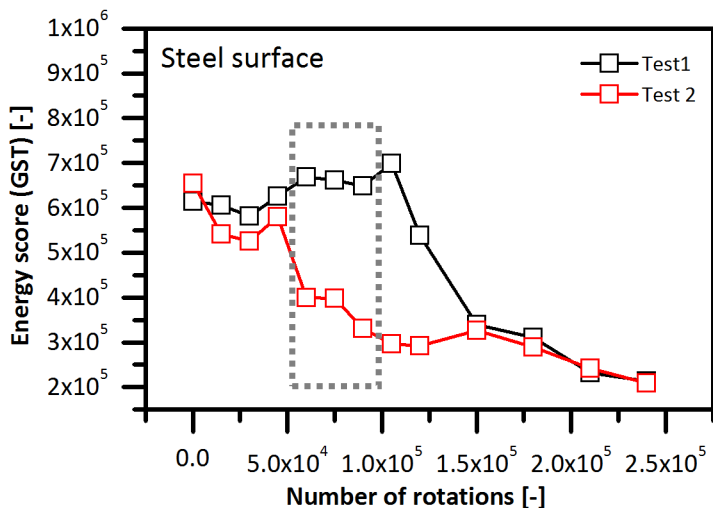
Figure 5-24 Energy score from GST of steel counter surface.

A decrease in energy score of micrographs from steel surface starting from $1.5 \cdot 10^4$ rotations is due to the reduction in light scattering effect of the steel caused by the transfer layer deposition (Figure 5-24). Even at the beginning of testing after $1.5 \cdot 10^4$ rotations, debris are generated from fractured polymer as seen earlier in Figure 5-11. These fragmented particles cause deposition of debris in-between asperities of the steel surface. As a consequence, darkening of steel surface occurs, which results in reduced energy score. A similar situation has been described by Sviridyonok *et al* stating that the formation of transfer layer is a consequence of detachment of micro particles from the parent material. It is after $1.2 \cdot 10^4$ rotation, a significant deposit of secondary layer can be found in steel surface. However, these layers on steel surface also peel off ($1.5 \cdot 10^5$). These peeled materials have higher chances of the transferring back polymer surface, which can be seen at $2.1 \cdot 10^5$ cycles.

## 5.4.2.2 Schematic representation of transfer layer characteristics

The transfer layer on the steel surface is investigated from the obtained micrographs (Figure 5-22). Based on the micrographs, two-staged process aiding to the formation of thin film on steel surface of transfer layer deposition can be determined. These two stages can be classified according to the nature of transfer layer formation: Stage 1 indicates the primary layer formation and Stage 2 indicates the secondary layer formation. From the micrographs, it is evident that the primary layer is uniform and distributed equally over the surface. However, the secondary layer is not globally present on the steel contact surface. The secondary layer after Stage 2 has an unstable state, which is responsible for the dynamicity in the contact condition. However, the significance of the secondary layer in affecting the tribological characteristic is not completely understood from the current research. The black deposit after $1.2 \cdot 10^5$ rotations is significantly larger than the earlier stage. Moreover, the deposited transfer layer is removed in the forthcoming stage ($1.5 \cdot 10^5$ rotations,

Figure 5-22), showing a dynamic behaviour. Similar characteristics were found in literature for sliding configuration of POM against steel [5. 23]. The formation of polymer layer on the counter surface continues until a significant thickness of transfer film is formed. Moreover, its presence depends on the adhesiveness of the transfer layer to the counterface material. Starting from the particle entrapment between asperities to the dynamic behaviour of the secondary layer, the schematic representation of Figure 5-25 clearly explains the dynamic process involved in transfer layer formation. The secondary layer formation is a cyclic process with peeling and redeposition.
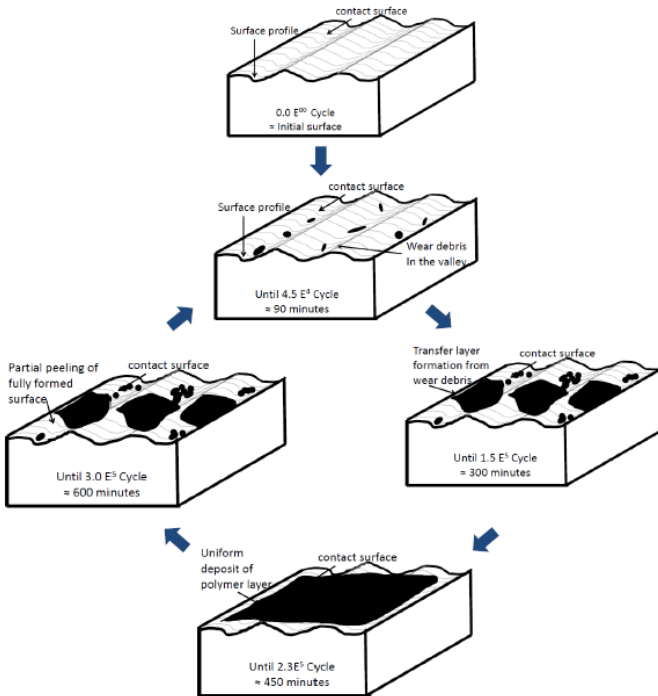


Figure 5-25 Schematic representation of transfer layer formation and its dynamic characteristics.

Though the DES stands effective in following the damage evolution process, there are few shortcomings in this approach. Dismounting the test material causes disturbances in the equilibrium of testing. The area under investigation is relatively small with a field of view (FOV) of 1300 μm. With the imaging techniques working well on such small FOV, a system with larger capabilities should be considered. An online monitoring system for microscopic images without stopping the test and investigations on a significantly large area can provide valuable information on the transfer layer dynamicity and its influence on tribological characteristics. Such an online system will be established in Chapter 6.

## 5.5 Summary and conclusion

Tests with intermediate observations using *ex-situ* methodology on the polymer composite against steel in rolling-sliding contacts resulted in two sets of conclusions concerning the use of imaging and image processing techniques followed by understanding the evolution process in polymer wear and transfer layer formation.

The damage evolution study (DES) shows various phenomena experienced in the wear process of polymer-metal tribo-pair in a rolling-sliding contact. The evolution of polymer surface shows that transfer layer formation is obvious on the polymer surface. These polymers surfaces are formed in two stages: 1) fracturing of sharp edges and plastic flow of polymers 2) back transfer of polymers from the counter material to form a new layer of polymer. However, these transfer layer of polymer are not consistent in their presence on the time scale.

The formed transfer layer on steel surface is characterized based on its texture. A uniformly spread polymer layer is referred as primary layer and it remains throughout the whole experiment. Bulky non uniform deposit of polymer on steel surface is called secondary layer and as a function of time, it is never consistent in its occurrence. For the polymer and its counter material, there exists a dynamicity in the transfer layer formation. However, the roughness change does not show these dynamic characteristics on all circumstances.

The particles in the polymer contact surface are effectively identified using dark field imaging. The image acquisition through relocation micrography is effective in tracking the same region of interest. The change in area of transfer layer deposit at different instants of testing in the steel and polymer surface was clearly understood by using relocation micrography. The image processing technique on registration precisely locates the same region for understanding sequence of event suffered by the polymer surface. The energy score of the grey scale texture (GST) can be used in both polymer and steel surface to track the change in surface characteristics.

# References

[5.1]   D. F. Charles, R. Gnanamoorthy, and P. Ravindran, "Rolling contact fatigue behavior of polyamide clay reinforced nanocomposite—Effect of load and speed," Wear, vol. 269, pp. 565-571, 2010.

[5.2]   Y. K. Chen, S. N. Kukureka, C. J. Hooke, and M. Rao, "Surface topography and wear mechanisms in polyamide 66 and its composites," Journal of Materials Science, vol. 35, pp. 1269-1281, 2000.

[5.3]   D. H. Gordon and S. N. Kukureka, "The wear and friction of polyamide 46 and polyamide 46/aramid-fibre composites in sliding-rolling contact," Wear, vol. 267, pp. 669-678, 2009.

[5.4]   C. J. Hooke, S. N. Kukureka, P. Liao, M. Rao, and Y. K. Chen, "Wear and friction of nylon-glass fibre composites in non-conformal contact under combined rolling and sliding," Wear, vol. 197, pp. 115-122, 1996.

[5.5]   S. N. Kukureka, C. J. Hooke, M. Rao, P. Liao, and Y. K. Chen, "The effect of fibre reinforcement on the friction and wear of polyamide 66 under dry rolling/sliding contact," Tribology International, vol. 32, pp. 107-116, 1999.

[5.6]   S. Apichartpattanasiri, J. N. Hay, and S. N. Kukureka, "A study of the tribological behaviour of polyamide 66 with varying injection-moulding parameters," Wear, vol. 251, pp. 1557-1566, 2001.

[5.7]   S. N. Kukureka, Y. K. Chen, C. J. Hooke, and P. Liao, "The wear mechanisms of acetal in unlubricated rolling-sliding contact," Wear, vol. 185, pp. 1-8, 1995.

[5.8]   C. C. Lawrence and T. A. Stolarski, "Rolling contact wear of polymers: A preliminary study," Wear, vol. 132, pp. 183-191, 1989.

[5.9]   D. Scott and G. H. Mills, "Scanning electron microscopical study of fibre reinforced polymeric cage materials for rolling bearings," Polymer, vol. 14, pp. 130-132, 1973.

[5.10]  T. A. Stolarski, S. M. Hosseini, and S. Tobe, "Surface fatigue of polymers in rolling contact," Wear, vol. 214, pp. 271-278, 1998.

[5.11]  A. I. Sviridyonok, V. A. Bely, V. A. Smurugov, and V. G. Savkin, "A study of transfer in frictional interaction of polymers," Wear, vol. 25, pp. 301-308, 1973.

[5.12]  T. Hermann, T. A. Blanchet, and N. F. Panayotou, "Evolution of wear, roughness, and friction of Alloy 600 superalloy surfaces in water-submersed sliding," Wear, vol. 268, pp. 126-132.

[5.13]  S. Kano, H. Homma, S. Sasaki, and H. Shimura, "In situ monitoring of friction surfaces and their sequence pattern analysis," Philos Trans A Math Phys Eng Sci, vol. 366, pp. 665-71, 2008.

[5.14]  V. Martinez-Fuentes, I. Dominguez-Lopez, and A. L. Garcia-Garcia, "Surface texture changes followed-up in real time during the initial wear transient of dry sliding of steel against several metals using laser light scattering," Wear, vol. 271, pp. 994-998.

[5.15]  Y. C. Tasan, M. B. de Rooij, and D. J. Schipper, "Measurement of wear on asperity level using image-processing techniques," Wear, vol. 258, pp. 83-91, 2005.

[5.16]   C. Q. Yuan, Z. Peng, X. C. Zhou, and X. P. Yan, "The surface roughness evolutions of wear particles and wear components under lubricated rolling wear condition," Wear, vol. 259, pp. 512-518, 2005.

[5.17]   D. F. Moore, "A history of research on surface texture effects," Wear, vol. 13, pp. 381-412, 1969.

[5.18]   J. Ye, H. S. Khare, and D. L. Burris, "Transfer film evolution and its role in promoting ultra-low wear of a PTFE nanocomposite," Wear, vol. 297, pp. 1095-1102.

[5.19]   J. Quintelier, "Online wear monitoring of polymer matrix composites with advanced measurement techniques," PhD desertation, Ghent University, 2007.

[5.20]   J. Zhang and P. Regtien, "Illumination methods for optical wear detection," 2007.

[5.21]   J. D. Huffington, "The frictional method of measuring contact area between surfaces and its relation to the surface microtopography of some abraded metals and polymers," Wear, vol. 12, pp. 343-356, 1968.

[5.22]   J. D. Huffington, "Abrasion groove sizes and shapes in relation to the mechanism of abrasion," Wear, vol. 49, pp. 327-337, 1978.

[5.23]   Y. J. Mergler, R. P. Schaake, and A. J. Huis in't Veld, "Material transfer of POM in sliding contact," Wear, vol. 256, pp. 294-301, 2004.

Chapter 6

# Development of a high speed online vision system
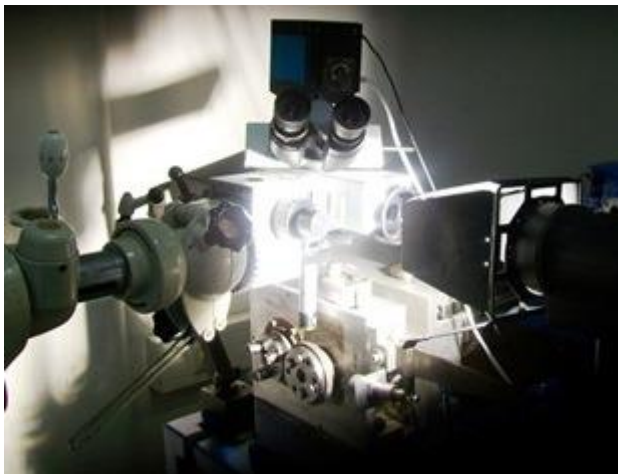
## Goal

In the chapter 5 it was evident from *ex-situ* monitoring that wear mechanisms changes as a function of time. Though damage evolution was clearly monitored, limitations in field of view and illumination mandates the use of advanced techniques. Moreover, the equilibrium of the test is disturbed both thermally and mechanically. Thus, it is necessary to have an *in-situ* system for monitoring the morphological changes which could provide a clear insight of the wear process without disturbing tribological equilibrium. In this chapter, attempts are made to describe how the moving polymer contact surface is visualized at micron scale. This is facilitated by the use of a high-speed camera in conjunction with a bright field optical microscope. Optical and imaging parameters are optimized and the obtained images post processed, for a better understanding of wear process. To understand the limits of this newly developed system, preliminary tests and a long duration test are performed. The capability of the system in terms of frame rate and shutter speed extends to a maximum of 35000 fps and 375 ns respectively. Periodical changes in wear mechanism are evident with resin back transfer, surface cracks and partial exposure of fibres. The obtained micrographs are processed and qualified for understanding online wear trends using blur estimation. Thus, from online images the wear process of polymers can be studied and used to validate wear hypothesis.

## 6.1 Introduction

In-lab wear investigations often make use of expensive scientific instruments such as sensitive and accurate displacement sensors (contact and contactless types). Nevertheless, measurements often do not provide a clear view on the wear process. When two materials come in contact, their surfaces are prone to change at asperity level even in no load condition. Such modification on the surface at micron scale can be clearly seen using microscopy techniques. Hence, in tribological investigation priority is always given to microscopic examination. The morphological investigation reveals various wear mechanisms such as abrasion, adhesion and surface fatigue from the observed wear scars. In the traditional post-mortem approach (TTS), it is obvious that the investigated surface has already been severely damaged. The important evidences such as wear pattern and its distribution in the contact surface significantly changed in the course of wear, thus leaving limited details for further investigation. This is revealed from our earlier studies (Chapter 5) using *ex-situ* monitoring. Considering the wear process, the intermediate wear mechanisms such as back transfer of polymers and peeling of transfer layer are clearly noticed in the DES. These intermediate mechanisms in rolling contacts of polymer indicates the dynamic tribological behaviour. Research on analysing the surface morphology exist at a quantitative level by means of topographic evaluation. However, more focus was given to roughness estimation than occurrence of phenomenon during the wear process [6. 1, 2, 3, 4]. Even though the *ex-situ* technique clearly monitors the morphological changes, the thermal equilibrium and the dimensional stability are disturbed. Each intermediate pause creates a new running-in period which was also observed by Clerico [6. 5] This intermediate running-in phase hinders the understanding of wear process. Surface modifications contributing to the dynamic

nature of the tribological process have to be monitored without disturbing the equilibrium of the test. Therefore a vision system for online monitoring of the moving surface at real test speeds is an absolute need to understand the tribological behaviour of the material.

## 6.2 Conceptualization of Online Vision System (OVS)

Visual inspection is a direct measure of surface morphology, especially in tribological investigation to understand the surface change. From methodologies of existing research, it is evident that any damage or defect on the contact surface is initially identified by visual inspection [6. 6]. The root cause of material removal and friction modification can be better understood from the sequential observations made on contact surface. This can be done by means of *in-situ* monitoring which is already in practice since early '70s [6. 7]. Series of *in-situ* observations using scanning electron microscope SEM were performed to understand dynamic friction characteristics, micro mechanisms and wear mode [6. 8, 9, 10, 11, 12]. Most existing research on *in-situ* monitoring studies the wear phenomenon during the running-in phase or initial material removal process. Given the situation where polymer is the subject of interest, the non-conductive nature of material impedes the use of SEM for *in-situ* investigations. Scientists also attempted to use charge free imaging for online observation of non-conductive material (polymers). However, this has constraints in terms of cost and geometry. It is evident from existing reports that SEM is more suitable for micro tribometer [6. 13]. Having known the "scale effects" influencing friction and wear characteristics of polymer, the micro-scale experiments cannot be considered for precise tribological investigation. Thus SEM which is the least favourable technique for polymers in rolling contact is averted in the current concept. It is noteworthy to mention that most existing *in-situ* techniques use optical means for surface characterisation. The images acquired using these various optical techniques use different methods and algorithms for topographic measurements. Image parameters such as grey level and intensity of scattered light were effectively used. However, these quantitative topographic measures are time consuming and tedious to analyse the wear mechanisms

Considering the flexibility of the optical system and the recent advancements in electronic imaging, a robust vision system can be designed based on these two factors. Thus, optical microscopy is considered to be most suitable *in-situ* technique, which is relatively inexpensive and optimal for medium-scale experiments. Additionally, it has also been proved to be effective in mapping the tribological process [6. 14]. In this regard, different types of optical microscopy techniques were surveyed to understand its suitability for OVS. Low cost optical techniques were adopted earlier for wear investigation by means of video zoom microscope (VZM) and tool makers microscope (TMM) [6. 14, 15] . Also most of the existing work using optical systems use a standalone charge-coupled device (CCD) for wear monitoring [6. 16, 17, 18, 19]. Recently, the frictional response as a consequence of surface damage was studied using an online monitoring system by means of optical microscope [6. 14]. A list of the different online techniques and their resolution is

given in Table 6-1. It is evident that the SEM and optical systems are used for mechanism monitoring and CCDs are used for topographic characterisation.

Table 6-1. Usage of online microscopy from literature

| Authors | Imaging system | Resolution/ magnification | Purpose |
|---|---|---|---|
| Kano *et al* [6. 14] | OM | 0.64 µm/pixel | Friction correlation from worn surface |
| Quintelier *et al* [6. 20] | OM | | Wear monitoring |
| Harold et al [6. 21] | OM | 250X | To understand the wear process (Lubricated surface) |
| Scharf et al [6. 22] | OM | | To understand the wear process (Lubricated surface) |
| Ovcharenko et al [6. 23] | OM | 1.2 µm/pixel | To understand the wear process (Lubricated surface) |
| Krick et al [6. 24] | OM | | To understand the wear process |
| Chromik et al [6. 25] | OM | | To understand the wear process (Lubricated surface) |
| Zhang *et al* [6. 26] | VZM | 4.4 µm/pixel | Laboratory scale wear testing |
| Kurada *et al* [6. 16] | VZM | 2.7 µm/pixel | Condition monitoring for tool wear |
| Su *et al* [6. 15] | TMM | 0.99 µm/pixel | Condition monitoring for tool wear |
| Glaeser *et al* [6. 8] | SEM | 1590X | Run-in wear |
| Hokkirigawa *et al* [6. 10] | SEM | | To understand the wear process |
| Lim *et al* [6. 12] | SEM | | To understand the wear process |
| Rigney et al [6. 27] | SEM | | To understand the wear process |
| Murarash et al [6. 13] | SEM | | Wear process of bio material |
| Michler et al [6. 28] | SEM | | To understand the wear process |
| Kayaba et al [6. 11] | SEM | | To understand the wear process |

Based on these considerations, an integrated microscopic high speed image acquisition system is essential to monitor the morphological changes of the contact

surface. Online imaging system, being a contactless method for tribological characteristic, would be appropriate to measure the damage and the influences without annihilating important evidences. However, major concerns for developing such a system are motion blur, locating the region of interest (ROI), large FOV and high resolution (2 – 10 µm/pixel). Such bottlenecks are resolved using a combination of microscope and high-speed camera supported by effective image processing techniques. The developed system at microscopic scale is particularly employed for rolling-sliding contacts using a twin-disc model. A rolling-sliding contact with surface curvature helps developing a system with maximum adaptability with regard to the optics, speed and investigated area. The high-speed imaging system is effective for twin disc model because, a rotating contact surface provides a self-exposure of the wear track to a statically mounted imaging system. Such an arrangement makes it viable to monitor significant area of contact surface. This novel technique in tribological investigation will elucidate the various intermediate mechanisms involved in the wear process. The baseline values of parameters related to optics and camera are calculated. The schematics of the online vision system is shown in Figure 6-1. An interesting feature in the instrumentation is the closed loop feedback system. In DES, a manual relocation micrography was used to locate the same ROI, however the OVS do not have intermediate pause for using the relocation micrography. Thus in case of OVS a closed loop feedback system was made using an encoder which is in line with the disc rotation. The signal from the encoder can be used as a trigger to acquire images of the same region.
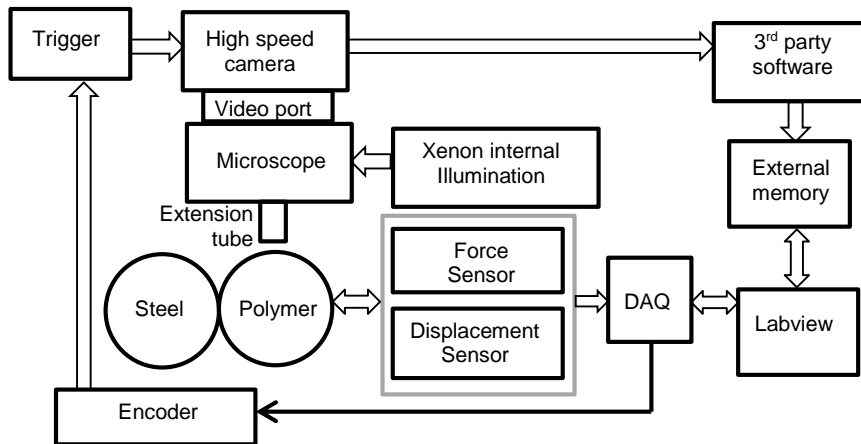


Figure 6-1. Schematics of twin-disc setup with imaging system.

## 6.3 Hardware design

The online vision system is developed for twin-disc model using the modified "Forschung und Getriebebau Zahnräder" (FZG) tester at Laboratory Soete. The complete set-up is divided into two separate components: 1. twin-disc test rig and its arrangement for continuous line contact, 2. Online Vision System (OVS) for monitoring the development of wear scars. Figure 6-2 shows the digital image of the online vision system mounted on the modified FZG. To our knowledge, no evidence

of such a system with a combination of **"high speed camera and optical microscope"** used for tribological investigation thereby making the OVS unique and novel. The OVS consist of two major modules: (i) microscope system module (MS), (ii) image acquisition module (IA). The OVS is isolated from the twin-disc by mounting the camera and microscope on a separate panoramic tripod. Thus the arrangement is flexible and also can be used for onsite inspection.
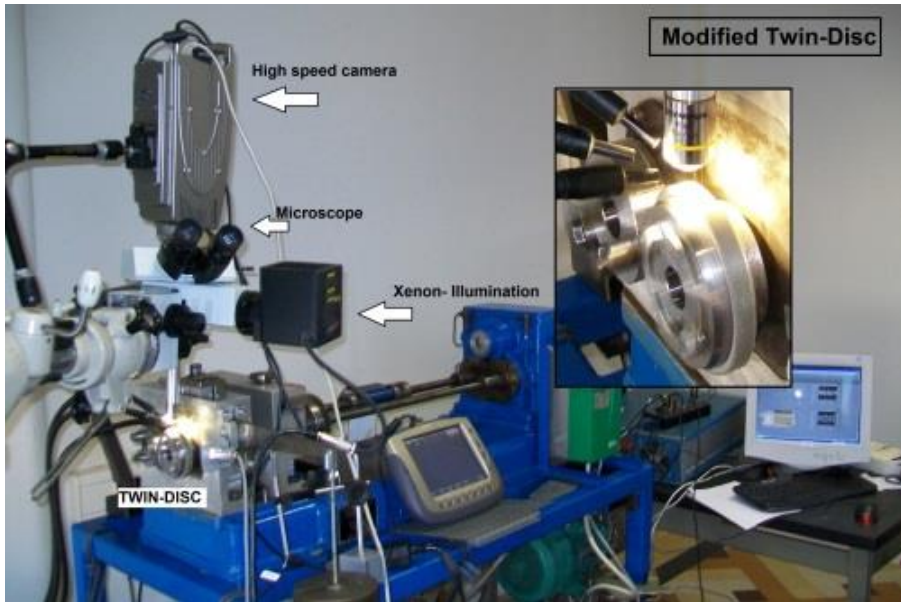


Figure 6-2. Twin-disc test rig and the online vision system.

## 6.3.1  Microscopic system module (MS)

The main components of the MS module are (a) focus mount (b) illumination (c) panoramic tripod and (d) extension tube. The light path and the schematic representation of the MS module are given in Figure 6-3. The microscope (Olympus BXFM) is attached to the cantilever arm of the tripod by bolting together the panoramic head and the focus mount. The optical microscope can be fitted with different light source such as metal halide or xenon. A reflected bright field microscopy technique which is commonly used for opaque objects is adopted. The lamp housing of the focus mount is adapted to accommodate the fibre optic guided illumination where a commercially available metal halide or xenon illumination is used.

## 6.3.1.1 Choice of microscope

Microscope as the main component of the online vision system has limitations particularly from the material to be investigated. In our case, polymers are opaque and requires a microscopic technique which uses diffused reflection for image formation. Thus, a reflected light bright field imaging is adopted in the MS module

which is rather common in metallographic inspections. The primary component of MS module is focus mount which is basically the complete optical unit. The focus mount accommodates a revolving nose, reflected light illuminator and focus column. The used focus mount is commercially available from Olympus (BXFM). A detailed description of the focus mount and the reflected light illumination is provided in Appendix F. In the OVS, the path of light from the illumination source is guided through the reflected light illuminator (U-KAS) and deflected 90° by a beam splitter to follow the vertical optic train. The schematic of the complete light path is given in Figure 6-3. Following the vertical path, light is passed through an extension tube and objective lens to reach the specimen surface. Then the reflected light from the specimen surface is back scattered through the objective lens and extension tube to reach the CCD for photomicrography.
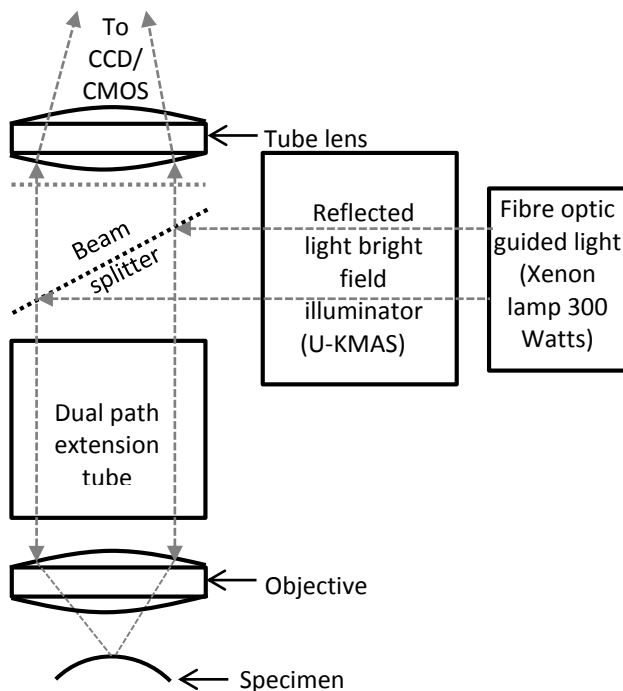


Figure 6-3. Light path and the schematics of the microscopic system (MS) module.

The OVS is an opto-electronic monitoring system where the MS module has a specific working distance (distance between the objective and the specimen surface) which changes in accordance with the used objective lens. Since geometrical constraints exists for accommodating the revolving nose in a confined space, an extension tube connecting the objective and the nosepiece is established. Thus, the distance between the beam splitter and the objective lens can be increased up to 90 mm. In addition to the test bench operations, this adaptation can lead to the usage of OVS in real life applications.

## 6.3.1.2 Selection of objective lens

The selection of a lens is a critical factor where consideration has to be given for working distance, microscopy technique, and morphological details. In the reflected light bright field microscopy, the objective lens guides the light source to the worn surface and collects the information back to the IA module to acquire photomicrographs. The limiting factors for lens selection are (1) FOV, (2) exposure time and (3) working distance.

Previous studies have shown that a resolution between 0.64 – 9.8 µm/pixel was attained in real-time monitoring of contact surfaces [6. 14, 16, 29]. Since the detectable size of wear scars range between 2 – 200 µm [6. 30, 31, 32, 33, 34, 35], the required resolution should not be more than 2 µm/pixel. Additionally, in medium/large scale experiments a significant FOV is required to know if the wear mechanism is globally present. Otherwise, the extracted details from micrographs might only represent the local damage. To start with, the baseline information for FOV of different lenses (5X, 10X, 20X, 40X, and 60X) is obtained using a micrometer resolution lined calibration scale (images acquired using QIcam with ½" CCD sensor). A bar chart representing the lens magnification and its corresponding FOV is shown in Figure 6-4. It is evident from Figure 6-4 that lenses with higher magnification above 20X have FOV less than 900 µm. Hence, higher magnification cannot be considered for our current investigation. Although FOV is significantly large for 5X lens the resolution is relatively lesser than 10X lens. Thus, 10X lens with a FOV of 1526 µm and high resolution is found to be optimal to accommodate a significant area for a global overview without losing the resolution. Also the asperity level changes can be understood from its high resolution of 1.16 microns/pixel. The resolution of these systems is also based on the video adaptor and size of the CCD which is subjected to change.
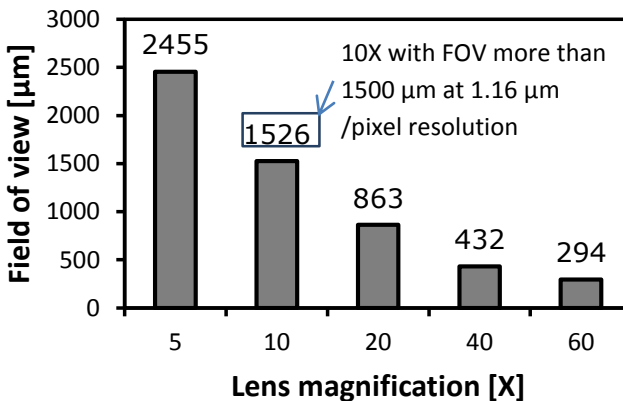


Figure 6-4 FOV calibration for different lenses using QIcam ½" sensor CCD.

Another factor to be considered for the choice of lens is blur, which partially depends on the disc velocity. From chapter 1, it is evident that the application range of polymers in rolling-sliding contacts has surface velocity between 0.1 and 1 m/s. Thus, calculations for lens selection were made based on the maximum speed limit (1 m/s). Besides FOV, the disc velocity has a significant influence on producing a blur free image. Motion blur is a typical distortion produced due to insufficient illumination and it occurs when the part velocity is higher than shutter speed. A transition less than 1 pixel is considered to produce a clear image, free from motion blur. The given expression is adapted from the literature to calculate the pixel blur [6. 36].

$$e = \frac{FOV}{v*NP} \qquad\qquad \text{eq. 6-1}$$

$$B = \frac{v*e*NP}{FOV} \qquad\qquad \text{eq. 6-2}$$

B is the blur in pixels [-],
$v$ is the part velocity [m/s],
FOV is the field-of-view size in the direction of motion [µm]
$e$ is the exposure time [seconds],
NP is the number of pixels spanning the field-of-view,

The exposure time of different lenses corresponding to the value of 1 pixel blur is calculated for speeds from 10 rpm (0.1 m/s) until 250 rpm (1.1 m/s). Figure 6-5 shows the calculated exposure time for a pixel blur of 1. It is evident that even at low speeds the lens with magnification above 20X requires an exposure time less that 1 µs. Also considering high speed, lenses such as 5X, 10X and 20X do not have significant difference in exposure time. However an exposure time with 1 µs can be achieved in a high speed camera.
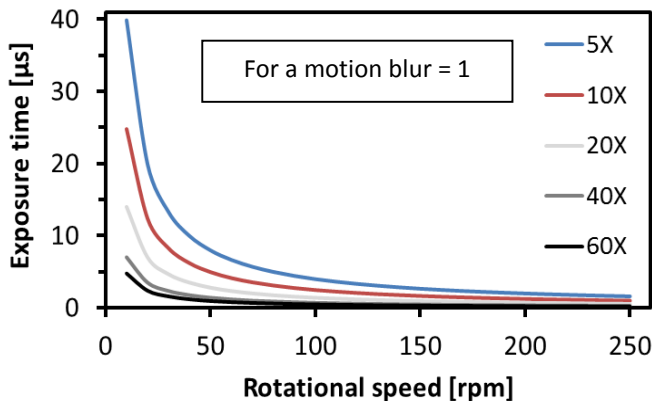


Figure 6-5 Exposure time required for different speeds.

Owing to reduced FOV, lens with magnification of 20X and above is considered as a poor choice. Moreover, the difference in exposure time between 10X and 5X at 200 rpm is only 0.60 µs for which 10X lens has a better resolution and optimal FOV, thus leaving no choice to exclude 5X lens for the setup and investigation.

Apart from image quality there are other reasons to exclude high magnification lenses. The impracticality involved in using 40X and 60X lens is the working distance which is rather small (30 – 65 μm). This may introduce contact between the lens and specimen surface due to eccentricity or from thermal expansion of polymer specimen. Moreover, with a narrow range in the depth of focus (less than 3 μm), a minute vibration during the test may produce distorted images. From chapter 3, it was understood that the depth of focus has limitation in acquiring clear images of both transfer layer and polymer surface at the same time. Thus, considering these factors such as FOV, depth of focus, disc velocity and working distance, the 10X objective lens is the most suitable for OVS.

## 6.3.1.3 Choice of illumination

In chapter 5, it was evident that by changing the illumination scheme minimally, intricate details are revealed. Illumination in high speed imaging is a critical factor and plays a vital role in acquiring blur free images. It is also noteworthy to understand that illumination partly relies on the limitation from camera dependant factor (exposure time) A system which effectively uses the illumination for defect detection is the machine vision. However, the machine vision has resolution only at a macro level. Reviewing such systems helps to adapt illumination for OVS [6. 37]. The choice of illumination is based on several factors such as working hours, heat generated, intensity and specimen characteristics. It is common to see a non-coherent light source in in-line inspection units. Different types of illumination were used in online monitoring of wear which includes diode flash light, ring light [6. 20], high power lighting (60 W), diffused lighting [6. 38], halogen light, laser diode [6. 18], incandescent light [6. 39] and florescent ring light [6. 40]. For microscopic inspection LED, Florescent, metal-halide, xenon and electroluminescence are used specifically. In our case, the major concern is the exposure time which is in micro second. Hence, an adequate light source is required to match the shorter exposure time. At high shutter speed, to acquire the image of fast moving surface the exposure time is at minimum thereby allowing less light for the sensor to grab the required details. Since high intensity is required for the short exposure time, LED, florescent and electroluminescence are excluded. Among the remaining two, metal-halide light source does not have substantial service life. Due to high intensity and adequate service life, the Xenon illumination source is found to be the most suitable for OVS. Thus, a powerful internal illumination is adapted with a fixed distance from the source. Two commercially available illumination systems with metal-halide and a Xenon illuminators of 120 and 300 W respectively are used. For the 300 Watt illumination, a flexible fibre optic light guide is the medium of transfer between source and the lamp housing mount. The used illumination has a high relative intensity, so that at a minimum exposure time images are acquired with full resolution without reducing the binning. The wavelength of the Xenon nova 300 watt lamp has a wide spectrum however, the peak is present only at 503.4 nm (the spectrum is measured using a USB2000 miniature fibre optic spectrometer for 1/3rd, 2/3rd and full intensity).

Apart from the source, type of illumination plays an important role based on opacity of the material [6. 29]. Having polymer as a work material, a reflected light

illumination scheme is chosen. This is facilitated by the reflected light bright field illuminator (U-KMAS). Moreover considering the illumination pathways, surface texture comprising asperities and fibre bundles, prevents the use of oblique illumination, because shadowing effects from the fibre bundles would be prevalent. Thus an internal illumination is used in the present configuration.

## 6.3.2 Image acquisition module (IA)

The image acquisition module is a flexible unit in which different types of camera can be used. A photograph of the complete set-up is shown in Figure 6-2. The main components of the IA module are (1) video port, (2) panoramic tripod and (3) high speed camera. In conventional microscopes, the camera is mounted using C-mount or F-mount by means of a single port tube. However, to compensate the infinity correction which was established by the extension tube, a video port similar to the F-mount was re-engineered in accordance with the RMS thread. This allows the camera to be directly connected to the focus mount without the tube lens. In this instance, the reflected light from the worn surface passing through the objective is guided towards the CCD by the beam splitter. However, while using conventional camera or video monitoring system, a standard adapter with 0.35X from Olympus (U-TV0.35xC-2.) is used. Apart from the adaptor, additional support to the camera is given by an articulate arm. The second most important component of the IA module is the panoramic tripod where 5 degrees of freedom is achieved. The imaging system on the panoramic tripod gives two degrees of freedom in translation (x and z) and three degrees of freedom in rotation ($\theta1$, $\theta2$ and $\theta3$) as shown in the Figure 6-6. This enables to monitor in a confined space at the required angle. However, limitations persist from the view point of depth of focus, and working distance is constrained by specimen geometry (twin-disc).
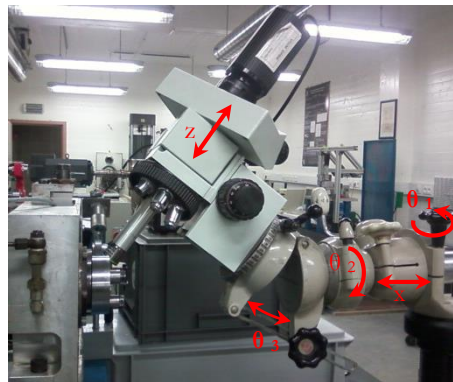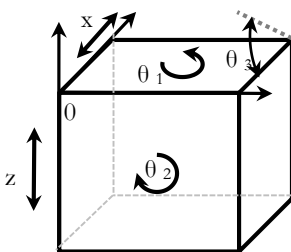


Figure 6-6 illustrates the degrees of freedom for the OVS.

## 6.3.3 Selection of high speed camera

Regarding microscopy for tribological investigation, there is no unique optimal choice for a camera. Thus, the selection of camera is dependent on many variables such as operating parameters, materials, methodology and the nature of study (For e. g. TTS or DES). The combination of high speed camera and microscope is still in the stage of

exploration where flexibility in the choice of camera can be introduced based on the disc speed. Cameras are being already used as an automated tool in vision systems for real time investigations of machined surface. The available camera system uses CCD (Charged Coupled Device) camera or CMOS (Complementary Metal-Oxide Semiconductor) sensors. However, due to sensitivity reasons, CCD is often used in surface investigation. Dutta *et al* has extensively reviewed on tool condition monitoring, from which it is evident that most vision systems use CCD sensors [6. 3, 20, 41, 42, 43, 44]. In our case both the high speed cameras are equipped with CMOS sensor.

Although high speed camera with microscope is commercially available, limitations persist based on the test parameter [6. 45]. The limitations exist in terms of frame rate, exposure time and illumination. Thus, a custom made online vision system from the commercially available individual components suits best for the IA module. The choice of camera is critical because specification of each device varies significantly. Four different cameras with variations in speed, spatial resolution, and exposure time are considered for calculation purpose. The used cameras and the respective specifications are given in Table 6-2. It is also evident from Table 6-2 that each camera has unique capabilities in terms of shutter speed and frame rate. The selection of camera varies based on the nature of study as well.

Table 6-2 Cameras and their spatial resolution, shutter speed and exposure time

| Camera | QICAM (QImaging) | AVT (GigE) | Olympus i-speed TR | Photron ARS |
|---|---|---|---|---|
| Type | Conventional | Conventional | High speed | High speed |
| Maximum resolution | 1280 X 1024 | 1024 X 1024 | 1280 X 1024 | 1024 X 1024 |
| Frame rate at full resolution (fps) | 30 | 110 | 2000 | 3000 |
| Minimum exposure time | 40 µs | 10 µs | 2.16 µs (HQ mode) | 375 ns |
| 3rd party software | Q-Imaging | Acquire control | i-speed | Photron FASTCAM viewer |

The cameras consider for the current investigation are as follows1) 10 bit QICAM color CCD sensor using Qimaging program, 2) AVT GigE a medium speed inspection or vision camera, (3) high speed camera i-speed TR from Olympus and 4) Photron ARS. In case of high speed camera, the images are temporarily stored in the buffer memory and eventually these images are transferred to the external storage.

Olympus is used in the preliminary test on time-series studies due to the high shutter speed and relatively increased spatial resolution (1280 X 1024). The exposure time is to be decided based on the speed of testing and the surface area covered for the given FOV. Based on the area covered in the circumferential direction, the approximately required 30% overlap between two images is maintained for post-processing (stitching) purpose. The QICam and AVT GiGE is favourable on speeds less than 3 rpm (0.01 m/s) and 10 rpm (0.04 m/s) respectively, due to their limitation in frame rate. I-speed TR and ARS suits well for high speed testing. The full resolution of the acquired micrograph varies with respect to the camera thus, the field of view changes correspondingly (see Figure 6-7). For a larger FOV the number of images to cover a significant area is relatively less. Thus the camera with higher resolution is more suitable for the time-series studies.
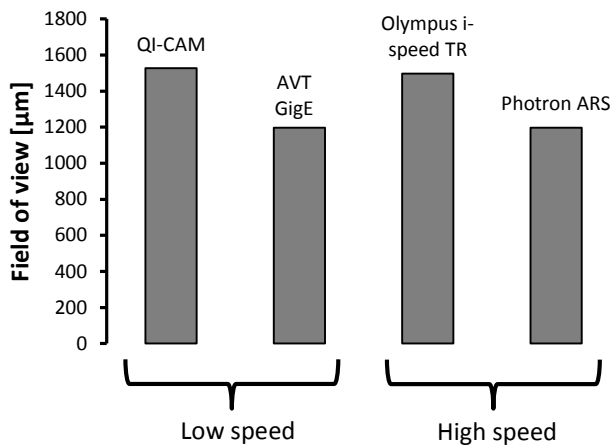


Figure 6-7. FOV at full resolution for the four different cameras.

The calculations for exposure time serves only as base line information, but the parameters are fine-tuned based on the details observed from real-time images. Thus, the working parameters and OVS limitations are finalized based on preliminary testing together with calculations for frame rate, exposure time etc. The capabilities of the OVS are also studied by acquiring images at extreme conditions (maximum speed).

## 6.4 Software

In OVS, the software plays a vital role on instrumentation control, image acquisition and image processing. To have more flexibility and for developmental purpose at the initial stage, these three entities are separated. The ultimate aim is to have a single dedicated software program combining all these three entities. For instrumentation control Labview 8.1 is already in use to control the speed of the FZG motor and also for acquiring signals from the sensoric devices such as torque sensor and linear variable differential transformer (LVDT). To effectively utilize the resources, the existing third party software (Table 6-2) provided by the camera manufacturer is used for image acquisition. These camera manufacturers also provide a software

development kit (SDK) which can be incorporated in the Labview for the combined program. The third entity which is the image processing module is performed using MATLAB, an algorithm for post-processing the acquired images is developed elsewhere (TELIN) [6. 46]. The image processing part is carried out by S. Soleimani and K. Douterloigne from IPI group of the TELIN department (telecommunication and information processing) of Ghent University.

## 6.5 Image processing

Effective use of image processing techniques can extract the surface features and severity of specific mechanism [6. 47]. It is evident from chapter 4 and chapter 5 that the image processing techniques can be effectively introduced in a tribological investigation. Momentary images of the contact surface produce valuable details about the morphological change as a function of time. As a first step, pre-processing of the acquired image is done for corrections on contrast, removal of vignette and tweaking. Further to which post processing of the image is done for stitching the images and to estimate the focus blur to perform the time-series study.

Considering the analysis of surface morphology in tribological investigation, a significant area at micrometer scale provides a global overview of the involved mechanisms. Thus, the adjacent images are stitched together to have a significant region. The schematic of the stitching process is shown in Figure 6-8. A similar technique is followed by Tasan *et al* in semi-online monitoring for pin on disc configuration [6. 48]. Stitching is used to combine the images and compare the changes in wear patterns of the surface between speculated cycles. The 30% overlap between images aids in identifying the surface features through image correlation and registration. These registered images are stitched together to make a continuous surface. Observation and analysis on the same surface sector as a function of time provides accurate information on the evolution of wear process. A detailed description about registration is mentioned elsewhere [6. 46].
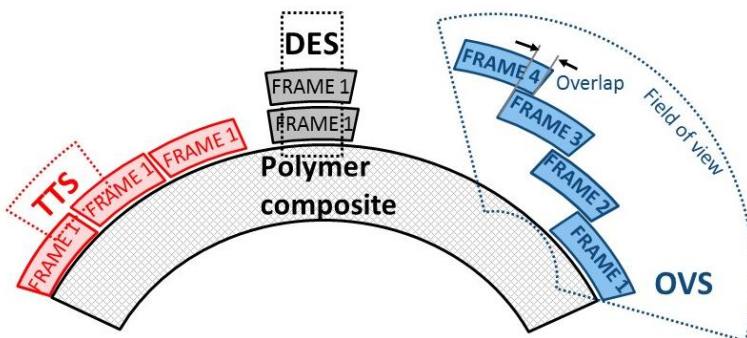


Figure 6-8 Schematics of the stitching procedure.

## 6.6 Materials

The material of choice is the commercially available polymer composite ORKOT (phenolic resin, polyester reinforcing fibres with PTFE filling) and steel counterface material (structural steel S355-J2). The properties of steel and the polymer composite are shown in Table 6-3. ORKOT used for marine bearing application is chosen for its specific surface patterns from the long continuous fibre. Composite morphology representing both phases (matrix and fibre) is more suitable for understanding the capability of OVS in distinguishing the mechanisms such as partial removal of individual phase. These materials were aimed to suffer individual phase damage which can be seen only on micron scale inspection. Thus, making this tribo-pair more suitable for the preliminary testing. The steel surface is machined using a turning centre with rough and finishing operations. On the other hand, no modification is done for the polymer composite. The initial arithmetical mean roughness (Ra) for the composite and the steel counter material are 1.04 µm and 2.55 µm respectively.

Table 6-3 Material properties of the polymer and steel.

| Properties | S355-J2 | Polyester composite |
| --- | --- | --- |
| Yield strength [MPa] | 355 | 55 |
| Elongation [%] | 16 - 20 | - |
| Young's modulus [GPa] | 220 | 3.3 |
| Hardness | 145HV | 100 Rockwell M |
| Thermal conductivity (20˚C) [W/(m·K)] | 34-45 | 0.293 |
| Maximum allowable service temp. [˚C] | - | 130 |

## 6.7 Real-time imaging

In the explorative approach, it is almost impossible to have a full understanding of the tribological behaviour from a single testing. Thus, two main test sequences are used: (1) a preliminary study to know the limitations of the system (effect of illumination and camera) and the features observed in the real-time micrographs, (2) a long duration test to understand the evolution of wear process. Series of attempts at a relatively high speed are made for understanding the maximum capability of the OCV system. Table 6-4 shows the test sequence and its objective.

Table 6-4 Test sequence followed in the OVS (19% slip ratio)

| Test Sequence | Part velocity | Frame rate (fps) | Exposure time (µs) | Lens used | Investigated |
|---|---|---|---|---|---|
| Preliminary test | Max 3.5 m/s | 7000-3500 | 0.375 - 500 | 10X 20X | Effect of: exposure time magnification camera morphological features |
| Long duration test | 1.0 m/s | 3000 | 66 µs | 10X | Evolution in surface morphology Wear trend |

## 6.7.1 Preliminary test

The objective of the preliminary test is to identify the microscopic details observed in real-time images which can point out specific damage/wear mechanisms. The test is made iteratively with both Photron and Olympus to find the maximum speed at which real-time images can be acquired. A common feature in all the images is the dark region which can be seen in Figure 6-9. This is due to the use of an extension tube to maintain the working distance between the objective and the contact surface. It is evident from the images that the illumination is highly influential to obtain a clear image. However, the intensity of the illumination allows to decide the exposure time. Initially on using 120 W metal halide light source, a shutter speed up to 33 µs at 3000 fps is achievable. However, for low exposure time (375 ns) a 300 W powerful Xenon illumination with fibre optic guided light is used.

Figure 6-9 clearly indicates the influence of exposure time images. It is important to note that the contact surface micrographs in tribological investigation have to provide sufficient details of the wear scars. It is evident from the images that with higher exposure time, the acquired images are brighter. Such bright images saturate the wear scar details and also leave less room for further processing. Additionally, in Figure 6-9 the influence of exposure time on motion blur is evident. Figure 6-9 (a) and (b) clearly shows the presence of blur as a consequence of low shutter speed while (c) and (d) with relatively low shutter speed displays a more clear contact surface.

The threshold for exposure time is chosen based on limitations of the individual camera. Figure 6-10 (a) and (b) show images taken at 500 (2.3 m/s) and 750 rpm (3.5 m/s) with frame rate of 7000 and 35000 fps respectively. The objective is to acquire clear images at a relatively high part velocity. Thus with the developed tools and instrumentation, the online images can be obtained up to a surface velocity of 3.5m/s. Scientists have already put forward wear hypothesis on damage of fibres based on the observed wear mechanisms such as pulverized fibre and partial resin removal [6. 49, 50, 51]. The fibre exposure in polymer is due to the failure of resin in the first place. Such details are also observed using the developed OVS system in

which fibre bundles being exposed as a consequence of resin removal (indicated by arrow) is indicated in the Figure 6-10 (b).
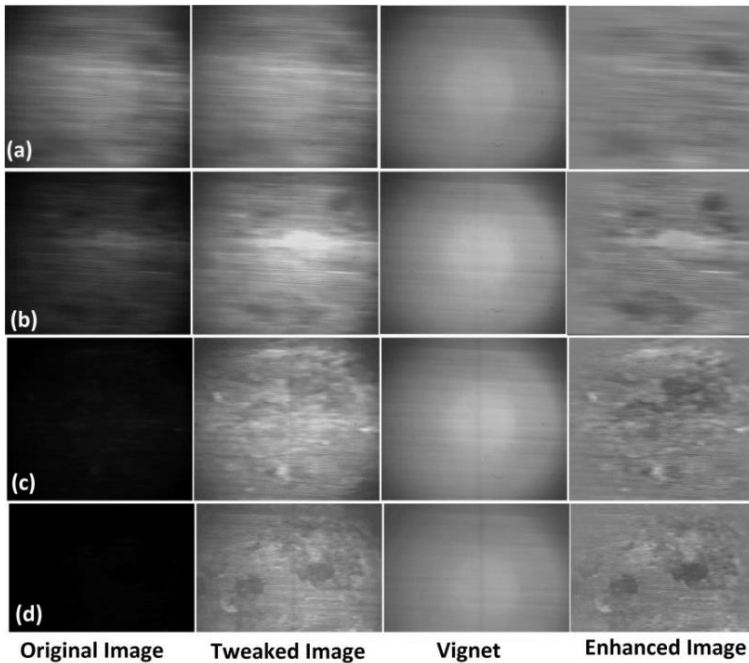


Figure 6-9 Online micrographs at different exposure time (b) Online images acquired at 3000fps and (a) 500µs, (b)166 µs, (c)66 µs and (d)33 µs exposure time.
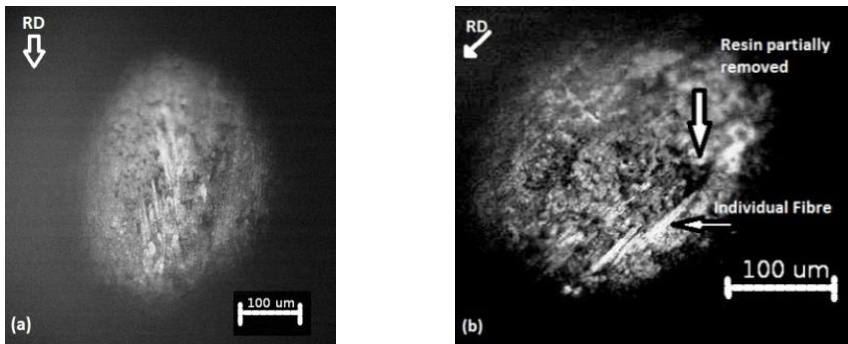


Figure 6-10. Real time micrographs acquired at (a) 7000 fps for 500 rpm and (b) 35000fps for 750 rpm.

Figure 6-11 shows the online micrographs of composite surface, but at different magnification (20X and 10X). The bright phase in the microstructure as seen from Figure 6-11 (a) are fibre bundles and the valleys between these bundles are indicated with arrows. Strands of fibres and the valley next to the fibres as a consequence of resin removal can be seen in Figure 6-11 (a). Valleys might have been formed due to two reasons: (1) plunging of machine marks from the counter material and (2) temporary displacement of fibre bundle.
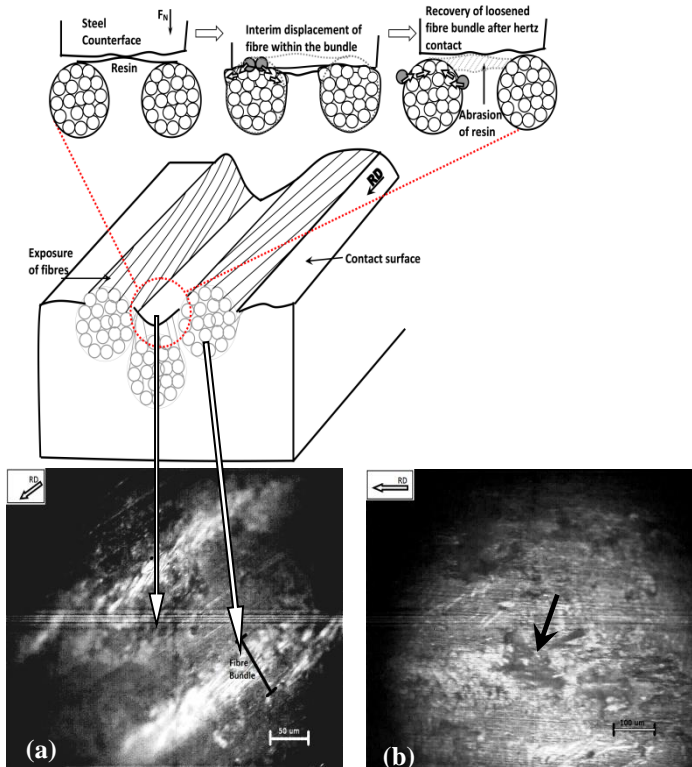
Figure 6-11 Online micrographs (a) 20X objective lens (b) 10X objective lens.

On comparing with 10X lens the field of view is relatively less for 20X objective thus showing intricate details (fibre bundles) than the overall surface morphology. It is also evident that a significant region is covered by 10X lens hence it will be used for long duration testing. Increased field of view allows covering more area for investigation. On having less field of view the frame rate has to be dramatically increased to obtain the overlap. Figure 6-11 (b) also shows with scars representing pitting phenomenon as one of the wear mechanism which is indicated with an arrow. Wear phenomenon correlating these morphological events can be represented in schematics for a better understanding of the wear behaviour. Nevertheless, these phenomena need a sequential observation to explain the evolution of particle generation. For that reason long duration test needs to be performed.

## 6.7.2 Long duration test

The main objective of OVS is to understand the evolution of wear which is studied by a time-series investigation. In the high speed real-time imaging Olympus, i-speed TR is used until 3000 fps. For understanding the morphological changes at a global level, approximately 30% overlap is required for stitching adjacent images. In regards to the illumination, threshold was selected based on motion blur and the details observed in the surface morphology during focusing.

Sequential evaluation of surface morphology is used to understand the wear behaviour of polymer metal contacts. It is evident from the image acquisition that the whole circumference of the image can be captured for investigation. However, in any given mechanical component the eccentricity is unavoidable for which focus blur is evident. Nevertheless, even after 30% overlap between images, a significant amount of frames can be stitched together. Previous experience had proved Orkot as a high performance material, thus a minimum 15 hours test duration is adopted. Initially both the discs are mounted and the contact surface is focused using a 10X objective at static condition. However, this is subjected to change during the commencement of the test from the initial Hertzian contact. Thus a fine focus is finally made after few contact cycles by visualizing the real-time images on the thin film transistor (TFT) screen.

The steel counterface which usually does not undergo a significant wear is not monitored online. Thus, post-mortem analysis is done only for counter material to understand the surface changes. From the surface investigation on steel, an uniform deposit of transfer film is observed. The steel contact surface is completely covered with polymer transfer layer and wear debris are found in the vicinity of the wear track (Figure 6-12). It is noteworthy to realize that these debris and transfer layer play an important role in controlling the tribological nature [6. 52].
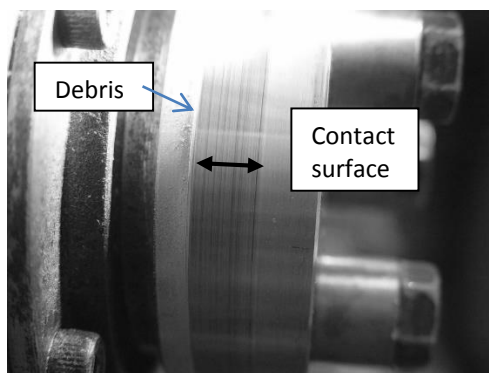


Figure 6-12 Photomacrographs of counter material contact surface.

Figure 6-13 shows the real-time image acquired during the initial period of testing (at 2 hours). 1000 images are acquired to cover the circumference of the specimen completely. These frames are acquired at 3000 fps and stitched together to form a significant surface for further investigation. Prior to stitching, the images, pre-processing is done for correcting the brightness and removing the vignette.

Subsequently registration is done for inter and intra video matching to identify the overlapping segments. Figure 6-13 shows image of 10 frames stitched together which is approximately more than 3 mm FOV. Considering a curved surface for investigation, this is significantly large area to understand the global presence of micro mechanism. Wear patterns such as surface cracks, craters, fibers are clearly seen from the high-speed micrographs. Both phases (resin and fiber) are differentiated from the grey scale intensity where the fiber bundle appears brighter in the micrograph. Craters which appear as a dark phase in the microstructure are pointed out using an arrow.
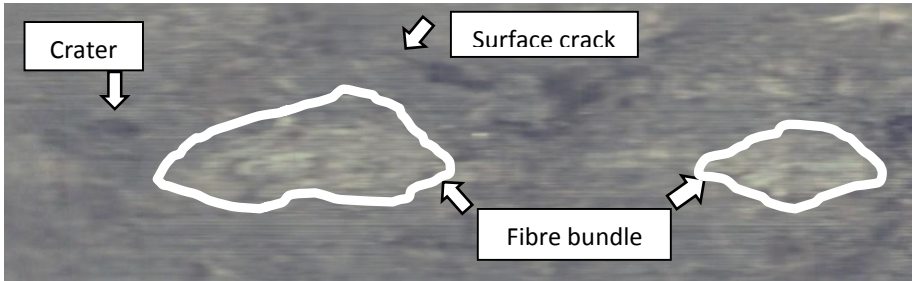


Figure 6-13 shows a stitched image from hour 2.

The real-time images at different cycles are stitched and compared with each other to understand the wear process. Craters which appear as a dark phase in the micrograph (Figure 6-14) are clearly seen even in the initial period of testing (hour 00). These craters are part of the surface texture where the space between the long 3D mesh of fibers are partially filled with resin. From the sequential images seen in Figure 6-14 it is evident that these craters disappear and reappear as a function of time. Craters present in hour 00 (indicated by arrow) disappear at hour 04, 06 and reappear at hour 08. Likewise, it is clear that the dark region within the square at hour 00 becomes partially bright at hour 08 and 14. It is evident from these images that the crater from the initial surface is filled with the resin due to back transfer phenomenon. This was also described in previous research without online evidences or chain of events [6. 49, 53, 54].

In our case, the online images give a clear picture with sequential images, proving the hypothesis of resin back transfer. Since the crater is occupied with resin, the filled in crater and the rest of the contact surface have similar height for having an equal scattering effect. Thus the dark phase disappears due to back transfer of resin from the steel surface to the parent material. This can be attributed to the dynamic nature of the backtransfered layer on the polymer surface. In a conventional post-mortem analysis this effect can also be misunderstood as a function of wear with global removal of material. But by observing the same region of interest the reappearance of crater in the image strongly emphasizes the back transfer of resin to the composite. An important feature as understood from the microstructure evolution is the closing of cracks. Figure 6-14 shows cracks located at the root of the craters (indicated with white circle) at hour zero. The surface crack present until hour 06 is partially closed at hour 08 and 14 (indicated by a circle) which can be observed from the micrograph. Cracks which are a critical factor for damage evolution are being repaired by means of back transfer of resin.
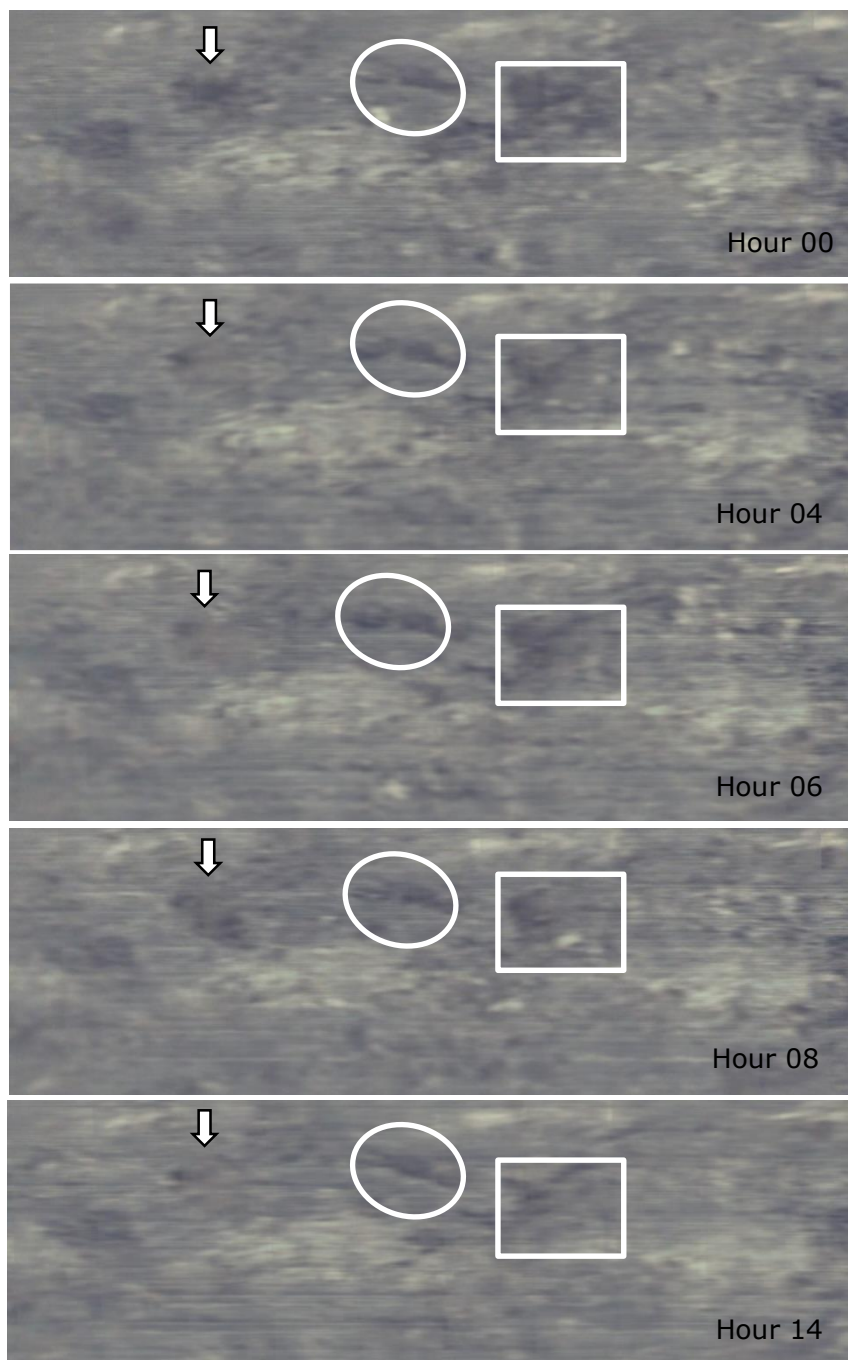
Figure 6-14. Online images acquired at 200 rpm (1 m/s).

The question of transfer layer playing a positive role in polymer tribology is partially answered by the time-series studies. In this case it is evident that the role of fibres which act not only as a structural member but also as a protective member of the

composite. The white region which represents the fibers in the worn surface morphology has not significantly changed. Thus, from the observations it is evident that these fibers are in contact with the steel counterface material to provide additional support to resist the damage caused by wear.

In any tribological study it is necessary to validate the wear process by quantitative means. Thus, change in dimension of the composite specimen is monitored online using a LVDT. Figure 6-15 shows the online data (average of 1000 points at 1kHz) of the diameter change as a function of time and the dots represents the time of image acquisition. In the first four hours, the diameter of the composite increases gradually however after hour 04 there is a sharp decrease in the diameter further to which oscillation in the diameter of the specimen is clearly observed. The increase in diameter can be attributed to the thermal expansion of the polymer.
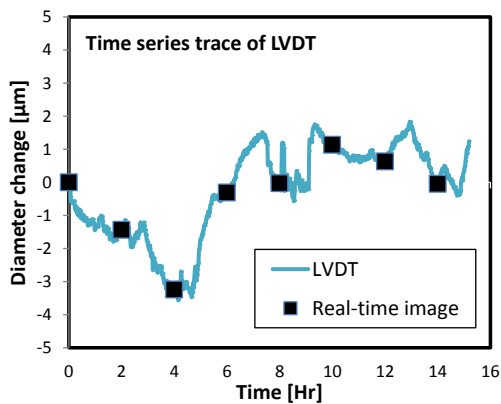


Figure 6-15 Diameter change as a function of time.

Since the dimensional changes are present in the course of testing, these changes should cause a focus blur. This "focus blur" serves as a variable in validating the dimensional change of the specimen. Thus, the acquired images from specific cycles (every two hours) were processed further to estimate blur. Fifteen blur estimation methods were used out of which three methods (gradient, variance and Reimannian tensor) have good correlation with the online signals from LVDT [6. 46]. Comparing the curves of estimated blur from the image gradient and diameter change, both follow a similar trend which agrees for the change in dimension (Figure 6-16).

Apart from monitoring the change in dimension, the different stages of wear process can be proven from the wear mode. The wear mode is characterized by the wear mechanism by which phenomenon like back transfer of resin from the steel counterface can be validated. By combining the quantitative measurement which is the estimated blur together with the wear phenomenon, a full understanding of the material removal process can be made. Here in our case even though polymer wear has detrimental-effect, the dynamic behaviour of the transfer layer as understood from the online images repairs the cracks and fills the craters to cover the surface defects. Thus, materials with properties complementing the formation of transfer layer can be considered effective in a polymer-metal tribo pair. The current research strongly recommends the use of online vision system for understanding the intermediate mechanisms which positively supports the wear behaviour.
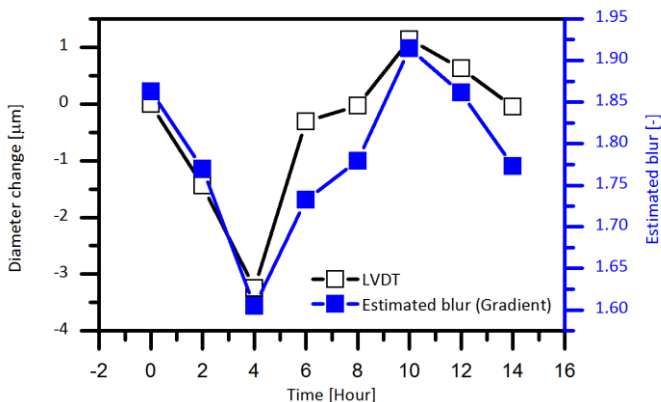
Figure 6-16 Online wear trend from the estimated blur and displacement measurements.

## 6.8 Conclusion

In an attempt towards developing a high speed online vision system, a new combination of bright field microscope in conjunction with high speed camera aids to investigate microstructure of moving surfaces. The following conclusions can be drawn from this exploratory approach.

- Parameters for optical and imaging system are optimized for which the 10X lens can elucidate micro mechanisms involved in the wear process.
- From the developed online vision system microscopic images with 1500 μm FOV can be acquired on a relatively fast moving body (3.5 m/s).
- Influence on exposure time clearly indicates the necessity of high intensity illumination (Xenon 300 Watt) for obtaining a blur free image.
- The unique combination of bright field microscope and high speed camera has capabilities to frame microscopic images at 35000 fps and 370 ns exposure time with the given Xenon illumination. At such a condition both the phases (resin and fiber) are clearly visualized in the micrograph.
- The test results strongly affirm the advantage of online monitoring by identifying the missed out intermediate mechanism such as back transfer of resin. Step by step progress of wear process is evident from online monitoring.
- The dynamic nature of polymer transfer film is clearly understood from the sequential image acquisition. Moreover, the repair mechanism of resin back transfer in closing the surface defects is very much evident in the real-time images.
- Additionally, focus blur can be used as an estimate to understand the wear trend from the online images, thus providing a complete package with qualitative (wear mode) and quantitative (estimated blur) information on the wear behaviour of the polymer composite.

# References

[6.1]    R. Kumar, P. Kulashekar, B. Dhanasekar, and B. Ramamoorthy, "Application of digital image magnification for surface roughness evaluation using machine vision," International Journal of Machine Tools and Manufacture, vol. 45, pp. 228-234, 2005.

[6.2]    S. Damodarasamy and S. Raman, "Texture analysis using computer vision," Computers in Industry, vol. 16, pp. 25-34, 1991.

[6.3]    D. E. P. Hoy and F. Yu, "Surface quality assessment using computer vision methods," Journal of Materials Processing Technology, vol. 28, pp. 265-274, 1991.

[6.4]    B. Y. Lee, S. F. Yu, and H. Juan, "The model of surface roughness inspection by vision system in turning," Mechatronics, vol. 14, pp. 129-141, 2004.

[6.5]    M. Clerico, "A study of the friction and wear of nylon against metal," Wear, vol. 13, pp. 183-197, 1969.

[6.6]    T. A. Stolarski, S. M. Hosseini, and S. Tobe, "Surface fatigue of polymers in rolling contact," Wear, vol. 214, pp. 271-278, 1998.

[6.7]    T. R. Bates Jr, K. C. Ludema, and W. A. Brainard, "A rheological mechanism of penetrative wear," Wear, vol. 30, pp. 365-375, 1974.

[6.8]    W. A. Glaeser, "Wear experiments in the scanning electron microscope," Wear, vol. 73, pp. 371-386, 1981.

[6.9]    P. Hedenqvist, M. Olsson, S. Jacobson, and S. Söderberg, "Failure mode analysis of TiN-coated high speed steel: In situ scratch adhesion testing in the scanning electron microscope," Surface and Coatings Technology, vol. 41, pp. 31-49, 1990.

[6.10]   K. Hokkirigawa and K. Kato, "An experimental and theoretical investigation of ploughing, cutting and wedge formation during abrasive wear," Tribology International, vol. 21, pp. 51-57, 1988.

[6.11]   T. Kayaba, K. Hokkirigawa, and K. Kato, "Analysis of the abrasive wear mechanism by successive observations of wear processes in a scanning electron microscope," Wear, vol. 110, pp. 419-430, 1986.

[6.12]   S. C. Lim and J. H. Brunton, "A dynamic wear rig for the scanning electron microscope," Wear, vol. 101, pp. 81-91, 1985.

[6.13]   B. Murarash and M. Varenberg, "Tribometer for In Situ Scanning Electron Microscopy of Microstructured Contacts," Tribology Letters, vol. 41, pp. 319-323, 2011.

[6.14]   S. Kano, H. Homma, S. Sasaki, and H. Shimura, "In situ monitoring of friction surfaces and their sequence pattern analysis," Philos Trans A Math Phys Eng Sci, vol. 366, pp. 665-71, 2008.

[6.15]   J. C. Su, C. K. Huang, and Y. S. Tarng, "An automated flank wear measurement of microdrills using machine vision," Journal of Materials Processing Technology, vol. 180, pp. 328-335, 2006.

[6.16]   S. Kurada and C. Bradley, "A machine vision system for tool wear assessment," Tribology International, vol. 30, pp. 295-304, 1997.

[6.17]   K. Niranjan Prasad and B. Ramamoorthy, "Tool wear evaluation by stereo vision and prediction by artificial neural network," Journal of Materials Processing Technology, vol. 112, pp. 43-52, 2001.

[6.18]   J. Jurkovic, M. Korosec, and J. Kopac, "New approach in tool wear measuring technique using CCD vision system," International Journal of Machine Tools and Manufacture, vol. 45, pp. 1023-1030, 2005.

[6.19]   K. B. Pedersen, "Wear measurement of cutting tools by computer vision," International Journal of Machine Tools and Manufacture, vol. 30, pp. 131-139, 1990.

[6.20]   J. Quintelier, "Online wear monitoring of polymer matrix composites with advanced measurement techniques," PhD dissertation, Ghent University, 2007.

[6.21]   H. E. Sliney, "Dynamics of Solid Lubrication as Observed by Optical Microscopy," A S L E Transactions, vol. 21, pp. 109-117, 1978.

[6.22]   T. W. Scharf and I. L. Singer, "Role of Third Bodies in Friction Behavior of Diamond-like Nanocomposite Coatings Studied by In Situ Tribometry," Tribology Transactions, vol. 45, pp. 363-371, 2002.

[6.23]   A. Ovcharenko, G. Halperin, I. Etsion, and M. Varenberg, "A novel test rig for in situ and real time optical measurement of the contact area evolution during pre-sliding of a spherical contact," Tribology Letters, vol. 23, pp. 55-63, 2006.

[6.24]   B. Krick, D. Hahn, and W. G. Sawyer, "Plasmonic Diagnostics for Tribology: In Situ Observations Using Surface Plasmon Resonance in Combination with Surface-Enhanced Raman Spectroscopy," Tribology Letters, vol. 49, pp. 95-102, 2013.

[6.25]   R. R. Chromik, C. C. Baker, A. A. Voevodin, and K. J. Wahl, "In situ tribometry of solid lubricant nanocomposite coatings," Wear, vol. 262, pp. 1239-1252, 2007.

[6.26]   S. W. Zhang, "State-of-the-art of polymer tribology," Tribology International, vol. 31, pp. 49-60, 1998.

[6.27]   D. A. Rigney, L. H. Chen, M. G. S. Naylor, and A. R. Rosenfield, "Wear processes in sliding systems," Wear, vol. 100, pp. 195-219, 1984.

[6.28]   J. Michler, R. Rabe, J. L. Bucaille, B. Moser, P. Schwaller, and J. M. Breguet, "Investigation of wear mechanisms through in situ observation during microscratching inside the scanning electron microscope," Wear, vol. 259, pp. 18-26, 2005.

[6.29]   J. Zhang, Detection and monitoring of wear using imaging methods: University of Twente, PhD dissertation, 2006.

[6.30]   V. K. Jain and S. Bahadur, "An investigation of the markings on wear and fatigue fracture surfaces," Wear, vol. 75, pp. 357-368, 1982.

[6.31]   H. Böhm, S. Betz, and A. Ball, "The wear resistance of polymers," Tribology International, vol. 23, pp. 399-406, 1990.

[6.32]   Z. Chen, T. Li, X. Liu, and R. Lü, "Friction and wear mechanisms of polyamide 66/high density polyethylene blends," Journal of Polymer Science Part B: Polymer Physics, vol. 43, pp. 2514-2523, 2005.

[6.33]   R. Cortellucci, C. J. Heim, T. D. Koshy, and P. J. Phillips, "Abrasion of plastics," Wear, vol. 47, pp. 397-405, 1978.

[6.34]   S. S. Kim, M. W. Shin, and H. Jang, "The Wear Mechanism of a Polyphenylene Sulfide (PPS) Composite Mixed with Ethylene Butyl Acrylate (EBA)," Tribology Letters, vol. 47, pp. 165-173, 2012.

[6.35]   L. Chang, Z. Zhang, H. Zhang, and A. K. Schlarb, "On the sliding wear of nanoparticle filled polyamide 66 composites," Composites Science and Technology, vol. 66, pp. 3188-3198, 2006.

[6.36]   P. C. West, "High speed real-time machine vision, Imagenation and Automated Vision Systems.

[6.37]   S. Kurada and C. Bradley, "A review of machine vision sensors for tool condition monitoring," Computers in Industry, vol. 34, pp. 55-72, 1997.

[6.38]   G. Galante, M. Piacentini, and V. F. Ruisi, "Surface roughness detection by tool image processing," Wear, vol. 148, pp. 211-220, 1991.

[6.39]   D. Fadare and A. Oni, "Development and application of a machine vision system for measurement of tool wear," Journal of Engineering and Applied Sciences, vol. 4, pp. 30-37, 2009.

[6.40]   D. Kerr, J. Pengilley, and R. Garwood, "Assessment and visualisation of machine tool wear using computer vision," The International Journal of Advanced Manufacturing Technology, vol. 28, pp. 781-791, 2006.

[6.41]   G. A. Al-Kindi and B. Shirinzadeh, "An evaluation of surface roughness parameters measurement using vision-based data," International Journal of Machine Tools and Manufacture, vol. 47, pp. 697-708, 2007.

[6.42]   S. Dutta, S. K. Pal, S. Mukhopadhyay, and R. Sen, "Application of digital image processing in tool condition monitoring: A review," CIRP Journal of Manufacturing Science and Technology, vol. 6, pp. 212-232, 2013.

[6.43]   E. S. Gadelmawla, "A vision system for surface roughness characterization using the gray level co-occurrence matrix," NDT & E International, vol. 37, pp. 577-588, 2004.

[6.44]   I. L. Rasmussen, M. Guibert, M. Belin, J. M. Martin, N. J. Mikkelsen, H. C. Pedersen, "Wear monitoring of protective nitride coatings using image processing," Surface and Coatings Technology, vol. 204, pp. 1970-1972, 2010.

[6.45]   "High Speed Camera and Microscope System pp 2-8, The dolomite cetre ltd..

[6.46]   S. Soleimani, J. P. Sukumaran, K. Douterloigne, F. Rooms, W. Philips, and P. De Baets, "Correction, stitching and blur estimation of micro-graphs obtained at high speed," Advanced Concepts for Intelligent Vision Systems, pp. 84-95, 2012.

[6.47]   J. Sukumaran, S. Soleimani, V. Rodriguez Fereira, M. Ando, W. Philips, and P. De Baets, "Transition of surface morphology in rolling/sliding of polymer-metal contacts," 5th World Tribology Congress 2013 , 2013.

[6.48]   Y. C. Tasan, M. B. de Rooij, and D. J. Schipper, "Measurement of wear on asperity level using image-processing techniques," Wear, vol. 258, pp. 83-91, 2005.

[6.49]   J. Bijwe and R. Rattan, "Influence of weave of carbon fabric in polyetherimide composites in various wear situations," Wear, vol. 263, pp. 984-991, 2007.

[6.50]   P. L. Rosin, "Thresholding for change detection," in Computer Vision, 1998. Sixth International Conference on, pp. 274-279, 1998.

[6.51]   R. C. Gonzalez, R. E. Woods, and S. L. Eddins, Digital image processing using MATLAB: Pearson Education India, 2004.

[6.52]   A. I. Sviridyonok, V. A. Bely, V. A. Smurugov, and V. G. Savkin, "A study of transfer in frictional interaction of polymers," Wear, vol. 25, pp. 301-308, 1973.

[6.53]   H. Czichos, "Influence of adhesive and abrasive mechanisms on the tribological behaviour of thermoplastic polymers," Wear, vol. 88, pp. 27-43, 1983.

[6.54]   H. Koike, K. Kida, E. C. Santos, J. Rozwadowska, Y. Kashima, and K. Kanemasu, "Self-lubrication of PEEK polymer bearings in rolling contact fatigue under radial loads," Tribology International, vol. 49, pp. 30-38, 2012.

# Chapter 7

# Summary and conclusion

# Vision assisted tribography of rolling-sliding contact of polymer-steel pairs

This chapter summarises the individual results from chapter 4, 5 and 6 and addresses the questions raised in chapter 1 and 2.

## 7.1 Polymer wear in rolling-sliding contacts

Chapter 1 was designed to understand the representativeness of engineering problems in scientific investigations. A comparison study was performed for polymers in rolling contacts with three modes: literature, retrieval analysis and real scale testing.

Even though rolling contacts of polymers are extensively used in engineering applications, their tribological importance are partially ignored. The few available polymer reports suggests that wear in rolling contacts is generally estimated from diametric loss or mass loss. However, the substantial difference in the dimensional scale of components and its corresponding wear does not allow for precise wear measurement. Having damages at an asperity level, the most suitable representation of wear is surface morphology. Thus, in the wear investigations of polymers in rolling contact, stereometric analysis could be replaced with morphological examination through worn surface micrographs. Results from the comparative study in chapter 1 clearly identifies micro-pitting as the dominant mechanism. It is also evident that the wear scars (pits) shows significant difference in size distribution and its coverage. Clear size distinction in diameter and depth of micro-pits and large craters were apparent. Thus, generalising the wear mechanism with qualitative information from surface morphologies is inadequate in wear analysis.

In most reported studies the micro-pitting phenomenon is prevalent in causing material loss. However, groove marks representing abrasion are also clearly observed in retrieval analysis and real scale testing. The cause of these groove marks are potentially from partial sliding, which is not well documented in the model testing. Besides, the model testing does not fully represent the real engineering problems. Thus chapter 1 clearly reveals the requirement for a fundamental understanding of wear process in rolling-sliding conditions. Moreover, it also points towards the direction of surface scar analysis as a prime indicator for wear characterisation.

## 7.2 Wear mechanisms, phenomenon and surface scars

Surface scars being proposed as a suitable variable for wear characterisation, an in-depth survey of literature on morphological features of polymer wear is described in Chapter 2. It was found that there is a misconception in the reported information between phenomena, wear scars and wear mechanisms. Thus, a tribo-tree was established for realizing the inter-relationship between the observed surface scars and wear mechanisms. The tribo-tree acts as an effective classification in segregating different mechanism incurred in polymer tribology. In the process of establishing

tribo-tree, mechanisms such as abrasion, adhesion, fatigue-wear and therformation are clearly understood and represented by specific wear scars. Despite of all available mechanism in literature, scars representing partial sliding condition are barely reported.

Generally, several techniques (OM, SEM, TEM, AFM, STM etc.) are available for morphological investigation. However, the most commonly used are SEM and optical microscopy. Though scanning electron microscopy is prevalent, it is relatively expensive when compared with optical microscopy. Also it was found that in general engineering practise the optical microscopy is still commonly used. However, standards and protocols in optical microscopy of polymers for investigating the worn surface are scarcely reported. In place where a combination of mechanism prevails a stringent protocol is required for representing global wear characteristics of the worn surface. Submicron level investigations provide information locally, but the wear in polymer rolling has a significant area of contact. Consequently, for representing the global wear process a substantial area ($\mu m^2$) is required. Thus, a protocol for image acquisition provides concurrent information from the view point of magnification, field of view, number of acquired images and ROI. This partly fulfils the criteria required for quantitative micrography of wear evaluation.

Two kinds of methods were proposed to understand the wear behaviour of polymer wear in rolling-sliding contacts: (1) traditional tribological study (TES) and (2) damage evolution study (DES). A precise protocol was developed for both studies based on preliminary testing.

## 7.3  Traditional tribological study (TTS)

In the traditional tribological study (TTS), tests were conducted for pure rolling and partial sliding condition with slip ratio ranging from 0 – 26%. On taking in account of partial sliding, the relative slip (9%, 18% and 26%) has an influence on wear behaviour. However, the topographic characteristics surpasses the influence from partial sliding condition. The post-mortem analysis revealed the presence of micropits in the contact surface of pure rolling condition However, partial sliding condition is dominated by micro-channels caused by abrasion. The wear rate at partial sliding condition shows an increased value for 9% slip ratio. The area of micropits and grooves occupied in the acquired images were calculated using quantitative micrography (image processing technique). This partly supports the existing engineering practise of visual inspection (macro level) for worn surface in wear parts. The polymer with 9% slipping showed high incidence of micro-channels. Both the tendency of wear rate and the image analysis for abrasion match well between each other. Knowing that the first-hand information of wear is from experts, the results from image processing are validated using a survey from expert opinion. The answers from expert showed similar tendency indicating severe abrasion for 9% slip condition. Therefore, the used technique with a new approach of quantitative micrography is effective in wear characterisation. One of the primary question in chapter 1 on the "establishment of any new technique" is answered by adopting the quantitative micrography for wear evaluation.

Also phenomena such as grooving and pitting are clearly identified by using the image processing technique (granulometry), for which, it can be used as a classifier for wear characterisation between the two wear phenomena.

There are numerous variables to be accounted for the wear characteristics in polymers, out of which the surface topography of the counter material is a critical factor. It is impossible to perform experimental evaluation to identify the influences of individual parameters. However, this is resolved by including all these parameters in a single dimensionless quantity derived from "Buckingham Pi" theorem. The developed wear equation has the topographic parameter "Rmax" and slip ratio as the primary component. The output (wear volume) of the wear equation is in good agreement with the experimental result on the wear rate.

This part of the dissertation also answers the question from chapter 2 on the effects of transfer layer. Describing the transfer film characteristics they are two types of (1) primary layer and (2) secondary layer. The primary layer is a thin uniform deposit of polymer on the steel counter material, and the secondary layer is a bulky material on top of the primary layer which is non-uniform in distribution. Both layers are formed from the particles generated as a consequence of wear. The thickness of the secondary layer is measured from a cross-sectional study as well as from the topographic profile Rmax. In pure rolling condition, the wear is substantially low and hence no secondary transfer layer is formed. This is also clearly seen from the micrograph. However, in partial sliding condition significant amount of wear result in formation of secondary layer. It is also evident that 9% partial sliding condition has the largest Rmax values representing the significant deposit of secondary transfer layer. From the traditional post-mortem analysis, by relating the micrographs, Rmax value, thickness from cross-section and the wear rate it can be concluded that transfer layer has neutral wear characteristics. However, the transfer layer formation can be a consequence of material removal only during the initial stage of wear. Also the transfer layer characteristics might be instant specific and short lived. Thus, further investigation was made using the damage evolution study to detect the occurrence of transfer layer and to study the wear process.

## 7.4 Damage evolution study (DES)

The unknowns of the transfer layer characteristics which are "protective element" and "friction modifier" are studied in chapter 5. Though the transfer layer characteristics were evaluated in the post-mortem analysis, its true nature in terms of occurrence is studied by means of "Damage evolution study". The DES has benefited from the newly developed "relocation micrography technique". This new technique stands effective in locating the same region of interest to understand the surface changes undergone by the polymer and steel specimen. The new technique clearly displays the evolution of the particles generated and the surface modification as a consequence of wear process.

The two tests performed with ideal condition (constant contact pressure and slip ratio) clearly showed variability in coefficient of friction. It is evident that, besides the operating parameters, the momentary change in surface morphology is reflected in

the friction characteristics. The variability in the surface characteristics are understood using image properties by man of energy of an image. Instantaneous image through *ex-situ* using dark field illumination explicated the momentary change in surface.

DES clearly explains the two staged global wear process of polymer in partial sliding. The first stage reveals fracturing and plastic deformation of polymer. Subsequently, the second stage establishes the transfer layer using the fractured debris. The debris are milled between the polymer and steel surface to form a thin layer of polymer on both the material (polymer and steel). However, this layer is not continuously present throughout the experiment which explicates the dynamic nature of its occurrence in the time-series study. This can be attributed to the change in friction characteristics of polymer as a function of surface morphology in both materials (steel and polymer). Since DES has an intermediate running-in which disturbs the equilibrium of the tribo system (Chapter 5). Also, a better understanding of the wear requires sequential data (images) of the wear process, for which advanced techniques are to be used.

## 7.5 High speed online micrography for polymers

After careful consideration, the online vision system (OVS) is developed with a combination of high speed camera in conjunction with optical microscope. With such a combination, images required for the quantitative micrography (as seen in Chapter 4 & 5) can be acquired during testing. In the course of developing the high-speed online imaging system, it was evident that 10X objective lens (FOV 1500 µm) is found to be more suitable based on the observed details such as grooves and micro-pits. From the newly developed system for online vision, microscopic images are acquired at extreme conditions. Images of moving contact surfaces at a surface velocity of 3.5 m/s are acquired using a high intensity illumination (Xenon 300 Watt). Short duration tests aimed at identifying the limitations of OVS acquired online images at 35000 fps and 375 ns exposure time. The geometry (disc) of the used configuration has an additional advantage from the self-exposure of the contact surface. In addition, the geometry also provides sufficient images from the circumference which are stitched together to have a significant area for investigation. Online images elucidate the back transfer of resin during the course of tribological interaction. The cracks present on the initial contact surface are filled by the back transferred resin to create a self-healing effect. These phenomenon remain only speculations without the online images. Besides, monitoring wear mechanism, quantitative micrography in terms of blur estimation stands effective in creating a wear curve for the time-series study. On the whole, the developed online vision system helps in understanding the wear behavior, quantitatively as well as qualitatively.

## 7.6 Future work

The particles in the polymer contact surface effectively identified using dark field imaging can be a source of inspiration to use dark field imaging for polymer tribography.

The newly developed relocation micrography is effective in laboratory scale. This can motivate designers to adapt such system to relocate ROI for condition monitoring to obtain momentary status of the critical component. The future work also aims at using these developed techniques in real scale component testing. The developed technique was used for studying one specific material, thus the research will be extended to investigate other material by using quantitative micrography.

To comply with the challenges in the use of polymers in tribological application it is necessary to develop a clear understanding on the physical interaction of contacting surface. For this reason the protective and self-lubricating capabilities of polymers are to be identified. Thus, an investigation on the basic variables such as load, speed, roughness of counter material and material characteristics (viscoelastic nature at Tg temperature) will be done to identify the dominating variable. *In-situ* observations will be done for monitoring the physical interaction between the polymer and the mating metal surface in dry sliding condition. To study the development of transfer layer image segmentation will be adopted for macroscopic images of contact surface. These physical interactions and the transfer layer observations will be thereafter converted to appropriate empirical model to describe the wear process and lubricating effect of the polymers.

# Appendix A

# Inspection report of elevator roller

The appendix here provides the measurements made on retrieved polymer roller from an elevator sliding door. The present case study deals with a critical component, which operates mostly in a contaminated environment. This component was chosen to understand the link between wear of real engineering component and laboratory scale testing. Inspection for morphological modification and topographic characteristics were performed to understand the incurred wear mechanism. These results on surface characteristics, elucidates the closeness of simulated lab scale experiments, to express real engineering problems. Beside elevator door, similar components in rolling contact are used in many applications as well. Thus, this is an appropriate representative of many engineering comments which are used in rolling/sliding contact.

## A.1 Background

Rolling/sliding in polymer metal pairs is one of the critical factors discussed in the current thesis. A comparable application is chosen and investigated for wear patterns and incurred damage mechanisms. The component chosen in the present investigation is the polymer rollers used in sliding doors for elevator rollers. These rollers generally have a service life of 2 – 3.5 years. The service life of rollers is considered to be crucial from the perspective of both elevator manufacturers and the end users. These rollers are replaced based on the vibrations and noise experienced from the doors. The individual rollers are replaced based on the operation condition. As a scheduled maintenance during the end of 3.5 years, these rollers are visually inspected for surface damage. Based on its operation with respect to the noise, vibration and surface damage these rollers in all the doors are completely replaced. This requires complete disassembly of the doors which is performed through shutdown maintenance. For a Small and medium scale enterprises (SME) the replacement of rollers can be routine. The understanding of the roller damage and its damage mechanism from the fundamental perspective can provide better solution to designers and manufacturers to select appropriate contact condition, materials and loads.

The roller presented in the case study was retrieved from Golden elevators company, India. The rollers were installed in a passenger (7 persons) car elevator doors operating on a ground plus three floors (G+3) of a commercial facility in Chennai, India. According to the elevator manufacturer, after careful consideration and visual inspection, all rollers in the elevators were fully replaced after an operational service life of 3.5 years. The doors of the elevators were operated manually, thus having approximately a sliding speed of 0.1 m/s.

## A.2 Polymer rollers

The elevator is equipped with manual single speed sliding door mechanism with two panels each for the landing and cabin doors. Each panel is supported by two rollers to fulfil the opening and closing condition. A panel weighed approximately 30 ± 0.25 kg, thus a normal force of 294 N was shared between the two rollers. The doors were partially supported by additional roller at bottom of the panel. However, due to the clearance between the door and the floor (sill) the full load from the panel acts on the polymer rollers A schematic of the loading condition is shown in Figure A-1. A drawing of the polymer roller and the assembly is shown in Figure A-2. The effective contact width of the roller and the thickness of the polymer are 10 and 3.7 mm respectively. Thus, a Hertzian contact pressure of 60 MPa will be implied on each roller.
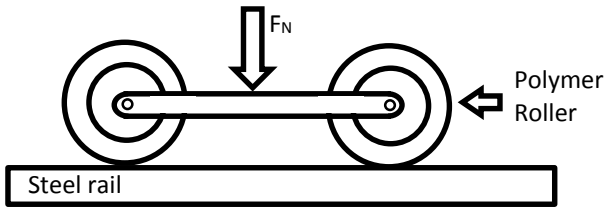
Figure A-1 Schematics of the loading condition of single panel in the elevator door.
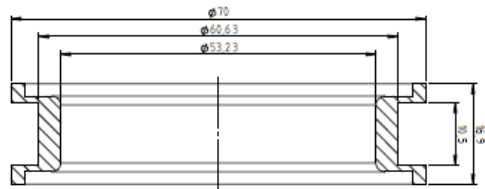


Figure A-2 dismantled roller assembly and part drawing of the polymer skeleton

## A.2.1 Visual observation.

Totally, 32 rollers were disassembled and most of them had pits and abrasions on the contact surface. The pits were occupied with contaminants such as dust on the polymer contact surface. Out of the 32 rollers, only two were used for further inspection, and were named as GL1 and GL2. The rollers were initially cleaned with distilled water and acetone in an ultrasonic bath for a period of 20 minutes. Despite of the rigorous cleaning process the polymer surface still had the black colouration in the pits. In the visual inspection, evidence of grooves were already visible, however these are only partially present in few sectors, thus, confirming partial sliding condition. From the visual observation, the dominating wear mechanism in the polymer contact is pitting. Similar pitting behaviour was observed by Gordan *et al* in model testing using a twin-disc test rig [A.1]. The shoulders of the polymer roller have experienced mild wear with random scratch patterns, this can be attributed to the effect of contaminants. The contact surface was fully occupied with pits ranging from micron size up to millimetre. To understand more about surface scars and its characteristics bright field optical microscopy and surface profilometry was performed.
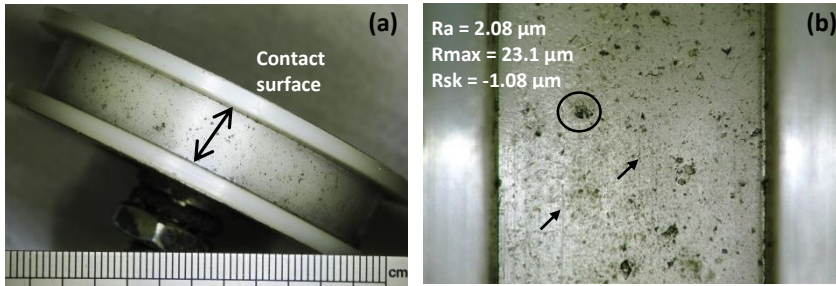
Figure A-3 Photomacrograph of the polymer roller (a) contact surface (b) exploded view

## A.2.2 Optical microscopy

The images of contact surface investigated under reflected brightfield microscope are presented in Figure A-4. Microscopic images were taken at different location to see the repetitiveness of the surface scars. Figure A-4 (a) shows contaminants as a white phase in the pure polymer specimen. Such contaminants were seen even with the naked eye during the retrieval. Craters were seen all over the contact surface, a typical example is shown in Figure A-4(a). The grooves from partial sliding is also visible in Figure A-4(b). From the appearance, it can be assumed that they are relatively shallow on comparing with the craters. However, the depth of these craters and grooves will be investigated further using stylus profilometry.
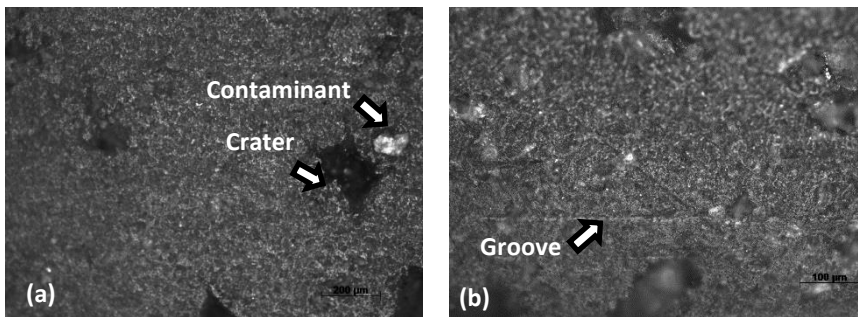


Figure A-4 Micrographs of the roller contact surface (a) pitting (b) grooving

## A.2.3 Topography measurement

The surface topography and contour of the wear scars were measured using 2D and 3D profiling respectively. In the surface characterization a cut-off wavelength $\lambda_c$= 0.8 mm at 0.3 mm/s traverse speed, and a sampling length $l_m$= 4 mm was used. The selection criterion for $\lambda_c$ and $l_m$ was based on DIN 4768 and ISO 4288 standards. The profile of the contact surface was traced in both along and across the .rolling direction. The average values of four different measurements are presented in Table A-1. The surface showed similar topographic characteristics in both direction (across and along) with negative skewness and a kurtosis value larger than 3. Depth of the

grooves, micro-pits and craters are clearly profiled where the crater was observed with depth of more than 100 µm. The micro-pits and the abrasion grooves have similar depth profile. The typical characteristic of groove with a ridge is clearly observed from the depth profile in

Figure A-6 (b).

Table A-1 Topographic information of contact surface [µm]

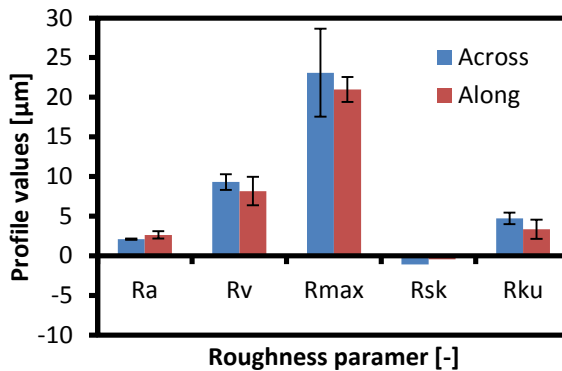| | Across | | | | | | Along | | | | |
|---|---|---|---|---|---|---|---|---|---|---|---|
| | Ra | Rv | Rmax | Rsk | Rku | | Ra | Rv | Rmax | Rsk | Rku |
| **Average** | 2.08 | 9.30 | 23.10 | -1.08 | 4.71 | | 2.63 | 8.15 | 21.00 | -0.47 | 3.36 |
| **Std.D.** | 0.07 | 0.97 | 5.55 | 0.18 | 0.73 | | 0.47 | 1.80 | 1.57 | 0.46 | 1.21 |



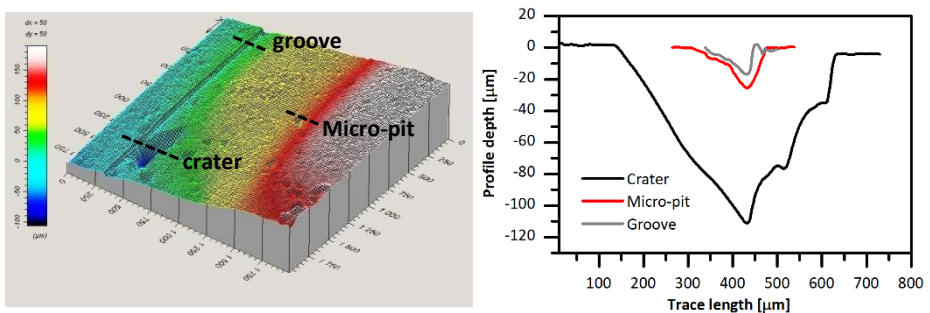Figure A-5 shows the roughness parameters and its values



Figure A-6 Polymer contact surface (a) 3D profile (b) depth profile

## A.3 Wear scar analysis

In regards to evaluating the surface scars three images representing the surface scars were acquired at different locations. The selected micrograph for image processing is presented in Figure A-7.
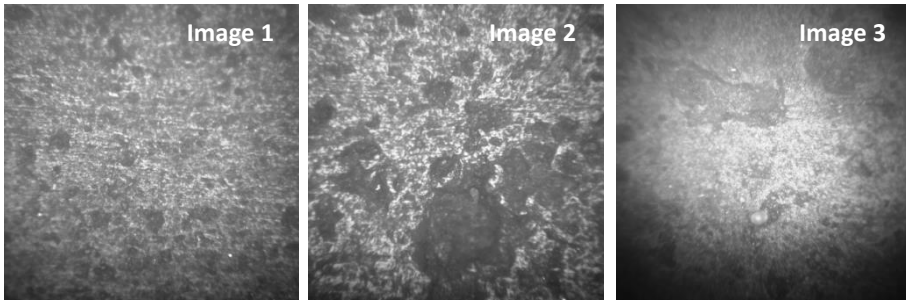
Figure A-7 Selected contact surface for characterizing the size distribution and the presence of wear scars

These images were segmented and the distribution of the surface scars based on its occupied area and its size were calculated using image processing technique (Granulometry). Amongst the three images, it is evident that micro-pits are dominantly present with diameter ranging from 50-100 µm. Also Image 1 and 2 does not show large craters above the size 1000 µm diameter.
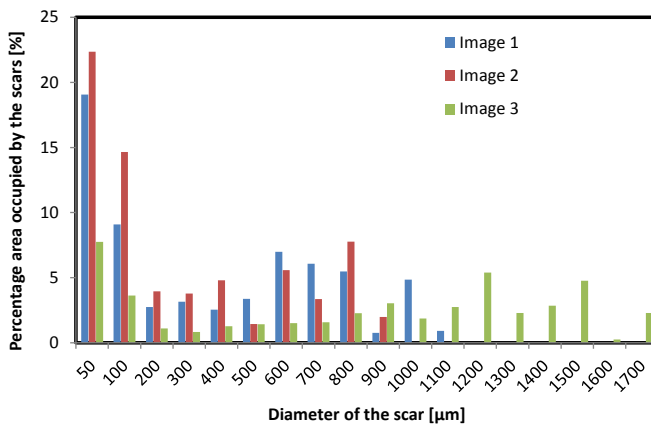


Figure A-8 Size distribution of craters and micro-pits from Figure A-7.

## A.4 Mechanical properties

According to the manufacturer the used material is PA6, for which the Shore D hardness was measured using Durometer Shore D (BAQ) in accordance with the ASTM D 2240. Five measurements were made on a contact surface with 5 mm apart from each other. A shore D hardness of 76 ± 1 was recorded in the observation from the dial.

## A.5 Discussion

The investigation was made to understand the wear mechanism underwent by the polymer rollers. All three modes of investigation: visible inspection, optical

microscopy and stylus profilometry revealed the presence of craters, micro-pits and grooves. On comparing with micro-pits, the crater has a relatively larger depth with factor of 5. The depth of the groove as observed from the contour is lesser than the micro-pits. The negative skewness shows prevalence of valleys in the contact surface, which can be attributed to the presence of several micropits. It is evident from the images that the micro-pitting is the dominant mechanism in rolling contacts for polymer metal tribo-pairs. Such mechanisms micro-pits) reported from laboratory testing indicate its relevance to industrial components. Additionally, partial sliding results with grooves on the contact surface. Nevertheless, this specific mechanism on partial sliding is limitedly reported.

## A.6 Conclusion

From the analysis made on the engineering component "polymer roller", the following conclusions can be drawn

- Micro-pits are the dominating mechanism in rolling contact of polymers.
- Particles seen on the polymer contact surface shows that, the third body as a contaminant has positive wear characteristics by filling the micro-pits.
- From the view point of micrographs, laboratory scale tests partially represent the wear of real engineering components.
- Partial sliding is evident from the observed wear scar (groove), this elucidates that even in pure rolling condition there is a involvement of sliding behaviour
- The inspection report raises a question on the use of quantitative microscopy for laboratory scale testing and also industrial inspection for such rollers.

## References

[A.1] Gordon, D. H., and Kukureka, S. N., 2009, "The wear and friction of polyamide 46 and polyamide 46/aramid-fibre composites in sliding/rolling contact," Wear, 267(1-4), pp. 669-678.

**Appendix B**

# Test report of conveyor roller testing

## B.1 Background:

Real scale wear analysis from applications takes years for having sever wear. This is primarily time consuming and expensive for tribological study. However, this can be experimentally simulated using an accelerated laboratory scale test representing the real application. The current test report details the conveyor chain tested in a laboratory scale conveyor wear tester at Laboratory Soete, Ghent University. A test was performed for conveyors with acetal (POM-H) rollers against steel counter material. Material removal and the incurred wear mechanism is studied from the post-mortem and online inspection of the microscopic images.

## B.2 Experimental data

Test number              : Conveyor chain test ADC_2014
Tribo system             : Closed system
Test equipment           : Conveyor chain wear test rig
Contact type             : Line contact
Condition                : Dry room temperature
Type of motion           : Combined rolling/sliding
Measurements             : Surface morphology, topography
                           and dimensional change

## B.2.1 Materials Used

In the current experimental study commercially available roller conveyor chains (Dongua) with POM-H rollers is tested against steel counter material. Specification of the conveyor and the technical drawing of the roller assembly is given Table B-1 and Figure B-1 respectively.

Table B-1 Specifications of the conveyor roller chain

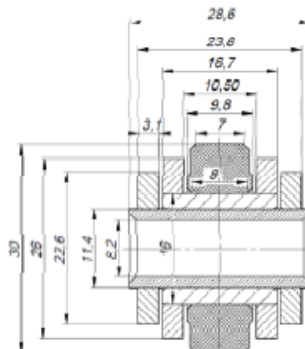| Chain material | RVS-AISI 304 |
|---|---|
| Roller material | POM-H (Delrin) |
| Chain pitch | 50,8 mm (2") |
| Roller outside diameter | 30 mm |
| Test chain length | 2438,4 mm |



Figure B-1 Schematics of the roller assembly

## B.2.2 Test configuration

The test parameters were selected accelerated test conditions as shown in Table B-2. A schematic of the test configuration is shown in Figure B-2. Accommodating 50 rollers in a chain the free end of the conveyor chain is linked together to have closed loop rotating roller chain. The chains will be fixed between a fixed sprocket driven by an electric motor and a movable shaft for inducing the tangential force as shown in Figure B-2.
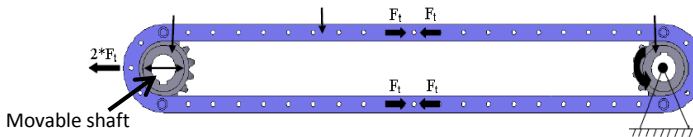


Figure B-2 the overall setup of the conveyor chain

A detailed description of the test rig capabilities and its assembly (see Figure B-3) is given in our earlier work [C.1]. The normal force is applied to the counter material, the loading schematic is given in Figure B-3. Out of 50 rollers, only 9 rollers at a time comes in contact with the counter material. The incurred motion on the rollers is pure rolling, however, partial sliding is experienced due to the several reasons such as presence of contaminants (wear debris), clearances between the roller and the bush.
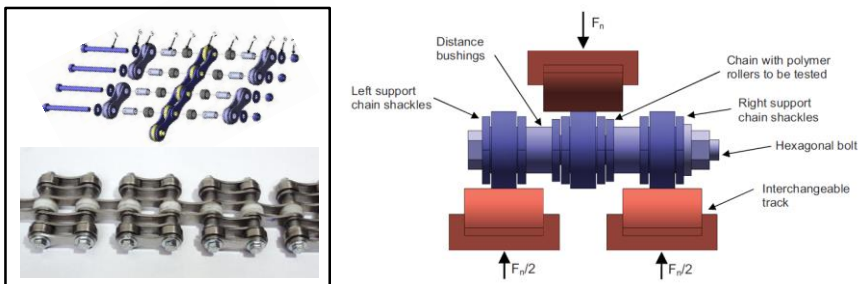


Figure B-3 Schematic of loading mechanism and the conveyor chain assembly [C.1].

Table B-2 Operational parameters

| Parameter | Unit | |
|---|---|---|
| Normal force | N | 2208 - 4908 |
| Tangential force | N | 3927 - 4412 |
| Width of contact | mm | 7 |
| Rotational speed | rpm | 174 - 275 |
| Lubrication | - | Dry contact condition |

## B.2.3 Test procedure

Step 1: Both test material and counter material are cleaned with Loctite 6040 cleaner.

Step 2: Out of 50 rollers, 8 were selected and markings were made for roughness measurement and microscopic inspection. (Starting from the coupled ends of the roller chain the rollers considered for investigations are 1, 6, 11, 17, 23, 29, 34, 39).

Step 3: The roughness profile of both the materials (conveyor rollers and steel counter material) were measured using stylus profilometry.

Step 4: The diameter of roller were measured using a digital Vernier calliper before testing.

Step 5: Micrographs and macrographs of the contact surface were acquired before testing.

Step 6: Continuous rolling/sliding wear test and post-mortem analysis of the worn rollers by following step 2 to step 6.

## B.3 Test results

The wear characteristics of the tribo-system were evaluated after 15 hours of testing. For morphological inspection, post-mortem analysis of contact surface was performed using reflected light bright-field microscopy. Tribological characterisation was done based on the changes observed in the diameter of the disc and roughness profile

## B.3.1 Offline measurements

The wear based on diameter change and profile depth was measured for the selected rollers are shown in the Table B-3 for test material. The diameter of the rollers are measured in five different locations (0°, 72°, 144°, 216°, 288) and its mean are presented in Table B-3. However, there is significant variability in wear considering the eight wheels. However, five rollers (wheel, 4, 5, 6, 7, and 8) has showed with no material loss or relatively 10 μm diameter loss. These variations can also be attributed to the clearances between the roller and the bush that can cause different contact condition.

Table B-3 Diameter loss from micrometer

|         | before test | after test | difference |
|---------|-------------|------------|------------|
| wheel 1 | 29.75       | 29.67      | 0.07       |
| wheel 2 | 29.78       | 29.67      | 0.11       |
| wheel 3 | 29.68       | 29.62      | 0.06       |
| wheel 4 | 29.59       | 29.59      | 0.00       |
| wheel 5 | 29.70       | 29.69      | 0.00       |
| wheel 6 | 29.60       | 29.60      | 0.00       |
| wheel 7 | 29.70       | 29.69      | 0.01       |
| wheel 8 | 29.58       | 29.58      | 0.01       |

## B.3.2 Visual inspection

Photomacrographs of the worn polymer contact surface are displayed in Figure B-4 Photomacrographs of (a) worn polymer contact surface. Different wear mechanisms were observed in rollers, significant amounts of debris were found, possibly due to polymer wear. The debris and the transfer layer are seen as dark coloration in Figure B-4. Amongst the various wear mechanism the dominant one is the transfer layer formation. Also transversal surface cracks were also present in few rollers (Table B-4). The counter material also showed with black deposit (see Table B-4 (c)) which might be due to the generated polymer particles. In the observation it was found that the black deposit is not uniformly spread on polymer and steel counterface material. Visual observations were also made with the endoscopic camera, where the partial sliding of polymer rollers was observed during the course of testing. These partial sliding was observed even in the beginning of testing. Thus, the partial sliding condition cannot be attributed to the debris or particle entrapped in the contact.
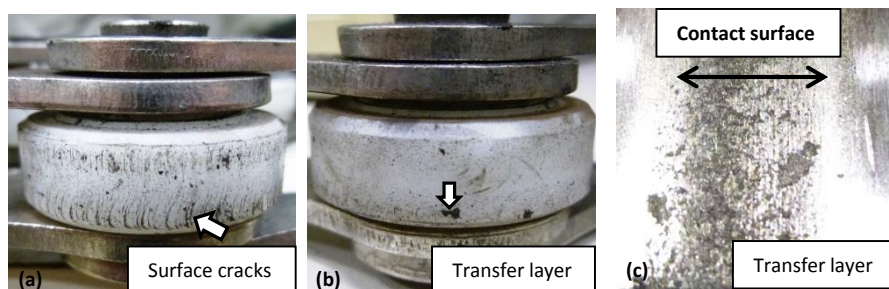


Figure B-4 Photomacrographs of (a) worn polymer contact surface with transversal cracks (b) transfer layer (c) counter material

## B.3.3 Surface morphology

Micrographs of the contact surface were acquired before and after the test for understanding the morphological changes. Figure B-5 and Figure B-6 shows the grey

scale micrographs of polymer rollers contact surface acquired before and after testing. A significant difference in surface morphology was observed on comparing the micrographs of initial and final surface (Figure B-5). This difference corresponds to the transversal cracks seen on the final surface of Figure B-5b (indicated by arrow). However, surface scars present in the post-mortem analysis (see the encircled region in Figure B-6(c)) represent a mixed information with micropits and abrasion grooves from partial sliding. Also, for better understanding of the involved mechanism, micrographs of contact surface were taken at higher magnification to learn more about the failure mode.
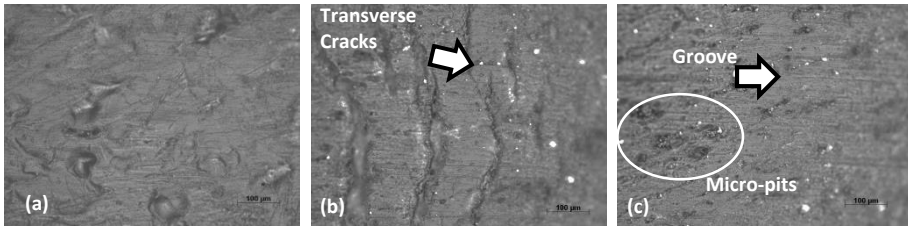


Figure B-5 Polymer contact surface (a) unworn roller (b) transversal cracks (c) abrasion grooves and micropits

On a higher magnification the grooves are clearly visible, similar type of grooves were seen often in the polymer contact surface of other rollers as well. On investigating the cracks further, debris were found between the cracks. These debris are still attached to the edge of the crack (see Figure B-6(b)) which indicates the tensile stress normal to the plane of crack. Also these debris are elongated in the direction of rolling which is from left to right in the shown micrograph. This can be attributed to the partial sliding condition. Also these cracks in most cases extended upto the chamfer edge of the rollers.
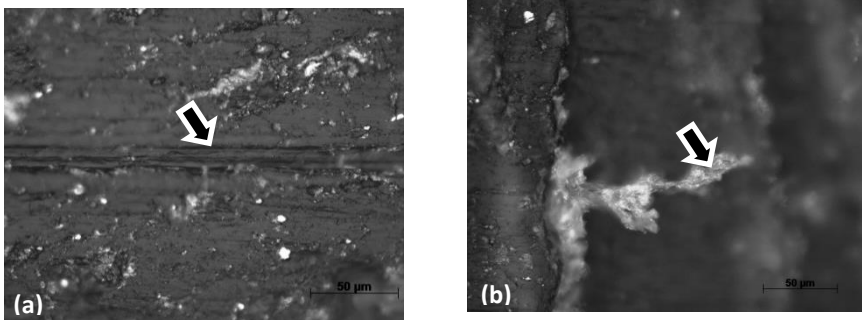


Figure B-6. Morphology of worn polymer contact for (a) grooving (b) cracks.

The steel counter material was also investigated before and after testing at higher magnification. The micrograph of the steel surface is shown in Figure B-7. It is evident from comparing both the surface a significant difference is seen in post-mortem with black colour deposit on the steel surface. Also it is noteworthy to see that these black colour patches have formed in a specific line pattern. All these patches are in a line format running in the direction of roiling. Similar patterns are present in the untested

steel surface. This can be attributed to the grinding marks, with roughness peaks, for which the valleys are filled with the wear particles in the course of wear.
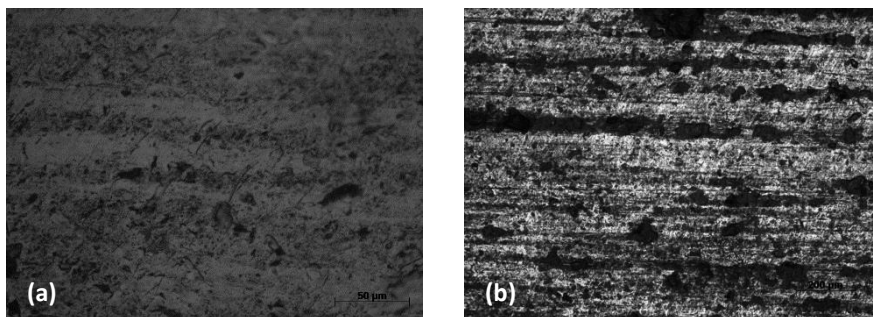


Figure B-7. Morphology of steel contact surface (a) before testing (b) after testing

## B.3.4 Roughness measurement

The roughness of the contact surface was measured before and after the tests across the wear track. An average of five measurements for the selected rollers were taken from the predefined regions. The measurements were made using a 3D-profilometer SURFASCAN 3D. Ra, and for polymer surface was calculated in accordance with an assessment length $l_t$ = 4.8 mm and cut off $\lambda_c$ = 0.80 mm for 0.1 µm < $R_a$ ≤ 2 µm. Table B-6 shows the change in arithmetic roughness average (Ra) of the chosen 8 rollers. The Ra of all the rollers has reduced significantly except for wheel 4. It is evident from the values smoothening of profile has occurred in the course of testing. Variability in roughness values between the eight rollers is evident, however the average roughness (Ra) of the eight polymer rollers has reduced from 2.4 to 0.98 µm.

Table B-4 Roughness characteristics of polymer roller [µm]

|  | Roughness average Ra | |
|---|---|---|
|  | before test | after test |
| **wheel 1** | 3.53 | 0.92 |
| **wheel 2** | 2.07 | 0.78 |
| **wheel 3** | 3.04 | 0.78 |
| **wheel 4** | 1.8 | 1.42 |
| **wheel 5** | 2.75 | 1.07 |
| **wheel 6** | 2.53 | 0.90 |
| **wheel 7** | 1.81 | 0.90 |
| **wheel 8** | 2.21 | 1.07 |

Individual profile for a trace length of 4 mm was extracted from polymers surface for comparing the depth profile before and after test. From the traced profile as shown in Figure B-8, it is evident that the polymer roller has a parabolic profile. Thus, line

contact will be brought only under severe loading condition. Variability in depth between each roller is evident even before testing (See Table B-5). Measurements on the change in profile depth shows significant difference between each roller.
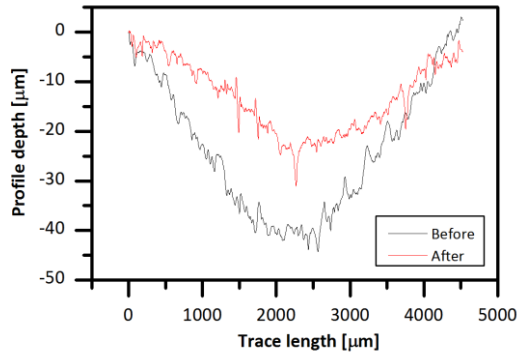


Figure B-8 Depth profile of polymer roller Wheel 1

Table B-5 Profile depth of the rollers [μm]

|         | profile depth | | |
|---------|-------------|------------|--------|
|         | before test | after test | Wear   |
| wheel 1 | 58.16       | 30.32      | 27.84  |
| wheel 2 | 50.78       | 27.4       | 23.38  |
| wheel 3 | 76.14       | 38.18      | 37.96  |
| wheel 4 | 77.46       | 69.42      | 8.04   |
| wheel 5 | 58.74       | 38.8       | 19.94  |
| wheel 6 | 63.7        | 42         | 21.7   |
| wheel 7 | 47.56       | 25.68      | 21.88  |
| wheel 8 | 70.06       | 55.9       | 14.16  |

The roughness of the counterface material was measured in four locations as shown in Figure B-9 (b). Ra and Rvk were calculated in accordance with an assessment length $l_t$ = 16.8 mm and cut off $\lambda_c$ = 0.80 mm for 0.1 μm < $R_a$ ≤ 2 μm. The roughness is measured across the rolling direction of the polymers on the counterface material. The Ra has increased, however, the variability in roughness value persist which can be attributed to the uneven deposition of the transfer layer. From Figure B-9 (a) it is evident that the change in surface profile has occurred only within the contact surface. This means the debris are mostly accommodated inside the parabolic profile of the polymer contact surface. Moreover, high peaks are found in the middle portion of the contact surface where the depth of the polymer profile was at its highest. The mean values of five measurement acquired in four locations are presented in Table B-6, from which it is evident that there is an increase in roughness peaks on the counter material after the testing.
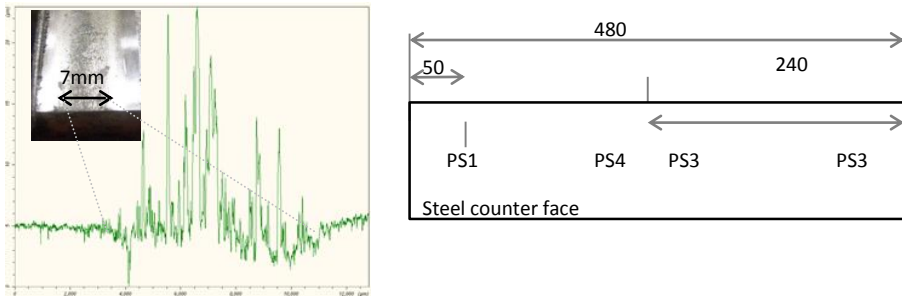
Figure B-9 (a) Roughness profile of the counterface material (b) locations of the roughness measurement

Table B-6 change in surface profile of the counterface material [μm]

|  | Ra | | Rpk | |
|---|---|---|---|---|
|  | before | after | before | after |
| PS 1 | 0.1676 | 0.237 | 0.5344 | 1.3892 |
| PS 2 | 0.2044 | 0.2534 | 0.2488 | 0.2914 |
| PS 3 | 0.211 | 0.3346 | 0.1754 | 1.1102 |
| PS 4 | 0.1046 | 0.1642 | 0.1324 | 0.322 |

## B.3.5 Online measurements

In order to understand the mode of wear online images were acquired during the course of testing by means of USB digital microscope. Few images taken during different stages of wear are shown in Figure B-10. Images from the initial period of wear have a bright white region in the middle of the roller. It is evident that in the initial period of wear there existed only a point contact on both sides of the parabolic profile. However, during the course of wear these dark patches, which might be due to the debris/ transfer layer covers the complete contact surface. Also the micrographs in the final stage of wear shows scratch marks which indicates the partial sliding condition.
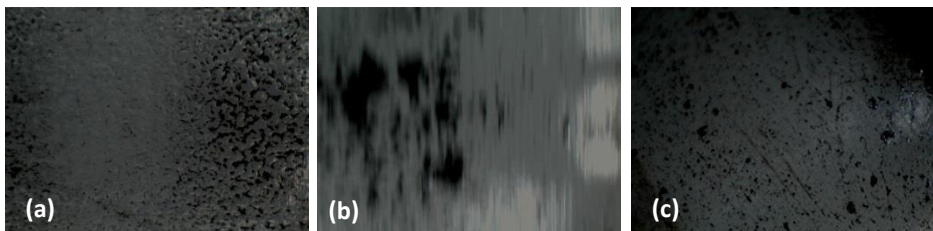


Figure B-10 Micrographs of polymer contact surface (a) Initial period, (b) transition (c) End of the testing

## B.4 Conclusions

**Test material: Polymer roller**

In regards to the evaluation of polymer roller for its wear behaviour, following conclusions are drawn based on the visual observations, micrographic inspections and topographic evaluation.

- Both the diameter and profile measurement for polymer roller wear characterisation in real scale testing shows variability to consider them for wear analysis.
- Transversal cracks and transfer layer formation are the dominant mechanism as observed from the micrographs.
- Grooves from partial sliding and pitting mechanisms are evident.
- The average roughness (Ra) of the eight polymer rollers has reduced from 2.4 to 0.98 µm.

**Counterface material:**

With respect to the surface inspections and analysis made on counterface material the following conclusion can be made:

- The counter material has dark layer of uneven deposition which is attributed to the wear debris and transfer film.
- From the topographic measurement it is evident that these debris are deposited to form roughness peaks (as observed from the increased Rpk in the post-mortem).
- With the applied normal force on a parabolic contact surface, will experience a high contact pressure in the edges and a relatively less contact pressure in the vertex. Thus the generated debris are trapped in the vertex of the parabolic surface which is reflected in the roughness profile of the counter material.
- On the average the roughness increased in the course of testing.

## References

[C.1] Kerremans, V., Rolly, T., De Baets, P., De Pauw, J., Sukumaran, J., and Perez Delgado, Y., "Wear of conveyor chains with polymer rolls," Proc. Sustainable Construction and Design 2011 (SCAD), Ghent University, Laboratory Soete, pp. 378-387.

# Appendix C

# Protocol for TTS and DES test

The appendix includes protocol for testing TTS, DES, working mechanism of the test rig and the used sensors. The protocol involved in testing of TTS and DES are specific and developed after several iterative processes to avoid the parasitic effects from illumination and cooling.
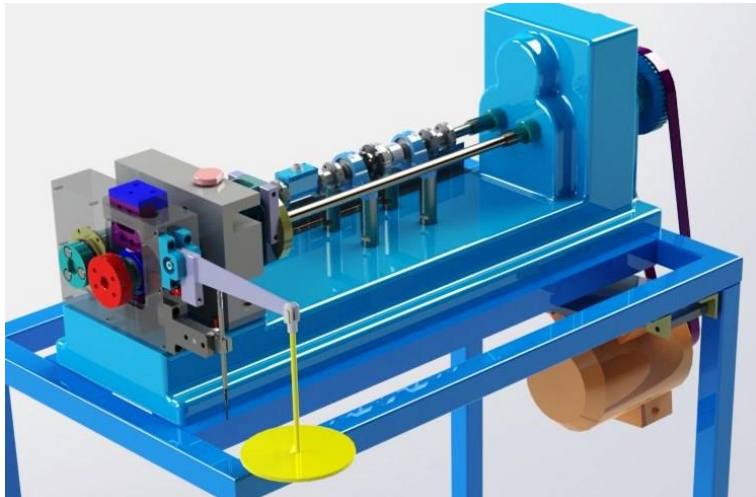
# C. 1 Protocol for traditional tribological study (TTS):

The procedure for traditional tribological test is developed based on preliminary tests and existing literature [C.1-4] on rolling sliding of polymers. The procedure consists of four steps 1. Sample preparation 2. Reference measurements before wear testing, 3. Tribo testing and 4. Post-mortem analysis

**TTS Step 1: Sample preparation:**

TTS Step 1.1: Machining of steel and polymer disc using indexable CCGT turning insert with 80° included angle coated insert. (4 markings were made on the flat face to locate the same region for roughness measurement). V-groove on the polymer specimen for contour profiling is made with a HSS tool.

TTS Step 1.2: Polishing of steel disc with SiC abrasive papers (in the following order P80D, P240, P320 and P400 from Buehler (Ø 305 mm))

TTS Step 1.3: The polymer discs are cleaned by gently wiping the surface with distilled water and later with acetone.

TTS Step 1.3: Drying of polymer specimen (20 hours at 70°C)

**Step 2: Reference measurement before wear:**

TTS Step 2.1: Immediately after drying, the reference mass ($m_1$) of the polymer specimen was measured for five consecutive times and its average is considered as mass loss.

TTS Step 2.2: The roughness and diameter of the specimen was measured in the marked locations. An average of five measurements was made for profile modification from the depth of the V-groove, V-groove contour ($VG_1$) and diameter reduction ($D_{1b}$). The roughness parameters measured for comparison purpose are Ra, Rz, Rsk, Rku, Rmax, Rpk and Rvk.

TTS Step 2.3: Optical micrographs of polymer and steel surface were made at four different locations with an exposure time of 1500 and 300 μs.

**TTS Step 3: Wear testing:**

TTS Step 3.1: Mounting of the polymer and steel disc followed by cleaning with acetone.

TTS Step 3.2: The test rig was warmed up for a period of 30 minutes at 500 rpm before each testing.

TTS Step 3.3: The base torque from the contacts is measured with the mounted specimen without contact at zero load. It is measured before and after testing

TTS Step 3.4: Wear testing of the specimen at continuous rolling for $3 \bullet 0 \ 10^5$ cycles at 500 rpm (10 hours).

**TTS Step 4: Post-mortem analysis**

TTS Step 4.1: Drying of polymer specimen at 70°C for 20 hours and measuring mass after testing ($m_2$).

The mass loss ($\Delta m$) is calculated from
$$(m_1 - m_2)$$

TTS Step 4.2: V-groove contour ($VG_1$) and diameter reduction ($D_{1a}$). All the roughness parameters mentioned in Step 2.2 is measured again for comparison purpose.

The diameter loss ($\Delta D$) is calculated from
$$(D_{1b} -. D_{1a}).$$

The reduction in height of the V-groove ($\Delta VG$) is calculated from
$$(VG_1 - VG_2).$$

TTS Step 4.3: The same region used in step 2.3 is located and micrographs of polymer and steel surface were made with the same exposure time of 1500 and 300 µs respectively.

TTS Step 4.4: Selected specimen (0% and 26% slip ratio) were further sectioned and investigated in the scanning electron microscopy for understanding the changes at sub-micron level.

TTS Step 4.5: Cross-sectional studies on the selected steel discs (0% and 26% slip ratio) were made to understand the transfer layer deposition.

## C. 2 Protocol for Damage Evolution Study (DES):

The procedure for Damage evolution study is typically an *ex-situ* monitoring technique with intermediate pauses. Existing research have already used the *ex-situ* techniques for transfer layer analysis from the view point of steel counterface [C.5]. However, in the current research the newly developed "relocation micrography" is used to locate the same region for tracking the modification on surface morphology. The procedure is similar to TTS, with four steps. 1. Sample preparation 2. Reference measurements at each intermediate pause, 3. Tribo testing. 4. Dismount specimen and make reference measurements and continuous testing.

**DES Step 1: Sample preparation:** (Same as TTS Step 1)

**DES Step 2: Reference measurement** are same as Step 2 of TTS, however, the mass loss is not considered in the case of DES because specimen are unmounted at each intermediate pause. For mass loss the specimen has to be dried for 20 hours, which is not feasible with the DES protocol.

**DES Step 3: Wear testing**

The wear testing was performed with intermediate pauses with the specific cycles as shown in Figure C-1. At every intermediate pause, the test rig continutes operation, but at zero load condition. Thus the ambient temperatur is maintained at 40°C to maintain the equilibrium.
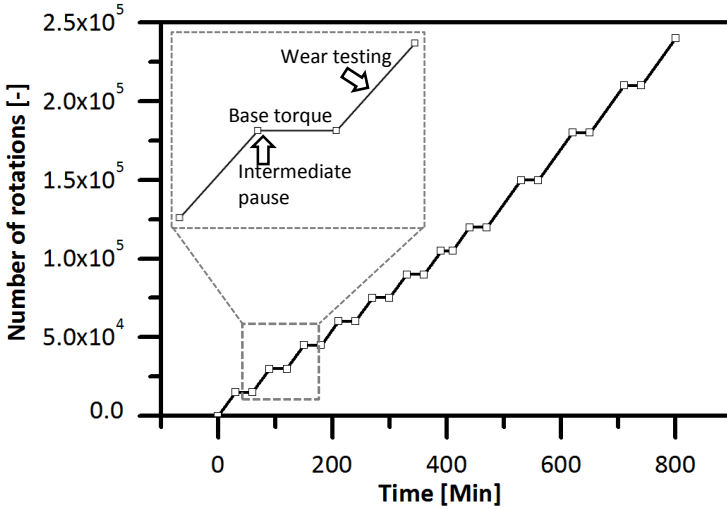
DES Step 3.1: Wear testing of polymer metal contact in the twin-disc setup

DES Step 3.2: Start measurement for base torque (free running)

DES Step 3.3: Mount disc specimen in the locating fixture of the microscope. Measure bright field image for both steel and polymer specimen (at 1500 µs shutter time) for 5X, 20X and 10X (Use same order).

DES Step 3.4: With the focus already set-up at 10X of the bright field imaging, acquire images for both steel and polymer specimen (at 25s shutter time) for dark field imaging.

DES Step 3.5: Following the previous two steps, images were also acquired on the opposite side.

DES Step 3.6: Acquire photo macrographs for both the polymer and steel specimen

DES Step 3.7: Measure roughness values for polymer and steel specimen. Continue testing for the next intermediate pause.

DES Step 4: continue step DES 3.3 until DES 3.7 after the intermediate pause.

## C.3 Brief description about the test rig

The testrig used for experimental simulation of rolling/sliding contact is a modified FZG tester. A schematic and the working principle of the testrig is shown in Figure C-2. The FZG is a modified gear oil tester, in which adaptation are done to perform experiments with non-conformal contact for pure rolling and partial sliding condition. The test rig consists of three main modules 1. driving module 2. loading module and 3. measuring module. Starting with the driving module, the primary components for creating rolling/sliding contact is the single speed gear box coupled to the electric motor through a belt drive. Since, both the polymer and steel disc are coupled to the single speed gear box, thus both are driven and have same rotational speed. The slip ratio is attained from the difference in slip velocity by having different diameter for the polymer and steel discs. The second is the loading module, which is just a dead weight; however the friction and wear measurements are based on this module. The normal force is applied by means of lever using dead weight mechanism. In the event of wear, to maintain the continuous line contact, one of the shaft is mounted with a self-aligning bearing as shown in Figure C-2.
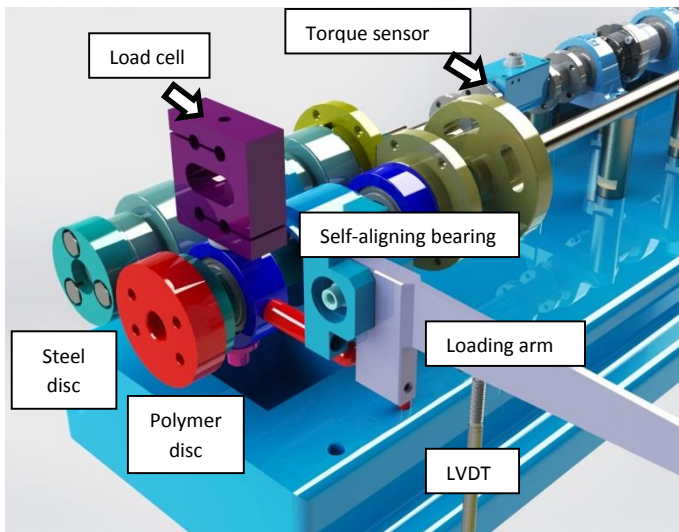


Figure C-2 Schematic overview of the twin-disc test setup

In the measuring module, the wear from linear displacement, surface temperature and the friction force are measured online. The displacement of the self-aligning bearing as a consequence of wear is reflected in the lever carrying the dead weight. A spring push LVDT is mounted against the lever to measure the online trend of wear. The friction force can be directly measured using the torque sensor and also by a load cell. For temperature measurement an infrared temperature sensor is mounted perpendicular to the polymer contact surface.

## C. 4 Instrumentation and calibration

A NI DAQ (National Instruments, BNC-2110) data acquisition card is used to receive and send signals for controlling and recording the measurements online. For tribological measurements, a sensor (LVDT) measuring linear displacement of the shaft and two sensors for measuring the friction force were used. The details and are mentioned in **Table C-1**

<div align="center">

**Table C-1 Shows the sensors, operational range, and their purpose**

</div>

| Sensor | Range/Accuracy | Purpose | Manufacturer |
|--------|----------------|---------|--------------|
| Spring push LVDT | ± 10 mm<br>0.7% of reading | Linear displacement | Solartron AX/10/S |
| load cell | 1-30 daN<br>0.1 % of reading | Friction force | Sensy 2712 Tension compression |
| Torque sensor | 1-10 N-m<br>0.1 % of reading | Friction force | Lorenz DR 20 |

From Figure C-2 it is evident that this system is a closed loop system where the given input from the motor is transferred to the contact. The friction torque is the difference between the measured torque at free running and the torque at contact load. This procedure helps in eliminating the possible parasitic effects from bearings and other moving parts of the test rig. An elaborate procedure for friction measurement, wear measurement is clearly mentioned later in the section with protocols for TTS and DES. The calibration of the sensors are shown in **Table C-2**

**Table C-2 Calibration for spring push LVDT**

| Displacement [µm] | Voltage [V] |
|-------------------|-------------|
| 0 | 0 |
| 10 | -0.009 |
| 20 | -0.0178 |
| 30 | -0.0259 |
| 40 | -0.0358 |
| 50 | -0.0437 |
| 60 | -0.0520 |
| 70 | -0.0607 |
| 80 | -0.0700 |



y = -1150x - 0.2712
R² = 0.9997
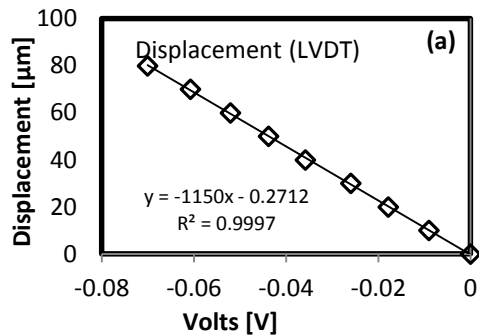
**Figure C-3 Calibration plot for torque sensor**

**Table C-3 Calibration for torque sensor (0-10 N-m)**

| Torque N-m | Volts V |
|---|---|
| 0 | 0 |
| 2.156 | 3.274125 |
| 4.312 | 6.21075 |
| 6.468 | 9.12025 |
| 8.624 | 12.0405 |
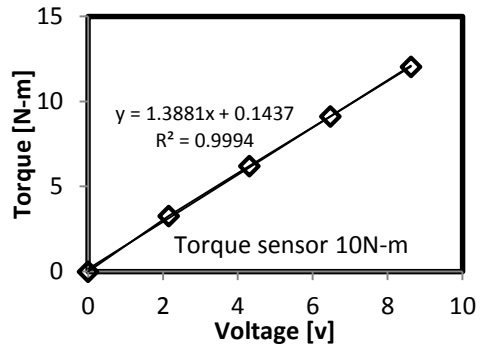


**Figure C-4 Calibration plot for Torque sensor**

**Table C-4 Calibration for Load cell**

| Load [N] | Voltage [V] |
|---|---|
| 0 | 0 |
| 19.673 | -1.001 |
| 39.347 | -2.002 |
| 59.013 | -3.001 |
| 78.607 | -3.997 |
| 98.082 | -4.988 |
| 117.756 | -5.988 |
| 137.430 | -7 |
| 157.095 | -8 |
| 176.697 | -9 |
| 196.115 | -10 |
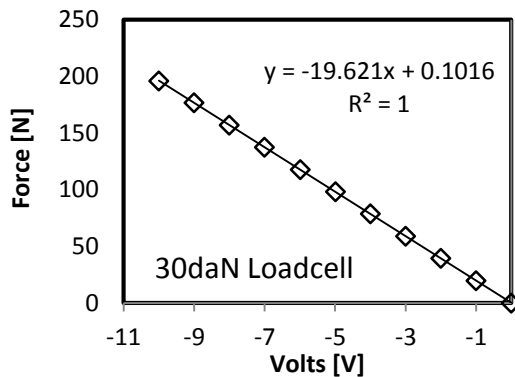


**Figure C-5 Calibration plot for Load cell**

# References

[C.1] Chen, Y. K., Kukureka, S. N., Hooke, C. J., and Rao, M., 2000, "Surface topography and wear mechanisms in polyamide 66 and its composites," Journal of Materials Science, 35(5), pp. 1269-1281.

[C.2] Gordon, D. H., and Kukureka, S. N., 2009, "The wear and friction of polyamide 46 and polyamide 46/aramid-fibre composites in sliding/rolling contact," Wear, 267(1-4), pp. 669-678.

[C.3] Kukureka, S. N., Chen, Y. K., Hooke, C. J., and Liao, P., 1995, "The wear mechanisms of acetal in unlubricated rolling-sliding contact," Wear, 185(1-2), pp. 1-8.

[C.4] Rao, M., Hooke, C. J., Kukureka, S. N., Liao, P., and Chen, Y. K., 1998, "The effect of PTFE on the friction and wear behavior of polymers in rolling-sliding contact," Polymer Engineering & Science, 38(12), pp. 1946-1958.

[C.5] Ye, J., Khare, H. S., and Burris, D. L., "Transfer film evolution and its role in promoting ultra-low wear of a PTFE nanocomposite," Wear, 297(1-2), pp. 1095-1102.

# Appendix D

# Dimension analysis

This section provides in the steps involved in deriving the dimensionless equations introduced in Chapter 4.

1) Identification of the variables associated with the system:

The used system is a twin disc model used for testing polymer composite against steel counter material. The first step is to identify independent variables which are the different parameters associated with the tribo system (F, s, Rmax,E, D, V ξ) that determine the value of a dependent variable (V) which is the wear volume. The relationship can be expressed as

V = f (F, s, Rmax,E, D, V ξ, )

Here the critical parameters are the relative sliding which is the difference between the surface velocity of the two disc. This includes the effect of partial sliding in the developed wear equation.

2) Determine the dimensional formula of each variable by assigning the fundamental units.

Dimensional formula is the relation that shows the fundamental units for any quantity raised to appropriate powers.

Dimensional formulae for the variables are listed in Table D-1

Table D-1 Fundamental units for the selected dimensional variables

| Variables | | Fundamental units |
|---|---|---|
| Normal force | F | [MLT-2] |
| Slip velocity | s | [LT-1] |
| Average peak height (initial) | Rmax | [L] |
| Elastic modulus | E | [ML-1T-2] |
| Sliding distance | D | [L] |
| Volume | V | [L3] |
| Relative slip | ξ | [L] |

3) Calculation of number of dimensionless pi parameter:

To equate the dimensionless parameters, we have used Buckingham pi theorem which is an important theorem in Dimension analysis. In Buckingham's Pi theorem, the number of dimensionless Pi parameter is calculated by subtracting the number of fundamental units (N = 3) from the number of variables (M = 7). This gives the number of pi parameters = M – N = 4.

4) Selection of core group:

A core group is selected with N = 3 variables. They are also called repeating variables. Some of the major restrictions for selection of core group involves 1) it should not be dimensionless 2) none of the variable should have the same dimension. Here, we have selected F, s, Rmax as the representative variables in the core group. Remaining variables are known as non-repeating variable.

5) Formation of Product groups:

Each product group comprises the core group and a non-repeating variable. Hence four product groups are formed and are listed below

[F, s, Rmax, E]                                                           (4.4)

[F, s, Rmax, D]                                                           (4.5)

[F, s, Rmax, V]                                                           (4.6)

[F, s, Rmax, ξ]                                                           (4.7)

Next, dimension formulae are applied for the product groups and arbitrary exponents are assigned for each variable.

$\Pi1 = [(F)a1, (s)b1, (Rmax)c1, (E)]$                                     (4.8)

$\Pi2 = [(F)a2, (s)b2, (Rmax)c2, (D)]$                                     (4.9)

$\Pi3 = [(F)a3, (s)b3, (Rmax)c3, (V)]$                                     (4.10)

$\Pi4 = [(F)a4, (s)b4, (Rmax)c4, (ξ)]$                                     (4.11)

6) Calculations:

By requiring each product group to be dimensionless, arbitrary exponents are solved.

Solving (4.8)

$M^0 L^0 T^0 = [MLT^{-2}]a1 \, [LT^{-1}]b1 \, [L]c1 \, [ML^{-1}T^{-2}]$

Equating the exponents on both sides gives the following equations

$0 = a1 + 0 + + 0 + 1$

$0 = a1 + b1 + c1 - 1$

$0 = -2a1 - b - 2C1 = 0$

Solving this equation gives $a1 = -1$, $b1 = 0$, $c1 = 2$

Subsequent substitution results in

$$\pi1 = \frac{(Rmax)^2 E}{F}$$

Equating the exponents for equation (4.9) (4.10) (4.11) it results in following pi groups

$$\pi2 = \frac{D}{Rmax}$$

$$\pi 3 = \frac{V}{Rmax^3}$$

$$\pi 4 = \frac{\xi}{Rmax}$$

The four groups can be put together as

$$\left(\frac{(Rmax)^2 E}{F}\right)\left(\frac{D}{Rmax}\right)\left(\frac{V}{Rmax^3}\right)\left(\frac{\xi}{Rmax}\right) k = 0 \qquad (4.12)$$

A constant K is added

$$\frac{V}{Rmax^3} = k\left(\frac{(Rmax)^2 E}{F}\right)\left(\frac{D}{Rmax}\right)\left(\frac{\xi}{Rmax}\right) \qquad (4.13)$$

Solving the above equation 4.13 results in

$$V = k.\frac{Rmax^3\ E\ \xi\ D}{F} \qquad (4.14)$$

Where k is the wear dependent constant.

$$k = \frac{V\ F}{Rmax^3 E\ \xi\ D} \qquad (4.15)$$

# Matlab code for filtering spectral analysis (PSD)

**Matlabcode for filtering of roughness profile and power spectrum density (PSD)**

```matlab
dimension=length(input);
start=1;
stop=1024;
for i=start:stop
   left(i)=input(i);
end
leftdata=left.';
j=0;
start=dimension-1023;
stop=dimension;
for i=start:stop
   j=j+1;
   right(j)=input(i);
end
rightdata=right.';


n=length(leftdata);
x=0:2:(2*(n-1));
fs = 0.5;
f  = linspace(0,fs,n);
t=f.^-1;
Time=t';
p=polyfit(x,leftdata',3);
leftformerror=x'.^3*p(1)+x'.^2*p(2)+x'*p(3)+p(4);
leftsign=leftdata-leftformerror;
lefta=((fft(leftsign,n)))/(n/2);
Leftabsa=abs(lefta);
for i=1:n
   if t(i)<2.5
      Leftabsa(i)=0;
   end
end;
n=length(rightdata);
x=0:2:(2*(n-1));
fs = 0.5;
f  = linspace(0,fs,n);
t=f.^-1;
Time=t';
p=polyfit(x,rightdata',3);
rightformerror=x'.^3*p(1)+x'.^2*p(2)+x'*p(3)+p(4);
rightsign=rightdata-rightformerror;
righta=((fft(rightsign,n)))/(n/2);
Rightabsa=abs(righta);
```

```matlab
for i=1:n
    if t(i)<2.5
        Rightabsa(i)=0;
    end
end


for i=2:n
    resultleft(i-1,1)=Time(i);
    resultright(i-1,1)=Time(i);
    resultleft(i-1,2)=Leftabsa(i);
    resultright(i-1,2)=Rightabsa(i);
end
resultleftsort = sortrows(resultleft,2);
resultrightsort= sortrows (resultright,2);
for i=1:n-1
    resultsort(i,1)=resultleftsort(n-i,1);
    resultsort(i,2)=resultleftsort(n-i,2);
    resultsort(i,3)=resultrightsort(n-i,1);
    resultsort(i,4)=resultrightsort(n-i,2);
end
%%resultsort=[resultleftsort,resultrightsort] ;
for i=2:n
    result(i-1,1)=Time(i);
    result(i-1,2)=Leftabsa(i);
    result(i-1,3)=Time(i);
    result(i-1,4)=Rightabsa(i);
end
xlswrite('result.xlsx',result,'sortedbyT');
xlswrite('result.xlsx',resultsort,'sortedbyA');
```

# Appendix F

# Focus mount and illumination

The present appendix presents the details about the focus mount adopted for the DES, TTS and OVS. The used illumination and its characteristics are described.

## F.1 Microscope

A solid model of the reflected light bright field imaging system is shown in Figure F-1. A stroke of 36 mm is for one full rotation of focus knob (coarse) and for the fine focus a 200 µm for one complete rotation with an adjustment graduation of 2 µm. The microscope system is equipped with UIS2 Optical system (infinity-corrected system). A six stage revolver is used in the microscope.
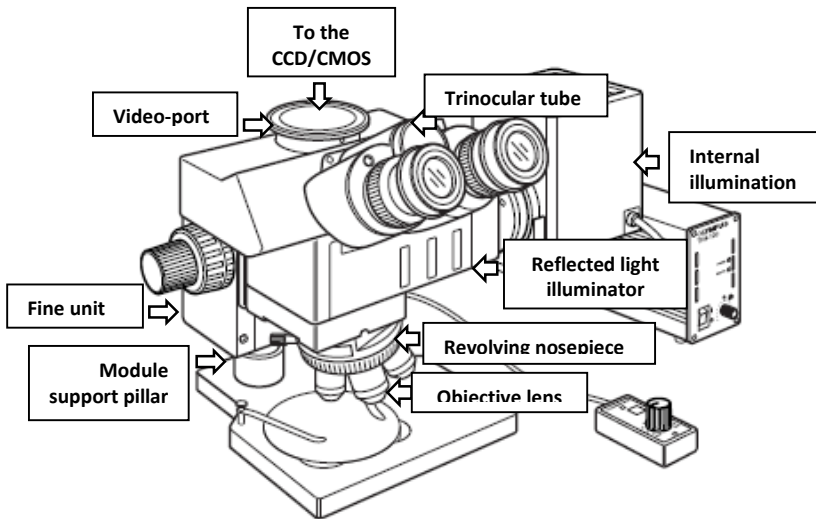


Figure F-1 Olympus BXFM focus mount with bright field imaging

## F.1.1 Procedure for bright field microscopy

Step 1: Mount the polymer/steel specimen in the locating fixture

Step 2: Ensure the optical path to the trinocular tube is closed for supressing the external noise.

Step 3: Use illumination at full intensity, set the required exposure time from the third party software.

Step 4: Engage the 10X objective lens and the worn contact surface is focused by adjusting the fine focus.

However, the dark field microscopy also follows the same steps as mentioned above except after focusing the specimen in step 4, the illumination is changed from internal illumination to external illumination. Furthermore, the required exposure time is selected in the third party software.

# F.1.2 Extension tube:

In regards to the OVS for framing online images, a high speed camera in conjunction with a microscope was used. The microscope was mounted using a panoramic mount, however, having a six station revolver, dimensional constraints persisted to use the appropriate working distance for objectives lens. Hence a tube lens was made in between the objective and the optical train. The tube was made of Aluminium A6061 alloy. Unlike other components the microscope had a different thread followed by the Royal microscopical standard (RMS) specification. The drawing was adopted from the standards and the same was manufactured in Laboratory Soete. The technical drawing of the extension tube and its assembly is shown in Figure F-2.
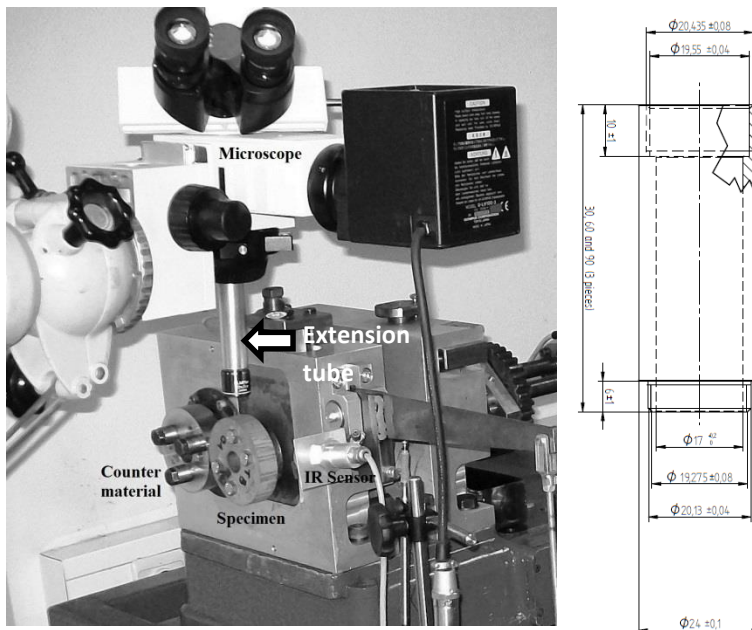


Figure F-2 Schematic view of the microscope arrangement with the extension tube and the technical drawing of the extension tube.

## F.1.3 Contact observations using panoramic tripod

Micrographs of composite (Orkot) edges taken at 5X magnification. Images taken at approximately an angle of 60° to the contact surface.
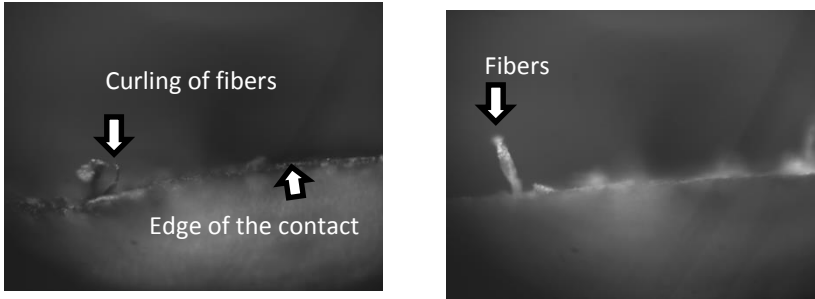


Figure F-3 Static image of composite (orkot) contact surface.

## F.5 Illumination

In all the experiments such as TTS, DES and high speed online microscopy a reflected light bright field illumination is used. Additionally, a dark field illumination is also used in case of DES. To accomplish these two type of illumination, modification in the light path is made. For bright field illumination the light internally passes through the condenser as the light sources is housed before the condenser. But for dark field illumination, external illumination is used. This is because, the light has to be in two direction to eliminate the shadowing effect. Also in the dark field illumination the objective acts only as a collector. Both the illumination is measured for its wavelength using the USB2000 miniature fiber optic spectrometer (see Figure F-4). The Xenon 300 Watt lamp showed with a peak profile at 503.4 nm. The Gossen GKL 300 has a wide spectrum with a dominant wavelength at 575 nm.
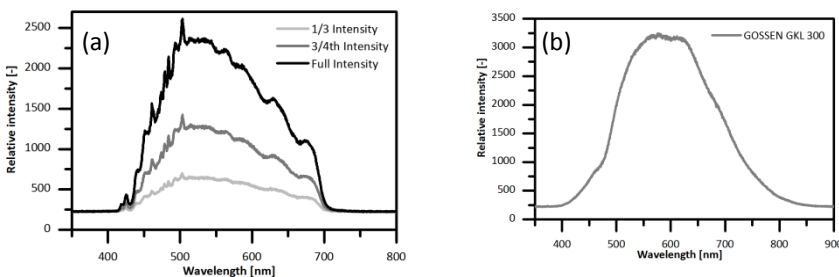


Figure F-4 Spectrum for (a) Xenon 300 Watt Storz illumination (b) Gossen GLK 300 haloen illumination

# Publications

List of scientific publications of Jacob Sukumaran (first author or co-author).

## A1 - Peer reviewed journal publications included in Science Citation Index

1. De Pauw J, De Baets P, Perez Delgado Y, **Sukumaran J**, Ost W. A full scale test rig for assessment of abrasive wear of shackle chains. WEAR. 2013; 302 (1–2): 1017–1025.
2. De Pauw J, **Sukumaran J**, Perez Delgado Y, Rodriguez Fereira V, De Baets P. Effect of hardness in shackle chain wear under harsh environmentally conditions. WEAR. 2013; 306 (1-2):131–7.
3. **Sukumaran J**, Soleimani S, De Baets P, Rodriguez Fereira V, Douterloigne K, Philips W, et al. High-speed imaging for online micrographs of polymer composites in tribological investigation. WEAR. 2012; 296(1–2):702–12.
4. Ando M, **Sukumaran J**. Effect on friction for different parameters in roll-slip of polyamide-steel nonconformal contacts. TRIBOLOGY TRANSACTIONS. 2012; 55 (1):109–16.
5. **Sukumaran J**, Ando M, De Baets P, Rodriguez Fereira V, Szabadi L, Kalacska G, et al. Modelling gear contact with twin-disc setup. TRIBOLOGY INTERNATIONAL. 2012; 49:1-7.
6. Bonny K, Perez Delgado Y, De Baets P, **Sukumaran J**, Vleugels J, Malek O, et al. Impact of wire-EDM on tribological characteristics of ZrO2-based composites in dry sliding contact with WC–Co-cemented carbide. TRIBOLOGY LETTERS. 2011; 43(1):1–15.
7. Krakhmalev P, **Sukumaran J**, Gåård A. Effect of microstructure on edge wear mechanisms in WC–Co. INTERNATIONAL JOURNAL OF REFRACTORY METALS & HARD MATERIALS. 2007; 25(2):171–8.

## A2 - Peer reviewed journal publications not included in Science Citation Index

1. Rodriguez Fereira V, **Sukumaran J**, Perez Delgado Y, Staia M, Iost A, De Baets P. Scratch evaluation on a high performance polymer. MECHANICAL ENGINEERING LETTERS. 2013. p. 76–84.

2. **Sukumaran J**, Rodriguez Fereira V, Irullappasamy S, Jebas Thangiah WJ, Ando M, De Baets P. Exploration of tribological characteristics of naturally woven fiber composites. Kalacska G, editor. MECHANICAL ENGINEERING LETTERS. 2013; 9:7–15.

3. **Sukumaran J**, Andó M, Rodriguez Fereira V, De Baets P, Neis PD. Friction torque, temperature and roughness in roll-slip phenomenon for polymer–steel contacts. MECHANICAL ENGINEERING LETTERS. 2012; 5.

4. Ando M, **Sukumaran J**, Rodriguez Fereira V, Neis P, Kalácska G, Czigany T, et al. Development of new PA6 composites. MECHANICAL ENGINEERING LETTERS. 2012; 5.

5. Krakhmalev P, **Sukumaran J**, Gåård A. How hardmetals react to wear: nano is not always the best. METAL POWDER REPORT. 2007;62 (2):30–5.

6. Rodriguez Fereira V, **Sukumaran J**, De Baets P, Ost W, Perez Delgado Y, Andó M. Friction and wear properties of polyamides filled with molybdenum disulphide ($MoS_2$). MECHANICAL ENGINEERING LETTERS. 2011; 5: 68–80.

## P1 - Conference proceedings included in Science Citation Index

Soleimani S, **Sukumaran J**, Douterloigne K, Rooms F, Philips W, De Baets P. Correction, stitching and blur estimation of micro-graphs obtained at high speed. In: Blanc-Talon J, Popescu D, Philips W, Scheunders P, editors. LECTURE NOTES IN COMPUTER SCIENCE. Berlin, Germany: Springer; 2012. p. 84–95.

## C1 - Publications in conference proceedings

1. **Sukumaran J**, Soleimani S, Rodriguez Fereira V, Ando M, Philips W, De Baets P. Transition of surface morphology in rolling/sliding of polymer-metal contacts. 5th World Tribology Congress 2013, Proceedings. Torino: Italian Tribology Association (AIT); 2013.

2. Rodriguez Fereira V, **Sukumaran J**, Perez Delgado Y, De Baets P. A review of the tribological performance on polymers filled with inorganic particulate fillers. SUSTAINABLE CONSTRUCTION & DESIGN. 2012.

3. Perez Delgado Y, Bonny K, De Baets P, Rodriguez Fereira V, Neis PD, **Sukumaran J**, et al. On-line and post-mortem wear measurement of static counterpart in a ball-on-disk test. SUSTAINABLE CONSTRUCTION & DESIGN. 2012.

4. **Sukumaran J**, Rodriguez Fereira V, Perez Delgado Y, De Baets P, Andó M, Dhieb H, et al. A review on water lubrication of polymers. SUSTAINABLE CONSTRUCTION & DESIGN. 2012.

5. Horvath Á, Csik Z, **Sukumaran J**, Neis PD, Andó M. Development of brake caliper for rally-car. SUSTAINABLE CONSTRUCTION & DESIGN. 2012.

6. Rodriguez Fereira V, **Sukumaran J**, Perez Delgado Y, De Baets P, Igartua A, Fernandez B, et al. Tribological behaviour of the low and high viscosity peek at various testing scales. In: Aranzabe A, Igartua A, Arnaiz A, Aranzabe E, Barriga J, editors. Lubrication, maintenance and tribotechnology. Eibar, Spain: IK4-TEKNIKER; 2012. p. 145–9.

7. Kerremans V, Rolly T, De Baets P, De Pauw J, **Sukumaran J**, Perez Delgado Y. Wear of conveyor chains with polymer rolls. In: Van Wittenberghe J, editor. SUSTAINABLE CONSTRUCTION AND DESIGN. Ghent, Belgium: Ghent University, Laboratory Soete; 2011. p. 378–87.

8. Rodriguez Fereira V, **Sukumaran J**, Andó M, De Baets P. Roughness measurement problems in tribological testing. In: Van Wittenberghe J, editor. SUSTAINABLE CONSTRUCTION AND DESIGN. Ghent, Belgium: Ghent University, Laboratory Soete; 2011. p. 115–21.

9. Van Steenkiste D, Plasschaert S, De Baets P, De Pauw J, Perez Delgado Y, **Sukumaran J**. Abrasive wear of link chains. In: Van Wittenberghe J, editor. SUSTAINABLE CONSTRUCTION AND DESIGN. Ghent, Belgium: Ghent University, Laboratory Soete; 2011. p. 388–96.

10. Andó M, **Sukumaran J**. Tribological behavior of composite-steel on rolling/sliding contacts for various loads. In: Van Wittenberghe J, editor. SUSTAINABLE CONSTRUCTION AND DESIGN. Ghent, Belgium: Ghent University, Laboratory Soete; 2011. p. 29–34.

11. Rodriguez Fereira V, **Sukumaran J**, De Baets P, Ost W, Perez Delgado Y, Ando M. Tribology properties of polyamides filled with nanoadditives. In: Kurják Z, Magó L, editors. Synergy in the technical development of agriculture and food industry (Synergy2011). Gödöllö, Hungary: Szent István University. Faculty of Mechanical Engineering; 2011.

12. **Sukumaran J**, Rodriguez Fereira V, De Pauw J, De Baets P, Ando M. A novel measuring technique to evaluate frictional characteristics of roll-slip contacts in polymer-metal pairs. Advanced Materials and Processing, International conference, Proceedings. Chennai, India: RMK College of Engineering; 2011. p. 153–9.

13. **Sukumaran J**, Andó M, Rodriguez Fereira V, De Baets P. Effect of velocity on roll/slip for low and high load conditions in polymer composite. In: Van Wittenberghe J, editor. SUSTAINABLE CONSTRUCTION AND DESIGN. Ghent, Belgium: Ghent University, Laboratory Soete; 2011. p. 122–7.

## C3 - Conference abstracts

1. **Sukumaran J**. Roll-slip wear of polymers: A worms eye view. FEA PhD symposium, 14th. Ghent, Belgium: Ghent University. Faculty of Engineering and Architecture; 2013.
2. **Sukumaran J**, De Baets P, Rodriguez Fereira V, Perez Delgado Y, De Pauw J, Ando M. The need for online microstructural image acquisition for tribological charecterisation in rolling/sliding contacts. In: Schipper D-J, Masen M, editors. Proceedings of the 29th Meeting of the International research group on wear of engineering materials IRG-OECD. 2013. p. 21–2.
3. **Sukumaran J**. Roll-slip phenomenon of polymer composites: online analysis assisted by computer vision. FEA PhD symposium, 12th. Ghent, Belgium: Ghent University. Faculty of Engineering and Architecture; 2011.